To my family

STUDY OF ELLIPSOMETRIC APPLICATIONS AND EXAMINATION OF OPTICAL ANISOTROPY IN ALUMINIUM AND SILICON OXIDES

by

Saud Jamil Yaghmour, B.Sc., M.Sc.,

A thesis submitted to the University of Aston in Birmingham for the Degree

of

DOCTOR OF PHILOSOPHY

Physics and Mathematics Department

June 1985

University of Aston in Birmingham

SUMMARY

STUDY OF ELLIPSOMETRIC APPLICATIONS AND EXAMINATION OF OPTICAL ANISOTROPY IN ALUMINIUM AND SILICON OXIDES

Saud Jamil Yaghmour Ph.D., 1985

The ellipsometric technique was used to study optical anisotropy in aluminium and silicon oxides by rotating the samples about their normal surface. The optical anisotropy in the aluminium oxide was detected in a Polycrystalline (as received) and electropolished single crystal. In silicon oxide, optical anisotropy was present only in thermally grown samples at a thickness higher than 400 nm.

The anisotrophy in the optical properties was attributed to the stress in the film, which arised from the differences in thermal expansion between the film and the substrate.

Anisotropy was reduced by annealing the sample in a temperature lower than the oxidation temperature. A reduction in the range of 83% was obtained in aluminium oxide (as received) after it was annealed for four hours at 500°C. However, a 91% reduction was achieved in silicon oxide when it was annealed for 90 minutes at 950°C.

The importance of using the correct refractive index for the film and substrate, using the same angle of incidence during the study and the sensitivity of measuring ψ and Δ angles was investigated, in order to obtain the most accurate results. We then calculated the optimum angle of incidence for silicon nitride on silicon and aluminium.

Key words: Ellipsometry/Optical anisotropy/SiO_2/Al_2O_3/Sensitivity

ACKNOWLEDGEMENTS

I would like to express my appreciation to those who have helped me with my research.

To my advisor Professor W E J Neal, I owe a great deal of thanks for his willing assistance. His confidence in me and the research I have performed, which has been demonstrated in both attitude and responsibilities given to me, will always be remembered.

I would like to thank my co-advisor, Mr J L Sullivan for providing assistance and helpful advice during this work.

In addition, thanks go to Mr Bassi for his technical help during this work. Also I would like to thank Mr H Arrowsmith for his help.

I am especially thankful to my family, for their continued love and encouragement, without whom this work would not have been possible.

CONTENTS

LIST OF TABLES

LIST OF FIGURES

CHAPTER I

INTRODUCTION

Since the publication of the experimental results of Cathcart et al.[1] in 1963, concerning anisotropy in the refractive index of Cu_2O, the theoretical verification of the phenomenon has received a considerable amount of attention by researchers in the fields of surface studies as will be described in the next chapter. Karwal and Neal[2] found there is a variation in the ellipsometer parameters ψ and Δ when a sample of commercial aluminium is rotated about a normal to its surface. They found that a rolled sheet gives a large difference between the measurement values of ψ and Δ for directions parallel and perpendicular to roll lines. This change in the ψ and Δ angles will have an effect on optical constant calculations.

The main objectives of this work will be to (1) investigate any optical anisotropy for the surface layers on different materials; (2) study the cause of this phenomenon and (3) determine whether it is possible to avoid the occurrence of anisotropy and its reduction when it exists. We will use Cathcart's technique which depends on the rotation of the specimen about a normal to the surface of the material under investigation. Any resulting change in the ellipsometer parameters ψ and Δ could be considered as due to optical anisotropy, because the optical constants are calculated from ψ and Δ as we will explain later. Another objective was to investigate the optical properties and the film thickness for surface layers of different materials on

different substrates and to study the ellipsometer sensitivity of measuring the angles ψ and Δ in such determinations.

CHAPTER II

SURVEY OF THE PUBLISHED LITERATURE

2.1 Ellipsometry

Interest in the physical properties of thin films has rapidly increased within the last two decades. There are various optical techniques available for the measurement of the refractive index and the thickness of metal films, e.g. the use of a multiple beam interferometer for thickness measurement developed by Tolansky[3]. Murmann[4,5] has shown that the optical properties can be determined by measuring the intensities of the light transmitted and reflected from both sides of films. These and other methods available for the determination of the optical properties and the thickness of thin films are summarised and discusssed by Heavens[6,7].

Ellipsometry is a sensitive technique which allows the determination of the optical properties of a surface. The theory of technique is based on the work of Drude[8,9]. In ellipsometry polarized monochromatic light is incident onto a surface and the resulting polarization state of light reflected from the surface is measured. In the most common case, the ellipsometer is adjusted so that the incoming light is polarized in such a way that light reflected from the surface is elliptically polarized or plane polarized (this depends on the compensator's position). Thus the technique is concerned with measuring the change in the state of polarization of light reflected from a surface. Such measurements may be interpreted to yield the optical constants n

and k of the reflecting material if it is film free or, the optical constants and or thickness t when the reflecting material is a film-covered substrate. The incident polarized light can be resolved into components parallel and perpendicular to the plane of incidence. The state of polarization is characterized by the phase and the amplitude relationships between the two components of a light beam.

Generally, for a clean surface, the reflection coefficients r_p and r_s can be obtained from basic electromagnetic theory in terms of the refractive index and the angle of incidence. For a clean dielectric surface, the plane of the polarization rotated due to a different amplitude ratio in the reflected light, but if the dielectric surface ($k_2 = 0$) is covered with a thin film there will be a phase difference between the two components $\Delta_p - \Delta_s$ and the ratio of the two amplitudes ρ_s/ρ_p undergo changes which are dependent upon the substrate, the thin film refractive index and thickness and the angle of incidence. In principle, with a complete knowledge of the state of polarization of the incidence ψ and reflected light (determined from the instrument parameters Ψ and Δ), the wave length of the light and the angle of incidence, the evaluation of the refractive index and the thickness can be obtained.

The historical development of the technique has been described by Winterbottom[10]. The earliest work on the influence of thin films at interfaces was carried out by Drude when he derived the fundamental equation of ellipsometry from Maxwell's equation with a suitable boundary condition. He was not able to solve the problem for n, k and t, but obtained approximate solutions for

films of thickness which were small compared to the wavelength of the light used.

At the same time as Drude[11] was investigating optical properties of light reflected from solids, Rayleigh[12] was examining the optical properties of light reflected from the surface of liquid. He found that light reflected from water at the Brewster angle had a small negative ellipticity which was contrary to the Fresnel equation. He concluded that the effect was due to a contaminating film of grease on the water surface which he estimated to be less than 1 nm in thickness.

Although the optical properties of metals were studied by means of reflectivity measurements[13,14], Trowstad and Feashem[15] studied the optical constants of a mercury surface which they used as a standard surface for the calibration and adjustment of the ellipsometer since it was found to give more reproducible results than any other surface produced by mechanical polishing. Trowstad and Haverstad[16] also produced the first experimental detailed work by using Drude's theory and technique and studied the chemically produced passivity of iron and steel mirrors.

Drude's approximate equations for a thinner film (i.e. less than 10 nm) were verified by Lebernight and Lustman[17] when they investigated the oxidation of iron and nickel. The instruments used until about 1940, were often modified spectrometers to carry the two polarizer prisms (polarizer and analyzer) and a quarter wave plate (compensator). Detection was by eye using half-shade devices, either Nakamura plates or Trowstad half-shade devices. But this way of detection ended in 1940 when the photomultiplier

was introduced. This made a great improvement in sensitivity and accuracy of the technique and it also made it possible to use a wide range of wavelengths for the same measurement. For example McPherson[18] measured the optical constant for copper-aluminium alloys over the wavelength range of 380 to 1000 nm.

Rothen[19] was the first to give the ellipsometer its name and before it had been called a polarization spectrometer. Later on Rothen and Hanson[20] used a coated surface with a known number of barium stearate monolayers for developing the calibration technique for the ellipsometer. Winterbottom[21] reviewed the results of optical constants for bulk materials (iron, aluminium and copper) in the visible region of the spectrum. The development of polarizing devices for infra-red (for e.g. selenium plates used by Elliott et al.[22]), helped Beattie[23] to develop a new ellipsometric technique for metals using a wide range of wavelengths up to 12 microns. But there are some limitations on the accuracy of such a measurement as shown theoretically by Beattie and Conn[24]. They became interested in the study of the state of the surface (rough or smooth), corrosion and oxidation of a surface by a simple instrument (ellipsometer) in order to see if it would give sufficient sensitivity and accuracy. The idea was adopted by Hayfield and White[25], by Neal et al.[26] in the investigation of the annealing of aluminium films and by Miller[27] in the investigation of optical properties of liquid metals.

McCrackin[28] investigated the importance of the alignment of the optical components, in the measurement of the ellipsometer parameters and illustrated the measurement of a very thin film

(e.g. films with a 2.3 to 2.7 nm and 0.2 to 0.5 nm thickness). Archer[29] studied a silicon surface using the exact theoretical equations of Drude. Gillham[30] introduced a new development by using the Faraday effect, which led to a highly sophisticated instrument. The rotation of the plane of polarization when light passes through a dielectric in the presence of magnetic fields is known as a "magneto-optic" or Faraday effect. Gillham[31] employed lead-zinc borate glass in the form of cyllindrical rods 10 cm in length overwound with a copper coil carrying an alternating current of 1 Amp at 50 Hz. With this arrangement, the plane of polarization was found to oscillate at 50 Hz through 6 degrees. When this light passed through the analyzer prism on to the photomultiplier, an alternating intensity of light was received, resulting in a convenient output signal. Gillham and King[32] modified their design, which led to the commercialization of the instrument, produced by Bendix Electronics. At the same time an equally accurate instrument was produced in the United States by Williamson et al.[33]. Since then several instruments have been developed on the basic design of King[34].

In 1963 the first ellipsometry conference was held in Washington D.C. by the National Bureau of Standards[35]. The programme of the conference included a historical review, theory, computational and measurement techniques and some application. Since then several conferences have been held[36-38] and some books about ellipsometry have been written[39,40].

At the same time many review articles have been written; for example by Neal[41,42] when he reviewed the theory and application of ellipsometry. Thomas and Allen[43] discussed the measurement

of optical properties by using ellipsometry and Neal and Fane[44] reviewed the ellipsometer application on surfaces (see references 45-49).

2.1.1 Automatic Ellipsometry

Until 1969 the ellipsometer was manually controlled and could easily be set-up on optical benches at a relatively low cost. With the aid of a suitable photomultiplier detector, the ellipsometer is a very sensitive tool for surface studies. The only disadvantage of the manual ellipsometer was the time consuming exercise to take a set of readings. With the increasing scientific research into ellipsometer applications, the need for a faster instrument, with a quick response to measuring the reaction rates and the film growth was needed. Hence, an automatic ellipsometer was produced. The first automatic ellipsometer was described by Cahan and Spanier[50], they give a very good description of a high speed automatic instrument. Since then more investigations about the automatic instrument have been made, which lead to the modified Cahan and Spanier instrument. Such an instrument is that of the modulated ellipsometer by Jasperson et al.[51] for studying thin layer optical properties and surface dynamics and by Cahan et al.[52] who studied the electrode-electrolyte interface with platinum and gold electrodes.

In a modulated ellipsometer, quantities related to the parameters ψ and Δ are extracted simultaneously by synchronous detection of reflected light intensities in two frequency channels. Signal processing is completed by an on-line computer

which samples the data at a repetition rate of approximately one a second. Once the optical system is aligned all elements remain rigidly in place so that precision and stability are high. ψ and Δ precision of the order of 0.001 and stability of the order of 0.01 over a period of one hour can be achieved.

Jerrard and Henty[53] describe an instrument for studying optical rotation, circular dichroism and an ellipsometer. The main characteristic of this instrument is that it records automatically and studies the surface over a wide range of wave lengths.

Muller and Mathieu[54] investigated the different types of automatic ellipsometry, because with the whole range of instruments now available, it becomes very difficult to compare performances. They checked these instruments by testing five characteristics: (1) accuracy and reproducibility, following any surface changes; (2) smallest variation which can be resolved (resolution); (3) maximum range of changes (dynamic range); (4) specimen area required for reflection; (5) maximum rate of change (slew rate). They suggested the use of rotating mirrors of slightly differing constants as a convenient method of characterisation. A comprehensive report on the classification of different types of automatic ellipsometry was written by Muller [55] when he divided them into two groups: (1) non-compensating, (2) compensating and compared their performances.

2.2 Surface Roughness

The exact equations used in ellipsometric studies require a

surface to be smooth and homogeneous. Usually this requires a small area to be examined but if the surface does not comply with these requirements, errors will arise in the measurement. Therefore it is very important in ellipsometric studies to have a smooth surface and because of this, some authors have tried to investigate the effects of varying degrees of roughness. The first theoretical investigation of the error produced by neglecting roughness of the surface were carried out by Fenstermaker and McCrackin[56]. They studied three models of surface roughness: square ridges, triangular ridges and pyramids. This will be discussed in more detail in Section 3.3 . They found large errors in the measured indices for some surfaces (glass, silicon, gold and other materials) with roughnesses of the order of 50 nm as compared with a smooth surface.

Sirohi[57] studied the effect of surface roughness by measuring the thickness and indices of a film grown on a rough surface (substrate). He assumed the irregularities were large compared with the light wavelength. The changes in ψ and Δ can be a few degrees different from the smooth surface values and he concluded that reports of measured variations in the refractive index with the angle of incidence could be partly attributed to the roughness. Azzam and Bashara[58] used Maxwell Garnett's theory and they suggested that the roughened surface layer is equivalent to a film whose refractive index is the average of the indices of surface material and the immersion or environmental medium. Chan and Morton[59,60] also followed the theory of Maxwell Garnett to study surface roughness. They showed that the variations in the angles ψ and Δ during their measurement were

not solely due to oxide layer changes but to that of the surface roughness. Smith[61] studied cracks in aluminium and observed a large change in ψ and Δ with the formation of sub-microscopic cracks. He concluded that the Fenstermaker and McCrackin[56] model is a useful approach for relating ellipsometric parameters to surface roughness (see Section 3.3). Hayfield[62] investigated the influence of surface roughness and inhomogeneous films. Ohlidal et al.[63,64] studied the refractive index of a polished and single crystal silicon and found that the polishing process is not reproducible because of the variation in the thickness of a damaged absorbing layer on non-absorbing oxide. But there was an increase in values of the refractive index as a result of mechanical polishing compared with surface etching. Smith[65] carried out experiments on controlled surface roughness on aluminium and showed the variation in the parameters ψ and Δ as a result of the effect of surface roughness.

Vedam[66] suggested that the surface roughness could be reduced by using angles of incidence less than 70 degrees. Pashley[67] theoretically investigated a water film on a slightly rough quartz with a substrate roughness in the same range as the film thickness and found that a large error in the ellipsometric parameters could occur. Smith and Lindberg[68] performed experiments to study a transparent film on a rough metal surface. They assumed two models to study the surface roughness: (1) if the refractive index of the smooth substrate are known, the roughness can be treated as a film with mixed properties of the substrate (the oxide, contamination and ambient); (2) if the refractive index of the smooth substrate are not known, the effective

refractive index of the rough surface will be used as the refractive index. If the roughness is very high then neither model can be used because ψ values fall outside the boundaries of any calculated possibilities. The thickness of the sample can be obtained from the values of Δ .

2.3 Optical Anisotropy

The ellipsometry theory was derived on the assumption of an ideal surface (perfectly smooth, specular reflecting, isotropic and homogeneous) to examine the optical properties, thin film growth and contamination. A real surface can be affected and depart from one or all of these conditions by the environment or by treatments such as mechanical or chemical polishing. The surface may be damaged, rough or corroded and the optical constants measured depend on its previous history. The application of ellipsometry is to examine optically the state of the surface. In some cases the stress on the surface will lead to a change in the optical constant and this has been reported by Cathcart et al.[1]. They were studying Cu_2O by rotating the sample under examination about an axis normal to the surface whilst keeping the same angle of incidence and found a change in the values of Ψ and Δ with rotation. They assumed constant values of optical constant and calculated thicknesses relating to the variation in the ψ and Δ values. When they plotted the thickness against the angle of rotation they found a cyclic curve, as shown in Fig. 2.1.

The study of the optical anisotropy effect using an ellipsometer has received little attention after Cathcart. There has been more theoretical studies than experimental work.

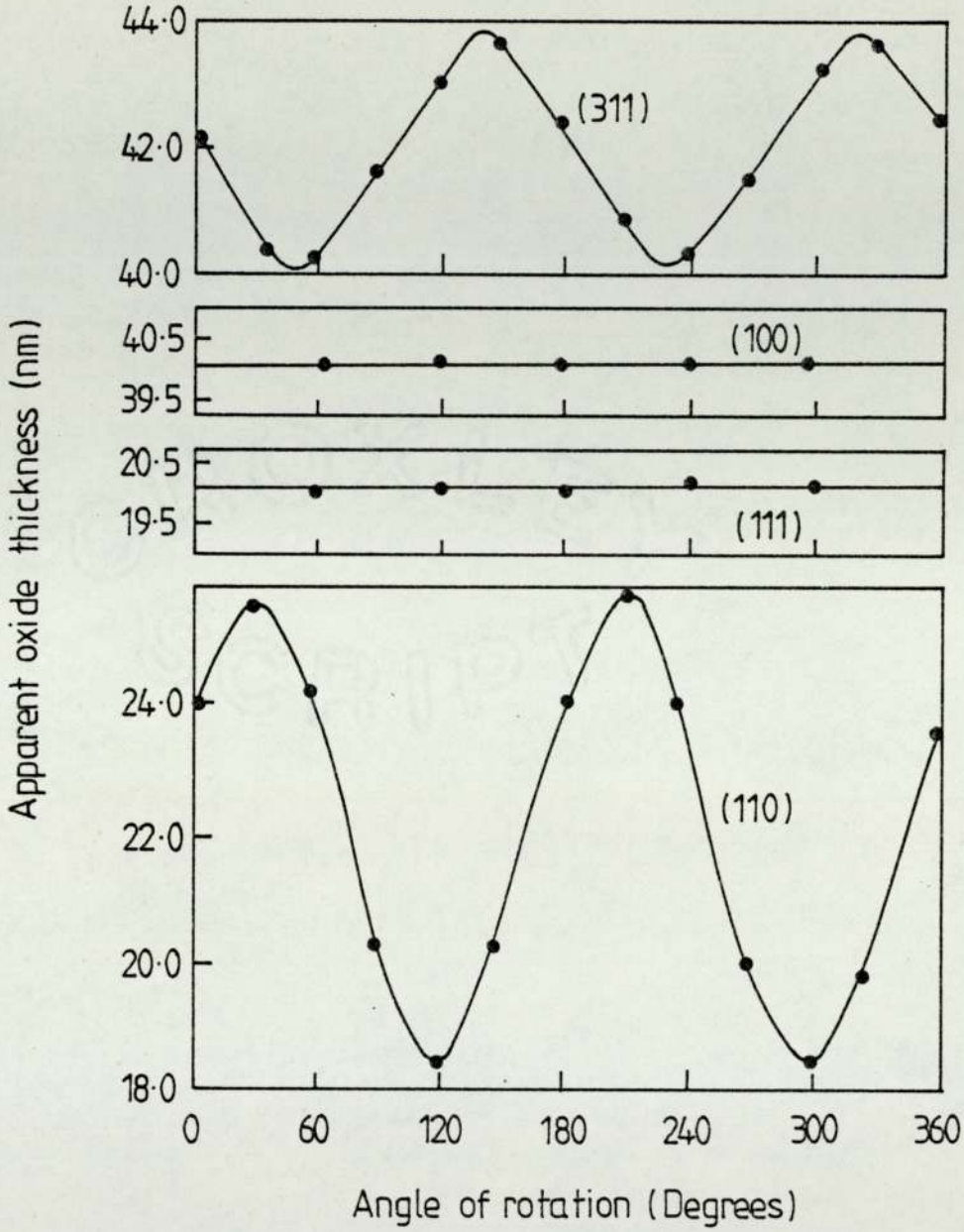

Figure 2·1 Variation in apparent oxide thickness on four planes of copper vs. angle of rotation about its normal. [After Calhcart et al. 1]

Winterbottom[21] discussed a few specific cases and presented total reflection coefficients for a uniaxial film and substrate with the optic axis parallel and normal to the film surface. Den Engelsen[69] treated the reflection and the transmission of polarized light by a thin uniaxial anisotropic layer with its optic axis either parallel or perpendicular to the plane of incidence (Appendix 1). Azzam and Bashara[70-74] in a series of papers, considered various configurations of ellipsometers in order to determine the arrangement of optical components most sensitive to anisotropy. Berreman[75] studied the transmitted and reflected light of a continuously varying anisotropic planar media and he applied it to liquid-crystal twist cells. De Smet[76] investigated the behaviour of ellipsometric parameters of a uniaxial anisotropic surface when it is rotated about a normal to the sample surface. He found that there are variations in the null settings (see Section 3.2) with the angle of the rotation. He then studied the uniaxial thin film on an isotropic substrate[77]. Meyer et al.[78] shows experimentally that the optical anisotropy does exist in uniaxial compounds and he studied GaSe which is a highly anisotropic structure. All these studies were about uniaxial surfaces until De Smet[79] modified his earlier work for biaxial surfaces and showed that the variation of the null setting (Section 3.2) is cyclic with the angle of the rotation when a specimen is rotated about a normal to its surface, as shown in Fig. 2.2.. In 1976 optical anisotropy was detected by Kawabata and Ichiji[80] in the plane parallel to the surface of evaporated gold films by using a return-path ellipsometer. At the same time Den Engelsen[81] reported on the refractive indices

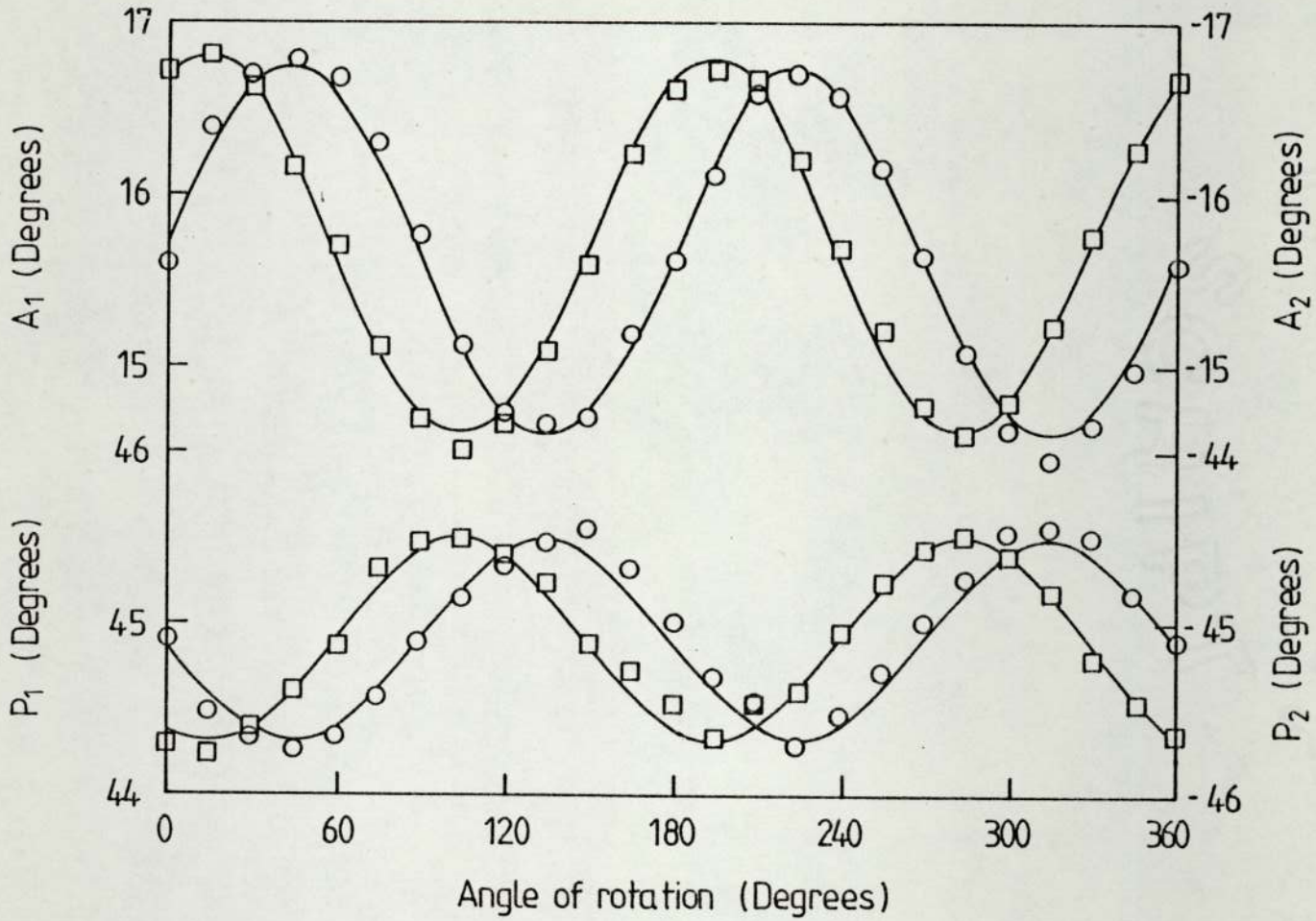

Figure 2·2 Ellipsometer null setting as function of angle of rotation about a surface normal
(□ :- represents P_1 and A_1 , and o :- represents P_2 and A_2 .
[After De Smet 79]

obtained from experiments on monolayers, bilayers and multilayers of various lipids. In the same year De Smet[82] predicted the extinction settings of a nulling setting for reflected light from almost any type of uniform film on a flat surface .

Pedinoff et al.[83] reported that optical anisotropy can arise from strain and stress in a film. They attributed the stress effect to lattice mismatch and thermal expansion coefficient difference between the film and the substrate. They measured the anisotropy in As_2S_3 , As_2 Se_3 and ZnSe films on KCL by using the multiple angle ellipsometer. Habraken et al.[84] modified the theory for the optical properties of (sub)monolayer film, with more attention to the anisotropic layers. A linear relationship between $\delta\Delta$ and the coverage of oxygen chemisorbed on Ag(110), Cu(100), Cu(111) and Cu(110) was found. The anisotropy in the Cu(110) plane (as measured by $\delta\psi$ and $\delta\Delta$) depend on the temperature as shown in Fig. 2.3. Pedinoff et al.[85] measured the optical anisotropy and stress in thermally grown SiO_2 for a film with a thickness of 400 nm by using the multiangle single-wave length ellipsometer. They attributed the anisotropy and the stress to the difference in thermal-expansion between the oxide and the substrate. A theoretical model of the sensitivity of measuring ψ and Δ has been presented as shown in Fig. 2.4, which shows the region in which optical anisotropy can be measured. Kotz and Hayden[86] present this evidence for optical anisotropy of a silver (110) surface covered with oxygen by using a single wave ellipsometer as well as a spectroscopic ellipsometer.

Whenever a specimen is strained, it can become optically

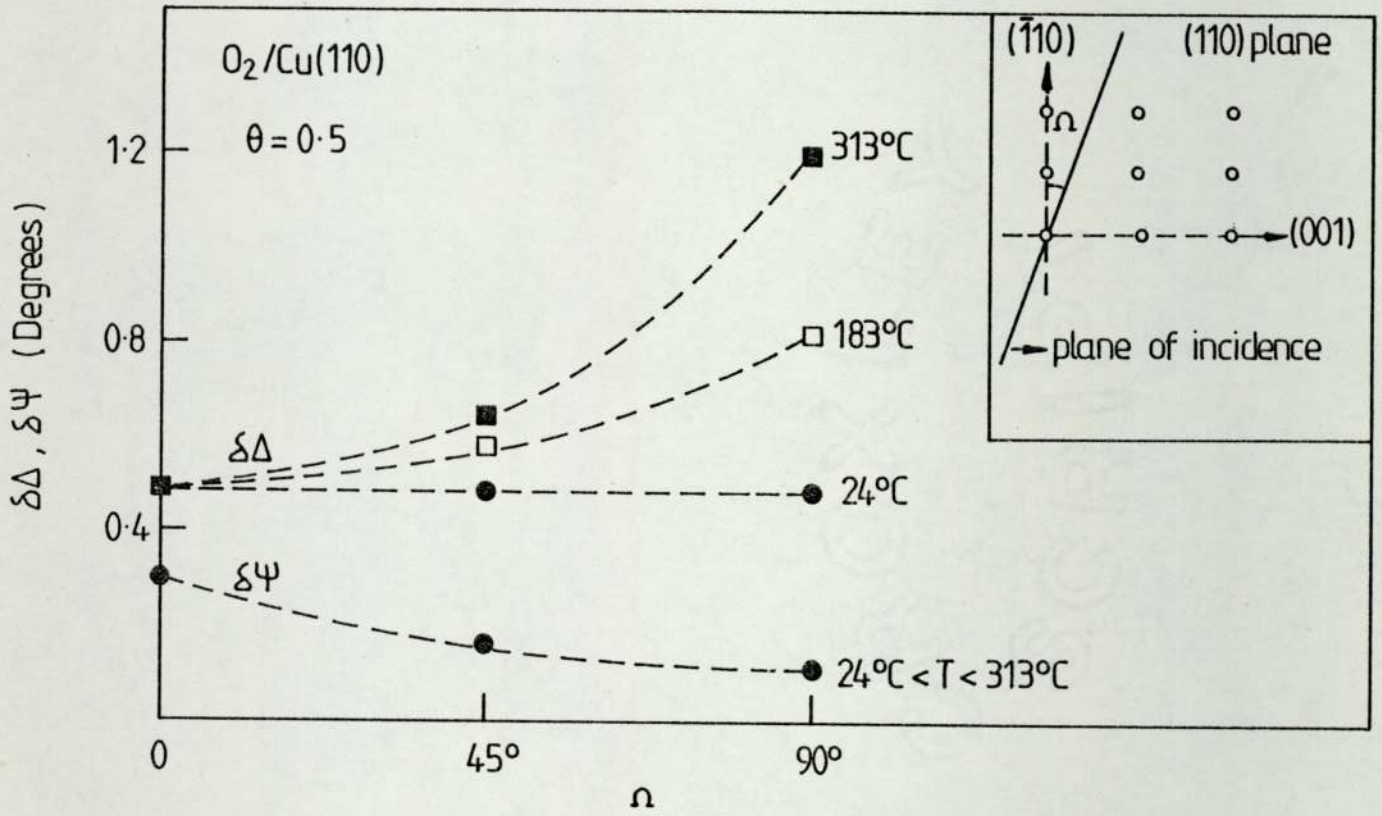

Figure 2·3 Experimental values of $\delta\Psi$ and $\delta\Delta$ of half a monolayer coverage of oxygen on Cu (110) as a function of the azimuth Ω at different temperatures.
[After Habraken et al. 8 4]

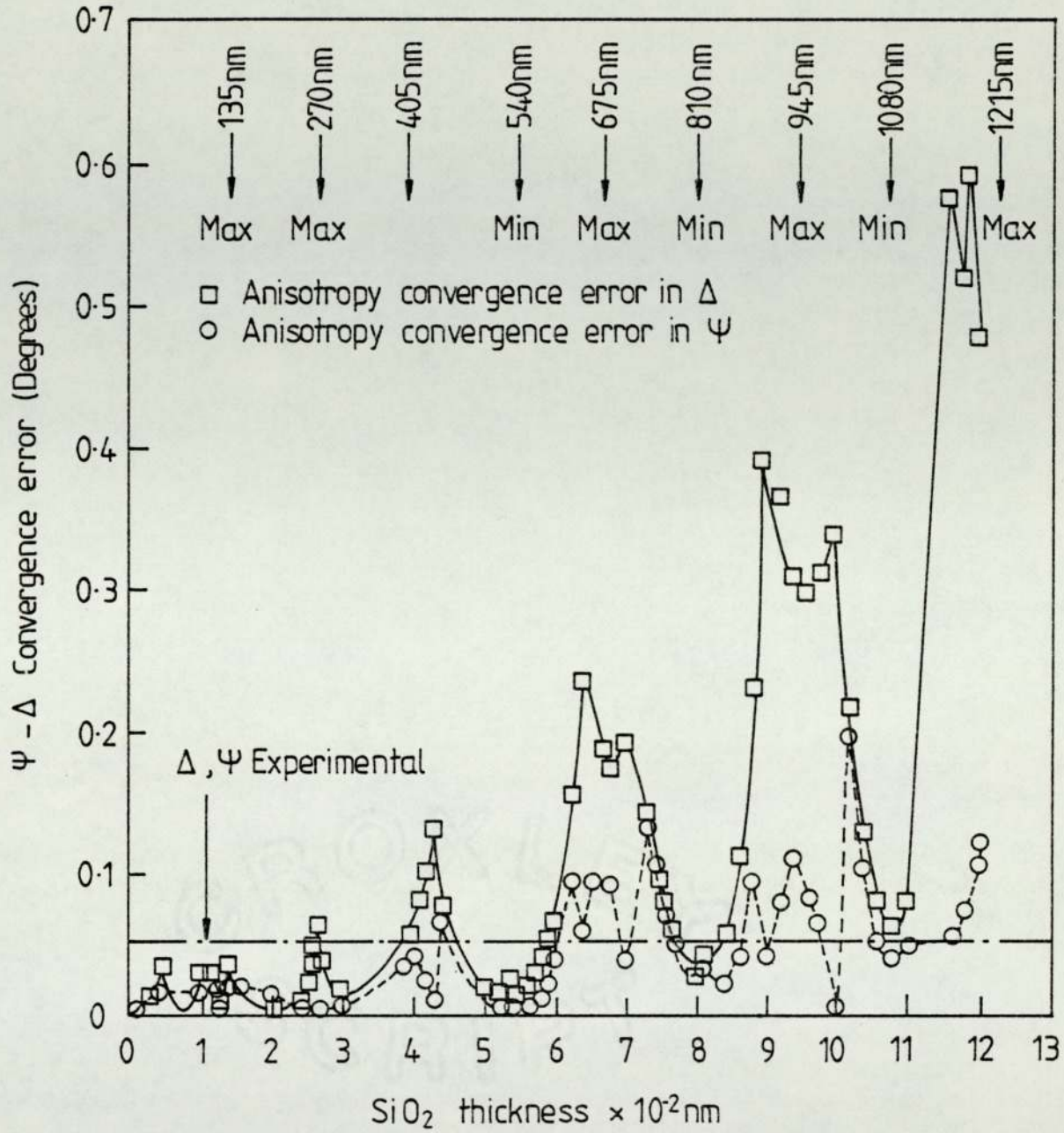

Figure 2·4 Anisotropy measurement sensitivity vs film thickness for SiO_2 on Si. [After Pedinoff et al 85]

anisotropic. The description of the changes in optical properties are due to the strain and stress as explained by Nye[87] which we will discuss in the next chapter.

Optical anisotropy was detected in anodic oxides of molybdenum, niobium and tantalum by De Smet and Ord[88], Matthews et al.[89] and Ord and Wang[90] respectively . Other investigations have been reported in this topic, see references from 91 to 96.

2.4 Oxidation of Metals

2.4.1 Introduction

At room temperature, most metals become covered with a film of oxide because they are unstable in the presence of oxygen. Initially, a film is formed rapidly, then the reaction is slowed down because the film which is formed acts as a protective layer. The thickness of such films are usually no more than a few nanometers. Review articles and books have been written on the subject and they give experimental results and theoretical explanations of the phenomena[97,98].

As a gas molecule approaches a clean solid surface with a potential energy as shown in Fig. 2.5, a weak interaction takes place, according to Van der Waals. A molecule with kinetic energy E_k has to lose at least this amount of energy to stay in the surface, this will occur if E_k is higher than the zero potential. If E_k is less than the zero potential, no interaction will occur. This reaction depends on the potential energy of the particular gas metal combination.

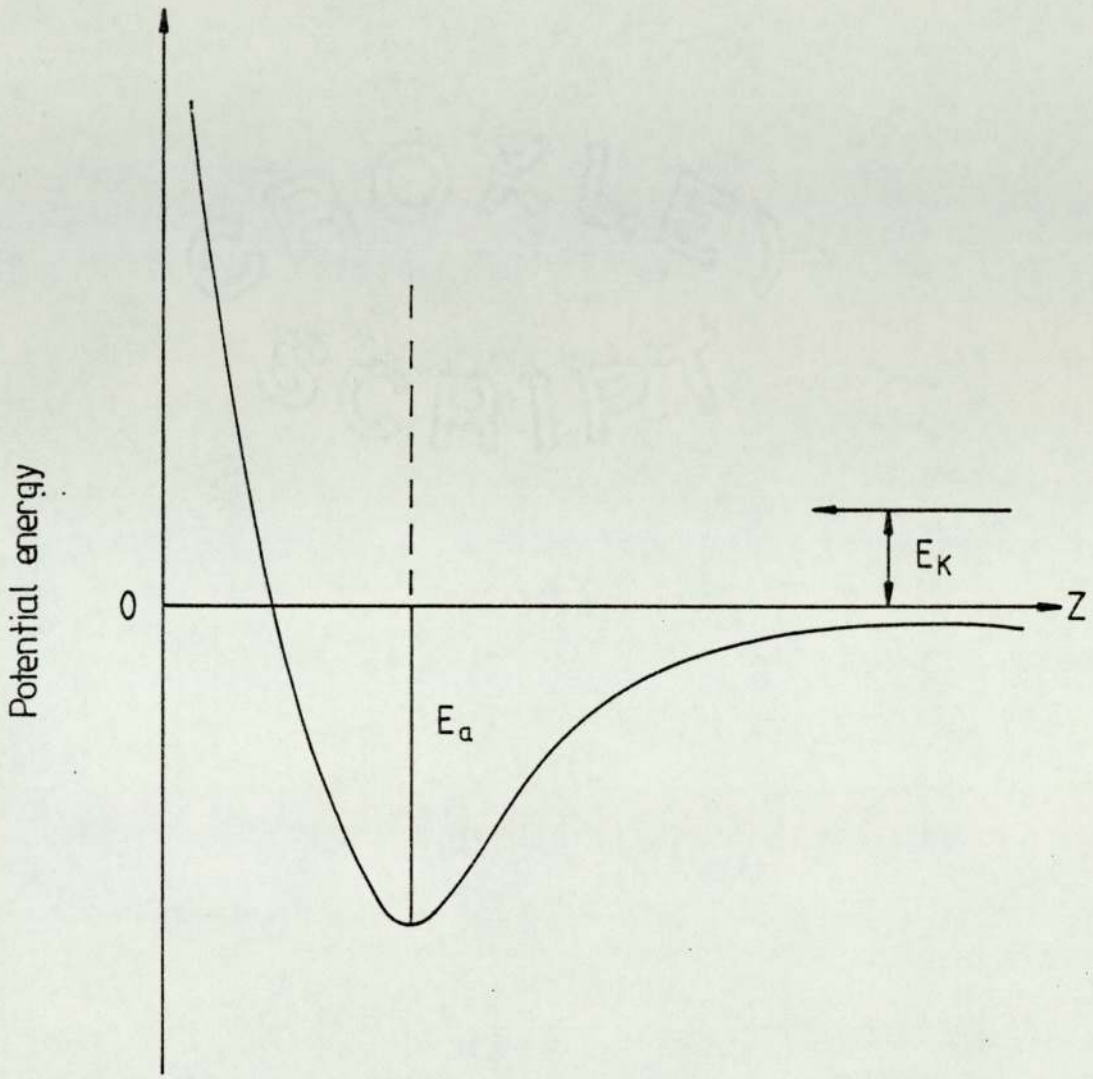

Figure 2·5 Potential energy of an adatom as a function of its distance Z from the surface.

2.4.2 Oxide Film Formation

When a thin film of oxide has been formed on a metal surface, this film will form a barrier between the environment and the metal which means no more reaction between the metal and the gas. Therefore a diffusion of cations, anions and electrons through the oxide layer is needed for the reaction to continue (more oxide layers can then be formed). The rate of the oxidation mechanism depends on many factors. A large number of theories and models have been proposed to explain the formation of oxide films[99].

2.4.3 Wagner's Theory

The nigh temperature oxidation of metal was studied by Wagner[100]. He assumed that transport of reactants implies an electrochemical mechanism where the current of anions, cations and electrons occurs under the double influence of chemical and electrical potentials. A thermodynamic equilibrium is established at a metal-gas interface. The current J_i of a particle i carrying a charge Z_i (anion, cation or electron) per unit of surface and per second is given by

$$\vec{J}_i = M_i \; C_i \frac{1}{N^2}\left[\frac{d\,\mu_i}{d\,\tilde{x}} + Z_i \; F \frac{d\,\phi}{d\,\tilde{x}}\right]$$

where M is the absolute mobility, C_i is the concentration, μ and ϕ are the chemical and electrical potentials, respectively. N is Avogadro's number and F is Faraday's constant.

Wagner maintained that when the simultaneous diffusion of anion and cation are controlling the oxidation rate, we get

$$\frac{dn}{dt'} \cdot \frac{1}{S} = \frac{1}{\delta\tilde{x}}\left[\frac{1}{|Z_2| F^2} \int_{\mu\tilde{x}}^{\mu''\tilde{x}} (t_1' + t_2')t_3' \, \tilde{x} \, d\mu\,\tilde{x}\right]$$

the first term is expressed as a number of equivalents formed per second per square centimetre, Z_2 is the charge of the anion; t'_1, t'_2, t'_3 are the transport numbers for cations, anions and electrons respectively; $\tilde{X}$ is the electrical conductivity, $\delta\tilde{x}$ is the thickness of the layer.

If t'_1, t'_2, t'_3, and X have the same value at each point in the layer, after integration we obtain

$$K_r = \frac{(t'_1 + t'_2)\, t_3}{F^2 |Z_2|} \tilde{\chi} \left[\ddot{\mu}\tilde{x} - \bar{\mu}\tilde{x}\right]$$

where $\dot{\mu}$ and $\ddot{\mu}$ are the chemical potentials of oxygen with oxide-metal interfaces and gas-oxide interface respectively. K_r is the parabolic rate constant. This equation is written in terms of chemical potential and an expression of the same type would be obtained if the diffusion coefficient was used instead of the chemical potential. Thus, the real value of Wagner's analysis lies in providing a complete understanding of the process of high temperature oxidation. For more information the reader should refer to references 101 to 102.

2.5 Stress in Thin Film

During the growth of an oxide film on a substrate, a problem of stress in the film may arise. In 1909 Stoney[103] reported about the existence of a large internal stress. Since then, studies in evaporated films to explain the origin of these stresses have been carried out.

There are two different types of stress, each one occurs under different conditions. Firstly, there is the intrinsic stress, which arises from the growth of the film - (a) epitaxial stress;

(b) defects stress; (c) volume difference stress; (d) recrystallisation stress, including other types. Secondly, there is thermal stress which arises during cooling because of the differences in thermal expansion of metal and film.

Stoney[103] was one of the early authors to measure internal stress in thin films. Hoffman[104] gave a general review and up-dated the experimental results, and the measurement techniques. He also presented models to explain the origin of the stress. Murbach and Wilman[105,106] studied the stress in deposited Ni, Cu, Al and other materials on copper strip in a high vacuum. They found that the degree of stress depends on the deposited material and they explain that stress is caused by thermal expansion coefficients. Buckel[107] investigated the stress in gallium, bismuth and other materials on aluminium and he attributed the stress to the crystal growth state. Hodgkinson and Walker[108] found that the SiO_2 films deposited by evaporation are in a compressive stress, but they were able to reduce the stress by irradiation by ultraviolet light. Reinhart and Logan[109] reported that the interface stress of $Al_x Ga_{1-x}$ As-Ga As, and explained that the existence of the stress was due to the difference in thermal expansion. They calculated the stress by using Nye's[87] method. Beleychera and Ziling[110] analyzed the stress in the two layer structures as a function of the geometrical dimension. They measured the stress along the coordinates and disc radius. Rossnagel et al.[111] used a simple technique to measure the stress in thin films. The technique required a laser, mirrors, and a diverging lens with simple geometric optics. Pulker[112] measured the stress in evaporated

silver, aluminium and chromium on glass substrate. Further studies have been presented for measuring the stress and studying the origin of this stress, e.g.[113–118].

2.5.1 Thermal Expansion

The curve in Fig. 2.6 shows that the potential energy against interatomic separation is not symmetric about the minimum at a distance ($\acute{X}$) at the absolute zero of temperature. But if there is a change in the temperature (T) when the atoms are not at rest, the volume of the solid is greater because the additional thermal energy causes an increase in vibrational amplitudes of the individual atoms, which will lead to an increase in the average separation between atoms. Therefore ($\acute{X}$) is increased by $\tilde{X}$ (as shown in Fig. 2.6). When the temperature $T \gg 0$, the relationship between the potential and $\acute{X}$ are linear, which gives rise to the constant volume of expansion coefficient[119].

Matching of thermal expansion coefficients of the film and substrate are very important to avoid thermal stress in the film. But if it is not possible to do so, the best way is to chose a film and substrate with a small difference between their thermal expansion coefficients, which will reduce a low stress[120].

2.5.1.1 Stress in Si-SiO_2 System

As described in the last section it is known that the existence of stress and strain is in a layer of material thermally grown on another material with differing thermal expansion. Jaccodine and Schlegel[121] investigated the strain in the interface of thermally grown SiO_2 on a single crystal silicon

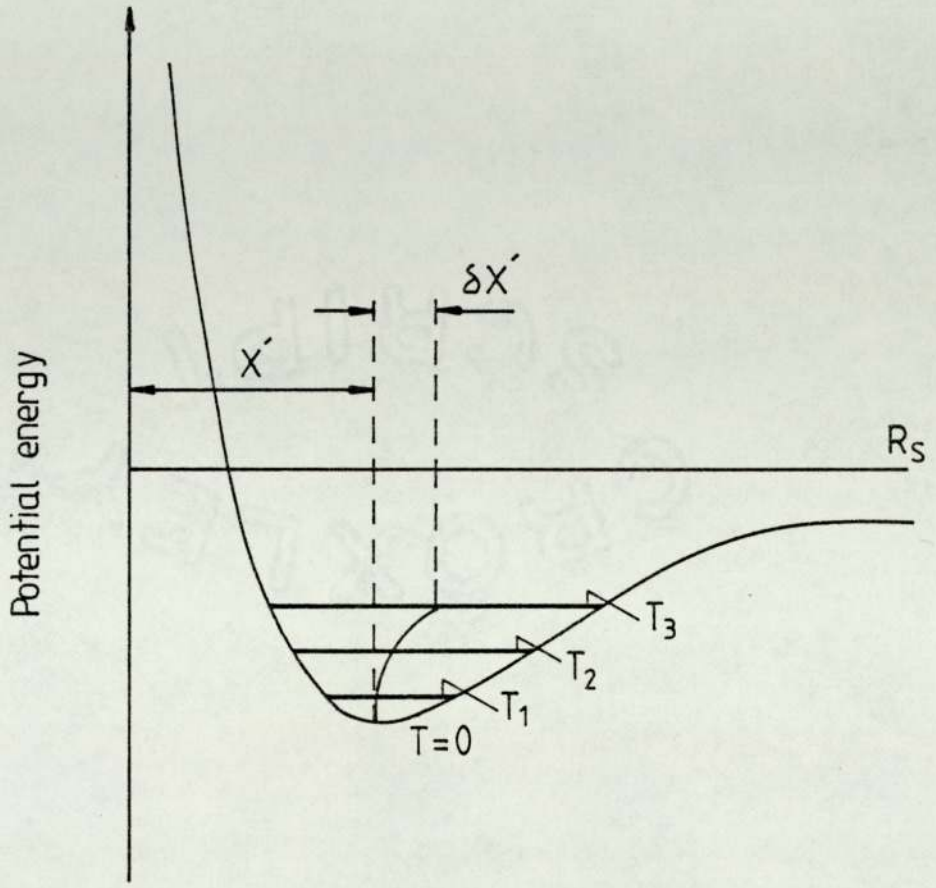

Figure 2·6 Variation of the potential energy of an ionic crystal lattice with ionic seperation R_S, at the absolute zero of temperature

substrate and they suggest the strain arises from the thermal mismatch of silicon and silicon oxide. No orientation dependence of stress was detected. Whelan et al.[122] studied the residual stress at the Si-SiO_2 interface and explained the existence of stress to the difference in thermal expansion between silicon and oxide. They show that the degree of stress depends firstly on the rate of cooling the sample after the oxidation process and secondly on the state of the oxygen (dry oxygen causes larger stress than wet oxygen). Lane[120] investigated the stress in Si-SiO_2 and used a vacancy model to explain the origin of the stress and he suggested that stress induced a surface state, which leads to a decrease in the surface density with increasing stress. Taft and Cordes[123] studied the interface layer between silicon and the silicon oxide and found a layer of 0.6 nm thickness having an index of 2.8 was needed to fit experimental data. The oxide index is not affected by the stress in a film less than 150 nm thick, but they suggest that the error in the index increases with the thickness. Aspnes and Theeten[124] investigated the effect of the interface layer on the optical properties and they suggested that the interface layer contained Si and O of average stoichiometry SiO and a refractive index of 3.2 ± 0.5 (for $\lambda =$ 546.1 nm) was needed to match experimental results. Pedinoff et al.[83] observed the strain-induced anisotropy in As_2S_3, As_2Se_3 and ZnSe films on KCl substrates and measured optical anisotropy by using a multiple angle ellipsometer. They presented a theoretical model for interpreting the results on strained films at a wide range of wavelengths. In 1982 Pedinoff and others presented for the first time an optical anisotropy in SiO_2 on Si

(thermally grown) by using the multiple angle ellipsometer. The anisotropy was reduced by annealing the sample at 925 °C (the oxidation temperature was 1100 °C) and the stress in each film was measured. They attributed optical anisotropy which arises from stress, to the thermal expansion difference between the Si and SiO_2.

There is a growing interest in the study of thermal stress, interface layer between the film and the substrate and optical anisotropy[125-144].

CHAPTER III

ESSENTIAL THEORY

3.1 Thin Film Optics

When polarized light is reflected from a metal surface covered with a thin film, the polarization state of the light is changed from that of a film free surface. This change in polarization state of the light depends on several parameters including the refractive index of the film and substrate and the thickness of the film. Even in the case of multiple films or optical anisotropy of the film, classical electromagnetic theory can be used to predict the change in the polarization state of the light upon reflection. The algebraic complexity of the problem increases for multiple layer or optical anisotropy of the film, and the use of high speed computers is essential for numerical evaluation of the relevant equations.

In principle, the amplitude and phase of a beam of light reflected or transmitted by a thin film, or combination of films may be determined by solving Maxwell's equations with the appropriate boundary conditions, which we will briefly outline in this study. Consider a plane electromagnetic wave incident on a smooth surface, Maxwell's equations are in the form of

$$\nabla . D = 0$$

$$\nabla . B = 0 \qquad 3.1$$

$$\nabla \times E = (-1/c)\ \partial B/\partial t$$

$$\nabla \times H = (-1/c)\ \partial D/\partial t + (4\pi/c)\ J$$

where we have assumed that there are free charges present. If the

media under consideration are assumed to be of uniform thickness, homogeneous, and isotropic, we have the constitutive relation

$$B = \mu H \qquad 3.2$$

$$D = \varepsilon E \qquad 3.3$$

$$J = \tilde{\sigma} E \qquad 3.4$$

where ε = relative permitivity = dielectric constant

$\tilde{\sigma}$ = electrical conductivity

μ = relative permeability

and E and H are electric field and magnetic field intensity all in cgs (Gaussian) system of unit. We will assume the material to be non-magnetic, i.e., $\mu = 1$. We will also assume that the monochromatic light is incident on the interface and consider the plane wave solution of the wave equation having the time dependence exp(iwt) and a spatial dependence exp(-in (w/c) s.r) where $(w/c = 2\pi/\lambda)$. Here s is a unit vector normal to planes of constant phase, and N, is the refractive index of the medium in which the wave is travelling. The problem of solving Maxwell's equation is considerably simplified by the use of Fresnel coefficients r and t, where r is the ratio of reflected to the incident amplitudes, and t is the ratio of transmitted amplitude to incident amplitude. Figure 3.1. illustrates schematically a situation in which a plane electromagnetic wave is incident from a medium of refractive index N_1, onto a medium of refractive index N_3 covered by a material of thickness d and refractive index N_2 . The incident and reflected waves are resolved into components parallel (p) and perpendicular (s) to the plane of incidence. For different boundaries between media the notation used here is adopted from that of Abelés[144] and used by Heavens[6,7]. A

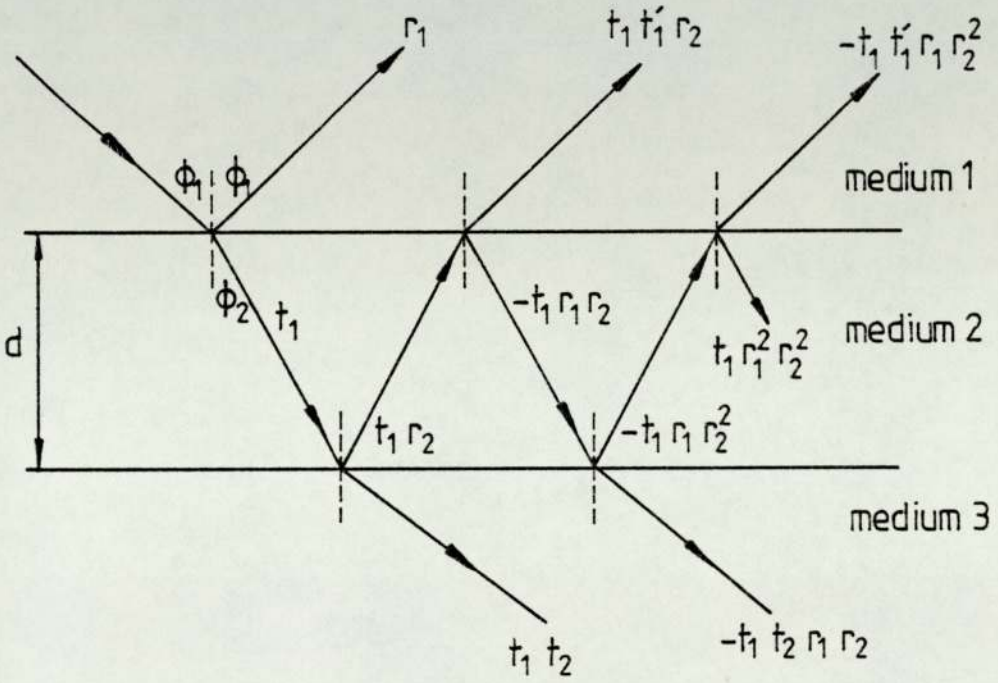

Figure 3·1 Multiple reflection and transmission of a light beam incident on a thin film.

subscript + or - indicates the direction of propagation with respect to the film (towards the film in the positive direction). The direction of the plane of polarization of any orientation is specified with respect to the plane of incidence. For an absorbing medium, the refractive index is a complex quantitiy N = n-ik, in which the imaginary part is related to the absorption of energy by the medium. For non-normal incidence, the angle of refraction becomes a complex quantity.

Let us consider Fresnel's equation for a single film, as shown in Fig. 3.1, which is assumed to be homogeneous and isotropic and to have parallel plane boundaries as indicated in the figure. This represents a parallel beam of plane polarized light of unit amplitude and wavelength λ falling on an absorbing film of thickness d and complex refractive index N_2, supported on an absorbing substrate of index N_3 . The complex amplitudes of the successive beams reflected and transmitted by the film are shown in Fig. 3.1, in which ξ_2 represents the amplitude and phase change in traversing the film once

$$\xi_2 = (2\pi/\lambda)\ N_2\, d_2 \cos\phi_2 \qquad 3.5$$

The reflected amplitude from the whole system is thus given by the infinite series:

$$r_{13} = r_{12} + t_{12}\, t'_{12}\, r_{23} \exp.\ (-2i\xi_2) - t_{12}\, t'_{12}\, r_{12}\, (r_{23})^2 \exp.\ (-4\, i\xi_2) + \ldots \qquad 3.6$$

which may be assumed to give:

$$r_{13} = r_{12} + \frac{t_{12}\, t'_{12}\, r_{23}\ \exp.\ (-2\, i\xi_2)}{1 + r_{12}\, r_{23}\ \exp.\ (-2\, i\xi_2)} \qquad 3.7$$

It follows from the conservation of energy, or from (Fresnel's

equation) that:

$$t_{12}\ t'_{12} = 1 - (r_{12})^2 \qquad 3.8$$

so that (eq.3.7) becomes, for the p-component

$$r^p_{13} = \frac{r^p_{13}\ r^p_{23}\ \exp.(-2\,i\xi_2)}{1 + r^p_{12}\ r^p_{23}\ \exp.(-2\,i\xi_2)} \qquad 3.9$$

and

$$r^p_{ij} = \frac{n_j \cos\Phi_i - n_i \cos\Phi_j}{n_j \cos\Phi_i + n_i \cos\Phi_j} \qquad 3.10$$

similarly, we have for the s-component

$$r^s_{13} = \frac{r^s_{12}\ r^s_{23}\ \exp.(-2i\xi_2)}{1 + r^s_{12}\ r^s_{23}\ \exp.(-2\,i\xi_2)} \qquad 3.11$$

with

$$r^s_{ij} = \frac{n_i \cos\Phi_i - n_j \cos\Phi_j}{n_i \cos\Phi_i + n_j \cos\Phi_j} \qquad 3.12$$

for waves travelling from medium 1 to medium 2 having an angle of incidence Φ_i and angle of refraction Φ_j. Similar expressions exist for the transmitted (p) and (s) components, these are known as Fresnel coefficients[146].

We can define $r_{13} = \rho \exp.(i\Delta)$ (from eq.3.9) where ρ is the amplitude ratio and Δ is the difference in phase of the reflected light compared to the incident light. Two identical expressions exist for the (p) and (s) components although the numerical values are different, because the Fresnel coefficients are themselves different. The ratio of amplitude changes for (p) and (s) components is given by

$$\frac{r_{13\,(p)}}{r_{13\,(s)}} = \frac{\rho_{(p)} \exp.(i\Delta_p)}{\rho_{(s)} \exp.(i\Delta_s)} = \frac{\rho_{(p)}}{\rho_{(s)}} \exp.\, i\,(\Delta_p - \Delta_s) \qquad 3.13$$

For convenience, this ratio is usually expressed in the form

$$\frac{r_{13\,(p)}}{r_{13\,(s)}} = \mathrm{Tan}\Psi \exp.(i\Delta) \qquad 3.14$$

$\mathrm{Tan}\psi$ is the relative amplitude reduction and Δ is the difference in phase change for the (p) and (s) components. The parameter Ψ and Δ are thus related, through the Fresnel coefficients, to the refractive index and the thickness of the film, and the angle of incidence. The derivation of n and k for the film from the measured values of ψ and Δ is extremely laborious, so that an electronic computer is very essential. For a clean opaque film surface, n and k are related to the instrument reading ψ and Δ through equations 3.15 and 3.16 are given in a form suitable for computation by Ditchburn[147].

$$n-k = \frac{\mathrm{Sin}^2\phi_1\,\mathrm{Tan}^2\phi_1\,(\mathrm{Cos}^2 2\psi - \mathrm{Sin}^2 2\psi\,\mathrm{Sin}^2\Delta)}{(1+\mathrm{Sin}2\psi\ \mathrm{Cos}\,\Delta)^2} + \mathrm{Sin}^2\phi_1 \qquad 3.15$$

$$2nk = \frac{\mathrm{Sin}^2\phi_1\,\mathrm{Tan}^2\phi_1\,\mathrm{Sin}4\psi\ \mathrm{Sin}\,\Delta}{(1+\mathrm{Sin}^2\psi\ \mathrm{Cos}\,\Delta)^2} \qquad 3.16$$

The extension of the calculation to several layers is possible since a single film, bounded by two surfaces, has an effective reflection coefficient and phase change. Such a film may be replaced by a single surface having the same properties as indicated in Fig. 3.1.

In this way, it is possible to start at the supporting substrate and work upwards through each layer to the surface as performed by Rovard[145] or to start at the surface and work downwards towards the substrate, as proposed by Vasicek[146]. For an oxidised surface, the angles Ψ and Δ are changed from the values for a clean surface. If the optical constants of the oxide free surface are known, then any subsequent changes of the instrument angles ψ and Δ can be used to determine the thickness of the oxide film formed.

The two basic programmes used in this work are given in appendices 2 and 3. In the first programme, the values of the optical constants n and k for a surface were computed for values of ψ and Δ at a given angle of incidence. These computed values n and k will be pseudo constants if a surface has a superimposed layer. If a layer is inadvertently present then the constants will not be for a clean surface.

The second programme was used to predict the thickness of the sample by matching the measured value of ψ and Δ with the computed value of ψ and Δ , for assumed constants of a superimposed layer on a substrate of known optical constants.

3.2. Theory of the Compensator Method of Ellipsometry

A simple method of optical phase shifting employs a thin parallel sided slab of birefringent material. If the optical axis lies parallel to the surface and when light falls on the slab at normal incidence as shown in Fig. 3.2 both ordinary (O) and extraordinary (E) rays will continue to propagate vertically in the same direction but with different velocities. The phase change produced by propagation will then be different for the two rays. The phase decrease in the distance d suffered by the O ray will be given by:

$$\Phi_o = \frac{2\pi d}{\lambda} n_o \qquad 3.17$$

and by E ray

$$\Phi_\varepsilon = \frac{2\pi d}{\lambda} n_e \qquad 3.18$$

The difference $\delta\Phi = \Phi_\varepsilon - \Phi_o = \frac{2\pi d}{\lambda} (n_E - n_o)$

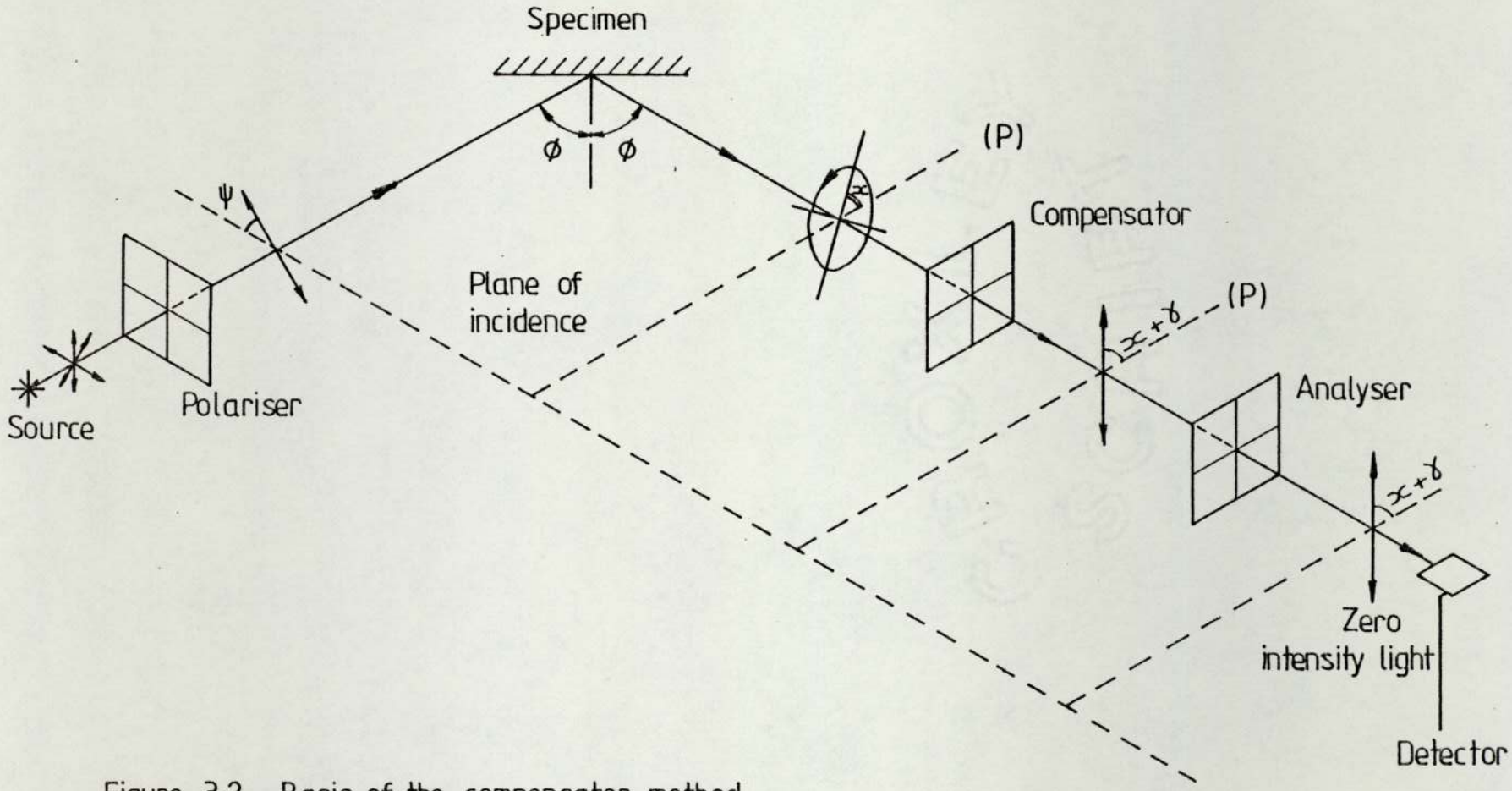

Figure 3·2 Basis of the compensator method of ellipsometry.

This phase shift device is often referred to as a compensator.

When the phase shift is $\delta\Phi = \frac{\pi}{2}$, a very useful device called a quarter wave plate is produced, that is when

$$(n_E - n_o)\, d = \lambda/4$$

The E ray is then advanced by a quarter of a cycle with respect to the O ray and, retardation occurs if $n_E > n_o$. The direction of the polarization that is advanced is along the fast axis, the retarded direction is the slow axis. The value of $\delta\Phi$ depends on λ, and this limits the practical wavelength range for precision work. When work is to be carried out with several wavelengths a phase-shifting device with variable thickness, called Babinent compensator is used.

A quarter wave plate (compensator) will convert plane-polarized light to elliptically polarized light or elliptically polarized to plane-polarized as in our case. The basis of the compensator method, as used in this work, is illustrated in Fig. 3.2. Plane-polarized light, produced by the polarizer p, is incident on the specimen with azimuth Ψ, i.e. its plane of polarization inclined at an angle Ψ to the plane of incidence. Conventionally, inclinations are considered positive if anti-clockwise from the plane of incidence, looking towards the oncoming light. On reflection from the sample the difference in amplitude reduction and the difference in phase change between the (p) and (s) component ensures that the reflected light is, in general, elliptically polarized i.e. the tip of the electric vector moves in an ellipse with azimuth of the major axis α, and ellipticity (ratio of minor to major axis) γ. This elliptically polarized light then passes through the compensator, which

consists of a birefringent sheet of mica. If the fast axis of the compensator is arranged to be parallel to the major axis of the reflected ellipse, the vibrations along the major and minor axis of the ellipse (for which a phase difference of 90 degrees exists) are again brought into phase, and plane polarized light results. The azimuth of this "compensated" plane polarized light will be at an angle γ to the major axis of the ellipse, as illustrated in Fig. 3.3.

Finally, the light passes through the analyzing polaroid A, which may be rotated until its transmission axis is perpendicular to the plane of polarization. In this condition and only in this condition, the light intensity received by the photomultiplier detector is zero. This is known as the null position.

The experimental procedure is considerably simplified if the compensator is first located with its fast axis at exactly 45 degrees to the plane of incidence. The polarizer and analyser are then adjusted for minimum light intensity received by the photomultiplier. The situation then corresponds to that shown in Fig.3.3. The azimuth of the reflected ellipse is always 45 degrees, or in other words, the amplitudes of the reflected (p) and (s) components are equal, i.e. E_p' and E_s' are equal.

The azimuth ψ of the polarizer is then equal to the parameter Ψ mentioned previously, in Figure 3.3.

$$\text{Tan } \psi = E_s^+ / E_p^+ \qquad 3.19$$

But
$$\text{Tan}\Psi = \frac{\rho_{(p)}}{\rho_{(s)}} = \frac{\left(\frac{E_p^-}{E_p^+}\right)}{\left(\frac{E_s^-}{E_s^+}\right)} = \frac{\left(\frac{E_p^-}{E_s^-}\right)}{\left(\frac{E_p^+}{E_s^+}\right)} \qquad 3.20$$

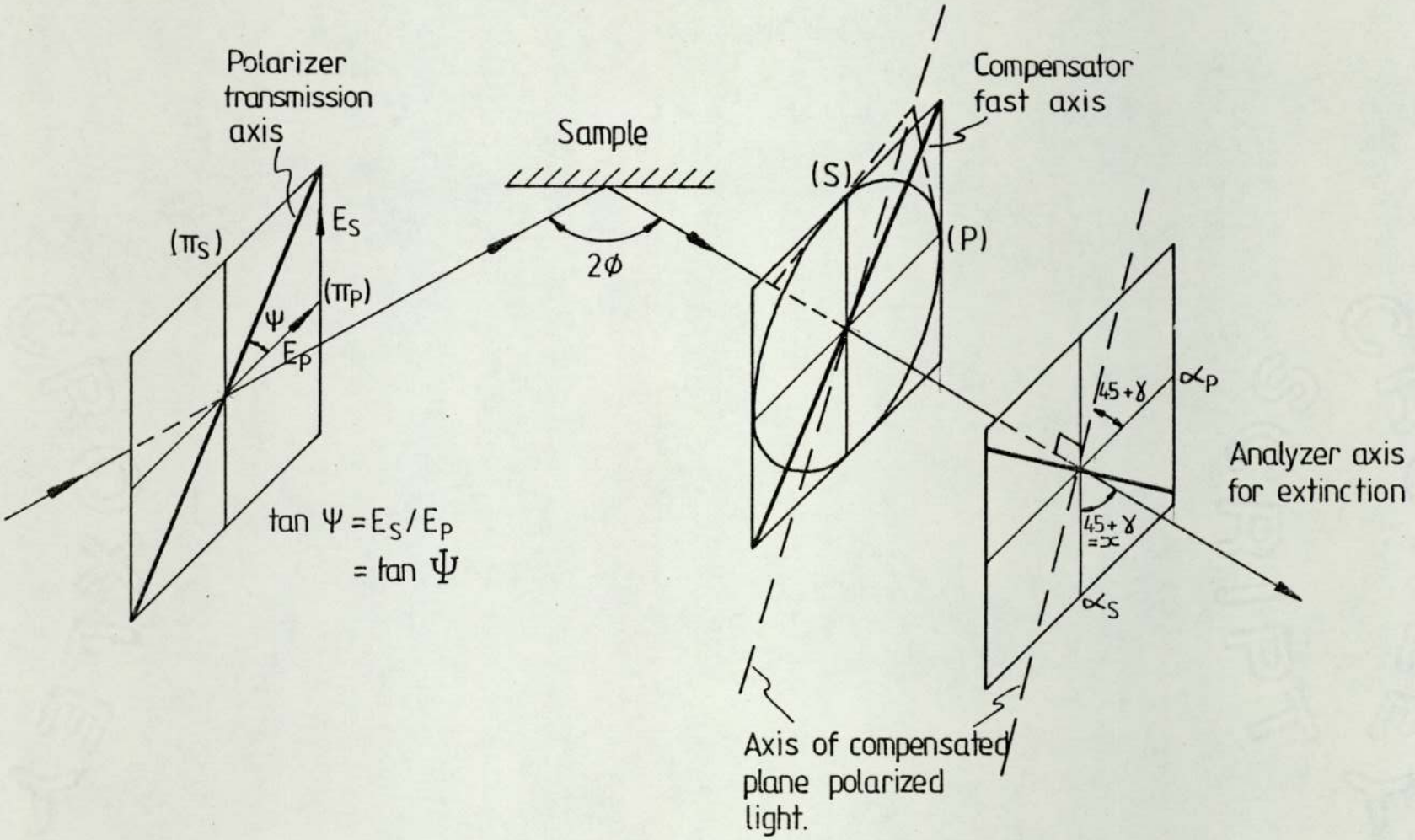

Figure 3·3 Experimental procedure for the compensator method.

since from above

$$E_p^-/E_s^- = 1.0 \qquad 3.21$$

then

$$\mathrm{Tan}\,\Psi = 1/(E_p^+/E_s^+) = E_s^+/E_p^+ \qquad 3.22$$

Hence, from (1)

$$\mathrm{Tan}\,\psi = \mathrm{Tan}\,\Psi \qquad 3.23$$

$$\psi = \Psi \qquad 3.24$$

The ellipticity ψ is related to the phase difference between the (p) and (s) component. In general, it may be shown that

$$\mathrm{Tan}\,\Delta = \frac{\mathrm{Tan}\,2\gamma}{\mathrm{Sin}\,2\alpha} \qquad 3.25$$

since, from above $\alpha = 45$, $\mathrm{Sin}\,2\alpha = 1.0$ and

$$\mathrm{Tan}\,\Delta = \mathrm{Tan}\,2\gamma \qquad 3.26$$

$$\Delta = 2\gamma \qquad 3.27$$

The ellipticity and hence the phase difference Δ is determined from the analyzer azimuth, as shown in Fig. 3.3. The azimuth of the compensated light is $45+\gamma$, so that the azimuth of the analyzer in the extinction position will be 45 with respect to α's , perpendicular to the plane of incidence. It is this quantity, marked α on Fig. 3.3 which is measured experimentally

$$\alpha = 45 + \gamma = 45 + (\Delta/2) \qquad 3.28$$

Then $$\Delta = 2\alpha - 90 \qquad 3.29$$

In general, pairs of polariser and analyzer azimuths for extinction occur which fall into four zones. McCrackin[28] gives a detailed explanation of the effect, although it should be noted that in his paper, the names 'polariser' and 'analyzer' are interchanged with those in this work, because his experimental arrangement has the compensator placed in the incident beam.

3.3. Surface Roughness

The optical refractive index for a material can be obtained from a clean isotropic smooth (homogeneous) and reflecting surface by using the ellipsometer. If one of these conditions does not apply the value of the refractive index will not be the exact value for that material. Therefore we have to have all these conditions to get the true result from the material.

If a surface has some degree of roughness the value of the refractive index and the thickness measurement of any superimposed layer will have an error i.e. if smooth conditions have been assumed. This error arises from the change in the ellipsometric parameters ψ and Δ which is observed during the study of the surface (in our case, the surfaces were polycrystalline aluminium). Because of the structure of the surface, light will be diffracted which means part of the scattered light will enter the acceptance angle of the photomultiplier which is set at a special angle (the angle of incidence) and the rest of the light will be scattered. The best treatment for such a rough surface is either chemical or electrochemical polishing.

The importance of this phenomena has led some authors to study it in order to try to either solve or minimize the effect on ellipsometric measurements. Maxwell Garnett[148,149] studied the effective dielectric constant of a composite material made up of dielectric constant in a medium. Chan and Morton[59,60] generalized the Maxwell Garnett theory. Fenstermaker and

McCrackin[56] investigated the error (effect) of the surface roughness on ellipsometric measurements. They assumed that the undulation of the roughness were small compared to the wavelength and they applied Maxwell Garnett's theory to study three theoretical models of the surface roughness: square ridges, triangular ridges and pyramids (as shown in Fig. 3.4) varying in height from 0 to 50 nm. Using the Maxwell Garnett theory, allowed them to assume that the equivalent polarizability of material of a rough surface is given by a simple volume average of polarizabilities of the substrate and air. The polarizability of a material of complex refractive index N = n-ik is given by $(N^2 - 1)/(N^2 + 2)$ and the polarizability of air is zero. therefore the effective refractive index N_e is given by

$$(N_e^2 - 1) / (N_e^2 + 2) = q\, r \qquad 3.30$$

solving for N_e

$$N_e^2 = (1 + 2\, r\, q)/(1 - r\, q) \qquad 3.31$$

where $r = (N_2^2 - 1)/(N_2^2 + 2)$

N_2 = refractive index of the substrate

$= n_2 - i\, k_2$

N = effective refractive index

$= n_e - i\, k_e$

q = The volume of fraction of the smooth substrate

$= 0 < q < 1$

They applied this method to six materials and changed the thickness of the roughness from 0 to 50 nm. All calculations of the effective refractive index and the degree of the surface roughness for the present work was calculated by a computer programme written by the author, and given in Appendix 4 and 5.

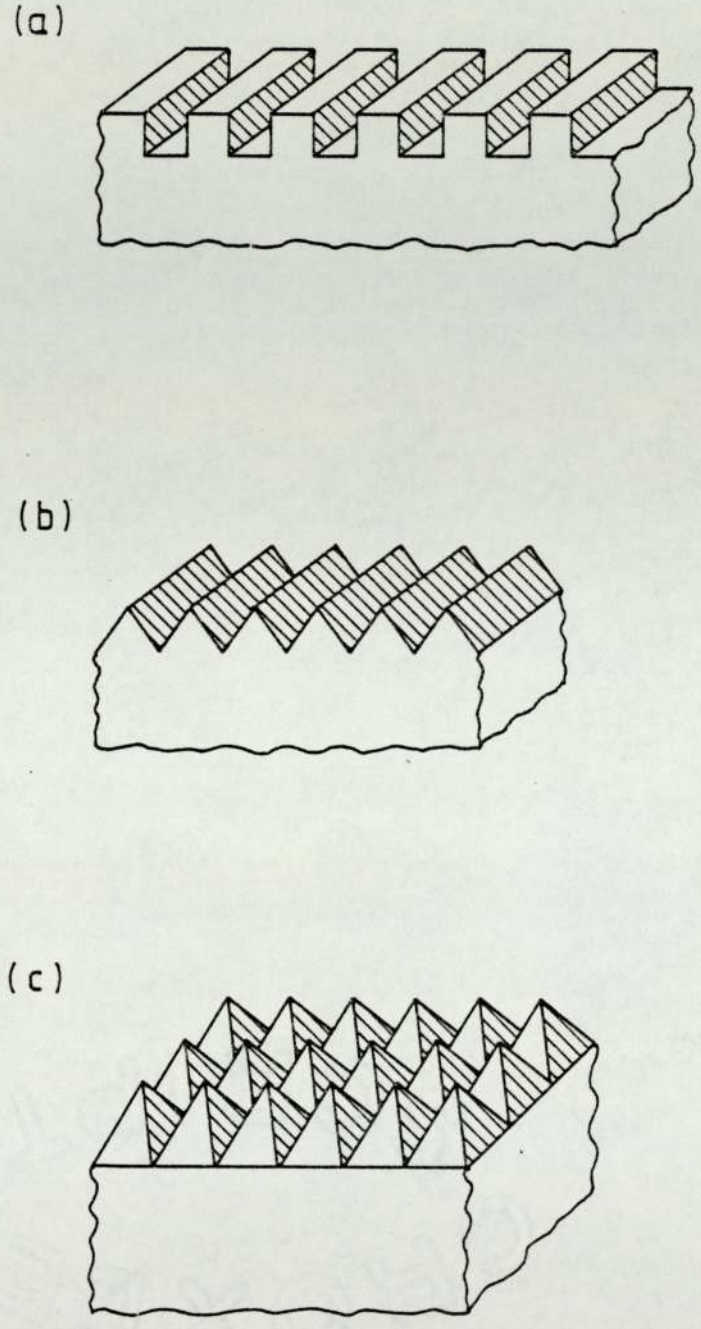

Figure 3·4 Three models of the surface roughness.
(a) square ridges
(b) triangular ridges
(c) pyramid ridges
[After Fenstermaker and McCrackin 56]

3.4. Optical Anisotropy (Photoelastic Effect)

Whenever a substance is subjected to stress it can change the refractive index and it is then optically anisotropic. The description of the change in the optical properties due to strain and stress is found by Nye[87,150-151]. The optical properties of any stress crystal can be explained by using tensors. There is a fourth order tensor that relates the relaxed crystal optical properties to the strain in such a way that the strained state will generally posess anisotropic optical properties even for cubic symmetry.

Nye describes the relation between the stress and the change in the optical constant. The dielectric impermeability tensor is defined to be $B_{ij} = k_o \partial E_i / \partial D_i$, where k_o the permitivity of vacuum, D dielectric and E electric field. Any small change of the refractive index will produce a change in the coefficience of B_{ij} . This change under the applied field and stress will be given as

$$\Delta B_{ij} = Z_{ijk} E_k + \pi_{ijkl} \sigma_{kl} \qquad 3.32$$

by neglecting the higher order terms. When Z_{jk} is the third-rank tensor this gives the electro-optical effect and the fourth-rank tensor gives a photoelastic effect. We will consider the fourth-rank because it gives the photoelastic effect that will make eq. 3.32 as follows:

$$\Delta B_{ij} = \pi_{ijkl} \sigma_{kl} \qquad 3.33$$

Because the stress is symmetric, it is possible to set

$$\pi_{ijkl} = \pi_{jikl}$$

and $\qquad 3.34$

$$\pi_{ijkl} = \pi_{ijlk}$$

equation 3.34 reduces the number of independent coefficients from 81 to 36, without loss of generality. Thus it is possible to change from the strict tensor notation to a matric notation by replacing symmetric pairs of subscripts according to the following scheme:

Matric notation		Tensor notation	
n = 1	if	ij = 11	
n = 2	if	ij = 22	
n = 3	if	ij = 33	3.35
n = 4	if	ij = 23 or 32	
n = 5	if	ij = 13 or 31	
n = 6	if	ij = 12 or 21	

In this notation the relation of the stress to the delectric impermeability is given by

$$\Delta B_i = \pi_{ij}\, \sigma_j \qquad 3.36$$

but it is to be emphasized that the quantities involved are matrices and not tensors specifically and do not obey the transormation law of tensors.

Take silicon as an example. Silicon is in the m3m symmetry group. Since the tensors describing a physical property of a crystal must have at least the symmetry of the crystal we can reduce the number of independent parameters from 36 to 3 for crystals of point group m3m. As an example of how the symmetry elements are reduced, consider the effect of operating on the π_{ijrs} tensor by rotating the coordinate axis (the (111) axis) by 120

degrees. This operation takes the X_1 into the X_2 axis, the X_2 into the X_3 , and the X_3 into the X_1. The matrix notation of this tensor will be to take subscript 1 into 2, 2 into 3, 3 into 1, 4 into 5, 5 into 6, and 6 into 4. Since the elastoptical matric must possess at least all the symmetry of the crystal, we have

$$
\begin{aligned}
\pi_{11} &= \pi_{22} = \pi_{33} \\
\pi_{12} &= \pi_{23} \quad , \quad \pi_{21} = \pi_{32} \\
\pi_{13} &= \pi_{21} \quad , \quad \pi_{23} = \pi_{31} \\
\pi_{14} &= \pi_{25} \quad , \quad \pi_{24} = \pi_{35} \\
\pi_{15} &= \pi_{26} \quad , \quad \pi_{25} = \pi_{36} \\
\pi_{16} &= \pi_{14} \quad , \quad \pi_{26} = \pi_{34}
\end{aligned}
\qquad 3.37
$$

etc. Continuing this way with other symmetry operations, the elastoptical matrix for symmetry class m3m is

$$
\pi_{ij} = \begin{bmatrix}
\pi_{11} & \pi_{12} & \pi_{12} & 0 & 0 & 0 \\
\pi_{12} & \pi_{11} & \pi_{12} & 0 & 0 & 0 \\
\pi_{12} & \pi_{12} & \pi_{11} & 0 & 0 & 0 \\
0 & 0 & 0 & \pi_{44} & 0 & 0 \\
0 & 0 & 0 & 0 & \pi_{44} & 0 \\
0 & 0 & 0 & 0 & 0 & \pi_{44}
\end{bmatrix} \qquad 3.38
$$

The zero result when a symmetry operation requires an element to equal its negative.

Now let us consider a crystal of m3m class (silicon class is m3m) and apply a parallel stress to the crystal axis. For a m3m crystal the principle axes are parallel to the edges and the

principle delectric impermeabilities are all equal, so the indicatrix is

$$B\,(X_1^2+X_2^2+X_3^2) = 1 \qquad 3.39$$

where X are the principle axes and $B_{ij}=B_o$. This is the equation of a sphere indicating that the optical properties are isotropic and the refractive index was given by $B_o = (1/n_o)^2$ and the matrix equation are given by

$$\Delta B_{ij} = \pi_{ij}\,\sigma_j \qquad 3.40$$

The change of the dielectric impermeability can be written as follows:

$$\begin{pmatrix} \Delta B_1 \\ \Delta B_2 \\ \Delta B_3 \\ \Delta B_4 \\ \Delta B_5 \\ \Delta B_6 \end{pmatrix} = \begin{pmatrix} \pi_{11} & \pi_{12} & \pi_{12} & 0 & 0 & 0 \\ \pi_{12} & \pi_{11} & \pi_{12} & 0 & 0 & 0 \\ \pi_{12} & \pi_{12} & \pi_{11} & 0 & 0 & 0 \\ 0 & 0 & 0 & \pi_{44} & 0 & 0 \\ 0 & 0 & 0 & 0 & \pi_{44} & 0 \\ 0 & 0 & 0 & 0 & 0 & \pi_{44} \end{pmatrix} = \begin{pmatrix} \pi_{11}\,\sigma \\ \pi_{12}\,\sigma \\ \pi_{12}\,\sigma \\ 0 \\ 0 \\ 0 \end{pmatrix} \qquad 3.41$$

Since the values of $B_4 = B_5 = B_6 = 0$, there are no off-diagonal terms of the dielectric impermeability tensor and there is no change in the direction of the principal axes of the dielectric tensor. The refractive index changes can be obtained by writing $B_1 = 1/n_1^2$. Therefore $\Delta B_1 = -(2/n_1^3)\Delta n_1$. For simplicity let us replace n_1 by n_o and obtain

$$\Delta n_1 = -1/2\,(n_o)^3\,\Delta B_1$$

$$= -1/2\,(n_o)^3\,\pi_{11}\,\sigma \qquad 3.42$$

$$\Delta n_2 = -1/2\,(n_o)^3\,\pi_{12}\,\sigma \qquad 3.43$$

$$\Delta n = \Delta n_1 - \Delta n_2$$

$$= -1/2 \, (n_0)^3 \, (\pi_{11} - \pi_{12}) \, \sigma \qquad 3.44$$

$$\Delta n = u \sigma$$

where $u = -1/2 \, (n_0)^3 \, (\pi_{11} - \pi_{12})$

$$\therefore \quad \sigma = 1/u \, \Delta n \qquad 3.45$$

This will be referred to later in the discussion in Section 6.3.

CHAPTER IV

EXPERIMENTAL EQUIPMENT AND PROCEDURE

4.1 Experimental Equipment (Basic Instruments)

The components of a basic instrument for ellipsometric measurement comprise a light source with a known wavelength, a suitable quarter wave plate, two polaroids (polarizer and analyzer), a detector and sample holder and arranged as shown in Fig. 4.1.

The light source used in this investigation was a He-Ne laser with a wavelength of 632.8 nm supplied by the Nippon Electronic Company Limited (N.E.C.). The sample holder was rotatable about the normal to the sample. The angle of the rotation which could be varied in the range between 0 to 360, was measured by a divided circle capable of reading to ±1.0. To avoid systematic errors during the rotation of the sample in a particular run, the sample was rotated about an axis perpendicular to the sample surface until a complete rotation of 360 degrees was accomplished. This facilitated the studying of any anisotropy in the sample surface. The angle of incidence was normally set at 60 degrees but the facility exists to change it from 45 - 85 degrees by adjusting the reflection arm position for determin roughness effect.

The detector used was a photomultiplier type 5-20 (9658B) supplied by EMI Electron Ltd., covering the range of 370 nm - 880 nm with a spectral response as shown in Fig. 4.2. The high voltage supply for the tube was a stabilised power supply type 530/D from Isotope Development Ltd. The connections for the

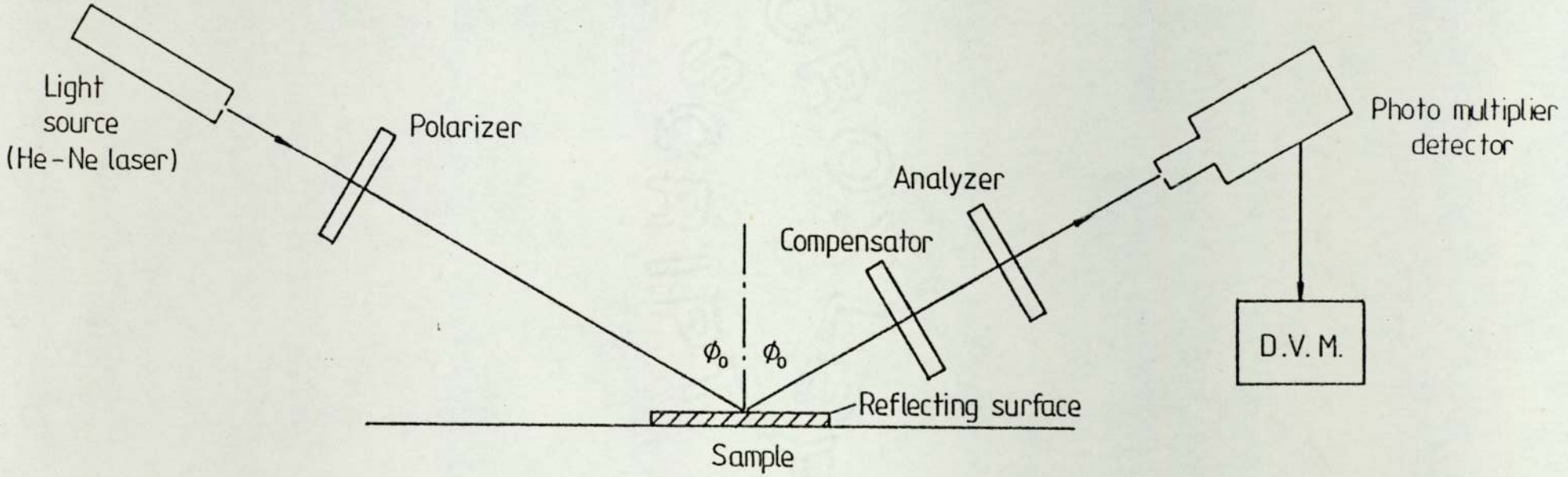

Figure 4.1 Components of the basic instrument.

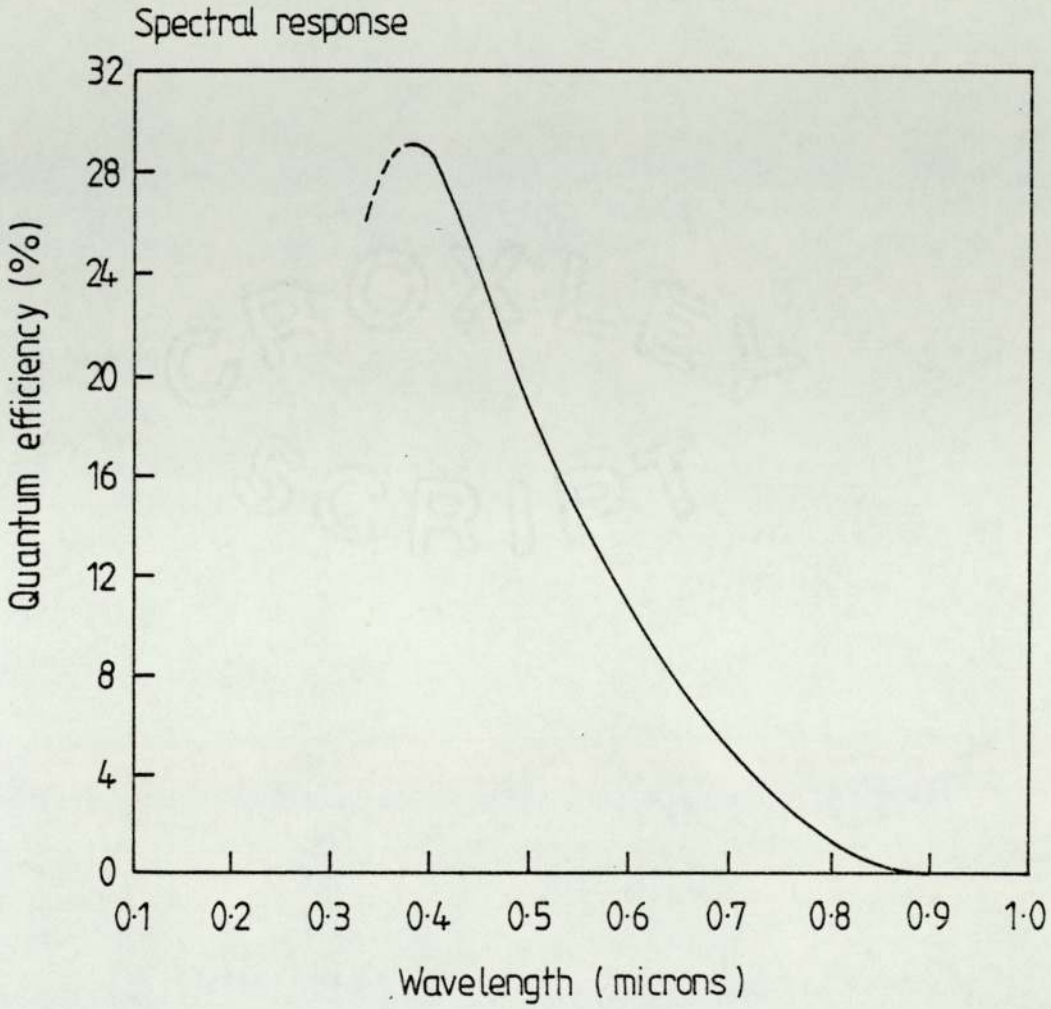

Figure 4·2 Spectral response for the photomultiplier.

dynode chain with an operational amplifier are shown in Fig. 4.3 a, b.

4.2 Single Wavelength Ellipsometer (632.8 nm)

A single wavelength ellipsometer which is called in some cases the compensator method of ellipsometry, is based on the theory of Winterbottom which has been described in Section 3.2. The two polaroid heads were interchangeable as a polarizer or an analyzer. Each polaroid carried a calcite Glan Thomson prism with a divided circle to determine the degree of polarization. A single index line actuated by a micrometer screw divided drum was incorporated into the head, enabling the 1/4 degree division on the scale of the divided circle to be subdivided directly to 0.01 degrees. It also carried scale readings with telescopes to provide readings at 180 degrees apart.

The phase compensator (Quarter-wave plate) can be constructed of a disc of birefringent material such as mica sheet (substance) which has a different refractive index for ordinary and extraordinary rays of n_o and n_e respectively. The phase difference between these two rays after passing through the plate will be given by $\zeta = \frac{2\pi d}{\lambda}(n_e - n_o)$ where d is the thickness of the plate. Therefore, in practice the compensator is cut so as to introduce a phase difference of odd multiples of $\lambda/4$. That is why it is so often referred to as a quarter-wave plate. The quarter-wave plate used was supplied by Ealing Beck Ltd. and produces a retardation of an odd multiple of $\frac{\pi}{2}$ for the wavelength used. The disc is mounted in a graduated circle reading to 0.01 degrees.

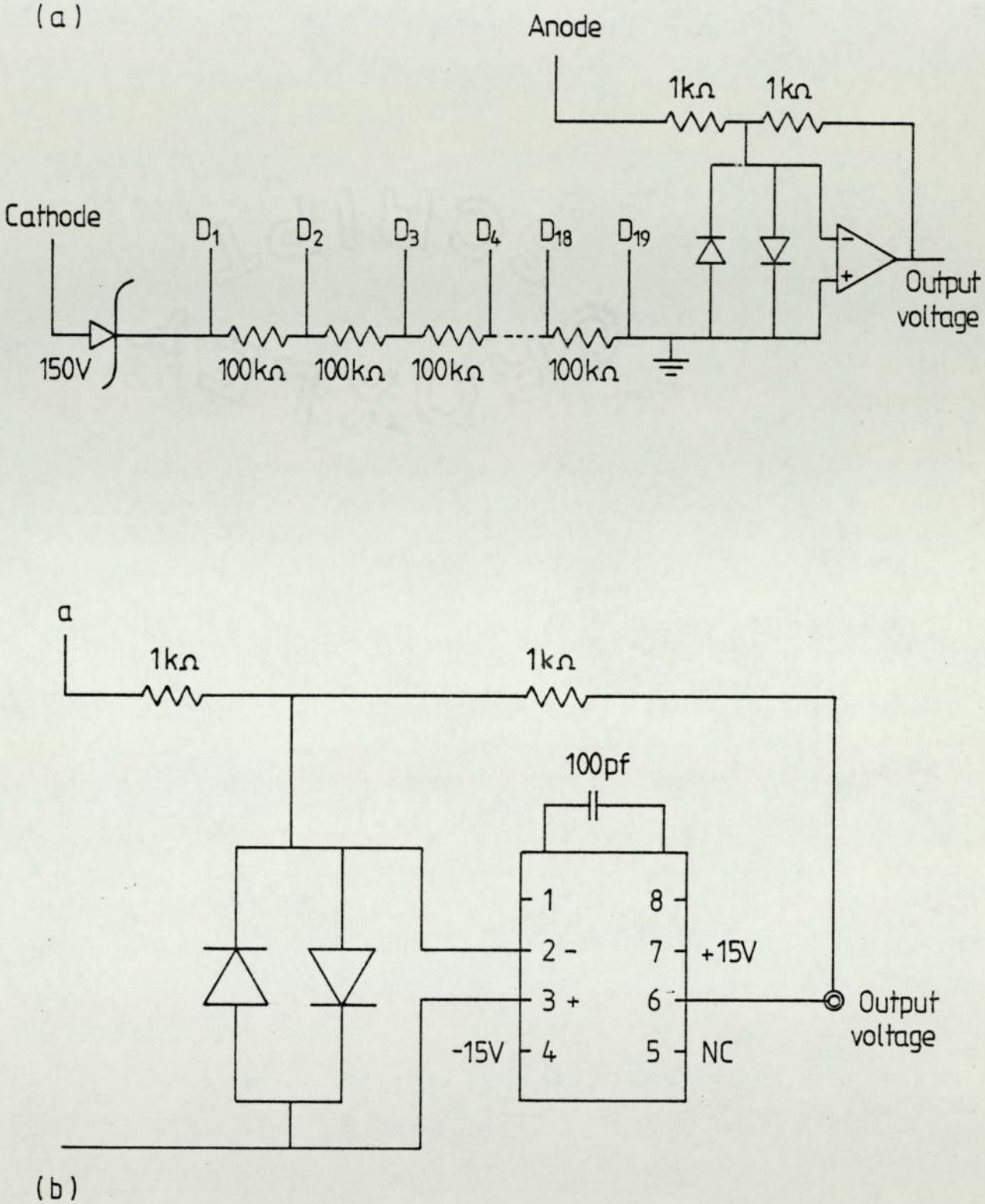

Figure 4·3 Diagram of the dynode chain circuit for the photomultiplier.

4.3 Experimental Procedure

4.3.1 Alignment of the Ellipsometer

(a) Establishing the horizontal plane

The correct alignment of the ellipsometer is a very important part of the measurement technique to achieve high instrument sensitivity. The first step of the alignment is to remove all the optical components from the bench, and replace them by six plates each with a central pin hole (all at the same height above the bench). The optical benches and the table supporting the samples are first set horizontal by a spirit level. The levels of the pin holes, the laser and a reflecting surface (gold or aluminium) are adjusted until the beam passes through all the pin holes, to confirm that both the incident and reflected beams are in a horizontal plane. Five plates with holes are then taken away, and when the last plate is moved along the incidence arm, the light should always pass through the pin hole in it. This is repeated in the reflecting arm, and the same result must be obtained. The bench is now ready for the placing of the components.

(b) Checks on the analylyzer and polarizer and achievement of minima

The alignment of the ellipsometer is accomplished essentially by the method described by McCrackin[28]. The alignment was achieved when the analyser and the polariser were placed in their positions and their heights adjusted until the beam passed through the centres of the prisms. Then both prisms were rotated to give minimum transmission intensity readings in the photomultiplier. There are four positions for this condition and the scale readings

differ in setting by 90 degrees, which means that the prisms are aligned. The azimuth reference can be obtained for the analyzer and the polarizer as described in the next section.

4.3.2 Determination of Azimuth Reference for the Instrument

For this exercise the compensator plate is not present. The readings on the divided circles of the polarizer and analyzer correspond to the transmission axis of the polaroids being parallel and perpendicular to the plane of incidence, known as the reference azimuth.

After aligning and setting the ellipsometer, the azimuth references can be determined i.e. readings on polarizer and analyzer which give light with electric vectors parallel and perpendicular to the plane of incidence. Approximate values are quickly obtained by removing the analyzer or the polarizer in turn from the ellipsometer and rotating the polaroid until the minimum intensity of the light is achieved (at an angle of incidence of 56 degrees) when the light is reflected from a glass block as shown in Fig. 4.4 (i.e. Brewster angle). The transmission axis is then perpendicular to the plane of incidence. On returning the polaroids to the ellipsometer on which the plane of incidence is approximately horizontal, the transmission axis are therefore set roughly perpendicular to the plane of incidence.

The approximate azimuths for the polarizer and analyzer were determined by adjusting for minimum intensity of light which has been reflected from a metal surface (aluminium or gold). With the compensator removed, the only direction for no light intensity with crossed polarizer and analyzer, will be parallel

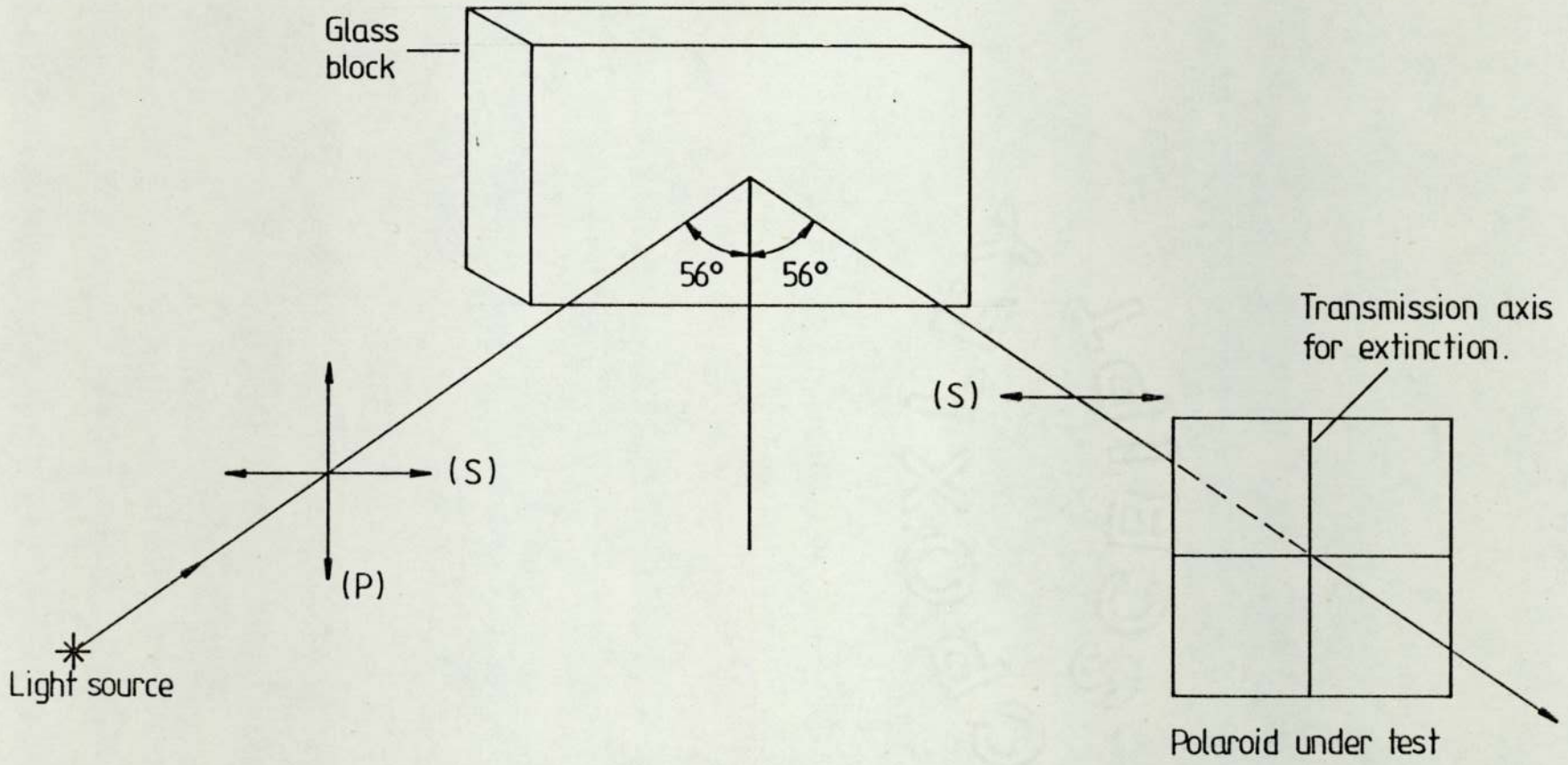

Figure 4·4 Determination of reference azimuths (approximate).

and perpendicular to the plane of incidence. The exact azimuth setting for the polarizer was determined by measuring polarizer angles P_1 and P_2 at equal intensity on each side of the minimum and the exact minimum $P_o(\pi_s)$ is the average of these two values. The method of determining the minimum is known as the bracketing method. The analyzer was then set at $A_o(\alpha_p)$ (exact minimum) obtained by the same method as that of the polarizer setting, giving equal intensity each side of the minimum. The method of setting the polarizer and the analyzer position P_o , A_o (the minimum values) is by taking the values of equal intensities on each side of the minimum by 5 to 10 degrees which are sufficient to attain the accuracy needed for the reference positions. Both polarizer and analyzer were then rotated by 90 degrees and the entire procedure repeated. These alternative positions correspond to the azimuths and there are non-significant positions at 180 degrees to each of the scale readings and these are represented by a dash (π', α').

To obtain the reference position for the compensator, the polarizer and the analyzer were set to a position (azimuth reference) to give a minimum and the compensator was placed in position as shown in Fig. 4.1. To obtain the exact azimuth for the compensator the same method of bracketing was used by measuring the intensity of both sides of the minimum required to get accurate results. This position corresponds to either the fast or slow axis of the compensator being parallel to the plane of incidence, because it is only when the light incident on the compensator is plane-polarized in a direction parallel to either the fast or slow axis that plane-polarized light emerges through

the compensator, enabling the analyzer to produce extinction. Thus for the given wavelength a phase difference of 90 degrees was introduced between light with electric vectors parallel and perpendicular with the plane of incidence. The procedure was repeated to get the rest of the compensator reference positions at the alternative positions which differ by 90 degrees from one to another, as shown in Table 4.1. We set the compensator to +45 or -45 degrees from a reference position (in order to satisfy equation 3.23) for determining Ψ and Δ. For example if we took 89.70 degree (compensator reference position), the two compensator positions of $\pm$45 degrees of the reference are 44.7 and 134.7 degrees. More explanation will be given in the next section.

4.3.3 Determination of Ψ and Δ for a Surface

The ellipsometer has recently gained much attention for the study of a surface and or any film growth on the surface, Section 2.1. It will be shown below, that by measuring the ellipsometer parameters Ψ and Δ and by running certain computer programs, the growth of an oxide layer can be accurately followed and its thickness and refractive index determined.

For any given sample there are a possible 32 polarizer, analyzer and compensator settings that produce the values of Ψ and Δ. The azimuth of the plane polarized light incident on the sample is arranged so that the reflected light has equal components in (p) and (s) directions (parallel and perpendicular to the plane of incidence respectively) which means that the reflected amplitude ratio $E_p^-/E_s^- = 1.0$. Because of the phase difference, Δ between these components, the reflected light will

Table 4.1

The values of the reference azimuth positions for the polarizer, analyzer and the compensator.

Polarizer Azimuth Position	Analyzer Azimuth Position	Compensator Azimuth Position
π_p = 138.50	α_s = 130.32	89.70
$\pi_{p'}$ = 318.49	$\alpha_{s'}$ = 310.25	179.69
π_s = 48.70	α_p = 40.40	269.80
$\pi_{s'}$ = 228.71	α_p = 220.40	359.71

in general be elliptically polarized with its major axis at 45 degrees to the plane of the incidence, and have an ellipticity that depends on Δ. If the compensator is set with its axis at 45 degrees to the reference positions, this ensures that the axes of the compensator coincide with the axes of the reflected ellipse (see Section 3.2). This will compensate any light with ellipticity, which means that the reflected light will be plane polarised after it passes through the compensator having an azimuth that depends on the ellipticity, and hence on Δ. This is shown in Fig. 3.3.

The compensator was set with its axis at +45 degrees to the reference position. Then, the minimum light intensity was found by rotating the analyser and the polarizer. The minimum position for the polarizer P was then found more precisely by the bracketing method. The polarizer was set at this position P, and the analyzer position A was also found by the bracketing method. The values of P_2 and A_2 for the polarizer and the analyzer respectively were found by the same method.

The values of A_1 and A_2 and P_1 and P_2 differ by 90 degrees. By using the same procedure the remainder of the polarizer positions P_3 and P_4 and the analyzer positions A_3 and A_4 were measured. It was found as expected that A_1 and A_2 were at 180 degrees to A_3 and A_4 respectively. The same difference was found in the polarizer reading between P_1 and P_2 and to P_3 and P_4 respectively.

The compensator was then set up at the fast axis azimuth -45 degrees, with respect to the plane of incidence which is 90 degrees from the first setting. The same procedure was repeated

to obtain the four different positions for each of A and P. Now we have found eight analyser and polariser positions at one reference position for the compensator, that means that there are thirty-two positions for the analyser and the polariser for all four reference positions for the compensator.

The values of A and P are not the values of ψ and Δ which we were looking for. These values are calculated as mentioned in Section 3.2. In the case of the analyser, it was found that A_1 and A_2 are symetrically placed at 90 degrees apart $\alpha_s - A_1$, should equal $\alpha_p - A_2$. In general the average is taken

$$\chi = \frac{(\alpha_s - A_1) + (\alpha_p - A_2)}{2}$$

where the angle $2\chi - 90 = \Delta$ and known as the relative phase retardation between the (p) and (s) components.

In the case of the reading of the polariser it was found that P_1 and P_2 were symetrically placed about π_p. In general, the polariser settings were symetrically placed about the plane of incidence i.e. $P_1 - \pi_p$ should equal $\pi_p - P_2$. The value of ψ is the average of both readings.

$$\psi = \frac{(P_1 - \pi_p) + (\pi_p - P_2)}{2}$$

4.3.4 Determination of Angle of Incidence

The angle of incidence was determined after each alignment of the ellipsometer by removing the optical components from the bench, and replacing them by four pencil like aluminium pins and a small telescope as shown in Fig. 4.5. The pins were adjusted so that their points all appeared to be in line A′ B′ C D with the

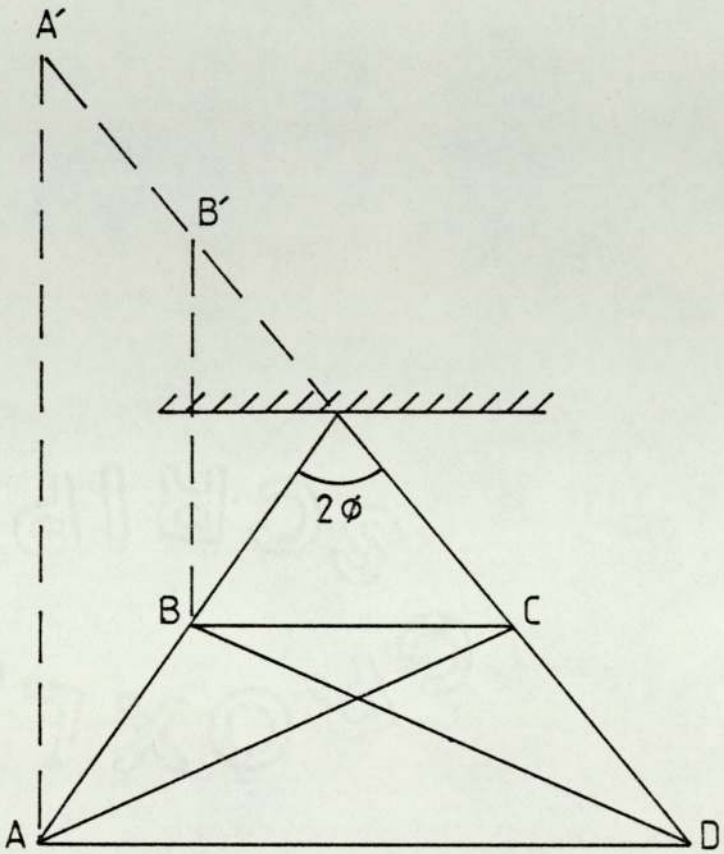

Figure 4·5 Determination of the angle of the incidence.

illuminated pins as seen through the telescope.

The distance between the points were measured and the angle of incidence, ϕ_o, calculated by simple trigonometry to within 0.05 degrees.

4.3.5 Determination of Optical Anisotropy

The ellipsometric parameters ψ and Δ for an ideal surface which is perfectly smooth, reflecting, isotropic and homogeneous under the same environment conditions will stay unchanged when the surface rotates about an axis normal to its surface. But if these parameters change on rotation, the surface is not isotropic. The equation (3.14) is then strictly not applicable. This phenomena found by Cathcart[1] is discussed in Section 2.3.

The samples in this investigation were mounted on a rotatable sample holder to determine the presence of any anisotropy. The anisotropy was studied by rotating the sample about an axis normal to its surface. This rotation could be determined to ± 1 degree. The measurement was taken in 10 degree steps which gave 36 sets of readings for each sample to identify the change in ψ and Δ with rotation. A change in ψ and Δ values were observed for oxides on polycrystalline and single crystal aluminium and thermally grown silicon oxide by using this method.

4.3.6 Preparation of Samples

All the ellipsometric measurements were performed on samples at room temperature. The aluminium and silicon materials which were used in this investigation were of high purity (99.999%). The samples included single crystals of silicon with orientations

of (111) and (100) and single crystals of aluminium of (110), (311) and (111) orientations. The orientations have been confirmed by X-ray differaction. Prior to testing the growth of oxide, hydroxide or contamination layers on a surface, it is necessary to characterise a clean reflecting surface. In most cases this necessitates the production of a surface with reproducible properties. The sample cleaning technique before forming a film is a very important stage of the study. In the case of aluminium all samples were first immersed in a 5% detergent solution in an ultrasonic bath. This was followed by repeated cleaning in distilled water in an ultrasonic bath. Finally the substrates were boiled in isopropyl alcohol and dried by drawing through the vapour. Aluminium samples were subjected to two polishing processes.

4.3.6.1 Diamond Polishing for Aluminium Surfaces

All the samples used for ellipsometric study require a specular reflecting surface. Some aluminium samples (single crystal and polycrystalline) were first mechanically polished using silicon carbide paper in grades 400, 600, 800 and 1200. Then the samples were viewed optically for any roughness from silicon carbide paper. Because the aluminium samples have a very high purity they are very soft and polishing material could be transferred to the surface very easily. To overcome this problem a further finer grade of polishing was needed (using 6μ then 1μ diamond paste) to remove the roughness from the surface. We then re-examined the sample optically to test that there was no more visible debris. The sample was then X-rayed to verify that

orientation of the crystal plane (for single crystal samples) was correct.

4.3.6.2 Electropolishing for Aluminium Samples

After the samples have been diamond polished they needed to be electropolished to give them a highly reflecting surface. The electropolishing solution for pure aluminium was 80% ethanol and 20% percloric acid[154]. The solution preparation condition is very critical and because this is an exothermic reaction, it was necessary to remove the heat generated. This was done by using liquid nitrogen as a bath for the mixing container and the mixture temperature was kept in the region of -35°C.

The three main parameters involved in the process of polishing are: voltage, current and temperature (see Appendix 6). In order to obtain the best conditions for good electropolishing, one of the parameters had to be fixed. In this case the temperature was kept constant at -10 degrees (by surrounding the solution container with 20% methanol and 80% water and liquid nitrogen. The electropolishing equipment, Fig. 4.7, consists of a beaker of electropolishing solution, the cathode which is formed from aluminium foil .25 mm thick and the anode which was the sample holder. Magnetic stirring was used to obtain uniform polishing. Both the cathode and the anode were connected to a power supply (Weir 762.1 model).

The simple relation between the anode potential against anode current density is shown in Fig. 4.7. This relation between the voltage and the current density is the main factor in the

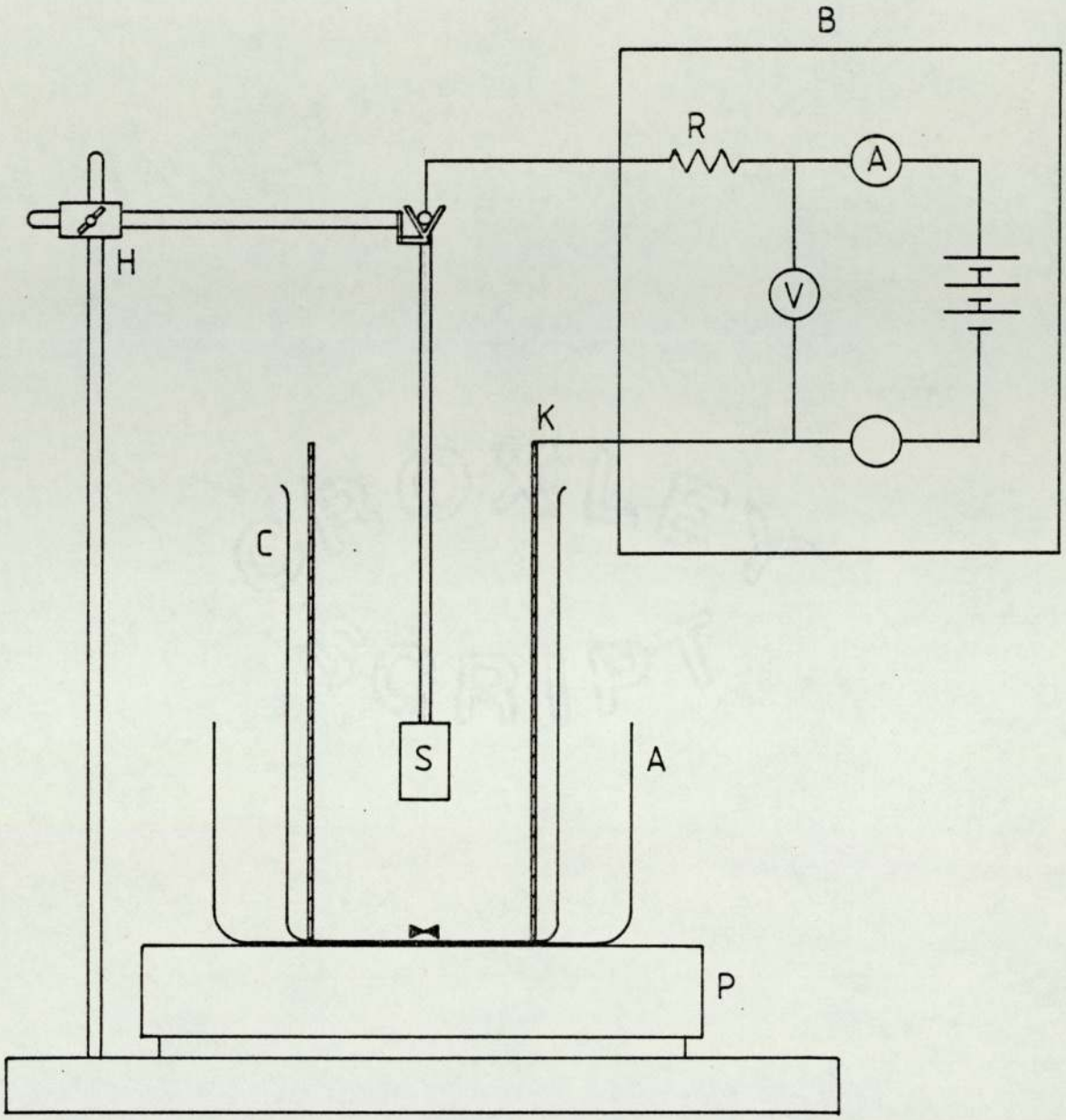

Figure 4·6 Electropolishing equipment.
H - Holder, S - Sample , K - Cathode,
C - Cell (beaker), A - Container,
P - Magnetic stirrer, B - Power supply

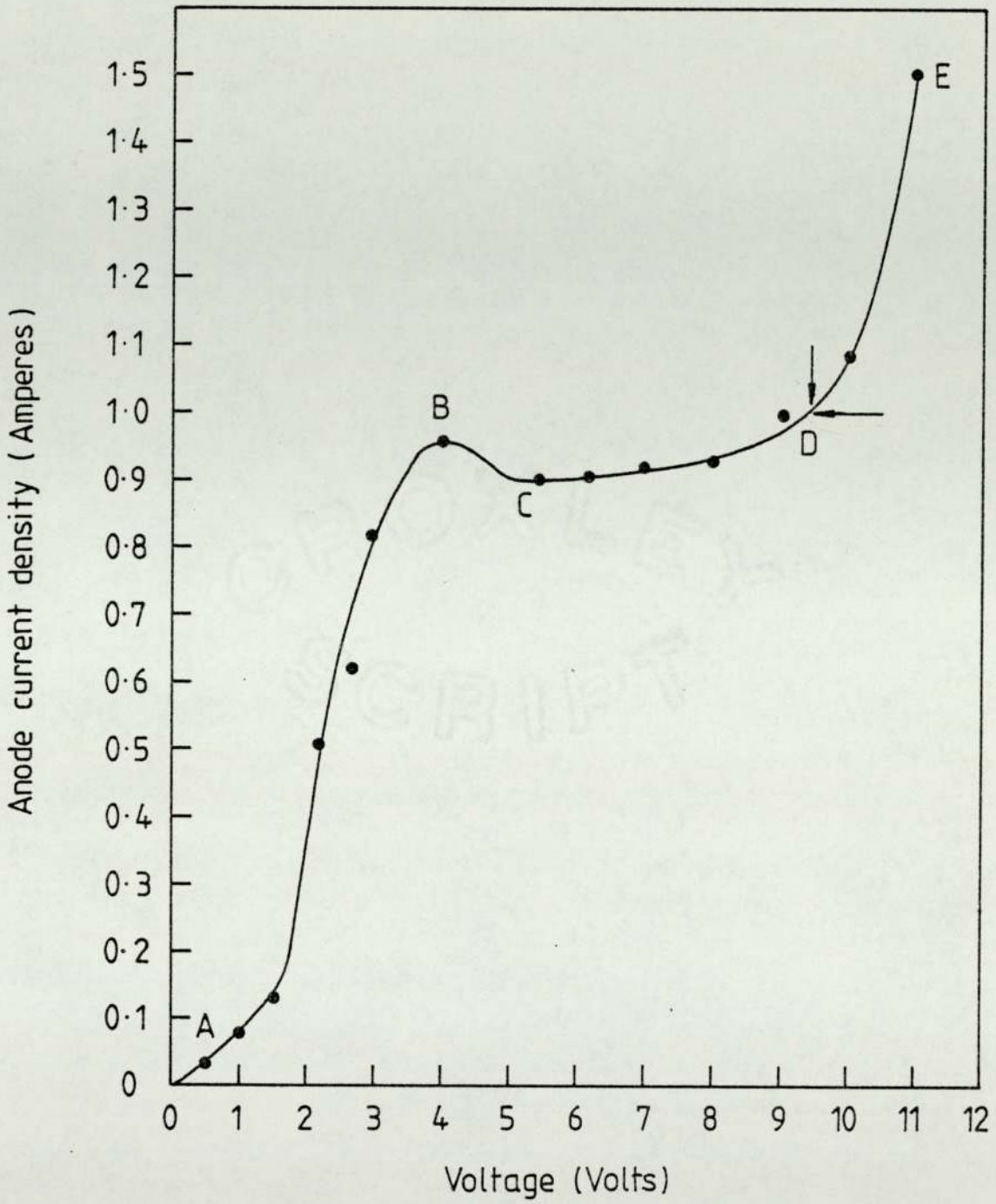

Figure 4·7 The electropolishing relationship between the cell voltage and the anode current density.

electropolishing because it explains the polishing mechanism[152-156]. The curve is divided into four regions: (i) Region A-B where the increase in the current is approximately proportional to the increase in the potential, and is often referred to as the "etching region", because at low voltage a film forms on the surface and a little or no current passes; thus, etching occurs with no polishing. (ii) The region B-C reflects an unstable polishing region. (iii) The region C-D indicates a stable plateau at which the polishing occurs, where the current density changes only slightly with the voltage. The optimum polishing condition occurs near D. (iv) In the region D-E the current rises sharply with a small increase in the voltage, which causes severe pitting. From the figure it can be seen that the current and the voltage which have been used in this experiment were about 0.95 amperℓ and about 9.5 volts repectively, which lie in the optimum region at (D).

4.3.6.3 Thermally Grown Silicon Dioxide Films

The silicon dioxide films were grown thermally in an oxygen atmosphere in a furnace supplied by Corbolit Furnace Ltd. The furnace was also used for the annealing process in a nitrogen atmosphere. The interior diameter of the tube was 25 mm. The eurotherm furnace temperature control was accurate to ±2°C at the centre. The silicon oxide was grown at a temperature of 1100°C and annealed at 950°C.

The procedure adopted for the growth of the oxide film was as follows: the furnace was preheated at 1100°C in a nitrogen atmosphere, the sample was inserted into the furnace against the

gas flow to avoid any oxidation or contamination from the air. Next the nitrogen was replaced by oxygen, in the furnace. The sample was left in the furnace until the required film thickness was obtained. A calibration curve of the oxidation growth is shown in Fig. 4.8.

The sample was cooled down in a nitrogen atmosphere at the rate of 20°C/min approximately and by moving the sample inwards in the direction of the gas flow, so as to minimize the stress[85] and the strain in the oxide surface film. Any annealing of the samples was also performed in a nitrogen atmosphere.

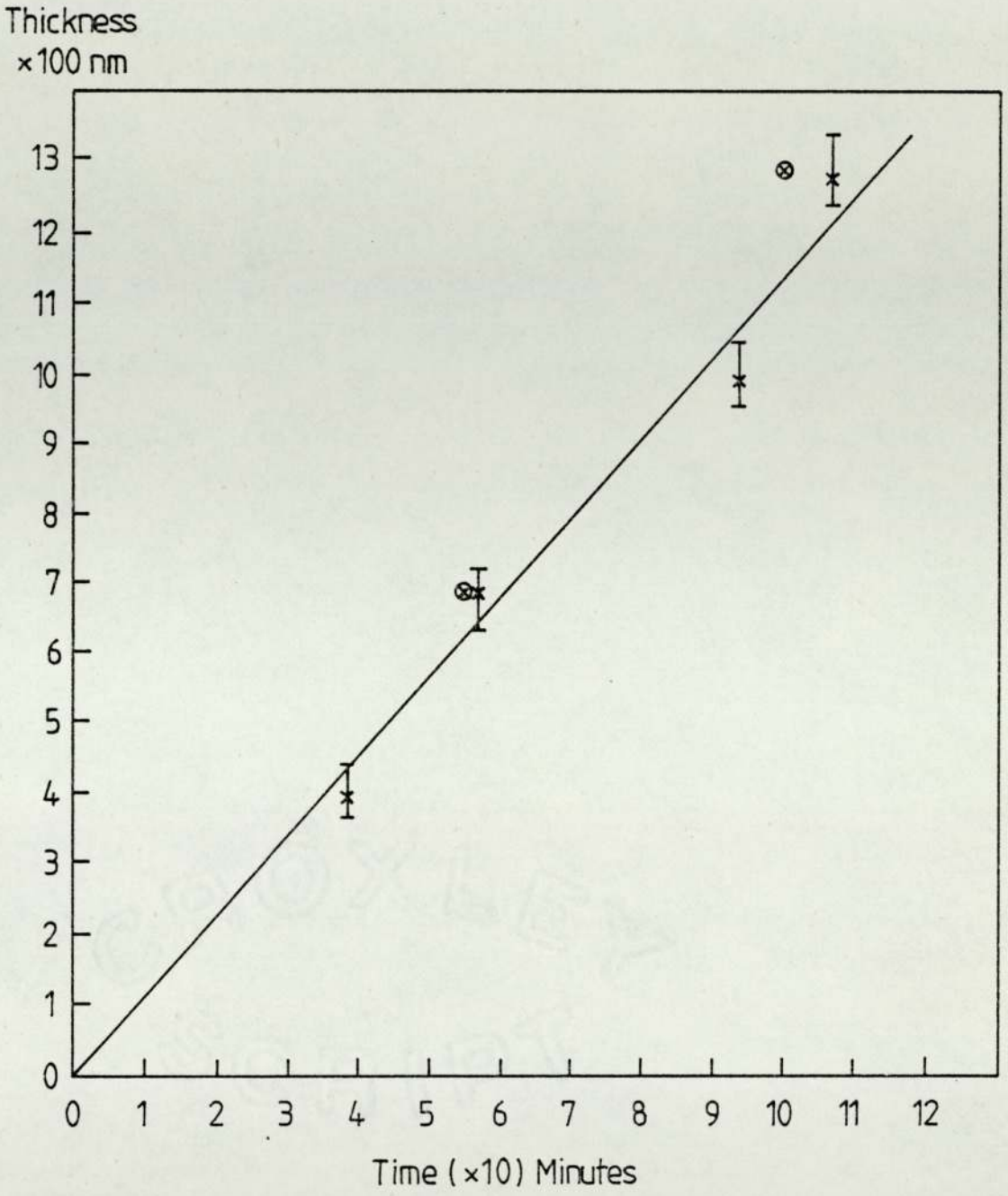

Figure 4·8 The growth rate for thermally grown silicon dioxide films on (111) and (100) silicon (× - 111, ⊗ - 100) at a temperature of 1100°C.

CHAPTER V

AN ASSESSMENT OF THE APPLICATION OF ELLIPSOMETRY FOR SURFACE FILM THICKNESS MEASUREMENTS

Ellipsometry is a very sensitive technique for measuring the optical properties and thicknesses of thin films, for examining growth of any contamination on a surface, and to study any optical anisotropy. The sensitivity of the instrument is dependent on the materials used and the angle of incidence. The object of the present section of the study was to obtain the optimum conditions for the instrument in order to investigate optical constants and thicknesses of film for the materials used in this work and to evaluate the optimum conditions for other materials. This investigation will show the ellipsometer sensitivity for measuring a small change in ψ and Δ which is very important for optical anisotropy studies because the changes in ψ and Δ on rotating the samples are small (this will be discussed in the next chapter). Since the light beam does not damage, change or contaminate the surface, ellipsometry is truly non-distructive and useful for measuring the surface properties. The two angles ψ and Δ measured by ellipsometry are discussed in Section 4.3.3. These two angles give information needed for the surface study. From the known wavelength of the light beam at the particular angle of incidence, the optical constants n and k of a surface can be calculated. For each film grown on a surface there are three unknown parameters (n, k and the thickness) and ellipsometry provides only two parameters, the two angles ψ and Δ. To

overcome the difficulty of lack of information, several procedures have been proposed. McCrackin and Colson[157] suggest that for any film with a real and imaginary part of unknown refractive index, an increased reading in the ellipsometry is needed. They investigated four different cases with different conditions: (i) using films of the same unknown optical constant with varying thicknesses but preferably with known thickness ratios, (ii) using different angles of incidence, (iii) using films in various surrounding media of known refractive index and (iv) using films on different substrates of known refractive index.

The first two methods are more practical to use because in case (i), the refractive index could be obtained for films between 10 - 100 nm, this is the most commonly used method in the ellipsometry technique, method (ii) is more complicated than (i) but much less complicated than methods (iii) and (iv), and has been reported in several papers[157-161]. Methods (iii) and (iv) are not very practical to do, because the effect of the different preparations on varying substrates may produce different films and also corrosion. But if the n and k of the substrates are unknown they can be measured by the ellipsometry before forming any subsequent film for testing. The ellipsometer sensitivity depends on many factors; the angle of the incidence, refractive index of the film and substrate and the components of the equipment. This matter will be discussed later.

5.1 The Film Refractive Index Effect on the Film Thickness Measurement

A computer model was used in order to assess the sensitivity

of the instrument for determining the thickness and properties of surface layers. In this model an aluminium oxide film on an aluminium substrate was used, because oxide film covers newly formed metal surfaces (in a local environment) in fractions of a second and quickly grows back when damaged and this will have an effect on the measured optical properties.

Fig 5.1 shows a plot of computed values of ψ vs Δ as a film of aluminium oxide grows on aluminiium. For a non-absorbing film layer ($k_2 = 0$) a closed loop is formed as the film thickness increases in that the ψ and Δ values repeat themselves i.e. the point corresponding to the start of the surface is shown at zero nm and it can be seen that for aluminium oxide films of about 235 nm, 470 nm and 705 nm the values of ψ and Δ correspond to the starting points of the second and third loops etc. The thickness can be obtained by matching the experimental values and the computed values of ψ and Δ . For a sample with an unknown oxide layer thickness we have to establish which loop we are looking for, and this can be obtained in two ways; firstly we may know the range of film thickness i.e. we can carry out tests on specially prepared samples.

In some instances it may be that the optical constant for the oxide (or any film) can be obtained from previous literature. To confirm these values of n_1 and k_1, different films with different thicknesses must be prepared experimentally. If the experimental measured values of ψ and Δ match with the computed values of ψ and Δ , it is reasonable to assume that n_1 and k_1 values are the correct values for that particular film. But if there is a difference between the two values, a change in the values of

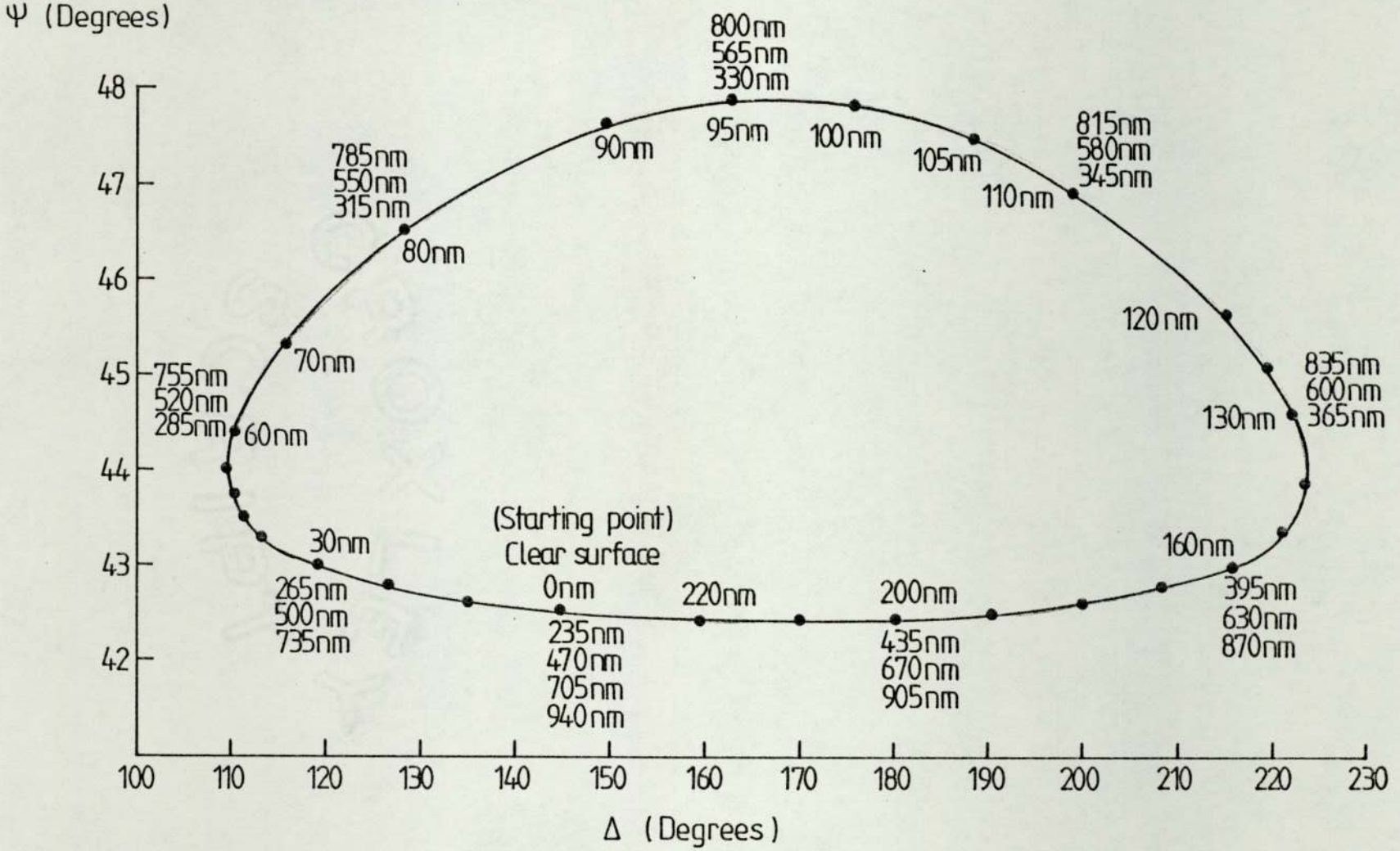

Figure 5·1 The loop of Ψ and Δ for the aluminium and show the thickness in the second, third and fourth loop at the same point of Ψ and Δ.

either or both n_2 and k_1 in the computer model may be needed until a match between the experimental values and the computed values of ψ and Δ is obtained.

To illustrate this approach we chose three different values of n_2 and k_2 for aluminium oxide on aluminium and we investigated the effect of these values on the thickness measurement. The effect of n_2 and k_2 on film thickness determination is also important if the films are anisotropic. In such cases the optical properties vary with orientation and the thicknesses determined would appear to depend on orientation if the variation in refractive index is ignored. For simplicity the left side only of the loop in the plot of ψ against Δ as shown in Fig. 5.1 will be expanded and presented in this study. Figures 5.2 and 5.3 show the effect on ψ and Δ for variation in $n_2 (k_2 = 0)$ for films of different thickness. In Fig. 5.2 the assumed values of n_2 are 1.6, 1.7 and 1.8. This will not give much variation between the model values for very thin films as shown in Fig. 5.2. For a thickness above 15 nm the error in the measurement of thickness is high, because, as n increases the curve moves up and to the left, which means that the values of $\delta\psi_{n=1.6-1.8}$ are increased. For example, Table 5.1 shows there is a large difference in the values of ψ and Δ where $\delta\psi_{n=1.6-1.8} = 2.7^\circ$ and $\delta\Delta_{n=1.6-1.8} = 18.58^\circ$ at 70 nm when n_2 is increased from 1.6 to 1.8. This indicates that a large error could be made by using the wrong refractive index.

Figure 5.3 shows the effect of change in the values of the absorbing coefficient k_2 from 0 to 0.025, 0.05 and 0.075 for $n_2 = 1.6$. The error caused by variation in k_2 can be neglected on a thin film, with a thickness less than 15 nm because the variation

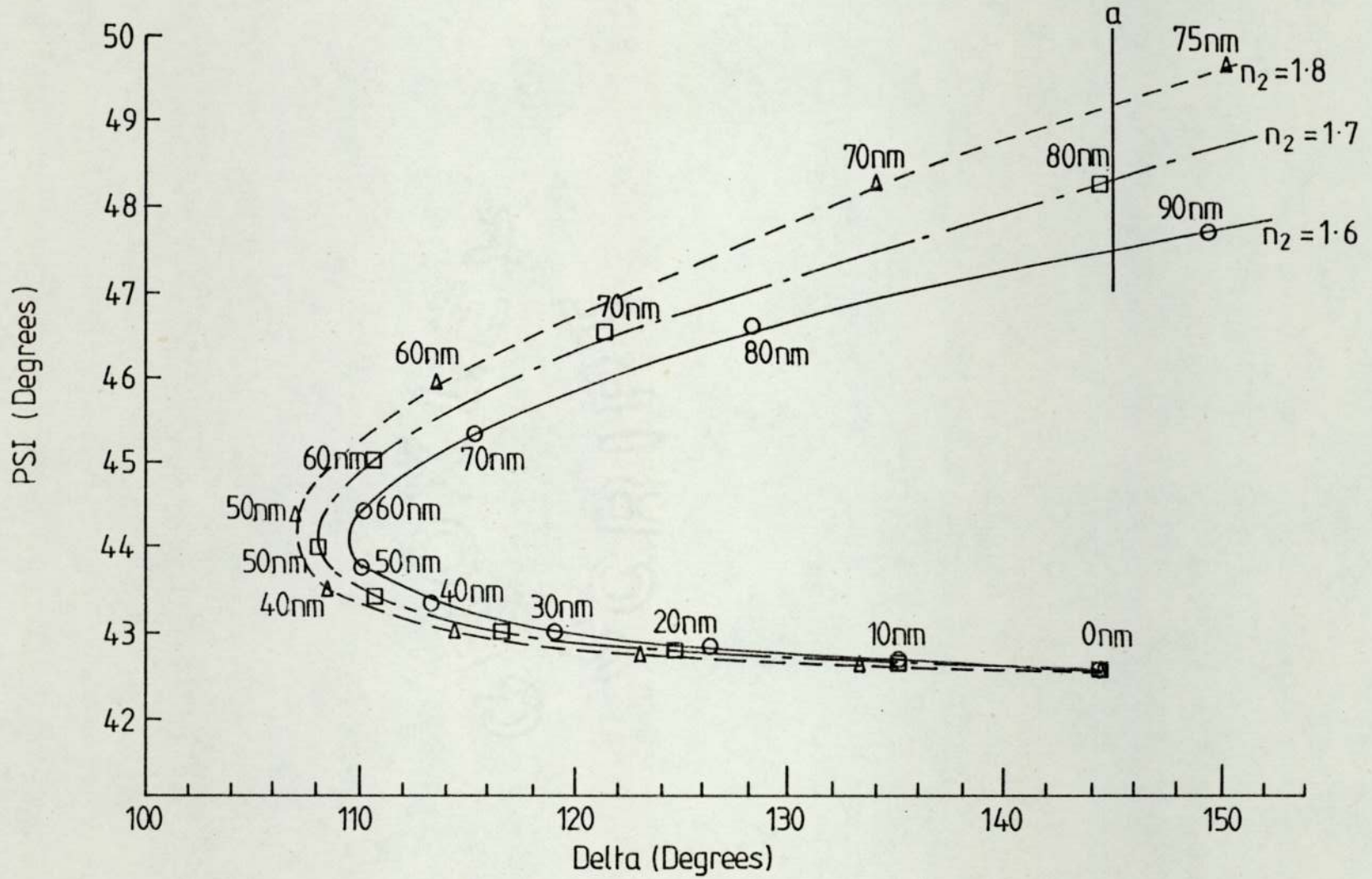

Figure 5·2 Expanded view of the theoretical Ψ vs Δ for different values of $n_2 = 1·6, 1·7$ and $1·8$, $k_2 = 0$, where $n_3 = 0·6926$ and $k_3 = 4·5229$.

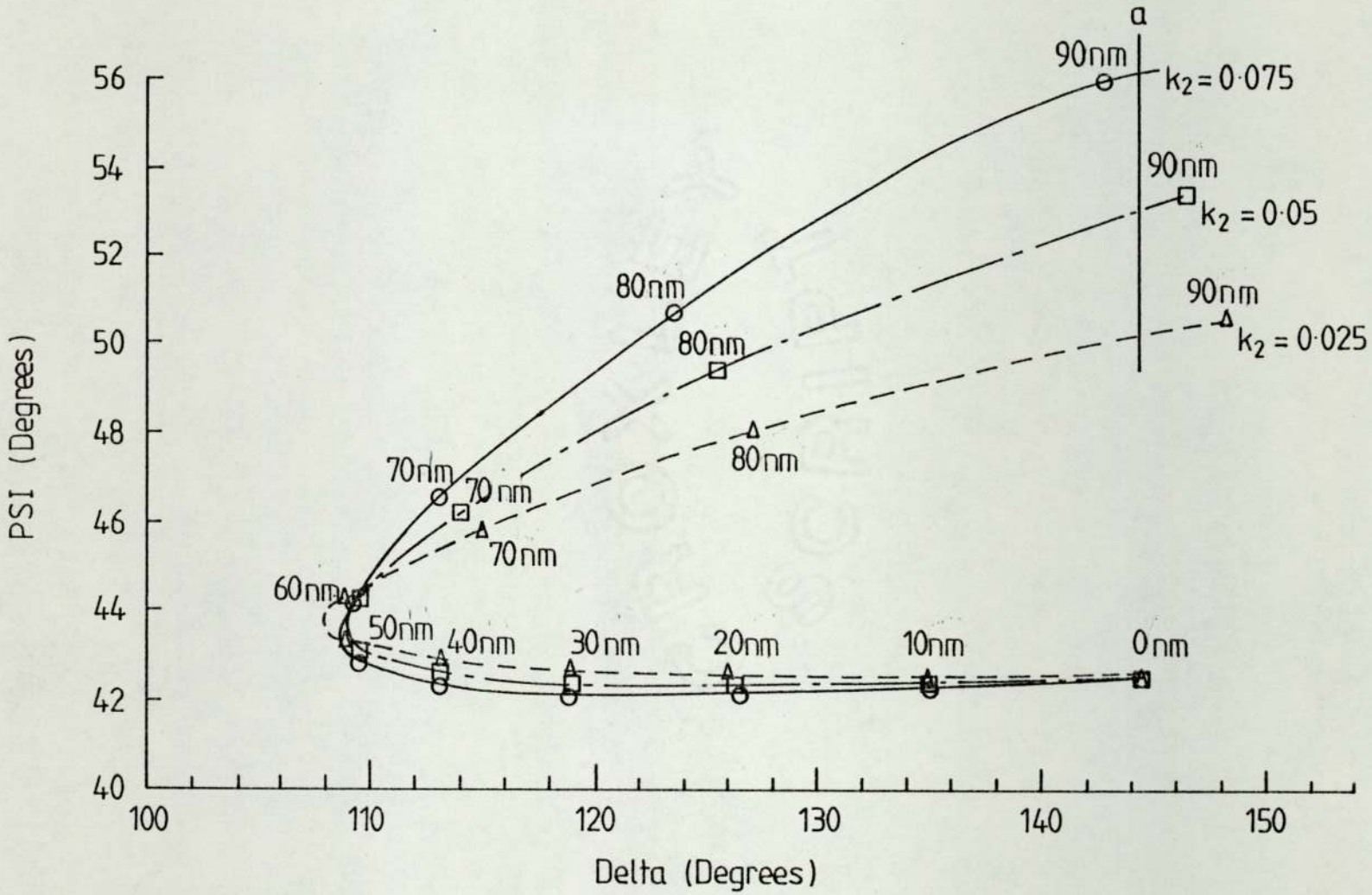

Figure 5·3 Expanded view of theoretical plot of Ψ vs Δ, for a different value of refractive index (absorption coefficient) of the film, $k_2 = 0.025, 0.05, 0.075$ and $n_2 = 1.6$, $n_3 = 0.6926$ and $k_3 = 4.5229$.

Table 5.1

The effect of changing n_2 in the values of Ψ and Δ at 0 nm and 70 nm.

n_2	k_2	Substrate Ψ	Substrate Δ	70 nm Oxide Film Ψ	70 nm Oxide Film Δ
1.6	0	42.55	144.56	45.53	115.60
1.7	0			46.50	121.75
1.8	0			48.23	134.18

Table 5.2

The effect of changing k_2 in the values of Ψ and Δ at zero film thickness (clean surface) and a film with 90 nm thickness.

n_2	k_2	Substrate Ψ	Substrate Δ	90 nm Oxide Film Ψ	90 nm Oxide Film Δ
1.6	.025	42.55	144.56	50.52	148.43
1.6	.050			53.34	146.67
1.6	.075			56.13	144.12

in ψ and Δ for changing k_2 are negligible. A film with a thickness of 90 nm will have a large error in the measurement because the difference between ψ values is $\delta\psi_{k=.025-.075} = 5.61$ and $\delta\Delta_{k=.025-.075} = 4.31$ between $k_2 = 0.025$ and 0.075. These differences are much greater than any errors in the measurement of ψ and Δ.

Consider one value of Δ in Figs. 5.2 and 5.3 i.e. $\Delta_a = 144.75$. Table 5.3 shows that there are thickness differences $\delta t = 14.67$ nm and 1.72 nm by using different n_2 and k_2 values respectively. This means that a large error in thickness evaluation will be made if the incorrect n_2 values for the film material are used in the computer model.

5.2 The Effect of the Substrate Refractive Index on Film Thickness Measurement

In the last section we discussed the effect of aluminium oxide constant n_2 and k_2 on the thickness measurement of the oxide on aluminium. As mentioned before, freshly prepared aluminium reacts with oxygen very quickly and an oxide layer is rapidly formed on its surface and this modifies the values of the substrate n_3 and k_3 (in air) when used as a substrate for subsequent additional layers. We consider three different values of n_3 and k_3 and investigated the effect on the thickness measurement of subsequent layers superimposed.

The effect of the change or error in the refractive index n_3 and k_3 of the substrate on the measurement of the film thickness can be seen in the shape of the plot of ψ against Δ as shown in Fig. 5.4. The shape of the plot is shifted down at the bottom

Table 5.3

The thickness variation at a point 'a' for different values of n_2 and k_2.

n_2	k_2	t nm	Ψ Degree	Δ Degree
1.6	0	88.05	144.75	47.50
1.7	0	80.00	144.75	48.22
1.8	0	73.33	144.75	48.95
1.6	.025	88.52	144.75	50.18
1.6	.050	89.24	144.75	53.06
1.6	.075	90.24	144.75	56.23

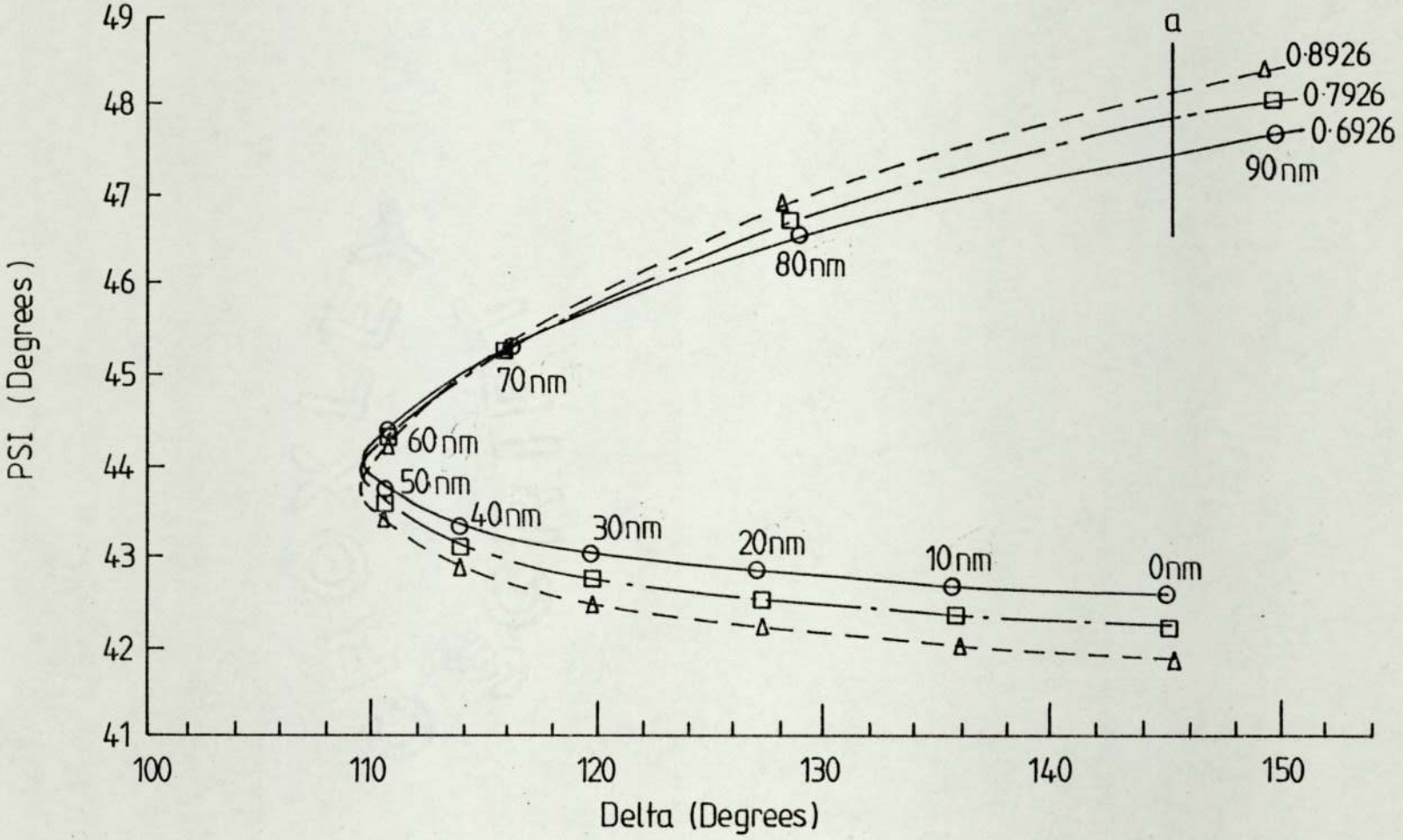

Figure 5·4 Expanded view of the theoretical curve of Ψ and Δ with different values of refractive index of the substrate. $n_3 = 0{\cdot}6926, 0{\cdot}7926, 0{\cdot}8926$, $k_3 = 4{\cdot}5229$, $n_2 = 1{\cdot}6$ and $k_2 = 0$.

of the curve and shifted up at the top of the curve, as n is increased from 0.6926 to 0.8926 (these values have been chosen because they lie in the range of the measured values). From the figure it is clear that the effect on very thin film thickness measurement is much higher than the effect from changing n_2 which is shown in Table 5.4 where $\delta\psi_{n_3=.6926-.8926} = .67$ and $\delta\Delta_{n_3=.6926-.8926} = .41$. However, the change in Δ is high, which will affect the thickness measurement of a thin film. The minimum error of the thickness can be obtained when ψ and Δ is very small, which is in the range of 60 nm - 75 nm and equal to $\delta\psi = 0.05$ and $\delta\Delta = 0.024$ at a 70 nm film thickness.

The effect of changing the substrate absorption k_3 on the thickness measurement and on the shape of the plot of ψ and Δ is shown in Fig. 5.5. Using the values of k_3 as 4.5229, 4.6229 and 4.7229, as shown in Table 5.5, it was found that $\delta\psi_o$ and $\delta\Delta_o$ are 0.17 and 1.32 respectively for a clean surface (zero oxide layer) and is equal to $\delta\psi_{900} = 0.25$ and $\delta\Delta_{900} = 1.41$ on a film of 90 nm thickness which will affect the measurement of the film thickness.

We took one value of $\Delta_a = 144.75$ to study the effect of the substrate optical constant on the thickness measurement. Table 5.6 shows the effect on the thickness measurement when n_3 and k_3 were changed. This means the change in n_3 will lead to an error in the thickness measurment of $\delta t = 0.26$ nm and by changing k_3 will lead to an error in the thickness of $\delta t = 0.56$ nm at this particular point ($\Delta_a = 144.7$). This shows that the error in point (a) is of the order of 0.6%.

Table 5.4

The effect of changing n_3 in the values of Ψ and Δ at 0 nm and 70 nm as shown in Fig.5.3.

		Substrate		70 nm Oxide Film	
n_3	k_3	Ψ	Δ	Ψ	Δ
0.6926	4.5229	42.55	144.56	45.33	115.60
0.7926	4.5229	42.21	144.75	45.35	115.48
0.8926	4.5229	41.88	144.97	45.38	115.36

Table 5.5

The effect of changing k_3 in the values of ψ and Δ at zero film thickness (clean surface) and a film with 90 nm thickness as shown in Fig.5.4.

		Substrate		90 nm Oxide Film	
n_3	k_3	Ψ	Δ	Ψ	Δ
0.6926	4.5229	42.55	144.56	47.68	149.50
0.6926	4.6229	42.64	145.23	47.55	148.77
0.6926	4.7229	42.72	145.88	47.43	148.09

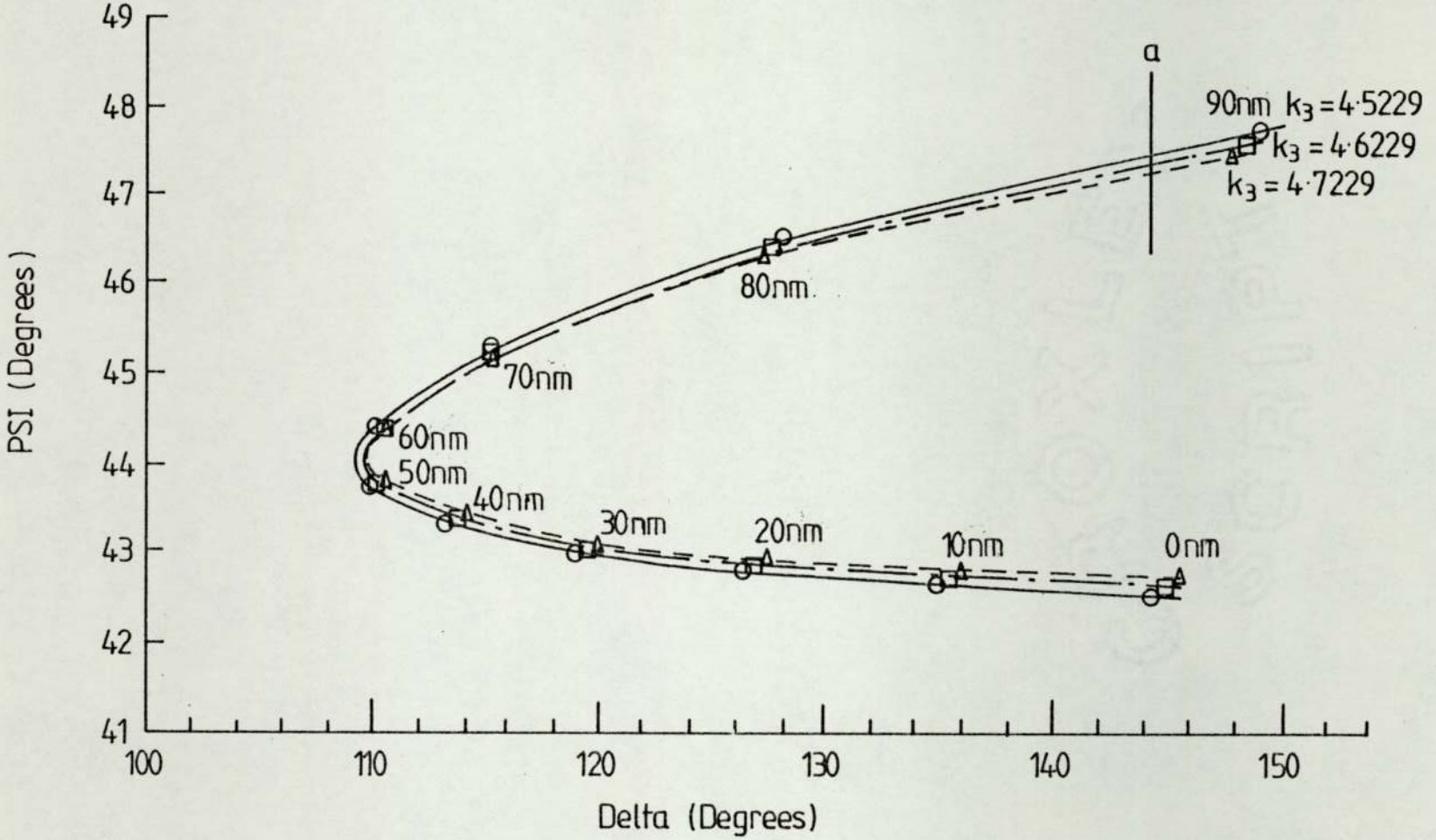

Figure 5·5 Expanded view of theoretical plots of Ψ vs Δ to show the effect of changing the absorption coefficient $k_3 = 4{\cdot}5229$, $4{\cdot}6229$, $n_3 = 0{\cdot}6926$, $n_2 = 1{\cdot}6$ and $k_2 = 0$.

Table 5.6

The thickness variation at a point 'a' for different values of n_3 and k_3.

n_3	k_3	t nm	Δ Degree	Ψ Degree
0.6926	4.5229	88.05	144.75	47.50
0.7926	4.5229	88.16	144.75	47.85
0.8926	4.5229	88.31	144.75	48.20
0.6926	4.5229	88.05	144.75	47.50
0.6926	4.6229	88.34	144.75	47.40
0.6926	4.7229	88.61	144.75	47.30

5.3 The Effect of the Angle of Incidence on Film Thickness Measurement

The effect of the angle of incidence ϕ_o in measuring the film thickness and the shape of the ψ vs Δ loop are shown in Fig. 5.6. It can be seen that the curve is displaced to the left along the Δ axis at t = 50 nm to 60 nm by three degrees as ϕ_o is changed from 60 to 61 degrees and another three degrees from 61 to 62 degrees. This is also shown in Table 5.7. This is making the error all around the loop of the order of three degrees. But the errors at the clean surface were $\delta\psi = 0.2$ and in $\delta\Delta = 3.46$, and $\delta\psi$ will decrease as the film thickness increases to 50 nm at which value $\delta\psi = 0.03$, but the $\delta\Delta$ will increase to be equal $\delta\Delta =$ 5.48 degrees at 50 nm.

We took one value Δ_a ($\Delta_a = 144.75$) and found the thickness changes at the three angles of incidence which are shown in Table 5.8. The variation in thickness measurement are in the range of $\delta t = \pm 1.8$ nm on the film thickness 88.05 nm for the $\phi_o = 60$. This shows how important it is to keep the angle of incidence constant during a set of measurements. As stated in Section 4.3.4 the angle of incidence can be measured to within 0.05 degrees. An error of 0.1 degrees in the angle of incidence is equivalent to 0.1 nm error in film thickness measurement.

5.4 The Instrument Sensitivity for ψ and Δ .

The ellipsometric study of the optical properties and film growth are a function of ψ and Δ . The film thickness measurement maximum sensitivity can be calculated at different thicknesses to find the variation of the sensitivity within their

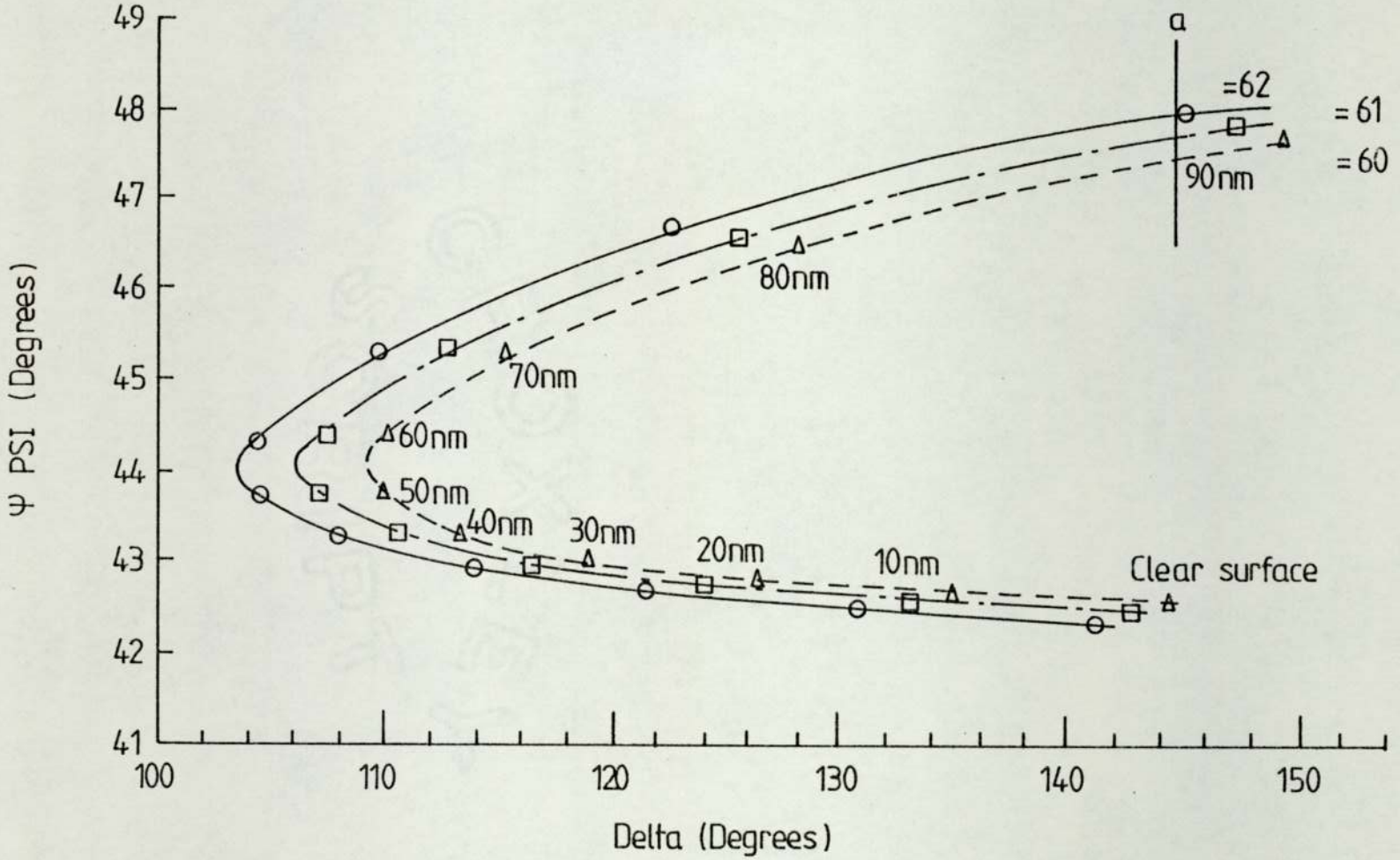

Figure 5·6 Expanded view of the theoretical plot of Ψ vs Δ , to show the effect of changing the angle of incidence = 60, 61 and 62 , where $n_2 = 1{\cdot}6$, $k_2 = 0$, and $k_3 = 4{\cdot}5229$, $n_3 = 0{\cdot}6926$

Table 5.7

The effect of changing the angle of the incidence (φ) in the values of ψ and Δ at 0 nm and 50 nm as shown in Fig. 5.5

φ	Substrate ψ	Substrate Δ	50 nm Oxide Film Ψ	50 nm Oxide Film Δ
62	42.35	141.10	43.75	104.56
61	42.45	142.90	43.76	107.38
60	42.55	144.56	43.78	110.04

Table 5.8

The thickness variation with a different angle of incidence at a point 'a' where Δ=144.70 degree.

φ Degree	t nm	Δ Degree	Ψ Degree
60	88.05	144.74	47.50
61	80.95	144.75	47.71
62	89.85	144.75	47.93

thickness and this can be done by applying the following equation:

$$\left|\frac{\delta\Delta}{\delta t}\right| = \left|\frac{\Delta_1 - \Delta_2}{t_1 - t_2}\right| \quad , \quad \left|\frac{\delta\psi}{\delta t}\right| = \left|\frac{\psi_1 - \psi_2}{t_1 - t_2}\right|$$

This relation will enable the instrument sensitivity to be determined over different ψ and Δ ranges i.e different film thicknesses. Since in part of this work the thicknesses of SiO_2 layers have been determined over a wide range of thickness , we will use SiO_2 layers on silicon as an example to look at this effect. Figure 5.7 gives the changes in the sensitivity for different thicknesses of oxide. This will be considered in the next section.

5.5 Film Thickness Measurement and Variations Across Samples

An assessment of the ellipsometer has beeen made for a range of silicon layer measurements as follows:- (a) Si_3N_4 on Si, (b) Si_3N_4 on Al, (c) SiO_2 on Si, (d) amorphous silicon on silicon, (e) Si_3N_4 on Si (glow discharge), (f) Si_3N_4 on Si. All the ellipsometric measurement evaluations were performed on samples at room temperature and supplied by courtesy of the Lucas Research Centre, Shirley. After being prepared in an r.f. system, the samples groups (a) to (d) (75.0 mm x 24.5 mm) were cut to fit the instrument holder. Some samples were of amorphous silicon, silicon oxide and silicon nitride films deposited on p-type crystalline (111) silicon substrates. In some cases the substrate were layers of aluminium ($\sim$100 nm thick) superimposed on silicon substrates. Samples were obtained from different wafers being originally placed at different positions in the deposition chamber during preparation. Figure 5.8 shows the two ways in which the wafers

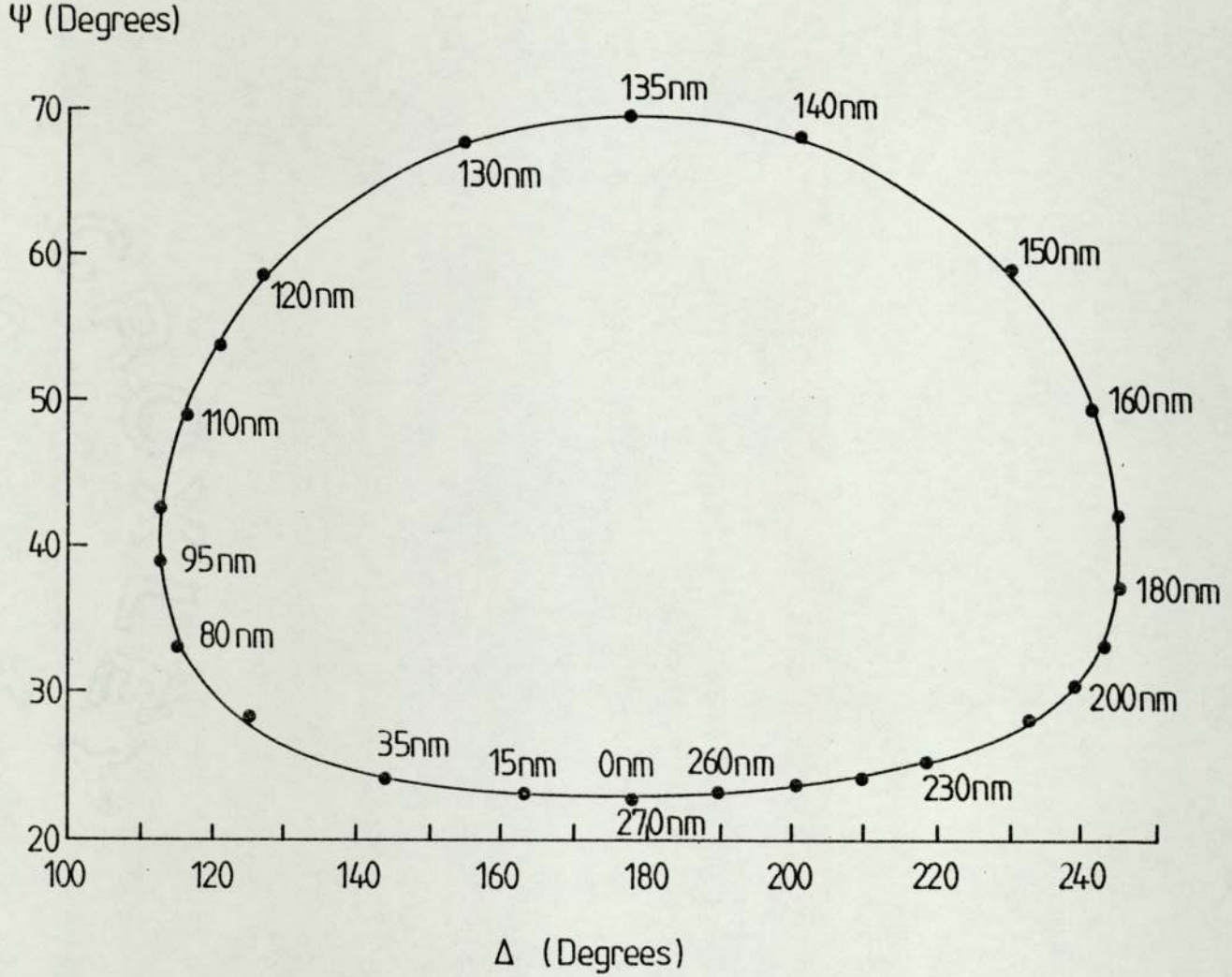

Thickness (nm)	δΔ/δt (deg/nm)	δΨ/δt (deg/nm)
0	1·0	0·03
30	0·91	0·09
50	0·74	0·15
70	0·48	0·25
90	0·11	0·45
110	0·71	0·83
130	3·7	0·47
150	1·96	0·93
170	0·2	0·63
190	0·31	0·33
210	0·61	0·2
230	0·83	0·12
250	0·98	0·06

Figure 5·7 The instrument sensitivity for Ψ and Δ for measuring the SiO_2 film thickness. (upto 10nm)

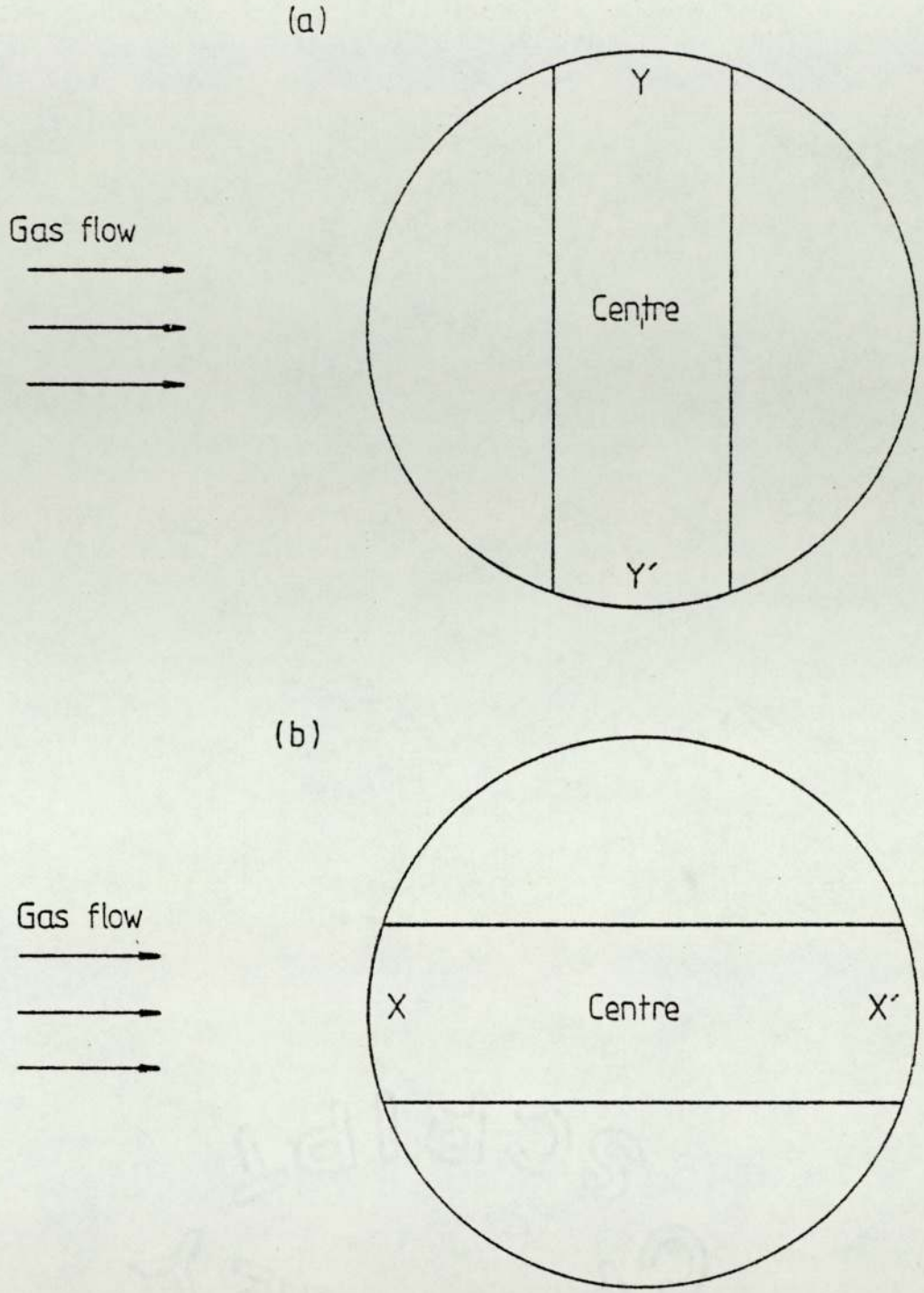

Figure 5.8 The position of the sample in the system during the oxidation. This shows the three positions where the measurement of Ψ and Δ were taken at the ellipsometer.

were orientated i.e. perpendicular (YŶ) and parallel (XX̄) to the gas flow in the production chamber. The distribution of wafers within the chamber and their coding is given in Figure 5.9. The coding also relates to the results on samples tested and shown in Table 5.10. The film thickness was measured in three different positions on the samples, the centre and the two ends.

a. Silicon Nitride on Silicon

The substrate test sample was p-type crystalline silicon (111) where the values of ψ and Δ for all three positions (the centre and both ends) were very close. The optical constant n_3 and k_3 of the test sample were calculated as described in Section 3.1 and were found to be 3.7585 and 0.0952 respectively. The first, second and third batches of samples of Si_3N_4 on Si were prepared by the sputtering technique, at a pressure of 2 Torr, and r.f. power of 300W, and a temperature of 380 °C. The optical constants for the Si_3N_4 given by the samples manufacturers for the conditions used were 2.0 and 0.0 for n_2 and k_3 respectively, and these values were confirmed in this work using a computer fit to data for layers of different thicknesses. Table 5.9 shows the values of ψ and Δ at three positions across each sample as indicated above and the values of pseudo constants, (see Section 3.1), n' and k' at the central position of the films. The last column of this Table 5.9 illustrates the variation in thicknesses evaluated by computer corresponding to the changes in ψ and Δ across the sample, and shows the uniformity or otherwise which existed in the layers across each specimen. But the variation of δt was not the same for all of the samples even though they were

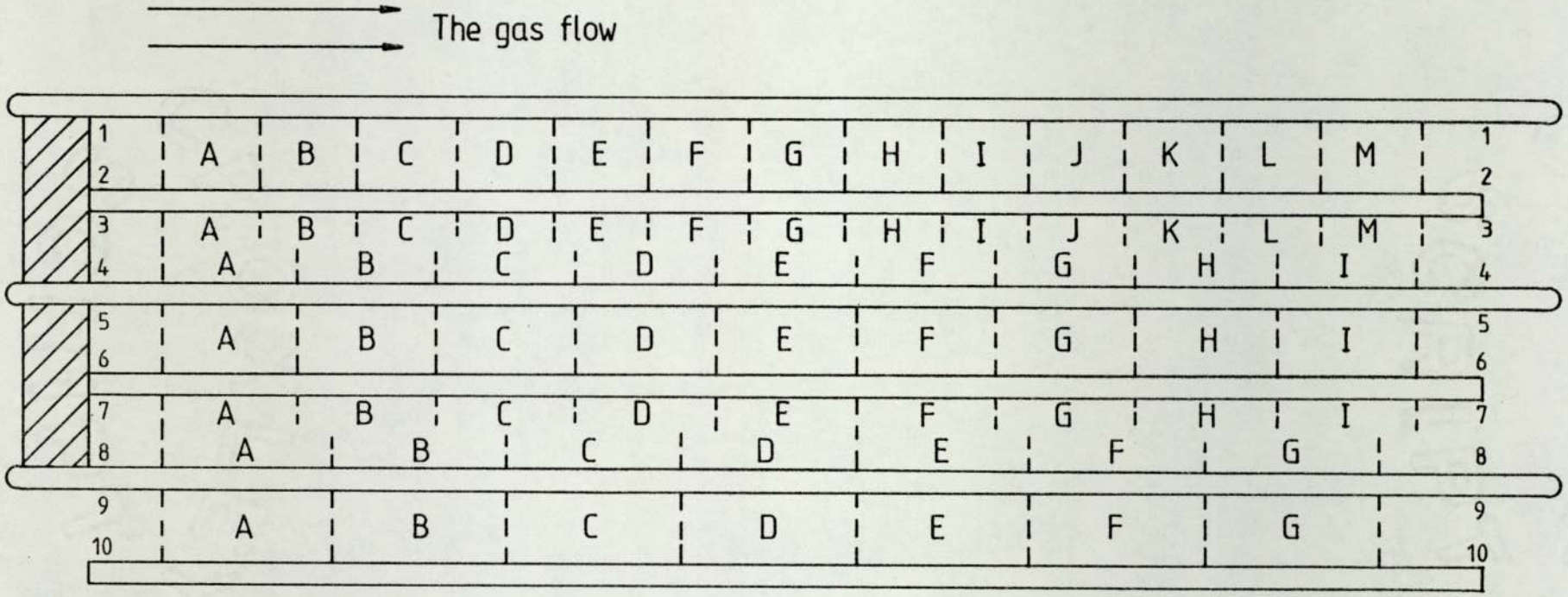

Figure 5.9 The relative positions of wafers in the preparation chamber.

Table 5.9

The values of ψ and Δ for Si_3N_4 on Si (batch one, two, and three) samples, in three different positions and the values of the pseudo constant (n' and k') for the central position only. $n_2 = 2.0$, $k_2 = 0$, $\lambda = 632.8$ nm and $\phi = 60$ degree.

Sample	ψ Degree			Δ Degree			Pseudo constant		δt
	C	X or Y	$\bar{X}$ or $\bar{Y}$	C	X or Y	$\bar{X}$ or $\bar{Y}$	n'	k'	nm
Sub.	22.72	22.69	22.85	181.51	182.13	182.38	-	-	-
5Da	26.09	25.56	25.60	90.04	98.00	97.72	1.0913	0.9997	2
5Ha	25.55	26.22	26.05	90.17	94.07	96.75	1.1176	0.9884	2
4Ga	24.59	24.01	26.27	100.64	107.64	92.76	1.2845	1.1323	3
5Da	27.58	27.26	26.51	93.49	90.39	94.87	1.0551	1.1057	1
7Ea	26.33	26.90	26.15	93.43	97.13	91.57	1.1159	1.0699	2
5Da	24.32	24.20	24.32	100.05	104.25	101.55	1.2969	1.1218	1
5Ia	24.90	23.61	24.30	96.31	103.77	101.91	1.2184	1.0783	3
6Ab	23.14	23.06	23.71	110.27	112.57	127.97	1.5270	1.2268	3
6Db	23.20	23.21	23.19	114.90	128.40	114.50	1.6249	1.2981	2

Table 5.10

The comparison between the experimental result with predicted computer result for appropriate thickness and optical properties for the Si_3N_4(batch one, two, and three) at the central position of the sample only and the film thickness.

Sample	Thickness nm	ψ Degree Exper.	Theor.	Δ Degree Exper.	Theor.	Instr. senst. $\delta\Delta/\delta t$	$\delta\psi/\delta t$
5Da	412.5	26.09	26.04	90.04	91.03	2.10	0.32
5Ha	412.0	25.55	25.93	90.17	90.07	2.10	0.31
4Ga	406.5	24.59	24.52	100.04	100.30	1.82	0.20
5Da	413.5	27.58	26.59	93.49	93.41	2.17	0.34
7Ea	413.5	26.33	26.59	93.47	93.41	2.17	0.34
5Da	406.5	24.32	24.52	100.05	100.30	1.82	0.20
5Ia	408.5	24.90	24.90	96.31	96.26	1.90	0.24
6Ab	401.0	23.14	23.65	110.27	110.27	1.66	0.13
6Db	398.5	23.20	23.38	114.90	114.58	1.63	0.11

prepared under the same conditions and in the same run. This was probably due to the varying position of the samples inside the preparation chamber. According to the manufacturer's of the production chamber, the variation in deposition layer thicknesses could be up to 20 nm and the results of the investigation confirmed this in most cases, see also Table 5.18 for silicon dioxide. Table 5.10 shows the variation in the film thicknesses and the different values of ψ and Δ from one sample to another. In general, it can be seen from this table that the computed values of thickness with the optical constant used in the computer model are in good agreement with the experimental results, showing the applicability of the model to these materials and on the applicability of the ellipsometric technique. The instrument sensitivity for each sample is listed in this table as $\delta\psi/\delta t$ and $\delta\Delta/\delta t$ which shows that the values of the sensitivity depend on film thickness at the appropriate point of the ψ and Δ curve.

The samples of batch four were also Si_3N_4 on Si , prepared under the same conditions as batches one, two and three but for different periods of time in order to produce different thicknesses, which were used for obtaining the non-absorbing curve between ψ and Δ . The values of ψ and Δ for the test sample (considered to be the substrate) enabled the theoretical curve to be generated. By matching these values to the measured values of ψ and Δ for samples, we were able to find the varying thicknesses, as shown in Fig. 5.10. As shown in Table 5.11, all samples are situated in the second loop of the ψ and Δ plot which means that the film is thick as explained in Section 5.1. Five of these lie in the bottom of the curve and the other three lie in differing

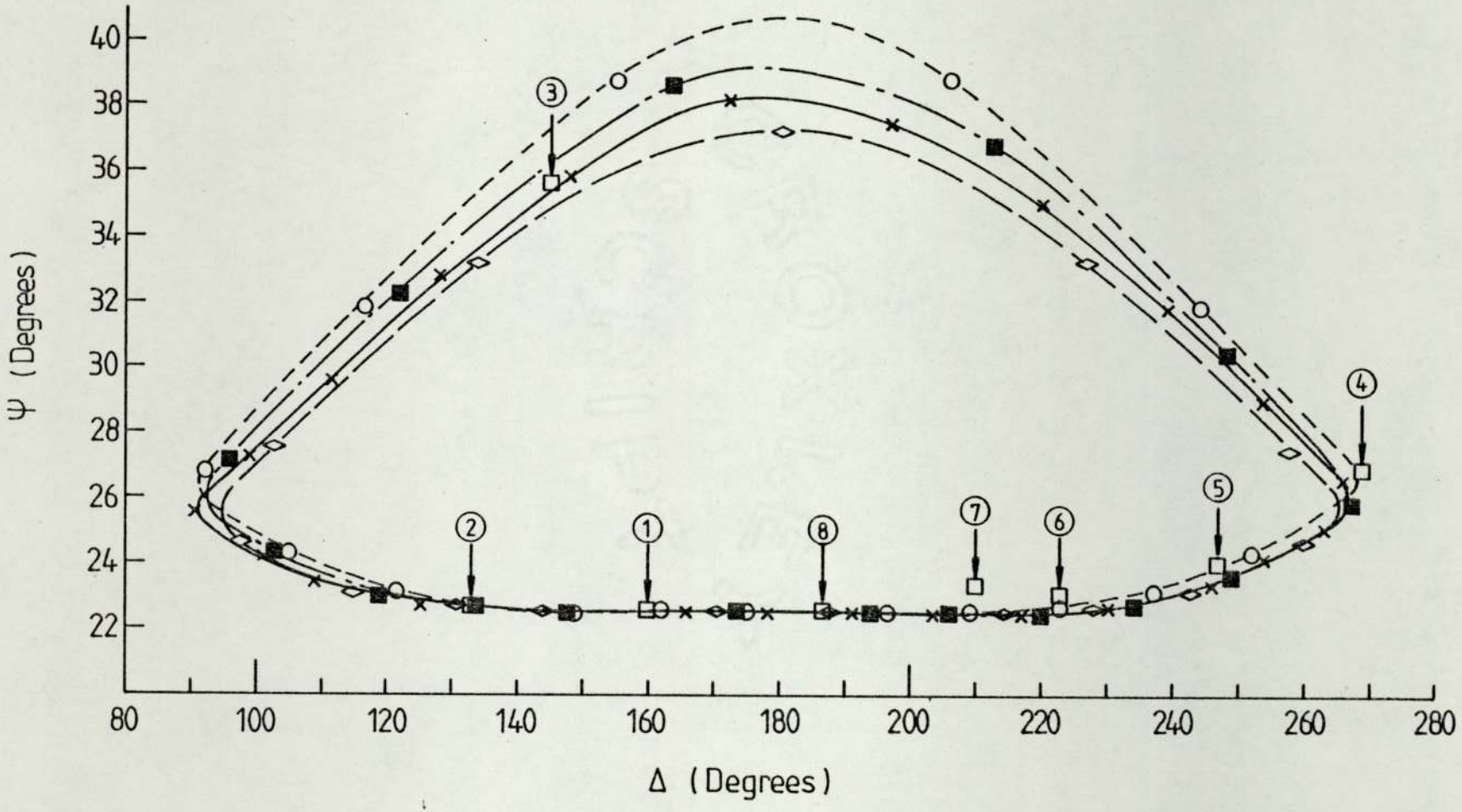

Figure 5·10 The growth of Si_3N_4 on a (111) Si substrate, with different values of n_2. The comparison is made between the experimental (points 1 to 8) and the theoretical values of Ψ and Δ, where $n_2 = 2, 1{\cdot}99, 1{\cdot}98$ and $2{\cdot}01$, $k_2 = 0$, $n_3 = 3{\cdot}7585$, $k_3 = 0{\cdot}0952$, $\phi = 60°$, and $\lambda = 632{\cdot}8$ nm.

Table 5.11

The measurement of ψ and Δ for Si_3N_4 on p-type silicon (batch four) with different thicknesses. $n_2 = 2$, $k_2 = 0$, $\lambda = 6328$ nm and $\phi = 60$ degrees.

Sample	Thickness nm	ψ Degree	Δ Degree
1	1880	22.58	161.33
2	2090	22.77	133.17
3	2690	35.82	145.96
4	2870	26.89	268.38
5	2980	24.15	246.97
6	3150	23.12	223.57
7	3250	23.60	210.67
8	3480	22.64	187.51

positions, which indicates that the instrument sensitivity is high. The results of four of the samples (4,5,6,7) did not match perfectly with the theoretical curve for $n_2 = 2$. We tried to modify this by changing the values of n as shown in Fig. 5.10. As can be seen in the figure using $n_2 = 1.98$ samples 1, 2, 4, 5 and 8 matched the theoretical curve.

b. Silicon Nitride on Aluminium

The samples of batch five were of Si_3N_4 on an aluminium substrate, prepared under the same conditions as batches 1, 2, 3 and 4. Table 5.12 shows the values of ψ and Δ for the different positions and shows the fluctuation in ψ and Δ values which is indicated by the variation in the thicknesses which is illustrated clearly in the values of δt which go up to 5.3 nm. This indicates that this run is not producing a uniform film as in the runs for batches 1, 2, 3 and 4 where δt were in the range of 3 nm. However, although these samples are not uniform, the values of δt still lie within the range predicted by the manufacturer's. Table 5.13 shows a good agreement between the experimental and the computed values of ψ and Δ, which again indicates the usefulness of the instrument and the model. The differences in the instrument sensitivity are as a result of the change in the sample thickness (i.e. in the position of ψ and Δ on the curve).

c. Silicon Nitride on Silicon by Glow-discharge

The sixth batch of samples were of Si_3N_4 with a refractive index of $n_2 = 2.0$ and $k_2 = 0.0$ on a silicon substrate. These samples were prepared by glow-discharge at a temperature of 315°C and 1.5 Torr. Table 5.14 shows the values of ψ and Δ at the

Table 5.12

The measurement of ψ and Δ for Si_3N_4 on Al substrate (batch five) in different positon and the values of n' and k' for the central position only, $n_1 = 2$, $k_2 = 0$, $\lambda = 632.8$ nm and $\phi = 60$ degree.

Sample	ψ Degree			Δ Degree			Pseudo constant		δt
	C	X or Y	$\bar{X}$ or $\bar{Y}$	C	X or Y	$\bar{X}$ or $\bar{Y}$	n'	k'	nm
Sub.	42.55	42.77	42.72	144.56	146.20	142.13	0.6926	4.5229	-
5Aa	42.26	42.13	44.26	147.21	147.21	167.11	0.8911	4.8815	5.3
5Da	42.26	43.26	41.31	143.38	136.38	150.62	0.7261	4.3466	3.0
5Ia	42.51	41.95	42.31	143.50	143.26	143.73	0.7586	4.3536	2.5
6Ib	42.33	41.78	42.23	147.89	153.69	146.79	0.9041	4.9955	2.0

Table 5.13

The comparison between the experimental and the theoretical values of Δ and ψ for Si_3N_4 on aluminium substrate (batch five) , for the central position and the thickness of the sample.

Sample	Thickness nm	ψ Degree Exper.	ψ Degree Theor.	Δ Degree Exper.	Δ Degree Theor.	Instr. $\delta\Delta/\delta t$	Senst. $\delta\psi/\delta t$
5Aa	349.0	42.26	42.25	147.21	147.13	1.27	5×10^{-4}
5Da	352.0	42.26	42.54	143.38	143.30	1.27	20×10^{-4}
5Ia	352.0	42.51	42.54	143.50	143.30	1.27	20×10^{-4}
6Ia	349.0	42.33	42.54	147.89	147.13	1.27	5×10^{-4}

Table 5.14

The measurement of ψ and Δ for the Si_3N_4 by glow discharge (batch six) in three different posititons and the values of n and k at the centre of the sample. $n_2 = 2$, $k_2 = 0$, $\lambda = 632.8$ nm and $\phi = 60$.

Sample	ψ Degree			Δ Degree			Pseudo const.	
	C	X or Y	$\bar{X}$ or $\bar{Y}$	C	X or Y	$\bar{X}$ or $\bar{Y}$	$\bar{n}$	$\bar{k}$
Batch six	25.09	58.25	50.94	115.73	125.60	103.73	1.5665	1.4323

different positions on a sample from the batch and gives the values of the pseudo constant n' and k' at the central position. The variation in ψ and Δ values indicate the difference in the thicknesses over the sample.

d. Amorphous Silicon on Silicon

The seventh batch of samples were amorphous silicon on a silicon substrate and these samples were prepared at a temperature of 380 °C, a pressure of 1 Torr, and a r.f. power of 500W. Table 5.15 shows the values of ψ and Δ at three points across each of three samples and illustrates the type of variation observed. The samples in this run had a uniform film which can be seen from the small difference between the values of ψ and Δ in the three points. The last column in the table shows the pseudo constant values for each film at the central point.

Since amorphous silicon is absorbing it was necessary to determine the limitations of the ellipsometer for measuring the thickness of amorphous silicon layers. Theoretically using the computer model we found the minimum thickness of the amorphous silicon film for which the substrate did not influence the results, and it is also the maximum thickness for which the technique can be used to measure film thicknesses. Fig. 5.11 shows the effect of increasing film thickness for an absorbing film. The minimum thickness was computed by allowing various thicknesses of amorphous silicon to be added to a glass substrate by using $n_3 = 3.437$ and $k_3 = 0.7113$ (the optical constant found for a 1.4 μm film thickness of amorphous silicon, produced by Dr. Fane's group in the department). After the minimum thickness the

Table 5.15

The measurement of ψ and Δ for a-Si on silicon (batch seven) in three different positions and the values of n' and k' at the centre of the sample. $\lambda = 632.8$ nm and $\phi = 60^{\circ}$.

Sample	ψ Degree			Δ Degree			Pseudo const.	
	C	X or Y	$\bar{X}$ or $\bar{Y}$	C	X or Y	$\bar{X}$ or $\bar{Y}$	n'	k'
5A(a)	23.85	24.63	23.93	174.90	175.16	171.62	3.9298	0.3654
5I(a)	25.68	24.08	23.96	173.23	174.94	174.18	4.2620	0.6022
5D(a)	24.68	24.17	24.83	172.28	175.28	175.78	4.126	0.2179

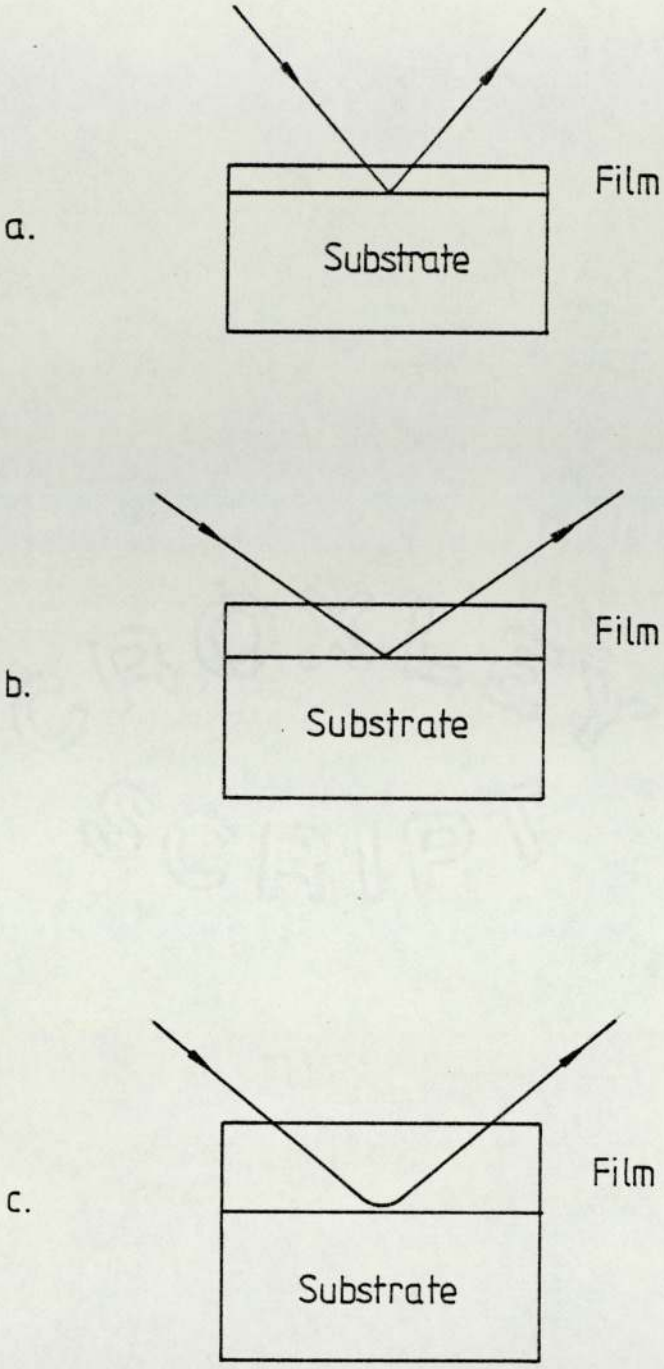

Figure 5-11 The substrate effect on the optical constant for the film. a) very thin film, b) thin film but the effect of the substrate on n_2 and k_2 there, c) the minimum thickness of the film for which the substrate has no influence. It is also the maximum film thickness which could be measured by the ellipsometric technique.

ψ and Δ values and pseudo constant should not change i.e. the film is absorbing the radiation and there is no penetration to the glass. The minimum thickness was obtained by assuming we had a glass substrate and by using the value of n_2 and k_2 of the glass as shown in Table 5.16. We found the value of ψ and Δ did not change after ~720 nm which means this is the minimum thickness. We then used these values of optical constants to find the thickness of the samples of batch seven of amorphous silicon on silicon. Table 5.17 shows the comparison between the computed and the experimental values and gives the thickness of the sample.

c. Silicon Dioxide on Silicon

1. The samples of batches eight and nine are silicon dioxide grown on a (111) silicon substrate at a temperature of 380°C and a pressure of 0.8 Torr with an r.f. power of 150W. The optical constants of the oxide layers for these conditions were stated by the equipment manufacturers to be $n_2 = 1.5$ and $k_2 = 0$, and the value was confirmed in this work using a computer fit to data for layers of different thickness as previously explained . Table 5.18 shows the values of ψ and Δ at different points across each sample, and shows the various values of ψ and Δ which indicate that the films are not absolutely uniform as can be seen clearly in the values of δt , which are in the range of 3 nm and 17 nm for batches eight and nine respectively. Table 5.19 shows the experimental and the computed values of ψ and Δ in the central position for each sample. The sensitivities for this group of samples are also listed in the table and it shows that the sensitivity can be given by $\delta\Delta/\delta t = 1.0$ deg/nm, and the values of $\delta\psi/\delta t$ are between 0.02

Table 5.16

The minimum thickness which is not influenced by the substrate for a-Si on Si. This is calculated by assuming that the values of n_3 and k_3 are the glass values.

Thickness nm	Δ Degree	Ψ Degree
500	166.825	21.983
520	166.801	21.990
540	166.781	21.986
560	166.787	21.980
580	166.800	21.981
600	166.802	21.984
620	166.795	21.985
640	166.792	21.983
660	166.794	21.982
680	166.797	21.983
700	166.796	21.984
720	166.795	21.984
740	166.795	21.983
760	166.795	21.983
780	166.796	21.983
800	166.795	21.983
820	166.795	21.983
840	166.795	21.983

Table 5.17

The comparison between the experimental and the computer values of amorphous silicon (batch seven) for the centre position and the thickness of the sample $n_2 = 3.437$, $k_2 = 0.7113$, $n_3 = 3.7585$, $k_3 = 0.0952$, $\Phi = 60^\circ$, $\lambda = 632.8$ nm.

Sample	Thickness nm	Ψ Degree		Δ Degree	
		Exper.	Theor.	Exper.	Theor.
5A(a)	7.7	23.85	24.12	174.90	174.90
5I(a)	12.8	25.68	24.49	173.24	173.22
5D(a)	11.0	24.67	24.64	172.28	172.28

Table 5.18

The values of ψ and Δ for SiO (batch eight and nine) samples, in three different positions and the values of n' and k' for the central position only. $n_2 = 1.5$, $k_2 = 0$, $\lambda = 632.8$ nm and $\phi = 60$ degree.

Sample	ψ Degree			Δ Degree			Pseudo cons.		δt
	C	X or Y	$\acute{X}$ or $\acute{Y}$	C	X or Y	$\acute{X}$ or $\acute{Y}$	n'	k'	nm
5Da	23.42	23.42	23.49	155.85	155.85	157.99	3.17	1.29	1
5Ia	23.87	22.10	22.30	187.77	181.97	182.37	3.87	0.58	3.6
6Ab	23.61	24.17	22.27	153.75	148.35	162.85	3.08	1.38	3
6Ib	22.63	22.69	23.08	186.39	182.03	184.93	3.69	0.39	3
5Aa	23.24	27.01	27.54	189.22	146.98	145.22	3.73	0.60	15.6
5Ia	27.69	27.26	26.39	235.50	231.70	210.54	1.70	1.79	16.5
4Ga	22.78	26.04	21.30	185.90	210.24	167.76	3.73	0.37	15.7
7Ea	23.02	23.02	23.75	188.57	187.03	125.27	3.71	0.54	17.0

Table 5.19

The comparison between the experimental and the theoretical values of ψ and Δ for SiO_2 (batch eight and nine) $n_2 = 1.5$ and $k_2 = 0$, centre position only and the film thickness.

Sample	Thickness nm	ψ Degree Exper.	ψ Degree Theor.	Δ Degree Exper.	Δ Degree Theor.	Inst. senst. $\delta\Delta/\delta t$	Inst. senst. $\delta\psi/\delta t$
5Da	280.0	23.42	23.47	155.85	155.41	1.02	0.07
5Ia	250.0	23.87	22.79	187.77	187.55	1.08	0.02
6Ab	282.0	23.61	23.61	153.75	153.38	1.00	0.07
6Db	278.6	23.24	23.34	157.76	157.47	1.03	0.06
6Ib	251.0	22.63	22.77	186.39	186.47	1.08	0.02
5Aa	248.0	23.24	22.84	189.22	189.71	1.08	0.03
5Ia	199.0	27.67	27.96	235.50	235.11	0.70	0.19
4Ga	252.0	22.78	22.75	185.90	185.39	1.09	0.02
7Ea	249.0	23.02	22.82	188.57	188.63	1.08	0.03

deg/nm and 0.19 deg/nm. This particular range of thicknesses, lie at the bottom of the loop of ψ against Δ, and this affects the value of $\delta\psi$. The significance of this will be seen when the results on anisotropy are discussed. For example $\delta\psi$ is equal to 0.31 and - 1.25 for 4G of batch nine and 6D for batch eight over a range of 20 nm.

2. The samples of batch ten are also silicon dioxide grown on silicon substrates with a refractive index of 1.45 which is stated by the equipment manufacturer's for the conditions used and was confirmed in this work by the computer model as discussed previously. The preparation conditions in this run were at a pressure of 0.8 Torr, and a r.f. power of 140W and a temperature of 380° C. Table 5.20 shows the variation between ψ and Δ for each sample. The difference in the values of ψ and Δ both across samples and below samples are very high in some cases. For example $\delta\psi$= 32.5 degrees and $\delta\Delta$= 108 degrees for sample 5D. The thickness variations (also given in Table 5.20) are of this order t = ±20 nm which are within the manufacturer's specification for the equipment used in the preparation process. Table 5.21 shows that ψ and Δ_λ values at the central point of the sample are in good agreement with the computed values to give thicknesses of each film, and to show the sensitivity of measurement which is in the range of 0.36, 0.67 for $\delta\Delta/\delta t$ and $\delta\psi/\delta t$ respectively, and these differences depend on the sample positions in the loop of ψ and Δ.

5.6 The Optimum Angle of Incidence

Initially the instrument was set up for the detection of oil contamination on gold layers and of aluminium hydroxide and oxide

Table 5.20

The measurement of ψ and Δ for SiO_2 (batch ten) in three different positions and the values of n' and k' at the central position only . $n_2=1.45, k_2=0, \lambda=632.8nm$ and $\phi=60$ degree

Sample	ψ Degree C	X or Y	$\bar{X}$ or $\bar{Y}$	Δ Degree C	X or Y	$\bar{X}$ or $\bar{Y}$	Pseudo constant n'	k'	t nm
5Da	50.50	54.75	18.03	116.37	127.27	224.43	0.5441	2.8160	13.5
6Ab	44.59	52.75	28.85	114.25	61.670	233.67	0.0393	2.1528	17.6
6Db	45.88	66.56	78.18	115.40	115.56	226.54	0.0866	2.2072	22.5
4Ga	51.46	44.96	50.22	115.22	111.91	247.42	0.6172	2.1022	20.0
7Ea	32.31	34.66	81.36	116.77	116.72	211.52	1.6661	1.8966	25.0

Table 5.21

The comparison between the experimental and the computer values of SiO (batch ten), n_2=1.45, k_2=0 for the centre position and the thickness of the sample.

Sample	Thickness nm	ψ Degree Exper.	ψ Degree Theor.	Δ Degree Exper.	Δ Degree Theor.	Instr. sensi. $\delta\Delta/\delta t$	Instr. sensi. $\delta\psi/\delta t$
5Da	383.0	50.50	50.14	116.37	117.94	0.69	0.85
6Ab	375.0	44.49	44.11	114.25	114.27	0.25	0.67
6Db	377.0	45.88	45.45	115.40	114.89	0.36	0.71
4Ga	379.0	51.46	46.92	115.22	115.69	0.45	0.76
7Ea	349.0	32.31	32.34	116.77	116.86	0.29	0.40

on aluminium and an angle of incidence of 60 - 65 degrees was used and when set the angle could not be varied. In the modified instrument there is an option of varying the angle of incidence. If the instrument is to be further used for silicon dioxide and silicon nitride on silicon or other combinations of substrate and surface layers it is important to optimise the angle of incidence for these materials. This section deals with the optimisation of the instrument for the detection of different materials based on the values of the optical constant already established in this work.

Figure 5.12 shows the curves of Ψ and Δ sensitivity as a function of angle of incidence for materials of different refractive index on a chromium base, when n = 2.97 and k_3 = 4.84 Smith and Hacskaylo[161]. Neal[2] determined the optimum angle of incidence for 304 stainless steel samples to be equal to 75 degrees and that for 304 oxide coated stainless samples to be equal to 72 degrees for thickness measurement in the range of 0-5 nm.

We investigated theoretically the optimum angles of incidence for both detection and thickness measurement for some samples which have been used in this work (Section 5.5). The theoretical results obtained for sensitivity (based on the presently determined values of optical constants) against angle of incidence are illustrated in Figs. 5.13, 5.14. The optimum angles for Si_3N_4 on Si, Si_3N_4 on Al, SiO_2 on Si were found to be 74.5, 77 and 75 degrees respectively, see Table 5.22. Table 5.23 shows the optimum angle for the detection of Si_3N_4 on Al, and shows the change in $\delta\Psi/\delta t$, $\delta\Delta/\delta t$, Ψ and Δ with the angle of incidence. The

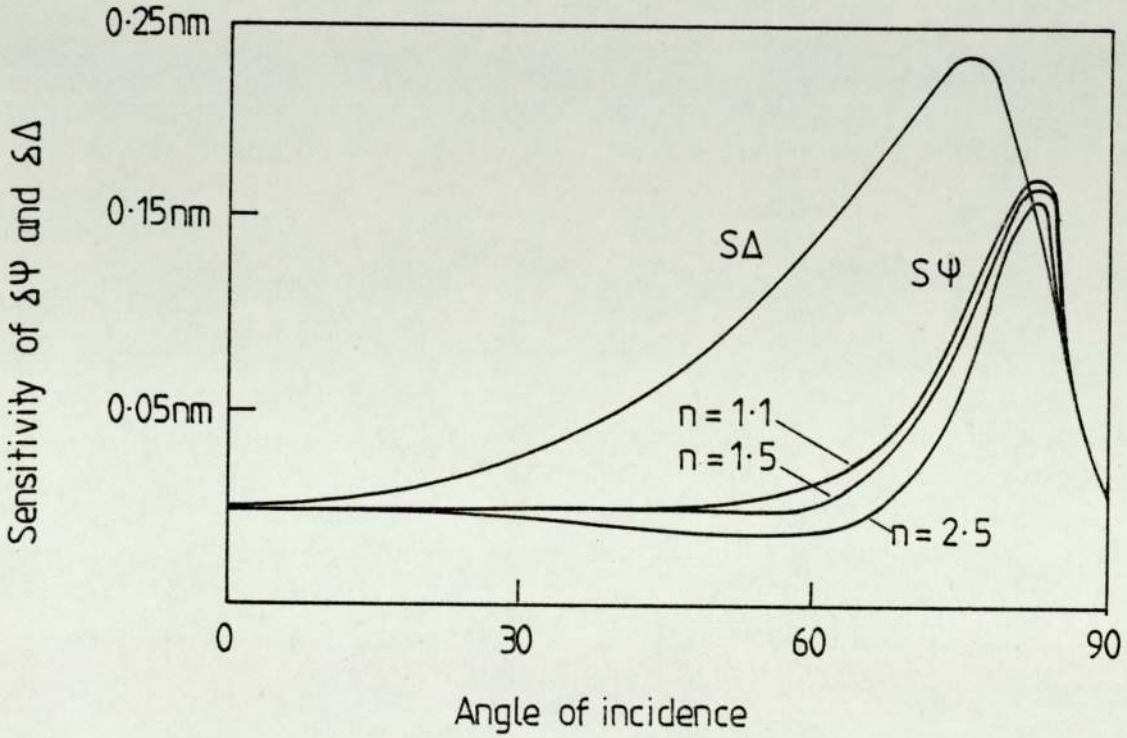

Figure 5·12 Ψ and Δ sensitivity vs. angle of incidence
[After Smith and Hacskaylo161]

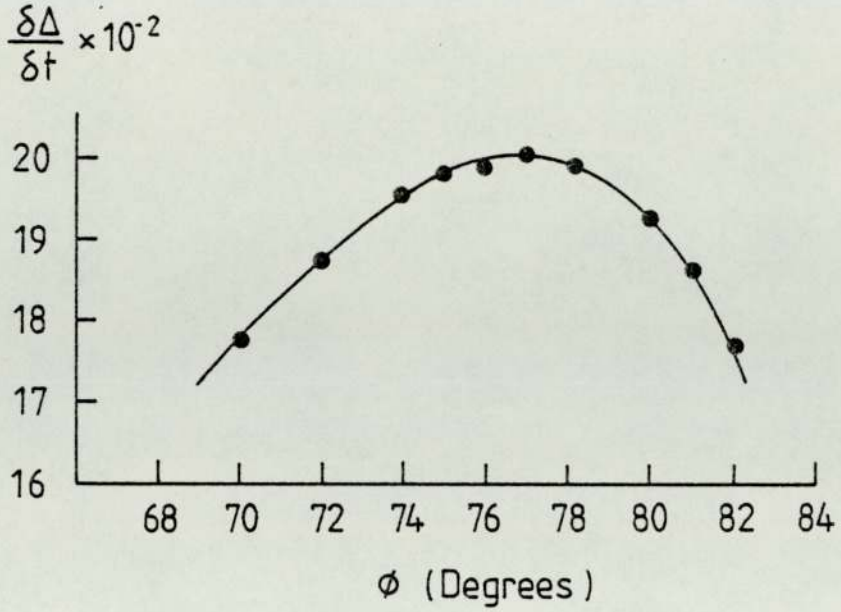

Figure 5·13 The optimum angle of incidence for the detection of a Si_3N_4 film on an Al substrate, where $n_2 = 2$, $k_2 = 0$, $n_3 = 0{\cdot}6926$ $k_3 = 4{\cdot}5229$ and $\lambda = 632{\cdot}8$ nm.

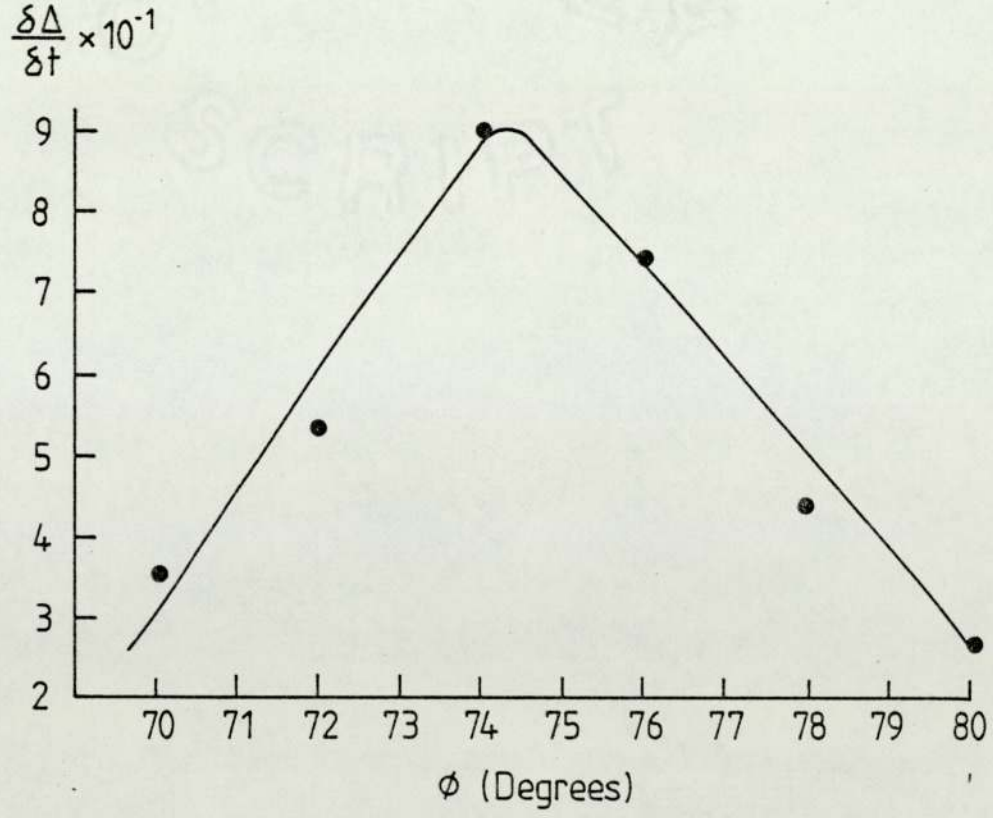

Figure 5·14 The optimum angle of incidence for the detection of a Si_3N_4 film on a Si substrate where $n_2 = 2$, $k_2 = 0$, $n_3 = 3{\cdot}7585$ $k_3 = 0{\cdot}0952$ and $\lambda = 632{\cdot}8$ nm

Table 5.22

The optimum angle of incidence for Si_3N_4 and SiO_2 and some assumed cases of thicknesses between 0 nm and 5 nm.

Sample	n_2	k_2	n_3	k_3	Optimum Angle
Case 1	2.0	0	1.31	1.14	60
Case 2	2.0	0	1.56	1.40	62
Case 3	2.0	0	2.0	0.5	64
Case 4	2.0	0	2.0	1.0	64
Case 5	2.0	0	1.0	2.0	66
Si N on Si	2.0	0	3.7585	0.0952	74.5
Si N on Al	2.0	0	0.6926	4.5229	77
Si O on Si	1.45	0	3.7585	0.0952	75

Table 5.23

The effect of the angle of incidence on the ellipsometer for detecting the Si_3N_4 film on Al, as shown in Fig.5.13. $n_2 = 2$, $k_2 = 0$, $n_3 = 0.69268$, $k_3 = 4.5229$ and $\lambda = 6328$ nm

Degree	Δ Degree	Ψ Degree	$\delta\Delta/\delta t$	$\delta\Psi/\delta t \times 10^{-2}$
70	122.48	41.47	0.178	.42
72	116.19	41.25	0.187	.58
74	109.02	41.05	0.195	.78
75	105.08	40.97	0.198	.88
76	100.90	40.91	0.199	.974
77	96.09	40.86	0.2006	1.20
78	91.13	40.83	0.199	.78
80	80.03	40.89	0..193	1.42
81	73.23	41.00	0.186	1.50
82	67.39	41.154	0.177	1.55
84	52.79	41.67	0.149	1.52

substrate affect on the optimum angle was very clear when the author used the pseudo constant for two samples of Si_3N_4 (Case (1) $n_3 = 1.3$ and $k_3 = 1.14$ prepared by r.f. sputtering method, Case (2) $n_3 = 1.56$, $k_3 = 1.4$ prepared by the glow discharge) as a substrate for a film with an optical constant of $n_2 = 2$ and $k_2 = 0$ (see Table 5.24). This is illustrated in Figures 5.15,16. The effect of this shows the optimum angle is shifted by two degrees. The author then assumed different values of n_3 and k_3 for the substrate (Case 3 where $n_3 = 2$, $k_3 = 0.5$ and Case 4 where $n_3 = 2.0$ and $k_3 = 1.0$ and Case 5 where $n_3 = 1.0$ and $k_3 = 2.0$) and assumed an optical constant for a film of $n_2 = 2$ and $k_2 = 0$ in all the cases Table 5.22. There was no affect on the optimum angle (64 degrees) when k_3 was changed from 0.5 to 1.0 in cases 3 and 4. It shifted by two degrees when $k_3 = 2$ and $n_3 = 1$ in case 5 where the optimum angle was found to be 66 degrees and the angle increased from 66 to 74.5 degrees with $n_3 = 3.7585$ and $k_3 = 0.0952$ for the Si_3N_4 on Si and to 75 for the SiO_2 on Si and reached 77 degrees for the Si_3N_4 on an aluminium substrate. The way in which the value of the optimum angle of incidence depends on the substrate used is clearly illustrated on the Si_3N_4 films because there are two optimum angles of incidence for the same film, but with a different substrate, where the optimum angle changes from 74.5 degrees to 77 degrees when the substrate was silicon and aluminium respectively.

The optimum angle of incidence varies with the film thickness changes as we found when we assumed a film of Si_3N_4 on Al of a thickness between 90 - 100 nm, 130 - 140 nm and 150 - 200 nm where the optimums were 74 , 82 and 70 for the three regions respectively, as shown in Table 5.25. But if the optimum angle

Table 5.24

The effect of the incidence angle on the ellipsometer for detecting the growth of a film on $Si_3 N_4$ (Glow discharge), the optimum angle is shown in Fig. 5.15, where $n_1 = 2$, $k_2 = 0$, $n_3 = 1.5662$, $k_3 = 1.4323$ and $\lambda = 6328$ n m.

Φ Degree	Δ Degree	ψ Degree	$\delta\Delta/\delta t$	$\delta\psi/\delta t \times 10^{-2}$
52	142.69	29.91	0.0984	.92
54	133.55	27.79	0.118	.526
56	128.24	26.80	0.127	.24
58	122.34	25.89	0.136	.12
60	115.72	25.09	0.1424	.56
62	108.72	24.47	0.1462	1.06
64	101.01	24.06	0.1462	1.58
66	92.79	23.09	0.142	2.12
68	84.23	24.03	0.134	2.60
70	75.37	24.49	0.122	3.02

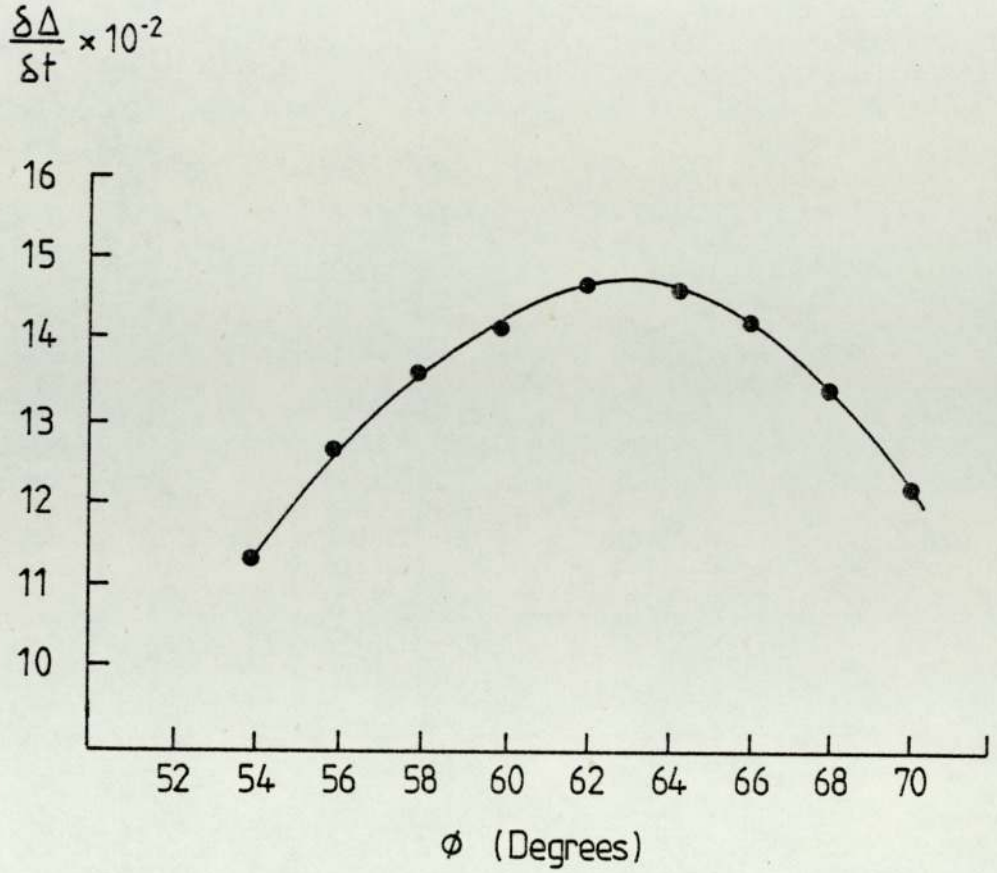

Figure 5·15 The optimum angle of incidence for the detection of a film with optical constant of $n_2 = 2$, $k_2 = 0$ on substrate of optical constant of $n_3 = 1{\cdot}566$ and $k_3 = 1{\cdot}4323$ (Case 2) and $\lambda = 632{\cdot}8$ nm. (Computer model)

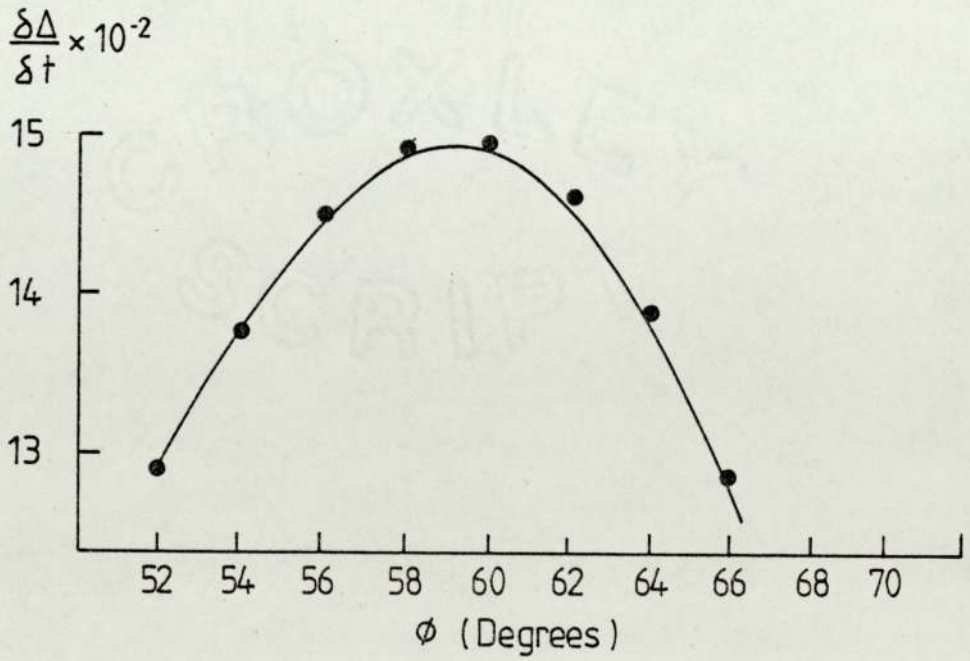

Figure 5·16 The optimum angle of incidence for the detection of a film with a refractive index of $n_2 = 2$, $k_2 = 0$ on substrate of refractive index of $n_3 = 1{\cdot}3082$ and $k_3 = 1{\cdot}1428$ (Case 1) $\lambda = 632{\cdot}8$ nm. (Computer model)

Table 5.25

The effect of the angle of the incidence on the ellipsometer for measuring the thickness of Si_3N_4 films on aluminium substrate in three different regions

Angle of Incidence	$\delta\Delta/\delta t$ Deg./nm (90 nm-100 nm)	$\delta\Psi/\delta t$ Deg./nm (90 nm-100 nm)	$\delta\Delta/\delta t$ Deg./nm (130 nm-140 nm)	$\delta\Psi/\delta t$ Deg./nm (130 nm-140 nm)	$\delta\Delta/\delta t$ Deg./nm (150 nm-200 nm)	$\delta\Psi/\delta t$ Deg./nm (150 nm-200 nm)
60	1.38×10^{-2}	1.21	12.31×10^{-1}	0.5×10^{-2}	1.23	0.6×10^{-2}
62	1.16×10^{-2}	1.33	13.53×10^{-1}	0.8×10^{-2}	1.34	0.88×10^{-2}
64	0.90×10^{-2}	1.44	14.88×10^{-1}	1.2×10^{-2}	1.45	1.26×10^{-2}
66	0.61×10^{-2}	1.55	16.36×10^{-1}	1.7×10^{-2}	1.58	1.78×10^{-2}
68	0.31×10^{-2}	1.64	17.98×10^{-1}	2.5×10^{-2}	1.72	2.4×10^{-2}
70	0.01×10^{-2}	1.71	19.71×10^{-1}	3.7×10^{-2}	1.87	3.2×10^{-2}
72	$0.2A \times 10^{-2}$	1.74	21.69×10^{-1}	5.3×10^{-2}	1.78	4.2×10^{-2}
74	0.54×10^{-2}	1.75	23.68×10^{-1}	7.6×10^{-2}	1.61	7.4×10^{-2}
76	0.75×10^{-2}	1.71	25.68×10^{-1}	10.8×10^{-2}	1.52	9.8×10^{-2}
78	0.82×10^{-2}	1.61	27.59×10^{-1}	15.3×10^{-2}	1.45	12.96×10^{-2}
80	0.94×10^{-2}	1.47	28.93×10^{-1}	21.2×10^{-2}	1.41	17.30×10^{-2}
82	0.91×10^{-2}	1.27	29.09×10^{-1}	27.8×10^{-2}	-	-
84	0.78×10^{-2}	1.20	27.09×10^{-1}	60.1×10^{-2}	-	-
86	0.57×10^{-2}	1.71	21.69×10^{-1}	34.7×10^{-2}	-	-

was calculated for the thickness range 0 - 50 nm and 0 - 200 nm, the optima were 73 degrees and 71 degrees as shown in Figs. 5.17,18. From this calculation we found that the optimum angle decreased with the thickness (when we neglect the range between 130 - 140 nm) and the best angle to use for an experimental measurement of a $Si_3 N_4$ film on aluminium up to 200 nm thick will be 73 degrees which is the average value. By using this value, the sensitivity will be reasonably high all over the range of the thicknesses.

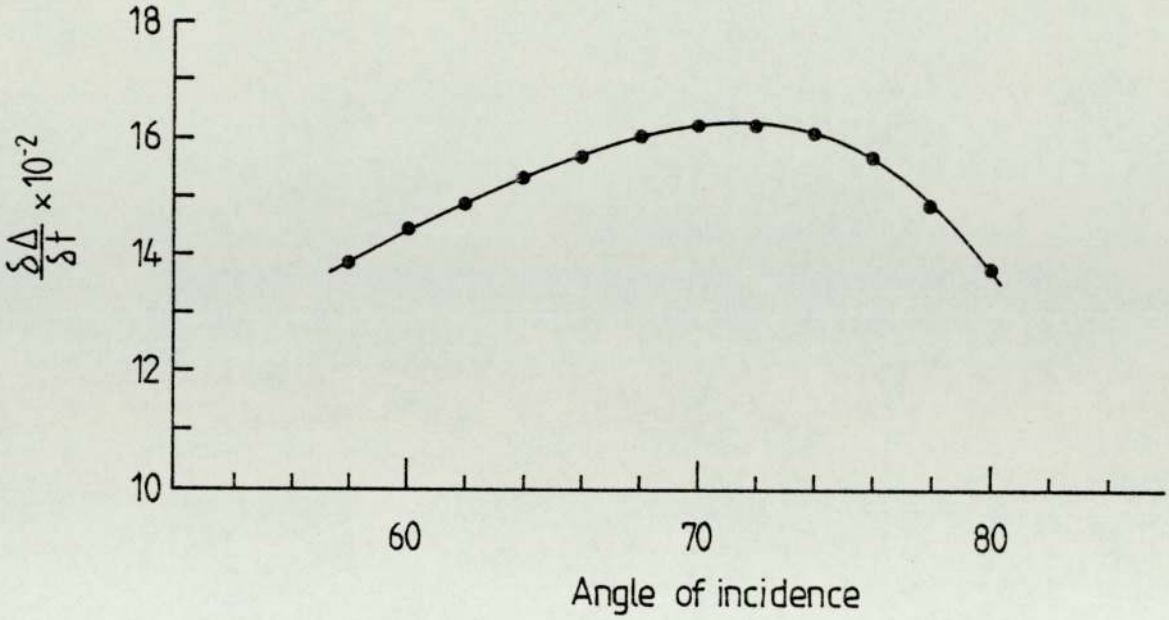

Figure 5·17 The optimum angle of incidence for Si_3N_4 on Al. For a range between 0 - 200nm.

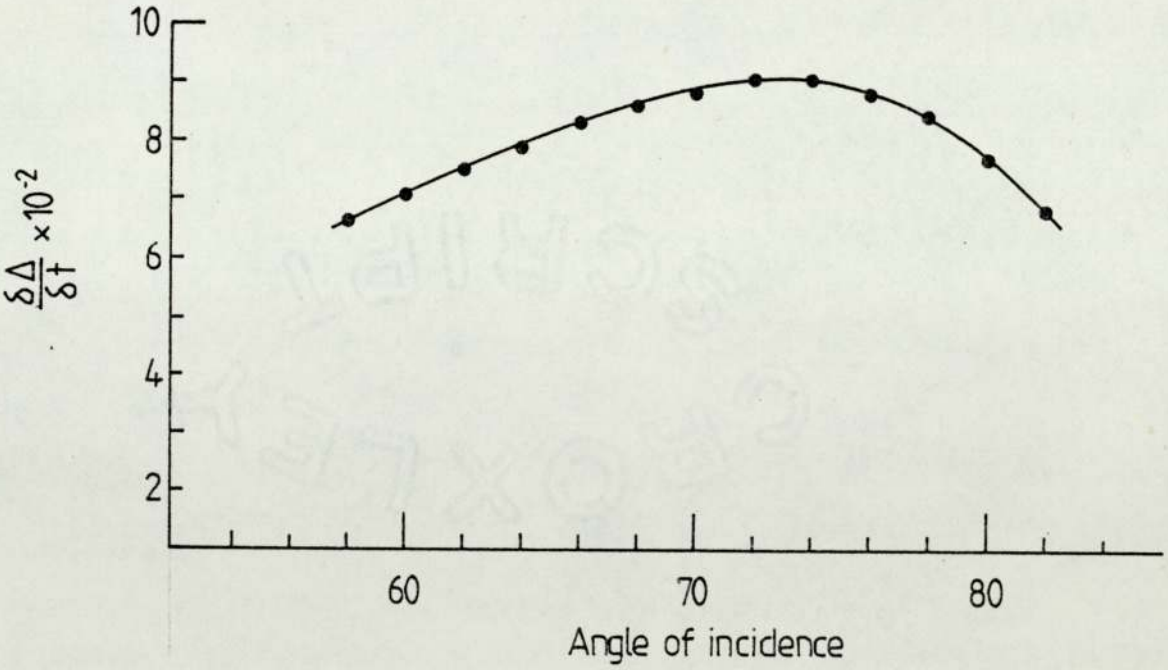

Figure 5·18 The optimum angle of incidence for Si_3N_4 on Al. For a range between 0 - 50 nm.

CHAPTER VI

ANISOTROPY IN SILICON
(RESULTS AND DISCUSSION)

6.1. R.F. Sputtered Films

Samples of different layers of SiO_2 and Si_3N_4 (supplied by the Lucas Research Centre and prepared by the r.f. sputtering technique) were initially used for sensitivity and for thickness measurements. These were also examined for optical anisotropy, as mentioned in Section 4.3.5, and no change in the measured values of Ψ and Δ were observed when the samples were rotated about a normal to its surface. This indicates that it was not possible to detect optical anisotropy in these samples. It should be noted that all samples were less than 400 nm thick.

6.2. Thermally Grown Silicon Dioxide Films

The variation of the ellipsometer parameters (Ψ and Δ) of a thermally grown silicon dioxide layer when a film is rotated about the normal to its surface as illustrated in Table 6.1. This indicates that anisotropy is present on its surface. In this particular film the amplitudes of the variations in Ψ and Δ were 0.22 degrees and 0.48 degrees respectively. Similar variations were detected in oxide films of 400 nm thickness and above, see Table 6.2. The films of silicon dioxide were thermally grown at 1100 °C and oxidation was carried out as described in Section 4.3.6.3.

The effects on the angles of Ψ and Δ by rotating samples of

Table 6.1

The variation of the angles ψ and Δ when a sample of thermally grown silicon dioxide is rotated 360 degrees about a normal to its surface .

Angle of rotation	Δ Degree	ψ Degree
0	237.62	29.57
40	237.97	29.75
80	237.54	29.96
120	237.24	29.87
160	237.75	29.65
200	237.76	29.63
240	237.28	29.86
280	237.55	29.97
320	237.06	29.75
360	237.62	29.56

Table 6.2

The amplitudes of the angles Ψ and Δ when samples of thermally grown silicon dioxide of varying thickness are rotaated about a normal to their surfaces.

Sample	Thickness nm	Amplitude Ψ Degree	Amplitude Δ Degree
20	664.5	0.12	0.25
24	128.15	0.22	0.48
25	995.9	0.17	0.395
28	700.9	0.13	0.275
31	400.2	0.09	0.14
45	1456.3	0.25	0.55
52	1545.2	0.25	0.575

films of thickness greater than 400 nm through 360 degrees at a constant angle of incidence are shown in Figs. 6.1 - 7. Table 6.2 shows that the measured amplitudes of ψ and Δ vary with film thickness and this is also illustrated in Fig. 6.8. Sample 24 (Fig. 6.1) gives an amplitude of ψ and Δ 0.22 and 0.48 degrees respectively. The lowest measureable amplitude was found to be in the region of 0.1 degrees and 0.2 degrees for ψ and Δ respectively and this was for a film thickness of 400 nm.

The changes in the values of ψ and Δ as the film is rotated, indicates a change in the values of the refractive index. The appropriate indices have been evaluated at three different positions a, b and c, in the cycle (see Fig. 6.1). for a number of flims and the appropriate values are given in Table 6.3

As previously stated optical anisotropy existed in all silicon dioxide samples greater than 400 nm thick. It was found that optical anisotropy (δN) ranged (between points a-c on different samples) from 1.0 X 10^{-3} to 8 X 10^{-3}, depending on the thickness of the film as shown in Table 6.3. The lowest change in optical constant was observed at 400 nm and 1200 nm where $\delta N_{ac} = 1.0 \times 10^{-3}$ and the highest value of δNac was for film thicknesses 999 nm and 1440 nm where $\delta N_{ac} = 8.0 \times 10^{-3}$. The remainder lay between these two values. This leads us to the initial conclusion that the optical anisotropy is dependent on the film thickness. However the sensitivity of the instrument depends on thickness as explained in Section 5.4, and this could affect the conclusion. The sensitivity influence will be discussed later.

As mentioned in Section 5.1 the error in the thickness measurement as a result of anisotropy, will affect the sensitivity

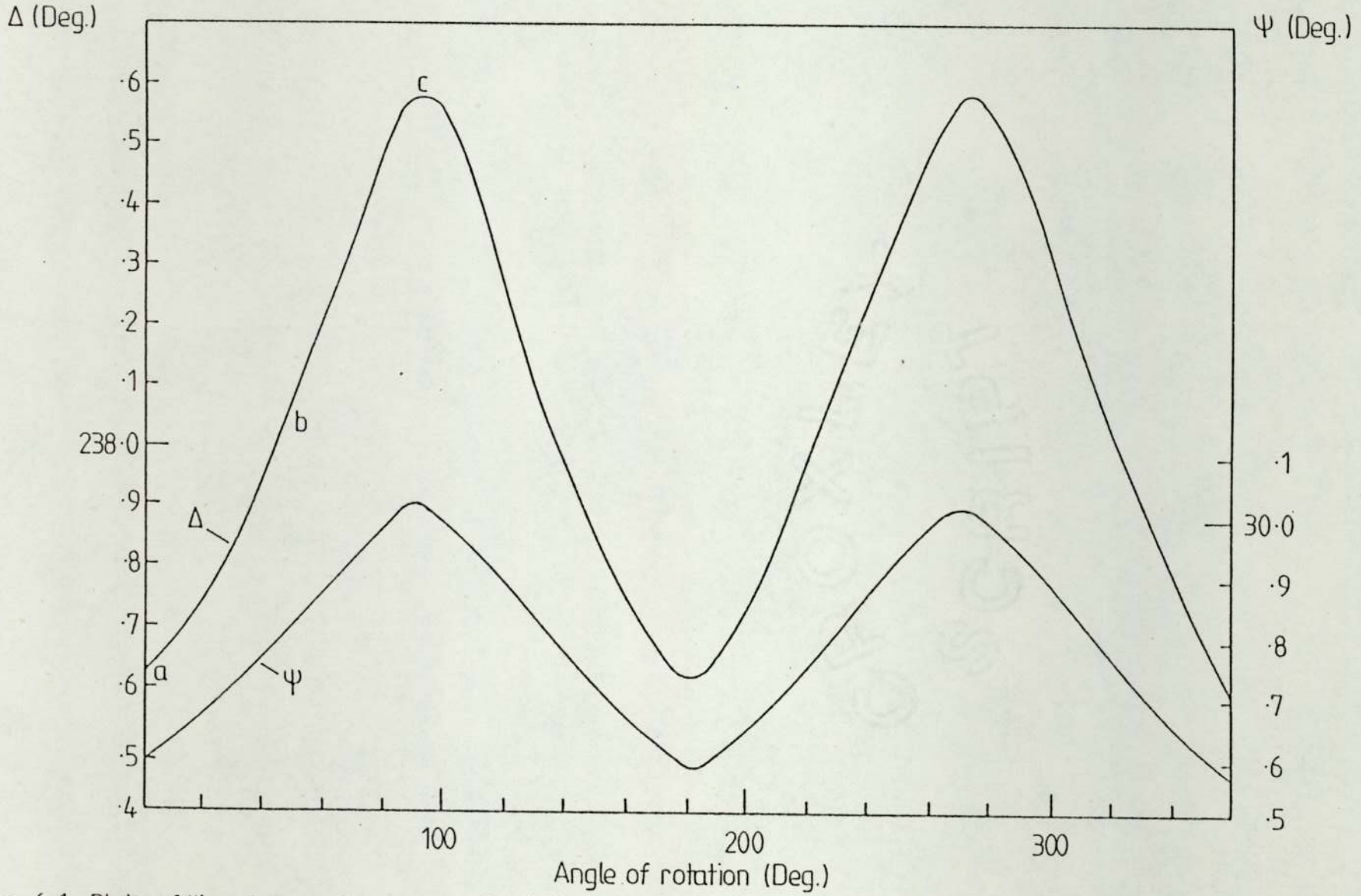

Figure 6·1 Plots of Ψ and Δ against angle of rotation for sample 24 (t = 1281·5 nm) for SiO_2. The positions a, b and c are the positions where the value of N was calculated. Instrument sensitivity at 1280 nm: $\frac{\delta t}{\delta \Delta}$ and $\frac{\delta t}{\delta \Psi}$ = 1·97 and 4·07 nm/deg. respectively

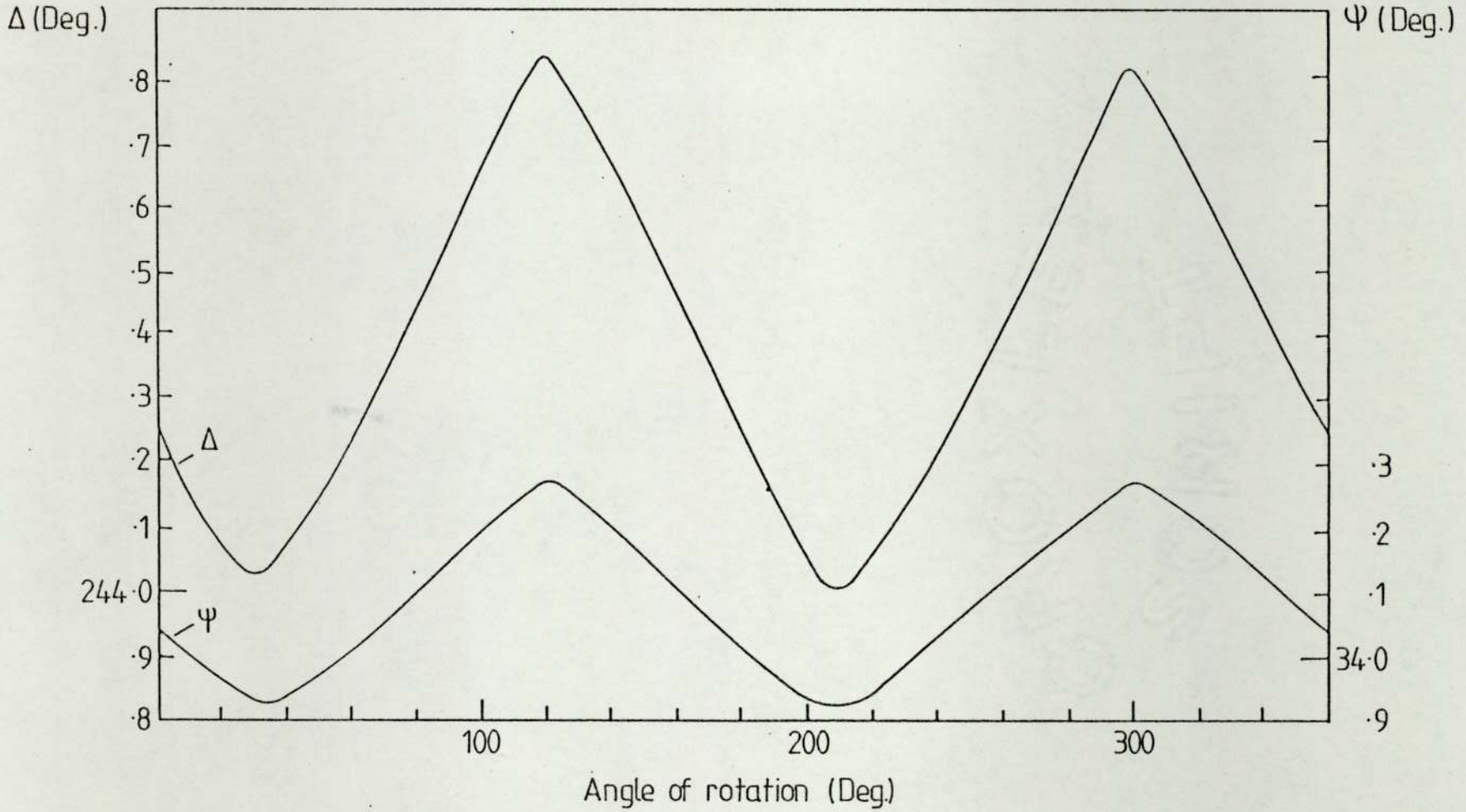

Figure 6·2 The variation of the values of Ψ and Δ against the angle of rotation for sample 25 ($t = 995{\cdot}9$nm) for SiO_2
Instrument sensitivity at 1000nm: $\frac{\delta t}{\delta \Delta}$ and $\frac{\delta t}{\delta \Psi}$ = 2·79 and 3·13nm/deg. respectively.

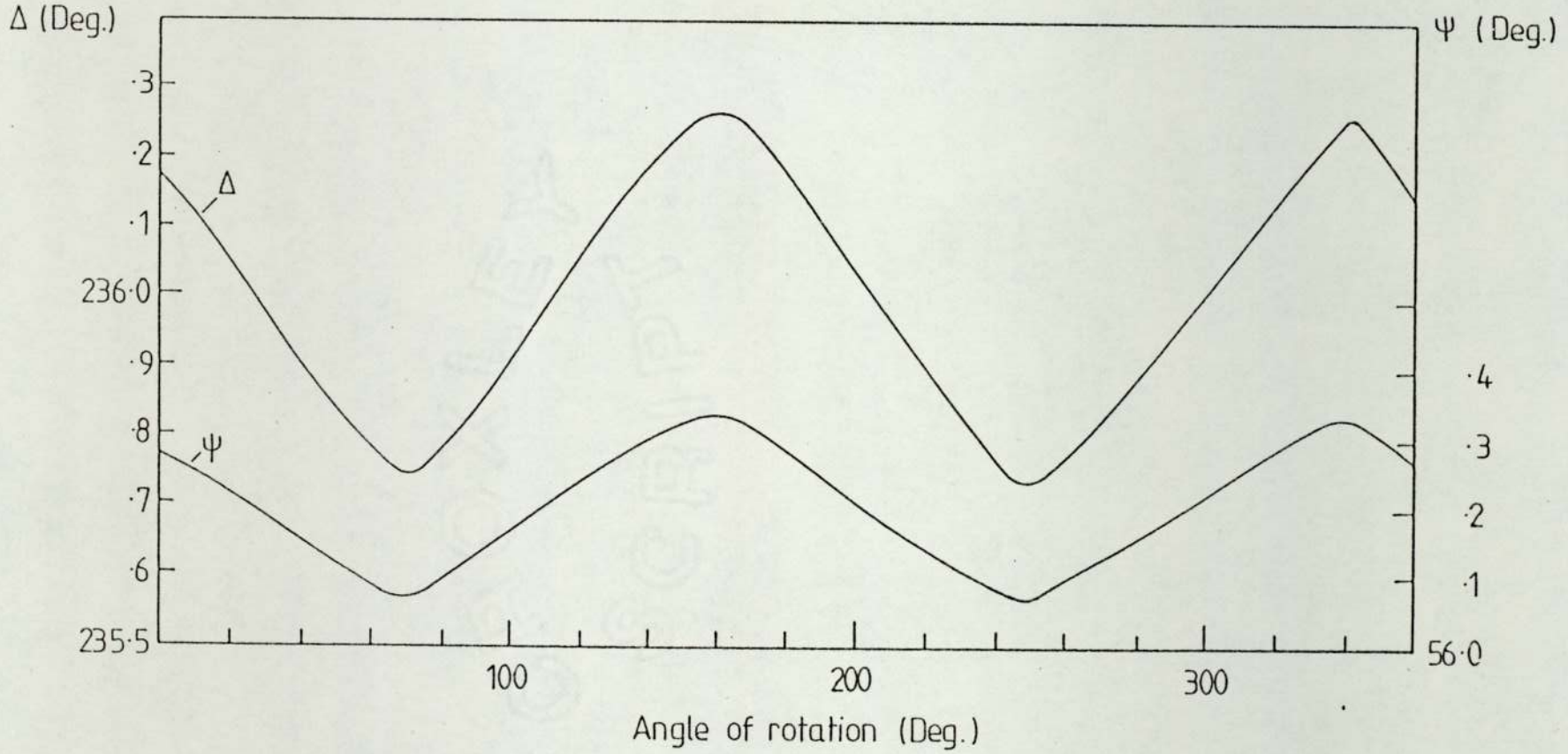

Figure 6·3 The variation of the Ψ and Δ as a function of the angle of rotation for sample 23 ($t = 692{\cdot}8$ nm) for SiO_2
Instrument sensitivity at 700 nm: $\frac{\delta t}{\delta \Delta}$ and $\frac{\delta t}{\delta \Psi}$ = -1·42 and 1·18 nm deg. respectively.

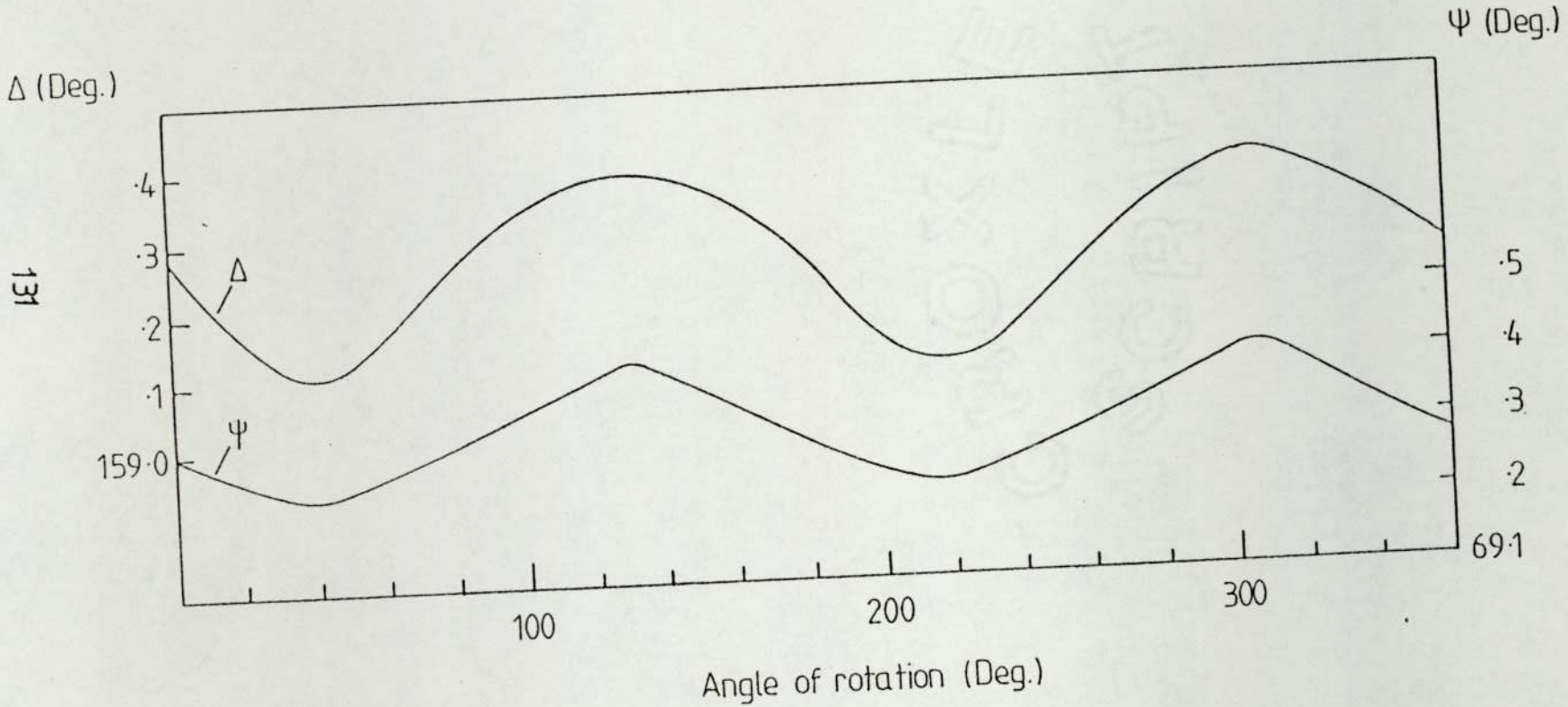

Figure 6·4 The change in Ψ and Δ as function of the angle of rotation for sample 31 (t=400·2nm) for SiO_2
Instrument sensitivity at 400nm: $\frac{\delta t}{\delta \Delta}$ and $\frac{\delta t}{\delta \Psi}$ = -0·25 and -2·45nm deg. respectively.

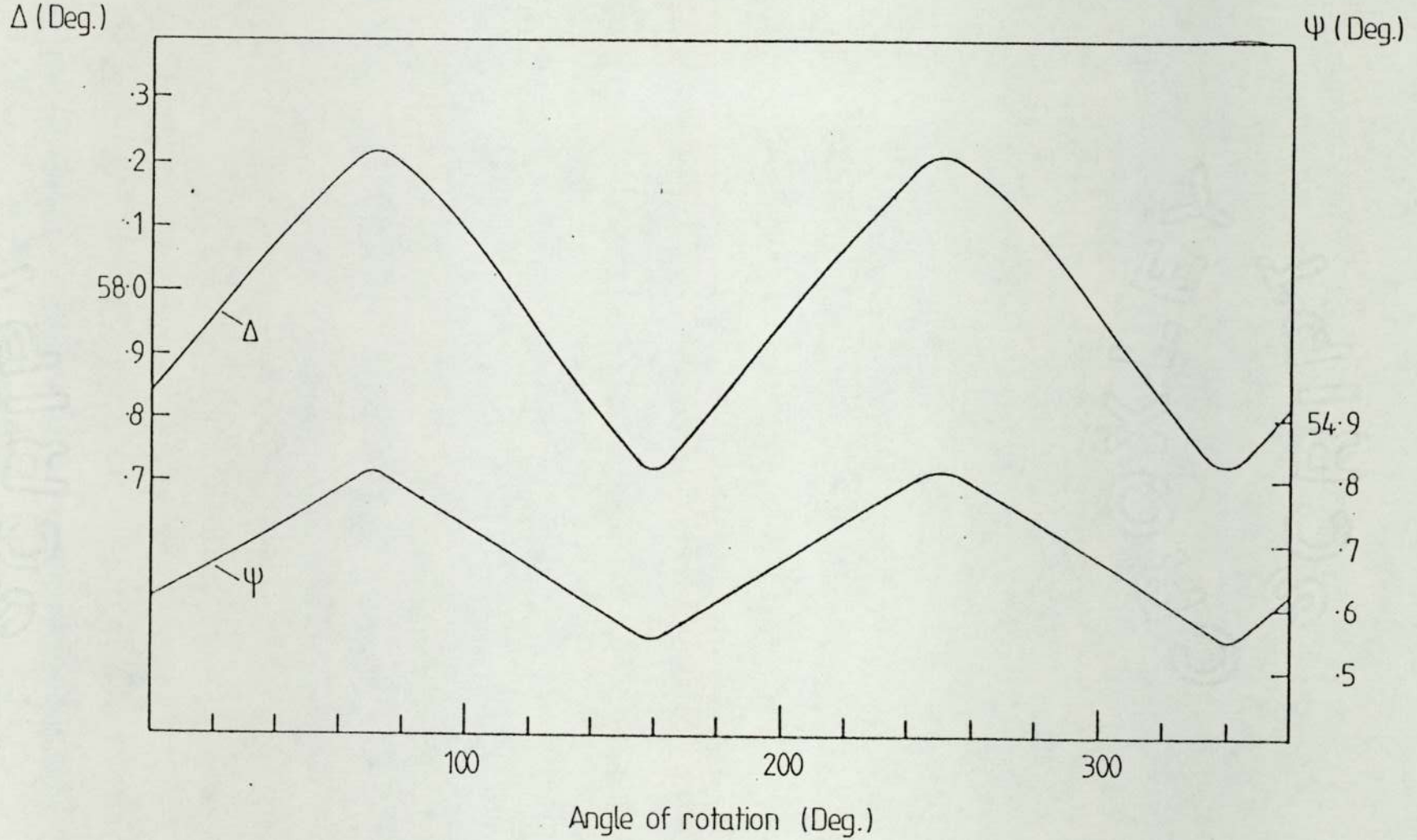

Figure 6·5 The change in Ψ and Δ as a function of the angle of rotation for sample 36 (t = 695 nm) for SiO_2 The substrate orientation is (100). Instrument sensitivity at 700 nm: $\frac{\delta t}{\delta \Delta}$ and $\frac{\delta t}{\delta \Psi}$ = 1·46 and 1·19 nm / deg. respectively.

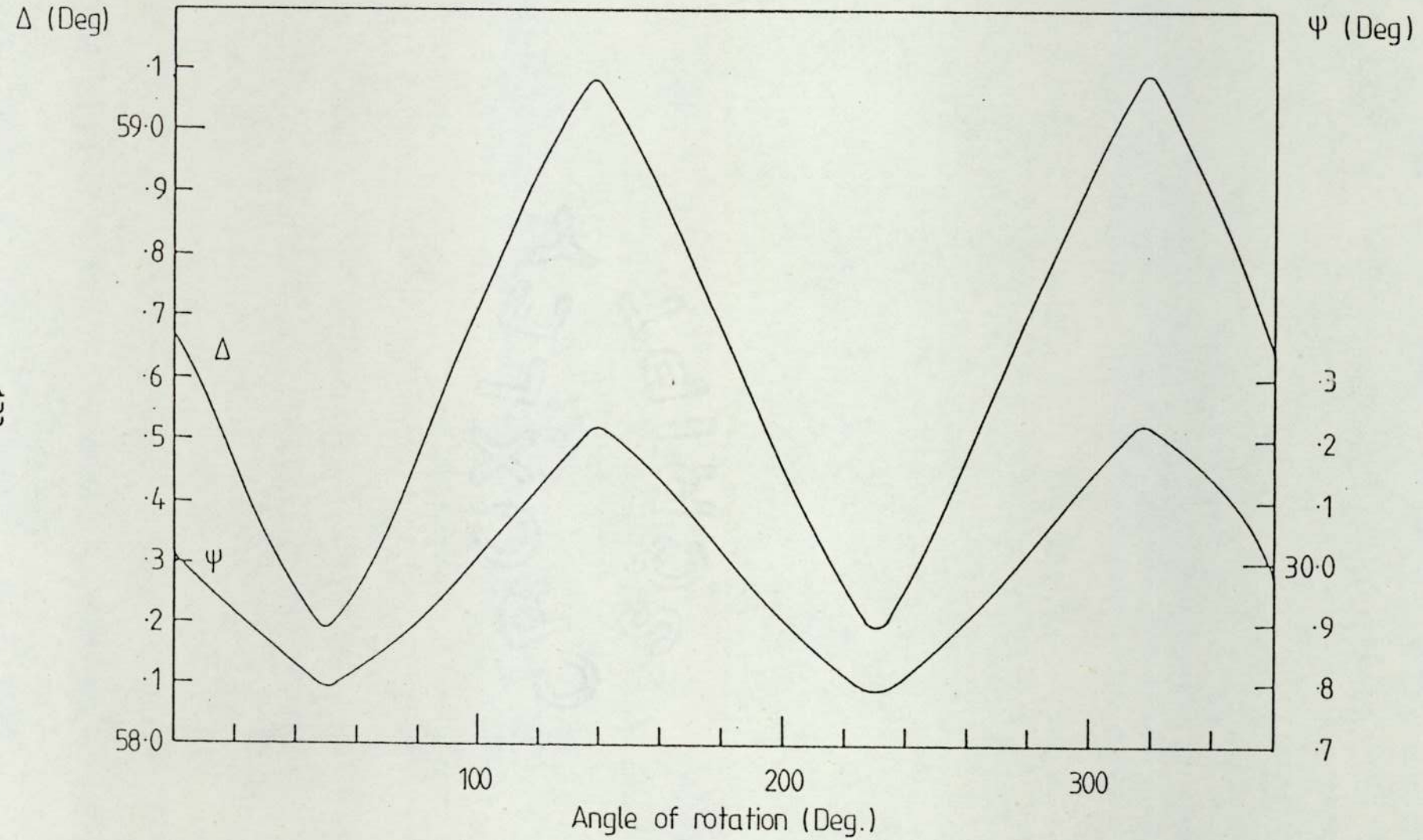

Figure 6·6 The change in Ψ and Δ as a function of the angle of rotation for sample 34 ($t = 1280{\cdot}2$ nm) for SiO_2
The substrate orientation is (100)
Instrument sensitivity at 1290 nm: $\frac{\delta t}{\delta \Delta}$ and $\frac{\delta t}{\delta \Psi}$ = 1·55 and 5·05 nm / deg. respectively.

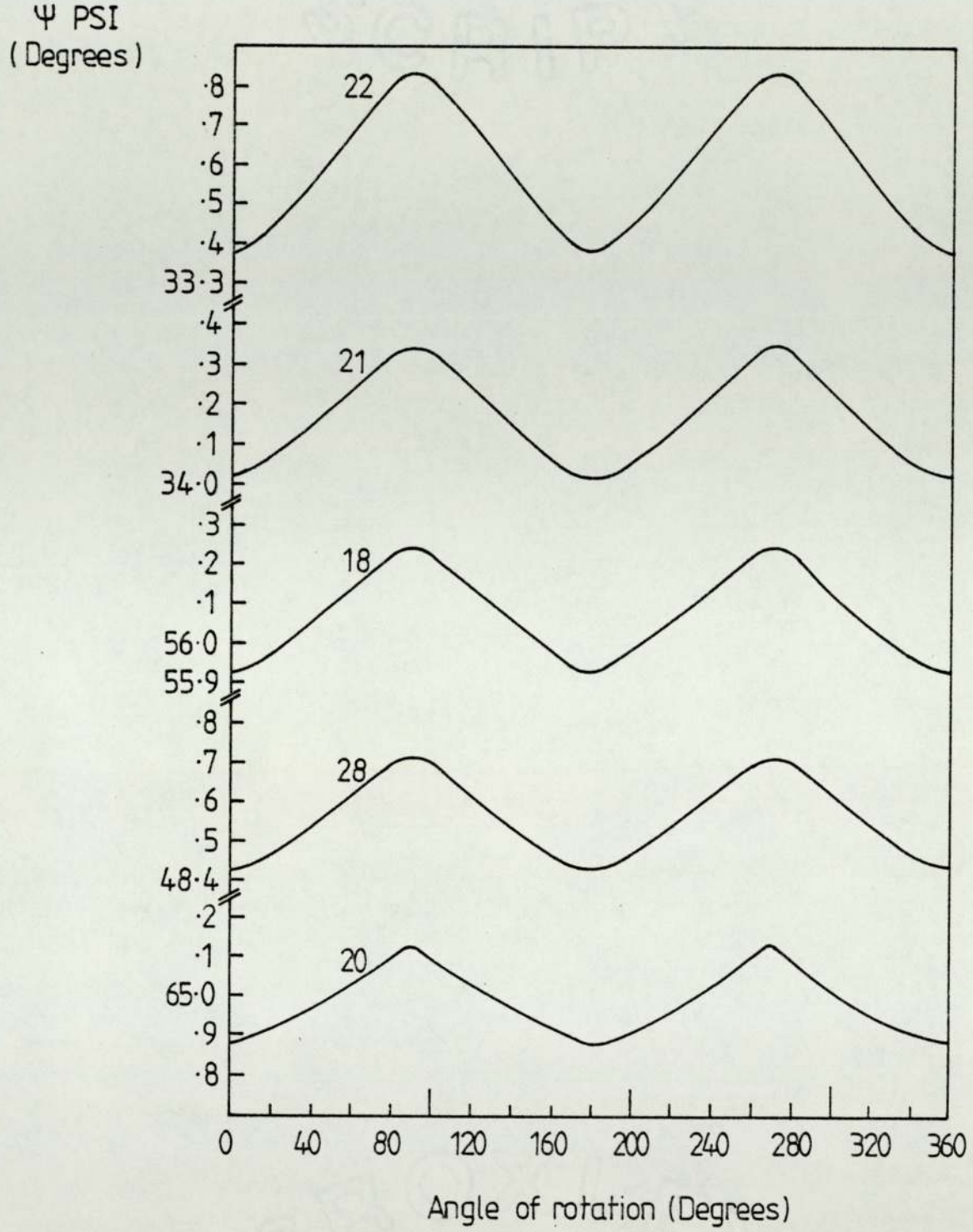

Figure 6·7a The change in the value of Ψ as a function of angle of rotation for different samples as illustrated in the plots. Samples (18, 20, 21, 22, 28)

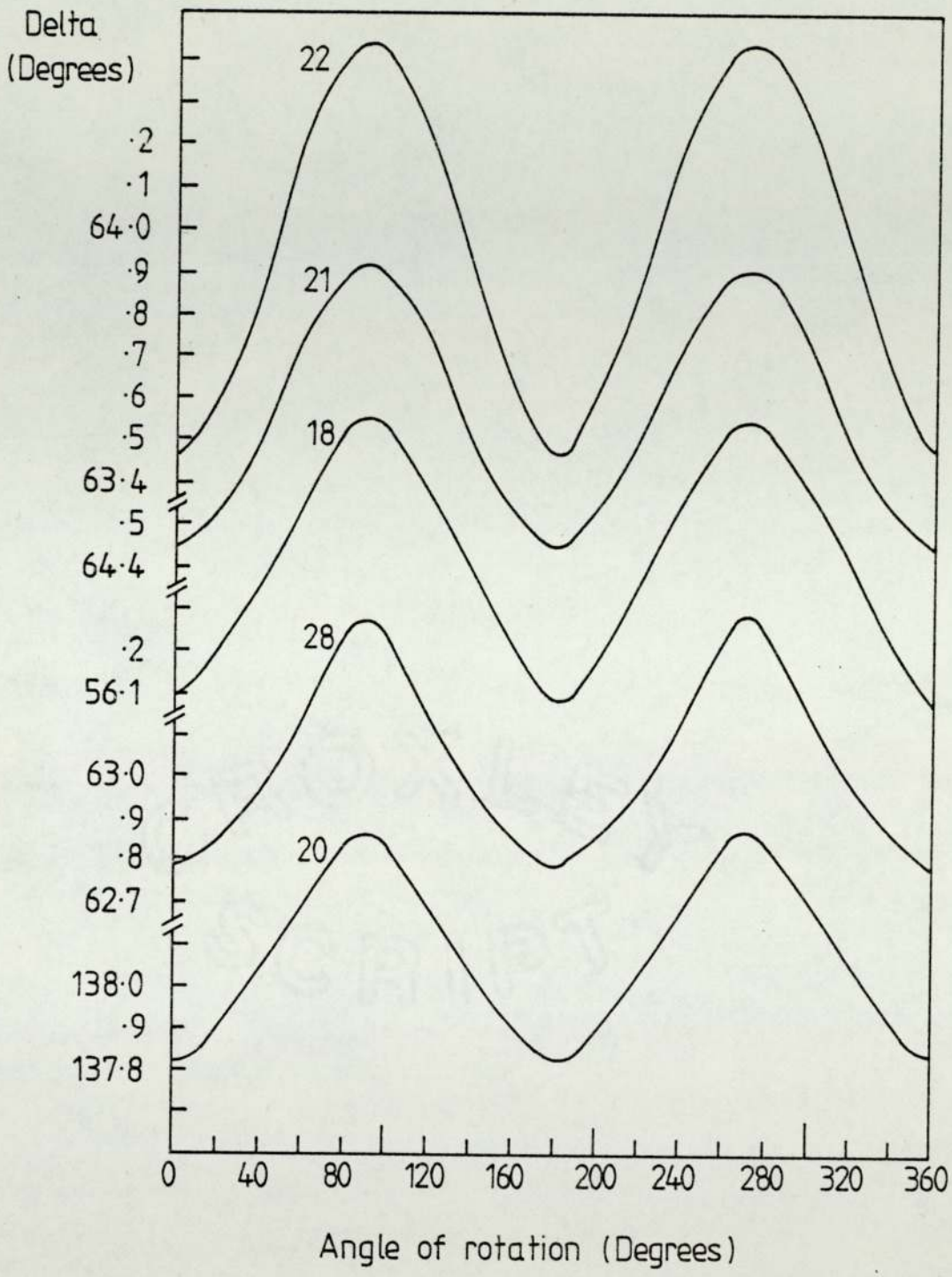

Figure 6·7b The variation of the Δ angle as a function of the angle of rotation for different samples, as shown in the plots. Samples (18, 20, 21, 22, 28)

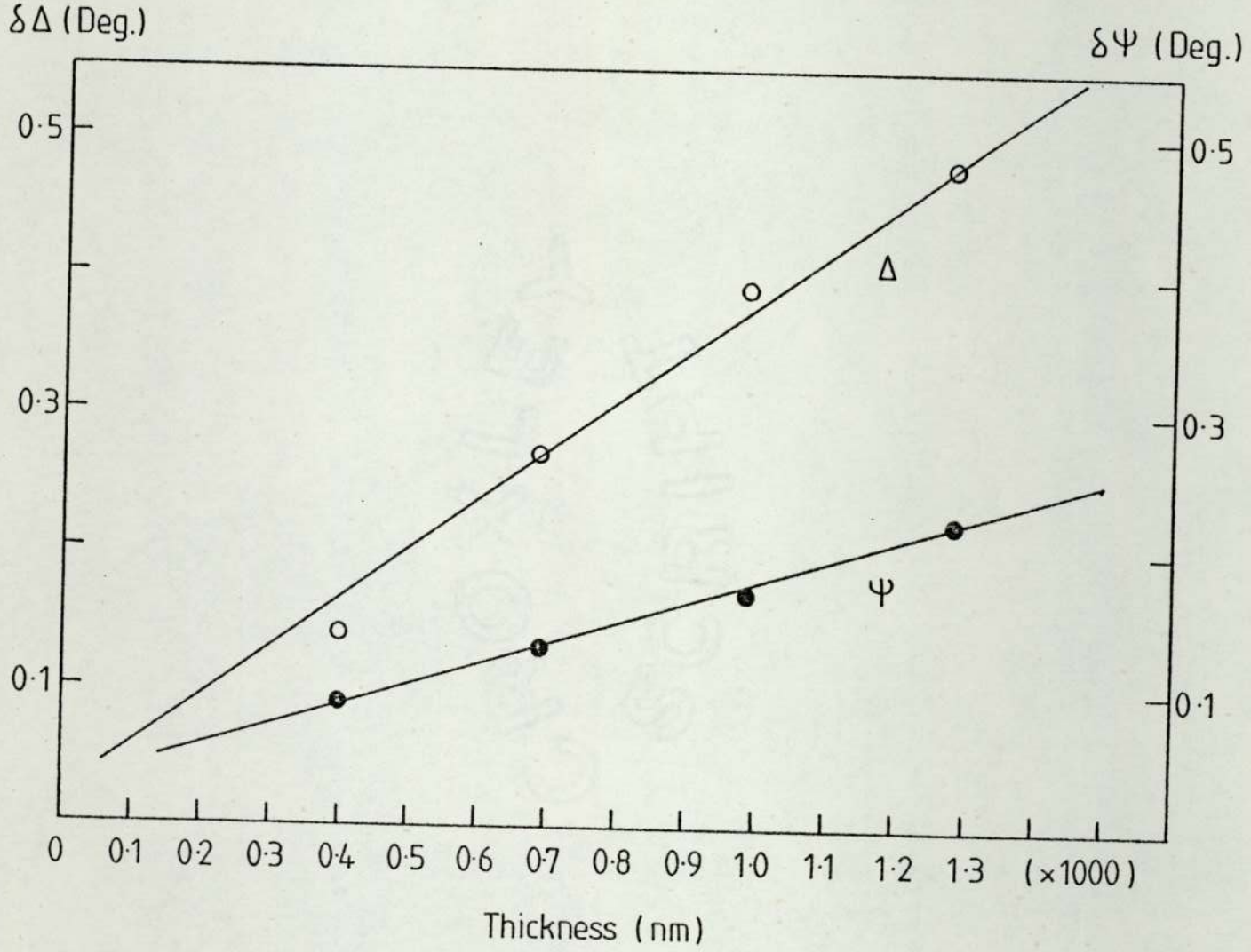

Figure 6.8 The changing amplitude for Ψ and Δ for oxide films of different thickness.

Table 6.3

The variation in the refractive index in three different position (see Fig. 6.1) for different samples .

Sample	Thickness (t_b) nm	n_a	n_b	n_c	δN_{ac}
11	926.1	1.4589	1.4554	1.4519	7.0×10^{-3}
16	899.4	1.4555	1.45925	1.4630	7.5×10^{-3}
18	961.8	1.4546	1.45740	1.4621	7.5×10^{-3}
20	664.5	1.4555	1.4570	1.4585	2.9×10^{-3}
21	991.4	1.45751	1.4614	1.4653	7.8×10^{-3}
22	1267.9	1.4587	1.4571	1.4577	1.0×10^{-3}
23	692.8	1.4540	1.4559	1.4578	3.8×10^{-3}
24	1281.5	1.4566	1.4571	1.4575	0.9×10^{-3}
25	995.9	1.4540	1.4575	1.4620	8.0×10^{-3}
28	700.9	1.4540	1.4560	1.4579	3.9×10^{-3}
29	916.8	1.4570	1.4540	1.4510	6.0×10^{-3}
31	400.2	1.4566	1.4571	1.4576	1.0×10^{-3}
36	695.0	1.4549	1.4565	1.4586	3.7×10^{-3}
40	1280.2	1.4577	1.4572	1.4567	1.0×10^{-3}
45	1456.3	1.4583	1.4514	1.4500	8.3×10^{-3}
52	1545.2	1.4499	1.4535	1.45917	9.3×10^{-3}

of the measurement. In Table 6.4, the thickness variation δt ranges from 0.1 nm for a film 400 nm thick (which is the lowest change that can be measured) to 13.6 nm for a film 1440 nm thick.

6.2.1 Stress Measurement

The optical anisotropy which was observed in the oxide film as described in Section 6.2, enabled the calculation of the stress in the film to be made by using eq. (3.45). Stress in thermally grown silicon dioxide has been observed by several authors as described in Section 2.5.1.1. The only stress calculation as far as the author is aware based on ellipsometry has been reported by Pedinoff[85] by using values of the optical anisotropy. He reported the stress $\sigma = -2.472 \times 10^{8}$ N/M^2 for a film with a thickness of 1185 nm. Taft and Corder[123] estimated that the stress would be in the range of $2 - 3 \times 10^{8}$ N/M^2 for a film thickness of more than 150 nm, and this aspect will be described later.

Table 6.5 shows how the stress 'σ' for the films observed in the present work depend on the value of the optical anisotropy. The stress was calculated by using eq. (3.45). The values of π_{11} of 0.43×10^{12} M/N and π_{12} of 2.7×10^{12} M/N were taken from Primak and Post[164] and Waxler et al.[165] respectively. The stress-optic facor is evaluated from eq.(3.45) by using the value of $n_2 = 1.457$ for the refractive index of the oxide as verified in this work (Section 5.5). Thus the stress can be obtained as follows:

$$\sigma = 2.85 \times 10^{11} \text{ N/M}^2 \times \delta N$$

Table 6.4

The variation in the film thickness in three different positions (see Fig.6.1) for different samples

Sample	Thickness nm(t_b)	t_a	t_b	t_c	δt nm
18	961.8	964.6	961.8	956.6	8.0
21	991.4	996.1	991.4	987.0	9.1
22	1267.9	1269.7	1267.9	1265.6	4.1
23	692.8	694.3	692.8	691.3	3.0
24	1281.5	1282.9	1281.5	1279.9	3.0
25	995.9	1000.1	995.9	990.6	9.5
36	695.0	695.2	693.9	692.3	2.9
45	1456.2	1449.5	1456.3	1463.1	13.6

Table 6.5

The optical anisotropy has been observed on all these samples by rotating the samples about a axis normal to the surface.

Sample	Thickness nm	δN_{ac}	σ N/M^2
11	926.1	7.0×10^{-3}	9.98×10^{8}
16	899.4	7.5×10^{-3}	1.07×10^{9}
18	961.8	7.5×10^{-3}	1.07×10^{9}
20	664.5	3.0×10^{-3}	4.28×10^{8}
21	991.4	7.8×10^{-3}	1.11×10
22	1267.9	1.0×10^{-3}	1.43×10^{8}
23	692.8	3.8×10^{-3}	5.42×10^{8}
24	1282.9	0.9×10^{-3}	1.28×10^{8}
25	995.9	8.0×10^{-3}	1.14×10^{9}
28	700.9	3.9×10^{-3}	5.56×10^{8}
29	917.0	6.0×10^{-3}	8.55×10^{8}
31	400.2	1.0×10^{-3}	1.43×10^{8}
36	695.0	3.7×10^{-3}	5.27×10^{8}
40	1280.2	1.0×10^{-3}	1.43×10^{8}
45	1456.3	8.3×10^{-3}	1.18×10^{9}
52	1545.2	7.3×10^{-3}	1.04×10^{9}

For the calculation of σ the value of δN_{ac} used was equal to $\delta N_{ac}/2$. From Table 6.6 it is clear that the highest values of σ are equal to 1.18×10^{9} N/M^2 for $\delta N_{ac} = 8.3 \times 10^{-3}$ for a film thickness of 1456.3 nm and the lowest value was 1.28×10^{8} N/M^2 when $\delta N_{ac} = 9 \times 10^{-4}$.

Pedinoff discussed the effect of reduction in anisotropy as a result of annealing oxide films. In our investigation the samples were annealed at 950 °C (which is below the temperature at which the oxide was grown) in a nitrogen atmosphere for different periods to examine the annealing effect on the stress measurement. Sample 24 was annealed for different periods (30 min., 60 min. and 90 min.) to study the change in Ψ, Δ and δN_{ac} and the results are shown in Table 6.6. A reduction in stress can be observed by the reduction on the variation in Ψ and Δ (see Fig.9 a,b) which in turn affects the optical constant and the stress through the stress-optical value. Fig.6.10 shows the reduction in the amplitude of Δ from 0.48 to 0.07 when annealing at 950 °C was continued for 90 minutes.

6.3 Discussion

Since there were some samples of silicon dioxide having thicknesses greater than 400 nm but exhibiting no detectable anisotropy the matter was further investigated in more detail. Those in which no variation in Ψ and Δ could be detected when rotated about their normals, were found to lie in the lowest part of each Ψ and Δ loop . i.e in the thickness ranges 490 nm - 590 nm and it can be assumed that this would recur in each cycle. More generally, this region "W" could be found by using the following

Table 6.6

The change in the values of Ψ , Δ , n, and t at three points (a,b,c;see Fig.6.1) and the optical anisotropy for three samples annealed for different times at 950 °C in a nitrogen atmosphere.

Sample		Annealing Time in Min.	Ψ Degree	Δ Degree	n_2	Thickness nm	δN_{ac}
24	a	0	29.57	57.62	1.4566	1282.9	0.9×10^{-3}
	b		29.73	58.02	1.4571	1281.5	
	c		30.01	58.58	1.4575	1279.9	
	a	30	29.36	57.13	1.4566	1283.8	5.0×10^{-4}
	b		29.53	57.44	1.45635	1283.5	
	c		29.70	57.75	1.4561	1283.3	
	a	60	29.80	58.16	1.4562	1282.4	1.7×10^{-4}
	b		29.91	58.34	1.4528	1281.9	
	c		30.02	58.52	1.45637	1281.5	
	a	90	29.97	58.58	1.45721	1280.3	1.2×10^{-4}
	b		30.01	58.65	1.45715	1280.2	
	c		30.06	58.72	1.45709	1280.2	
21	a	0	34.02	64.40	1.45575	996.1	7.8×10^{-3}
	b		34.17	64.74	1.4614	991.4	
	c		34.32	65.08	1.4653	987.0	
	a	60	34.55	64.72	1.45720	994.9	6.0×10^{-4}
	b		34.65	64.91	1.45718	994.5	
	c		34.75	65.10	1.45660	994.0	
	a	90	34.95	65.03	1.45750	993.5	3.0×10^{-4}
	b		34.98	65.07	1.45735	993.5	
	c		34.01	65.10	1.45720	993.5	
22	a	0	33.38	63.44	1.4587	1269.7	1.0×10^{-3}
	b		33.50	63.91	1.4571	1267.9	
	c		33.83	64.42	1.4577	1265.6	
	a	90	32.88	63.22	1.4580	1268.8	1.5×10^{-4}
	b		32.91	63.26	1.45793	1268.8	
	c		32.93	63.30	1.45785	1268.8	

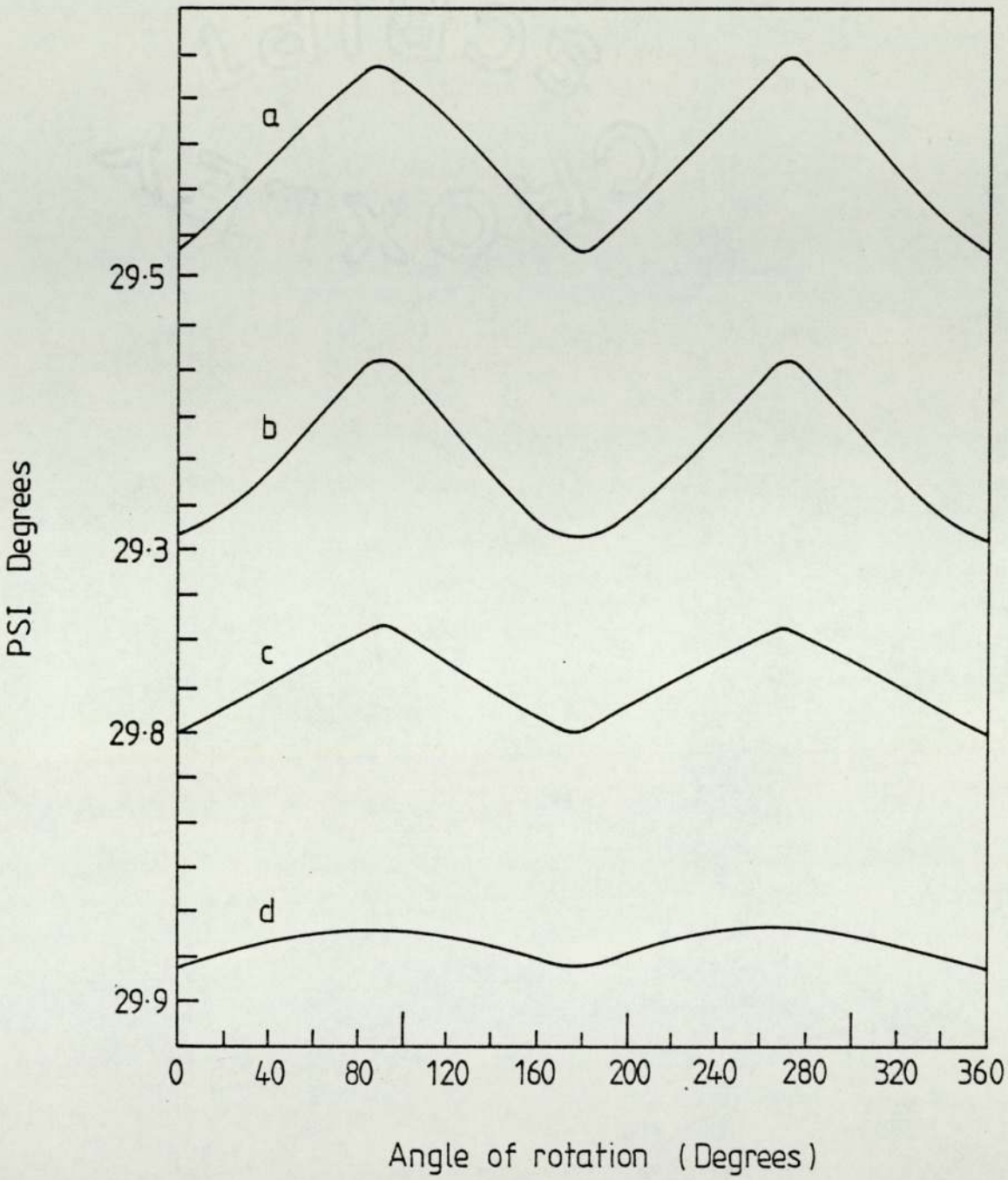

Figure 6·9a The reduction on the amplitude of the measurement of Ψ degree after annealing the sample (24) for different periods of time (a - no annealing, b - 30 mins, c - 60 mins, d - 90 mins) at 950°C

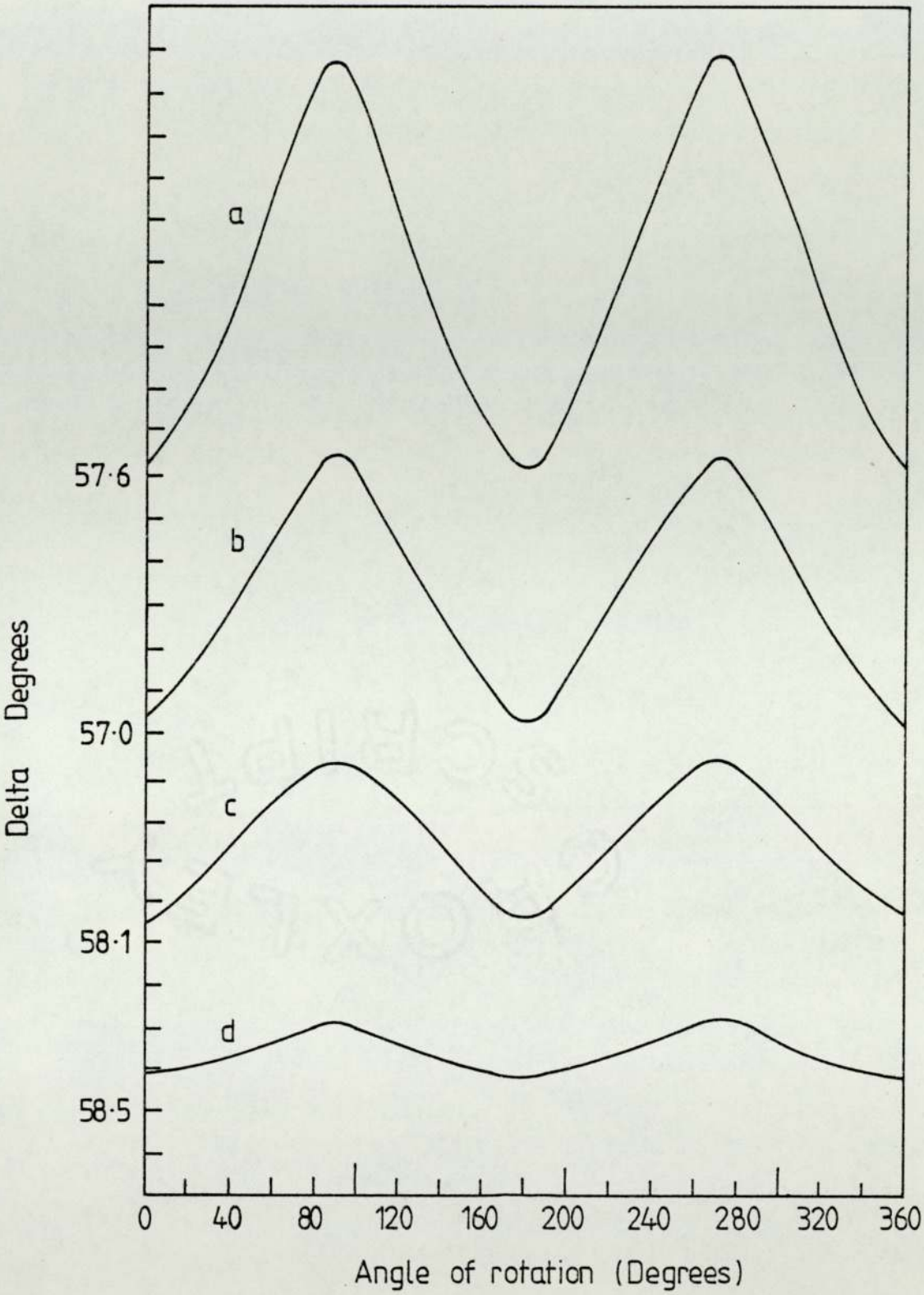

Figure 6·9b The reduction on the amplitude of the measurement of the Δ degree after annealing the sample (24) for different periods of time (a - no annealing , b - 30 mins, c - 60 mins, and d - 90 mins) at 950°C.

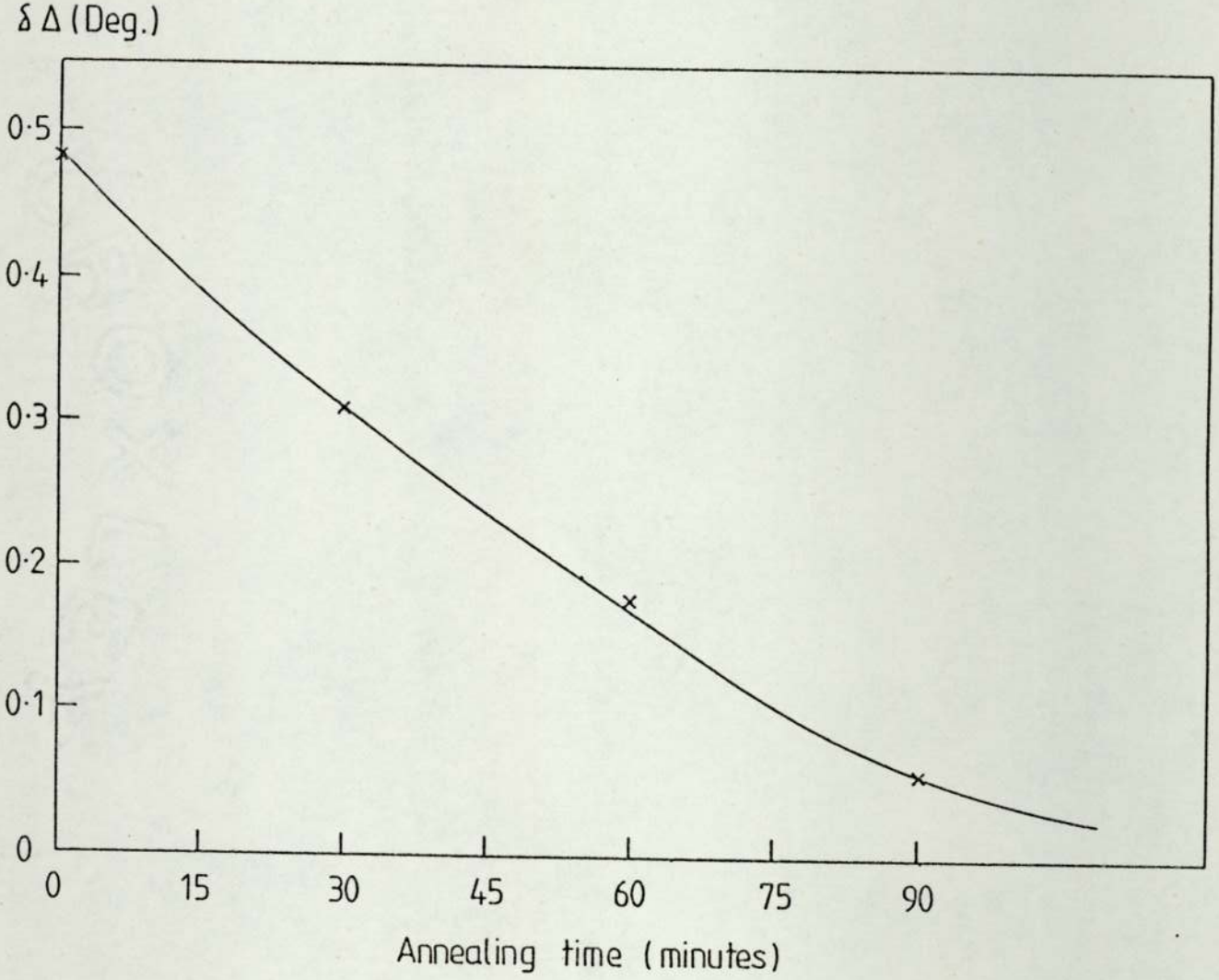

Figure 6.10 The reduction in the values of Δ as a result of annealing sample SS24 at 950°C in a nitrogen atmosphere.

formula

$$W \approx (X\bar{n} + 50) \text{ to } (X\bar{n} - 50)$$

where X = 268 nm (the first loop) and n is an integer ≥ 2 and refers to the loop number. This means that in this region of the loop the change in the value of ψ is small. Table 6.7 shows that all the samples have a value of ψ (less than 26.67). The absolute values of instrument sensitivites $\left|\frac{\partial\psi}{\partial t}\right|$ and $\left|\frac{\partial\Delta}{\partial t}\right|$ for different thicknesses of oxide were calculated. The absolute values of ψ and Δ for a 5 nm thickness change were plotted against thickness and the results are shown in Fig. 6.11 for one cycle of the ψ v Δ curve. From this figure we observed that all the samples on which no anisotropy could be detected lie in between the points L-M and E-F. This suggested that optical anisotropy can be observed when the sensitivity of $\left|\frac{\partial\psi}{\partial t}\right|$ is higher than the sensitivity of $\left|\frac{\partial\Delta}{\partial t}\right|$. It also indicates that it could be difficult to observe anisotropy for thicknesses corresponding to the peak of the ψ v Δ plot (Fig.5.7) where again $\left|\frac{\partial\psi}{\partial t}\right|$ is $\left|\frac{\partial\Delta}{\partial t}\right|$ and where optical anisotropy was observed to be small, as shown in Fig. 6.11.

Our observations in this regard are in general agreement with those of Pedinoff[85] who also was unable to detect anisotropy at certain film thicknesses corresponding to the minimal in his ψ and Δ versus thickness curves as shown in Fig. 2.4. If we take the minimum sensitivity of anisotropy measurement from his curve, it can be seen that the minimum sensitivity lies approximately between 490 nm - 590 nm, 770 nm - 830 nm and 1080 nm -1100 nm. In these thickness regions his maximum value of Δ are less than the

Table 6.7

Optical anisotropy was not found in these samples, even though their thickness was greater than 400 nm.

Sample	Thickness nm	Ψ Degree	Δ Degree	n_2
2	493.9	25.67	222.98	1.4570
4	518.6	23.30	200.54	1.4572
13	1349.3	22.83	179.40	1.4570
17	1846.7	25.27	220.68	1.4571
19	523.2	22.99	196.06	1.4569
44	797.4	22.93	191.60	1.4571
47	1100.6	23.36	157.41	1.4571
50	1566.8	26.69	228.02	1.4574

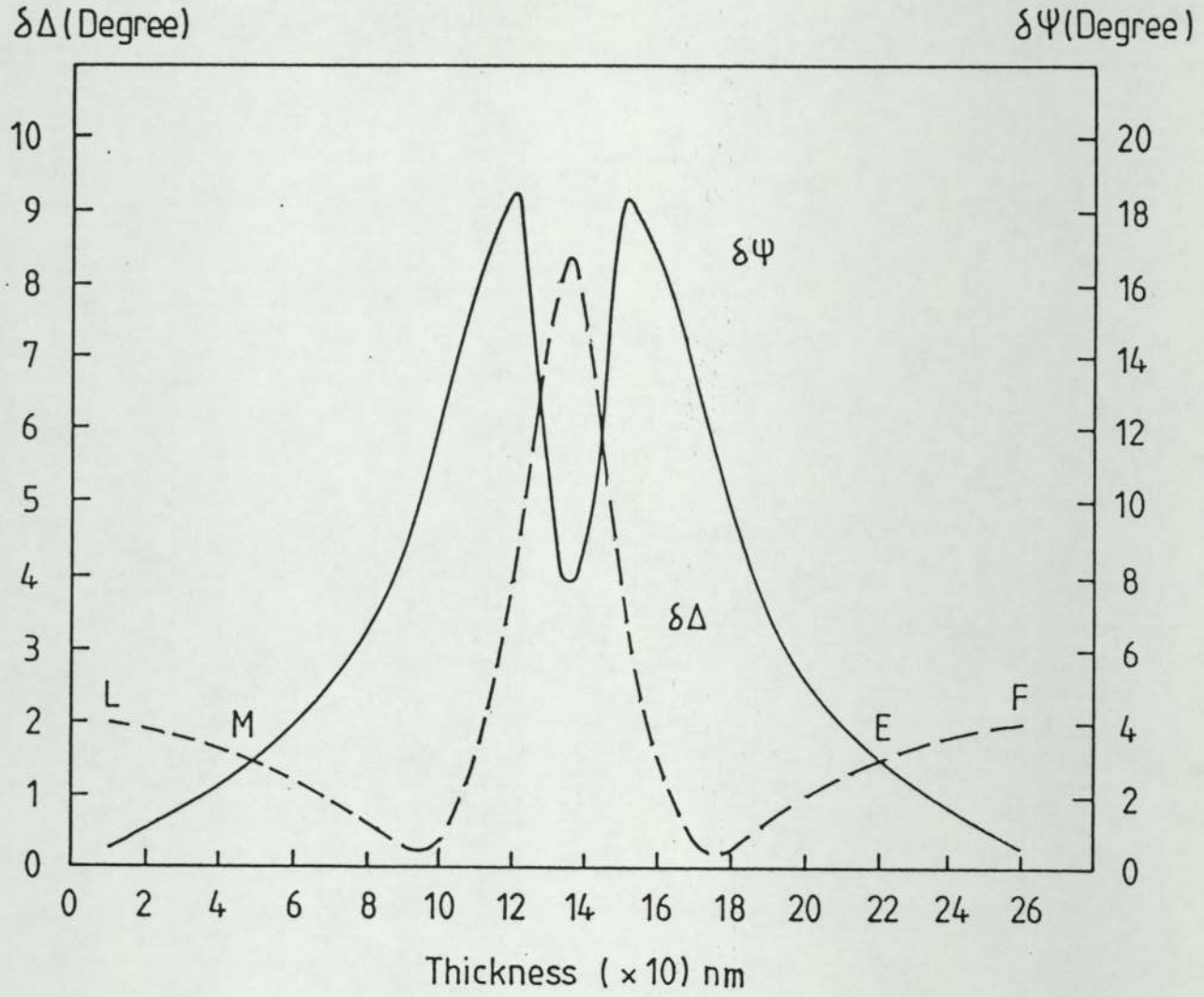

Figure 6.11 Sensitivity of the measurement of optical anisotropy . L-M and E-F are the regions where the technique was unable to find any optical anisotropy, but it was found in the M-E region.

other values shown in the figure and show that the value of $\delta\Psi$ is less than the value of $\delta\Delta$. Our observations are in general agreement. Table 6.7 shows the samples in this work which lie in the L-M and E-F regions in which we could not detect any change in the Ψ and Δ measurement. It should be noted that Pedinoff used the multiple angle ellipsometer technique as opposed to the sample rotation method used in this work. However, stress has been reported in this range of thicknesses before[121] and therefore it is possible that optical anisotropy is present in the silicon dioxide samples but not detectable by ellipsometry. Let us consider the measurement in sensitivity of the optical anisotropy further. We changed the value of n_2 for the oxide film by 1.45 ± 0.1 and studied this change at one point only on the curve, for example at $\Delta = 150.65$ as shown in Fig. 6.12. Table 6.8 shows the change in $\delta n/\delta\Psi$ and $\delta n/\delta\Delta$ which indicates the change in the sensitivity for the measurements. Fig. 6.12 and Table 6.9 show the sensitivity dependence on the refractive index of the film at a fixed value of Δ, where we have a large difference in the value of psi and in the thickness at the same point.

From Figures 6.1 - 7 it can be seen that silicon dioxide films grown thermally on silicon substrates at 1100 °C, and thicker than 400 nm exhibit optical anisotropy (all the samples produced by the r.f. system were less than 400 nm which may be why we could not detect any anisotropy). The changing amplitude of the angles $\delta\Psi$ and $\delta\Delta$ for thermally grown films changed with the thickness as shown in Fig. 6.8. The values of δN_{ac} which depend on the amplitudes, are computed by matching the model values and measured values of Ψ and Δ at the three points (a,b,c) as shown in Fig.

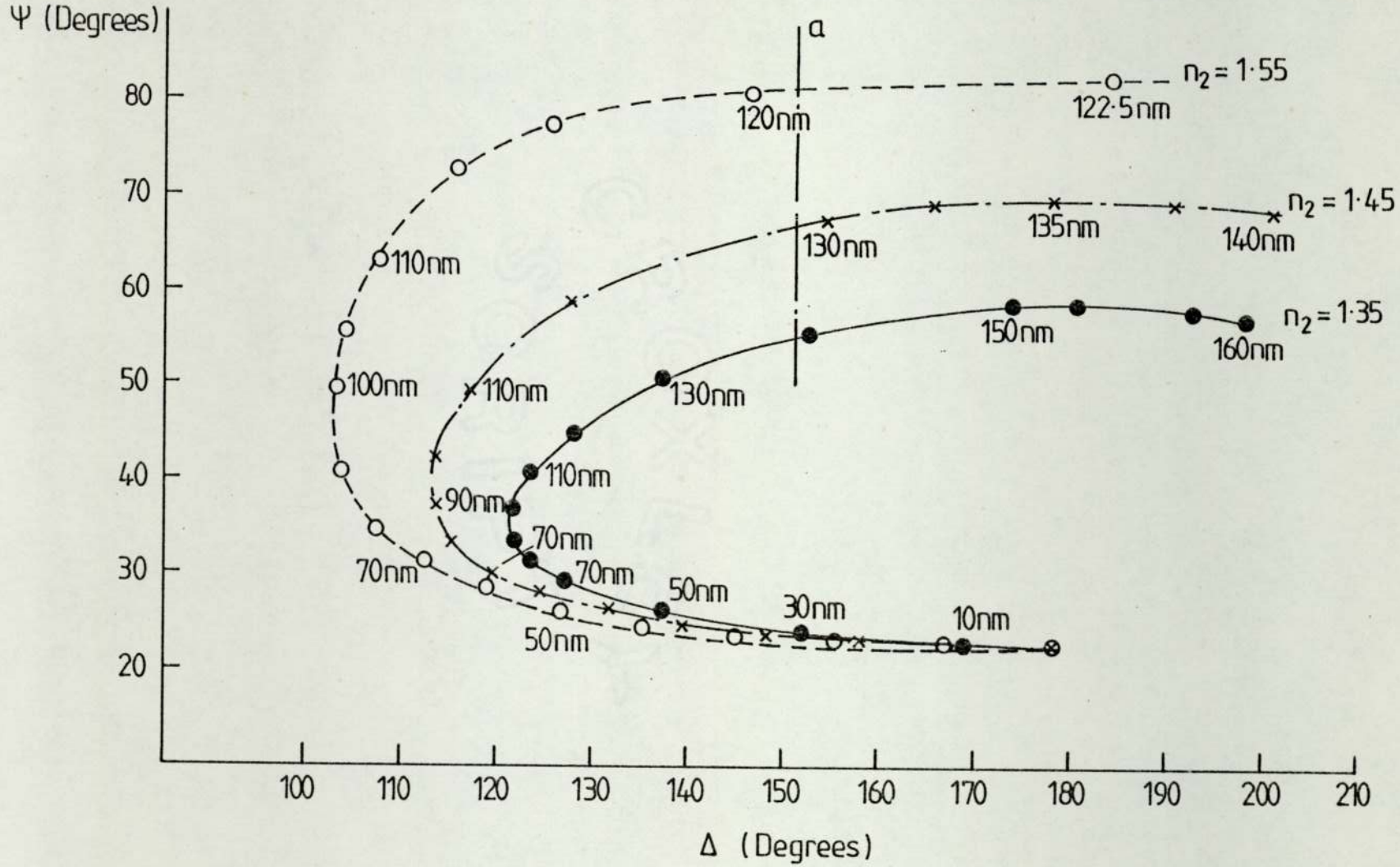

Figure 6·12 The change in the curve of Ψ vs Δ when using different values of n_2, which indicate the optical anisotropy at that point.

Table 6.8

The change in Ψ, Δ, $\delta N/\delta\Delta$ and $\delta N/\delta\Psi$ at point 'a' where Δ = 150.65 degrees for different values of n_2 = 1.55, 1.45 and 1.35. k_2 = 0, λ = 623.8 nm and Φ = 60 degrees.

n_2	k_2	Degree	Degree	$\delta N/\delta\Delta$	$\delta N/\delta\Psi$
1.55	0	81.99	150.56	1.11*	0.69 X 10^{-2}
1.45	0	67.04	150.65	10.00**	0.83 X 10^{-2}
1.35	0	55.21	150.66	1.00***	0.38 X 10^{-2}

* for n = 1.55 to 1.45

** for n = 1.45 to 1.35

*** for n = 1.55 to 1.35

Table 6.9

The change of the value of $\delta N/\delta\Delta$ and $\delta N/\delta\Psi$ along the curve as shown in Fig. 6.12.

Thickness nm	$\delta N_2 = 1.45 - 1.35$ $\delta N/\delta\Delta$ deg^{-1}	$\delta N/\delta\Psi$ deg^{-1}	$\delta N_2 = 1.55 - 1.45$ $\delta N/\delta\Delta$ deg^{-1}	$\delta N/\delta\Psi$ deg^{-1}
10	8.06×10^{-2}	0.9×10^{-2}	11.11×10^{-2}	10.00
30	2.74×10^{-2}	1.11	3.58	2.5
50	1.7×10^{-2}	2.7×10^{-1}	2.05	1.11
70	1.32×10^{-2}	9.0×10^{-2}	1.42	0.11
90	1.19×10^{-2}	3.15×10^{-2}	1.08	2.5×10^{-2}
110	1.6×10^{-2}	1.15×10^{-2}	1.03	6.9×10^{-3}
130	0.56×10^{-2}	5.78×10^{-3}	0.1	2.7×10^{-2}

6.1. By assuming values of N_2, an increase in δN_{ac} from 1 X 10^{-3} to 8 X 10^{-3} was found for films ranging in thickness from 400 nm to 995.9 nm respectively, and then a drop to 1 X 10^{-3} in a 1280 nm film and in the latter case the amplitude of Ψ and Δ are .22 and .48 respectively. But when the amplitude increases to .23 and .52, the optical anisotropy increased to 3.2 X 10^{-3} . The effect is illustrated in Table 6.5. Table 6.10 shows the change in the parameters Ψ and Δ of three samples at three different positions a, b and c, which would result in different calculated thicknesses if no anisotropy was assumed.

The variation in the angles of Ψ and Δ measured during the rotation will affect the thickness measurement if no anisotropy is assumed to be present. The change in Ψ and Δ of .25 and .55 respectively for sample 45 with a 1456.3 nm thickness will affect the thickness by 13.6 nm, which means that if we do not consider the optical anisotropy there will be an error in thickness measurement of the order of 1%. Table 6.4 shows that the value of δt_{ac} for some samples gives us an idea about the error in the thickness measurement when anisotropy is present.

Having looked at the effect of anisotropy on thickness measurement we now return to the variation in thickness measured across the samples supplied by Lucas and prepared by the r.f. discharge process. We investigated the variation in the thickness measurement in Section 5.5, and we found that the variation is in the range of 1-3 nm for batch one, two and three and 2.5 nm in batch five and increased to 13.25 nm for batch ten, and this was measured between the centre and the two ends of the sample. No variation in the measurement of Ψ and Δ was observed when these

Table 6.10

The variation on three samples at three different positions (a, b, c; see Fig.6.1.).

Sample	ψ Degree	Δ Degree	n_2	Thickness nm
a	64.85	137.84	1.4555	665.4
20 - b	64.97	138.09	1.4570	664.5
c	65.09	138.34	1.4585	663.8
a	34.02	64.40	1.4575	996.1
21 - b	34.17	64.74	1.4614	991.4
c	34.32	65.08	1.4653	987.0
a	29.57	57.62	1.4566	1282.9
24 - b	29.73	58.02	1.4571	1281.5
c	30.01	58.58	1.4575	1279.9

samples were rotated about the normal to their surfaces which indicates no anisotropy exists in these samples. Therefore the variation in thickness measurement on the Lucas samples could be attributed to the preparation conditions and not to optical anisotropy.

Thickness errors might however be attributed to the size of the light beam if there are thickness variations across a sample. To investigate this let us consider a light beam with a light spot size of 0.5 mm (which correspond to the beam diameter of the He-Ne laser used in this investigation), and examine a sample of 70 mm x 24.5 mm, Section 5.5. Errors arising from the light spot size in the thickness measurement would only be of the order of 0.3 nm over all the Lucas samples. This is a small error compared to the measured differences between the batches one to ten. Therefore in the thermally grown silicon dioxide samples the thickness error due to spot size would not be greater than 0.3 nm. More explanation about the measurement of sensitivity has been discussed in Section 5.1 - 5.4, by changing n_2, k_2, n_3, k_3, and Φ_2 for aluminium, and the same is relevant for the silicon dioxide. Such errors in thickness measurements can be minimized by annealing samples for about 90 minutes.

There was an observable decrease in the optical anisotropy with annealing. This indicates that the anisotropy in thermally grown silicon dioxide layers can be attributed to stress in the oxide layer. The stress in the thermally grown silicon dioxide has been known for several years as reported in Section 2.5.1. The stress could originate at the surface as a result of the difference in the thermal expansion coefficient between the

silicon and the oxide[121]. Other theories explain the stress on the silicon oxide to the surface density[120],the effect of the surface mobility[120], the impurity[121] and the effect of the vacancies[120]. It has not been possible to conduct further tests in the present work to be able to specify the sources of the stress.

In most of the previous work authors state that the difference in thermal expansion could be a second explanation for the stress mechanism. The thermal expansion for the silicon is $4.5 \times 10^{-6}/C^{\circ}$ and thermal expansion for oxide is $6 \times 10^{-6}/C^{\circ}$. The observed stress can be attributed to the cooling of the oxide after its formation at the surface temperature which must be several hundred degrees centrigrade (1100 °C in our work). Evans and Wilman[165] explain the formation of the stress on the surface when the silicon crystals are growing on the deposited surface in addition to the arriving atoms which are thermally expanded. This layer will then be covered by another layer and these layers deposited on the one before, which will reduce the temperature of the layer below. This reduction in temperature is progressively in accordance with the temperature of the deposit and the crystals will contract. The recrystallization will occur in these layers until the temperature falls below the recrystallization temperature and thereafter the further cooling causes a stress to develop through the deposit. The stress in the material could be avoided if we chose either a material which has the same thermal expansion or with only a small difference in the coefficient between the two materials and if this is not possible as in the case of SiO and some other materials then the stress can be

reduced by annealing[120]. The method of reducing the optical anisotropy and stress on materials by the annealing process has been used for a long time. If the material is annealed at a temperature lower than the oxidation temperature and left to cool down slowly, the annealing technique can be used to remove the stress which has been produced during the preparation process. Pedinoff[85] found that 20% of the stress can be reduced by annealling a sample (thickness 1185 nm) at 925 °C for 15 minutes and by 43% by annealing a sample (1168 nm) for 30 minutes at the same temperature. In this work the samples were annealed for different periods of time at 950°C. Sample 24 was annealed for three different periods of time (30 min., 60 min. and 90 min) and the longer the period of annealling, the greater the reduction of optical anisotropy ie. 44% after 30 minutes, 81% after 60 minutes and 86% after 90 minutes. The annealing process was carried out on sample 21 for 60 and 90 minutes and the optical anisotropy reduced from $\delta N = 7.8 \times 10^{-3}$ to $\delta N = 6.0 \times 10^{-4}$ and $\delta N = 3.0 \times 10^{-4}$ for 60 and 90 minutes respectively and sample 22 was annealed for 90 minutes. By annealing the samples the change in the amplitude of the measured angles ψ and Δ indicated a reduction in the optical anisotropy and the stress, which is shown in Table 6.11. It is reasonable to assume that in the annealing process the Si-SiO_2 system re-crystallizes and at a lower temperature than the oxidation temperature. The stress was reduced by as much as 80% when the sample was annealed for 90 minutes. Table 6.9 shows the variation of the value of the stress for different samples with annealing.

Table 6.11

The annealing effect on the optical anistropy and the surface stress.

Sample	Annealing Time in Min.	δN_{ac}	σ N/M^2
21	0	7.8 x 10	1.11 x 10^9
	60	6.0 x 10	8.5 x 10^7
	90	3.0 x 10	4.28 x 10^7
22	0	1.0 x 10	1.43 x 10^8
	90	1.5 x 10	2.40 x 10^7
24	0	0.9 x 10	1.28 x 10^9
	30	5.0 x 10	7.13 x 10^7
	60	1.7 x 10	2.42 x 10^7
	90	1.2 x 10	1.71 x 10^7

The stress was reduced by 44%, 81% and 86% when sample 24 was annealed for 30, 60 and 90 minutes respectively. The stress value before annealing was 1.28 x 10^8 N/M^2 and after annealing for 30, 60 and 90 minutes the stress values reduced to 7.13 x 10^7 N/M^2, 2.42 x 10^7 N/M^2 and 1.71 x 10^7 N/M^2 respectively, as shown in Fig. 6.13. Pedinoff reduced the stress by 43% when he annealed samples for 30 minutes at 925°C, which is in good agreement with our results. According to the present results the stress is almost completely eliminated after annealing for 90 minutes. Unfortunately Pedinoff did not prolong the annealing process to 90 minutes.

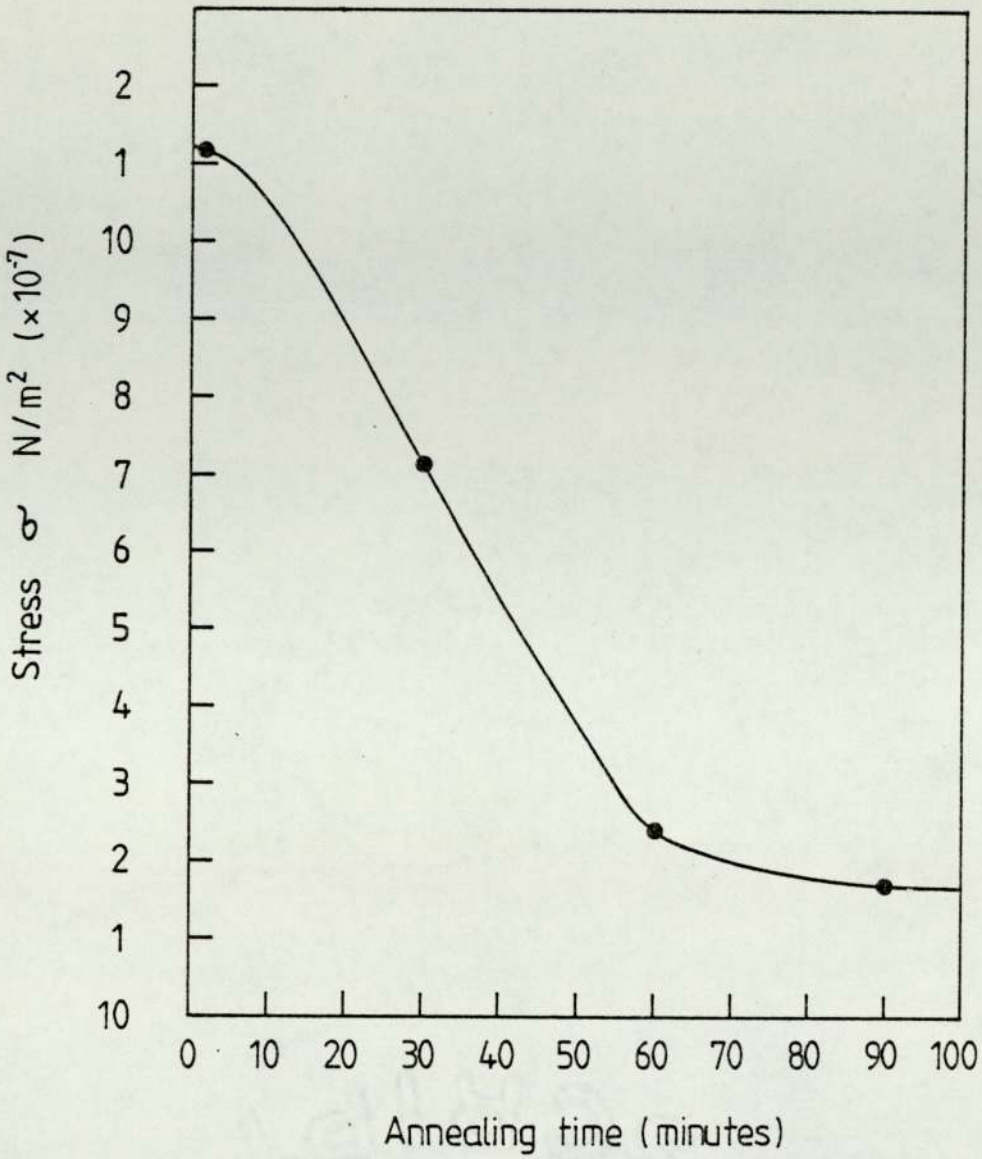

Figure 6·13 The reduction in the stress for sample 24 for different periods at 950 °C in nitrogen atmosphere.

CHAPTER VII

ANISOTROPY IN ALUMINIUM
(RESULTS AND DISCUSSION)

Optical anisotropy was detected in single crystal and polycrystalline aluminium by using the same technique which was used in the thermally grown silicon dioxide as discussed in Chapter 6. The variation in the ellipsometer parameter Ψ and Δ was detected by Karwal and Neal[2] when a commercial aluminium sheet was rotated about a normal to its surface. In this chapter we will investigate the variation in Ψ and Δ for pure polycrystalline aluminium "as supplied" and single crystal(311), (111) and (110) aluminium and look for the optical anisotropy in these samples. We found that optical anisotropy existed on the pure aluminium "as supplied" and on the electropolished single crystal which we will discuss next.

7.1 Polycrystalline Aluminium (as supplied)

The polycrystalline pure aluminium was supplied in 100 mm x 100 mm sheets and it was cut into 15 mm x 20 mm for ellipsometer use. The samples as supplied were then cleaned in an ultrasonic bath as explained in Section 4.36.

The pseudo optical constants of these samples was found to lie in a very wide range, as shown in Table 7.1. But the value of the refractive index we used in Chapter 5 was $n_3 = 0.6926$ and $k_3 = 4.5229$ for 100 nm Aluminium sputtered on single crystal silicon (111), which is quite different from the value obtained in a

Table 7.1

The variation in the value of the pseudo constant for samples of aluminium oxide on pollycrystalline aluminium.

Sample	Ψ Degree	Δ Degree	Pseudo n'	constant k'
GA 1	43.04	141.35	0.4742	4.1436
GA 2	43.18	140.18	0.4171	4.0142
GA 4	43.01	136.97	0.3949	3.6715
GB 1	39.57	108.16	0.4486	1.18315
GB 3	41.19	110.05	0.3294	1.9347
GB 4	44.93	107.89	0.58303	1.695

vacuum preparation, where n_3 = 1.12 and k_3 = 6.40[167]. In Section 5.2 we discussed what effect an incorrect value of refractive index would make to the film thickness measurement. We also calculated the pseudo constant for different thicknesses of the oxide on aluminium by using n_3 and k_3 for aluminium prepared in a vacuum. The pseudo values n_3 = 0.6926 k_3 = 4.5229 which we used as substrate values are equivalent to an oxide film thickness of 9 nm, as shown in Table 7.2 and this shows the difference between the measurements in both air and under high vacuum conditions. The samples used in this work would already have an oxide layer present.

To calculate the optical anisotropy we found that the various samples needed different values of n_3 and k_3 for the substrate to match the experimental values of ψ and Δ with the computed values. For convenience they have been sorted in different groups. As shown in Tables 7.3,4,5 where n_3 are in the range of 1.3 to 1.9 and k_3 are in the range of 7.1 to 7.5 for Group A, Group B have a small absorption coefficient where k_3 = 3.09 and n_3 = 1.699 and Group c where n_3 = 1.15 and k_3 = 6.33 which shows the large difference in the substrate and the effect on the thickness measurement of the film on the surface, which varies from 15 nm to 48 nm (see appendix 7) for some samples which is much higher than the expected value of the order of 5-10 nm. But it might be the combined effects of surface roughness and optical anisotropy as suggested by[56.57]. The effect on the angles of ψ and Δ by rotating the sample about the normal to their surfaces are clearly shown in Figure 7.1 - 5. Surface roughness would not have any significant affect on the variations in refractive index on

Table 7.2

The pseudo constant for the aluminium oxide on aluminium where $n_2 = 1.65$, $k_2 = 0$, $n_3 = 1.45$, $k_3 = 6.12$, $\phi = 60$ and $\lambda = 632.8$ nm.

Oxide Thickness nm	Ψ Degree	Δ Degree	Pseudo Constant n'	k'
0	42.09	153.99	1.45	6.12*
1	42.09	152.94	1.35	5.89
2	42.11	151.89	1.25	5.68
3	42.11	150.86	1.17	5.48
4	42.12	149.82	1.09	5.29
5	42.13	148.79	1.02	5.12
6	42.14	147.77	0.96	4.96
7	42.15	146.75	0.90	4.80
8	42.16	145.74	0.85	4.65
9	42.17	144.73	0.80	4.52
10	42.18	143.73	0.76	4.39

* Clean surface

Table 7.3

The optical anisotropy for the polycrystalline aluminium for group 'A' where n_3= 1.3-1.9, k_3 = 7.1-7.5, Φ = 60 degrees and λ= 632.8 nm .

Sample	Ψ Degree	Δ Degree	Amplitude $\delta\Psi$	Amplitude $\delta\Delta$	n_2	SN_{ac}
GA 1	43.04	141.35	1.95	2.60	1.599	0.080
GA 2	43.18	140.18	1.375	2.39	1.662	0.217
GA 3	42.90	141.94	1.32	2.60	1.600	0.345
GA 4	43.01	136.97	1.445	2.71	1.825	0.39
GA 5	42.16	141.35	2.10	2.625	1.756	0.258
GA 6	43.48	132.45	1.8	2.41	1.189	0.49
GA 7	43.21	136.99	2.275	2.31	1.29	0.59
GA 8	43.10	147.70	1.87	2.11	1.73	0.11
GA 9	43.20	139.51	1.32	1.685	1.65	0.16

Table 7.4

The optical anisotropy for oxide on polycrsytalline aluminium for group 'B' where $n_3 = 1.699$, $k_3 = 3.09$, $\phi = 60^\circ$ and $\lambda = 632.8$ nm.

Sample	Degree	Degree	n_2	δN_{ac}
GB 1	39.57	108.16	1.5000	8.6×10^{-2}
GB 2	44.13	109.19	1.514	6.9×10^{-2}
GB 3	41.19	110.95	1.3965	3.25×10^{-2}
GB 4	44.93	107.87	1.579	4.2×10^{-2}
GB 5	36.94	119.14	1.508	3.33×10^{-2}
GB 6	37.79	113.65	1.5801	10.04×10^{-2}

Table 7.5

The optical anisotropy for oxide on polycrsytalline aluminium for group 'C' where $n_3 = 1.15$, $k_3 = 6.33$, $\phi = 60^\circ$ and $\lambda = 632.8$ nm.

Sample	Degree	Degree	n	δN_{ac}
GC 1	42.85	139.61	1.871	5.62×10^{-1}
GC 2	42.82	144.79	1.867	5.46×10^{-1}
GC 3	42.83	144.90	1.850	5.10×10^{-1}
GC 4	42.87	136.26	1.840	5.50×10^{-1}

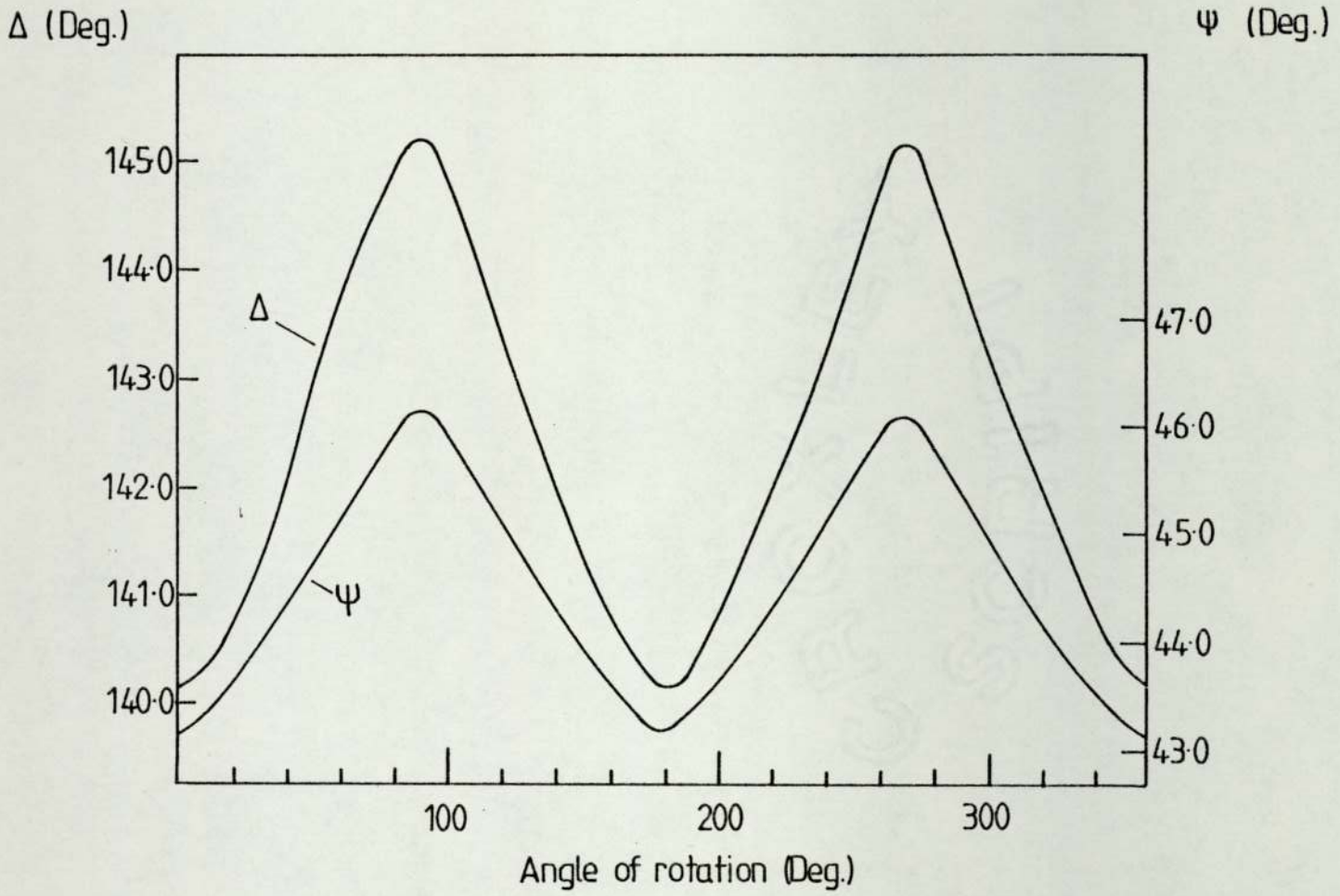

Figure 7·1 The change in Ψ and Δ angles as a function of the angle of rotation for polycrystalline aluminium, sample GA 2.

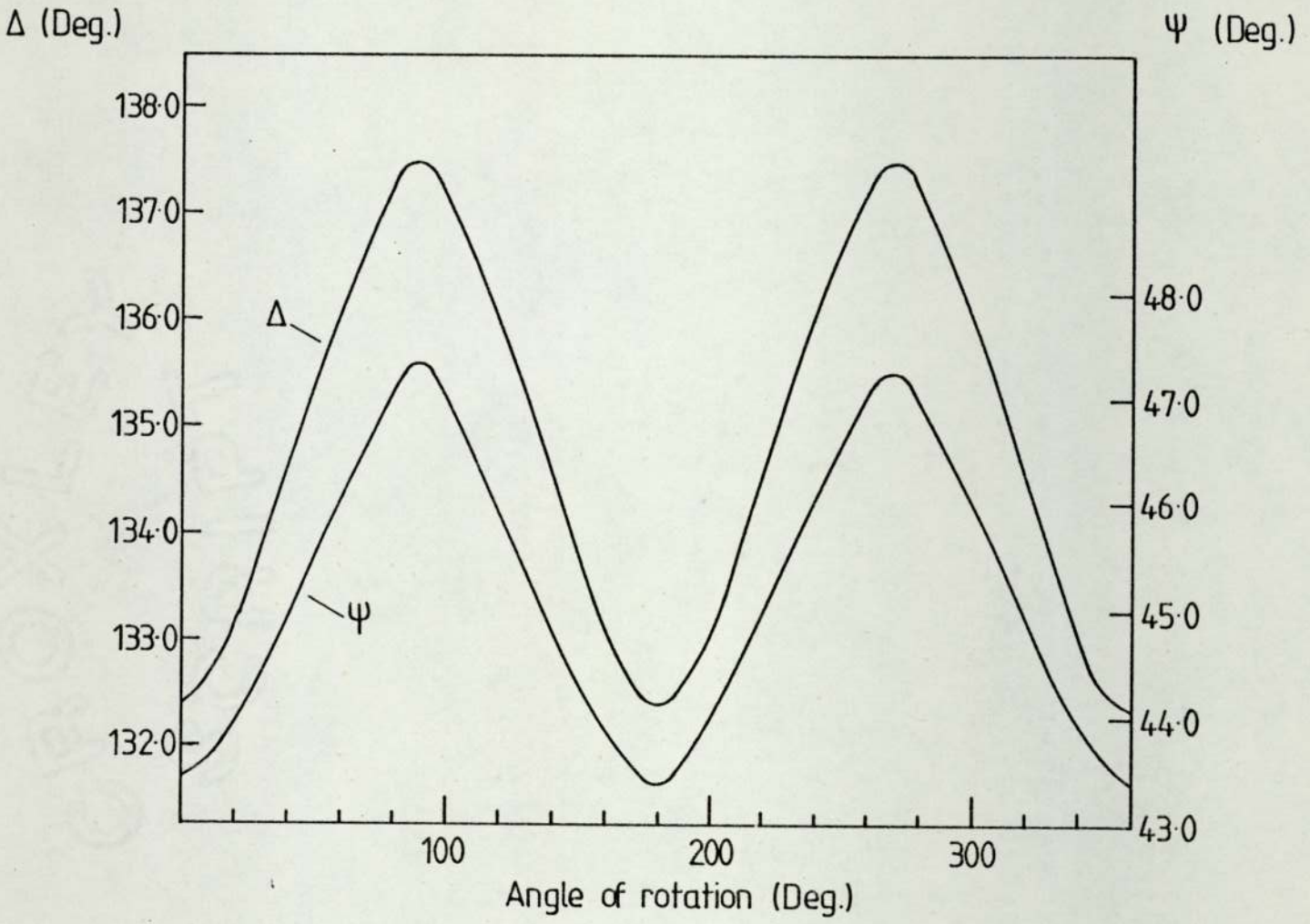

Figure 7·2 The change in Ψ and Δ as a function of the angle of rotation for polycrystalline aluminium, sample GA 6.

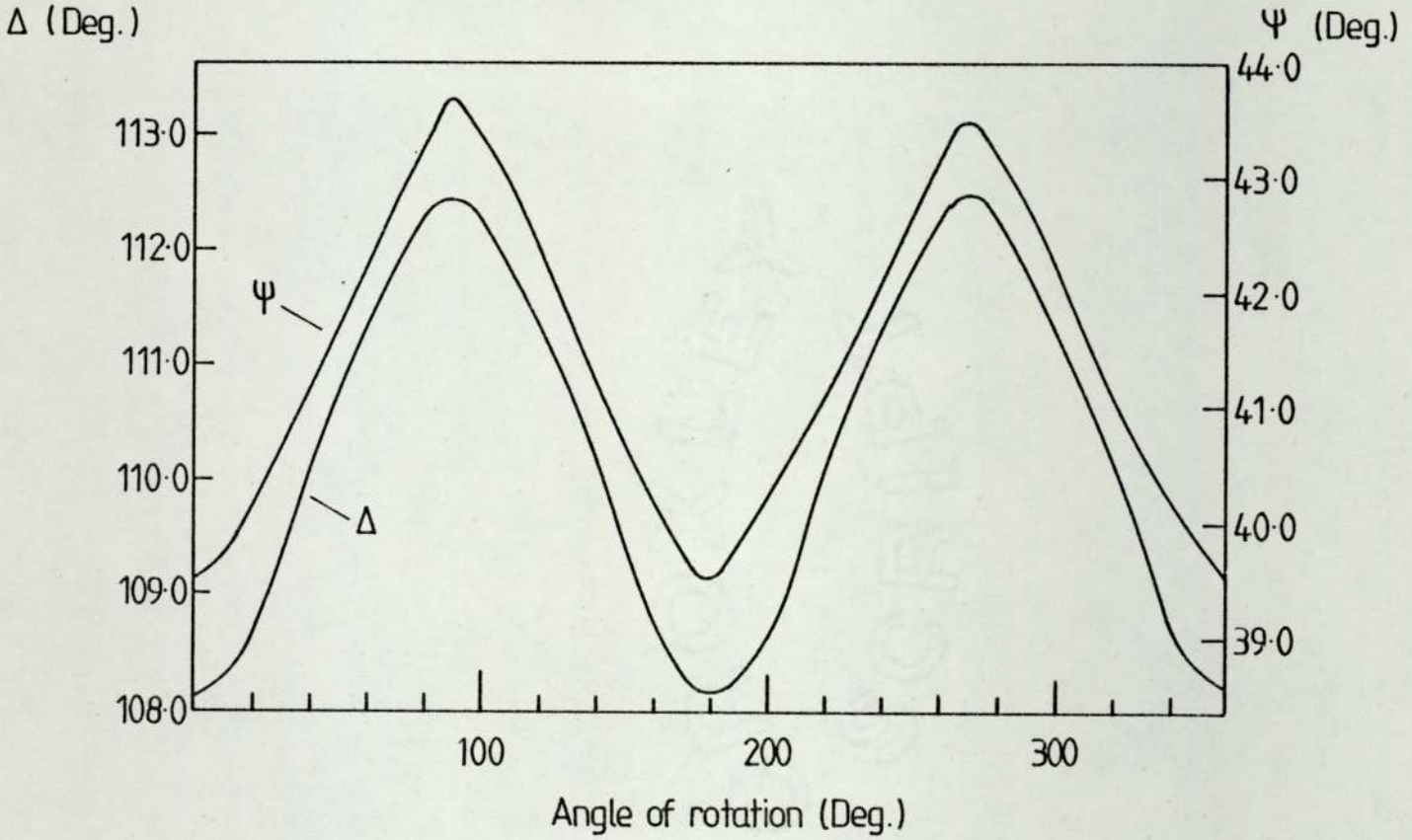

Figure 7·3 The change in the angles Ψ and Δ as a function of the angle of rotation for a polycrystalline aluminium for sample GB 1.

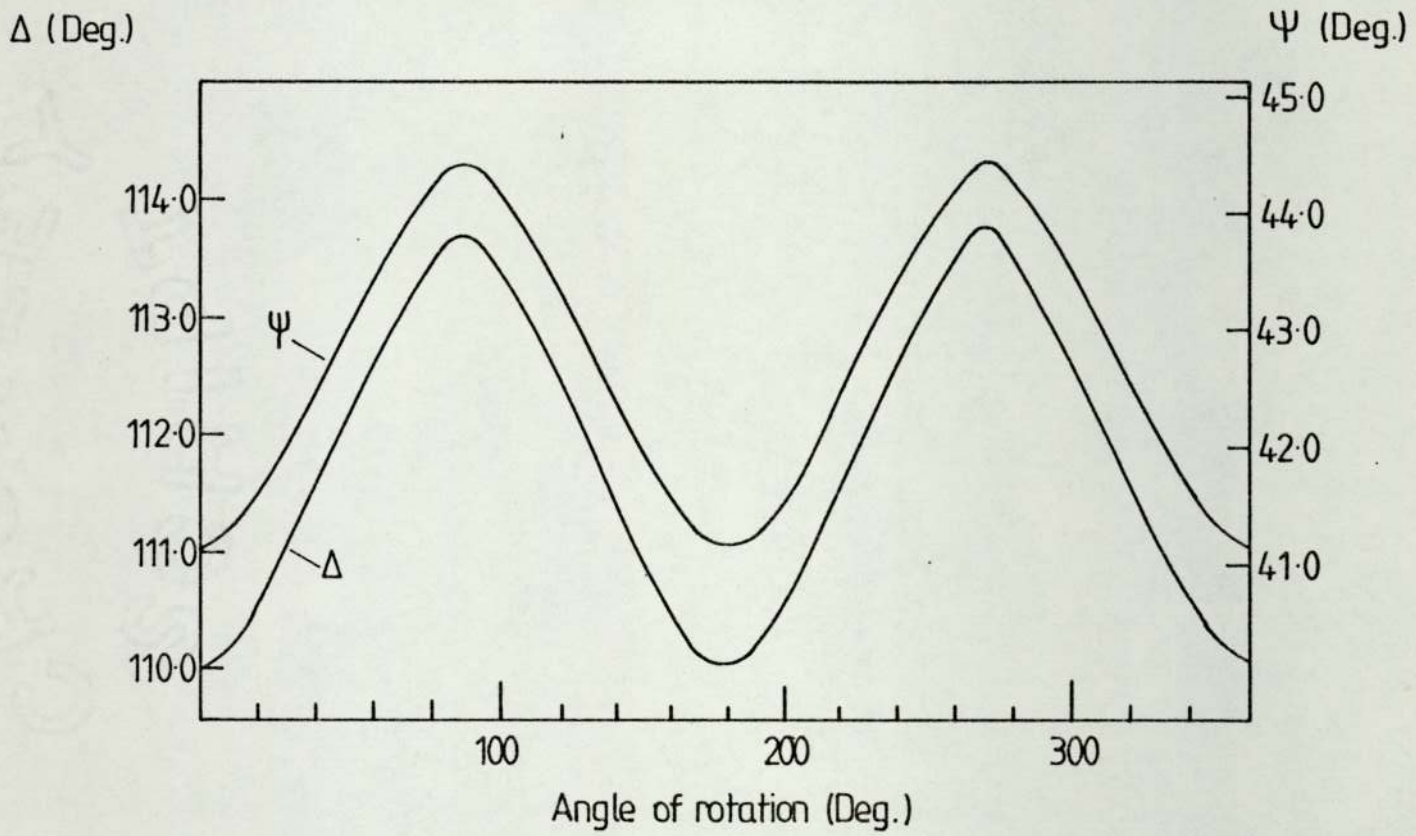

Figure 7·4 The variation in the Ψ and Δ measurement as a function of the angle of rotation for polycrystalline aluminium for sample GB 3.

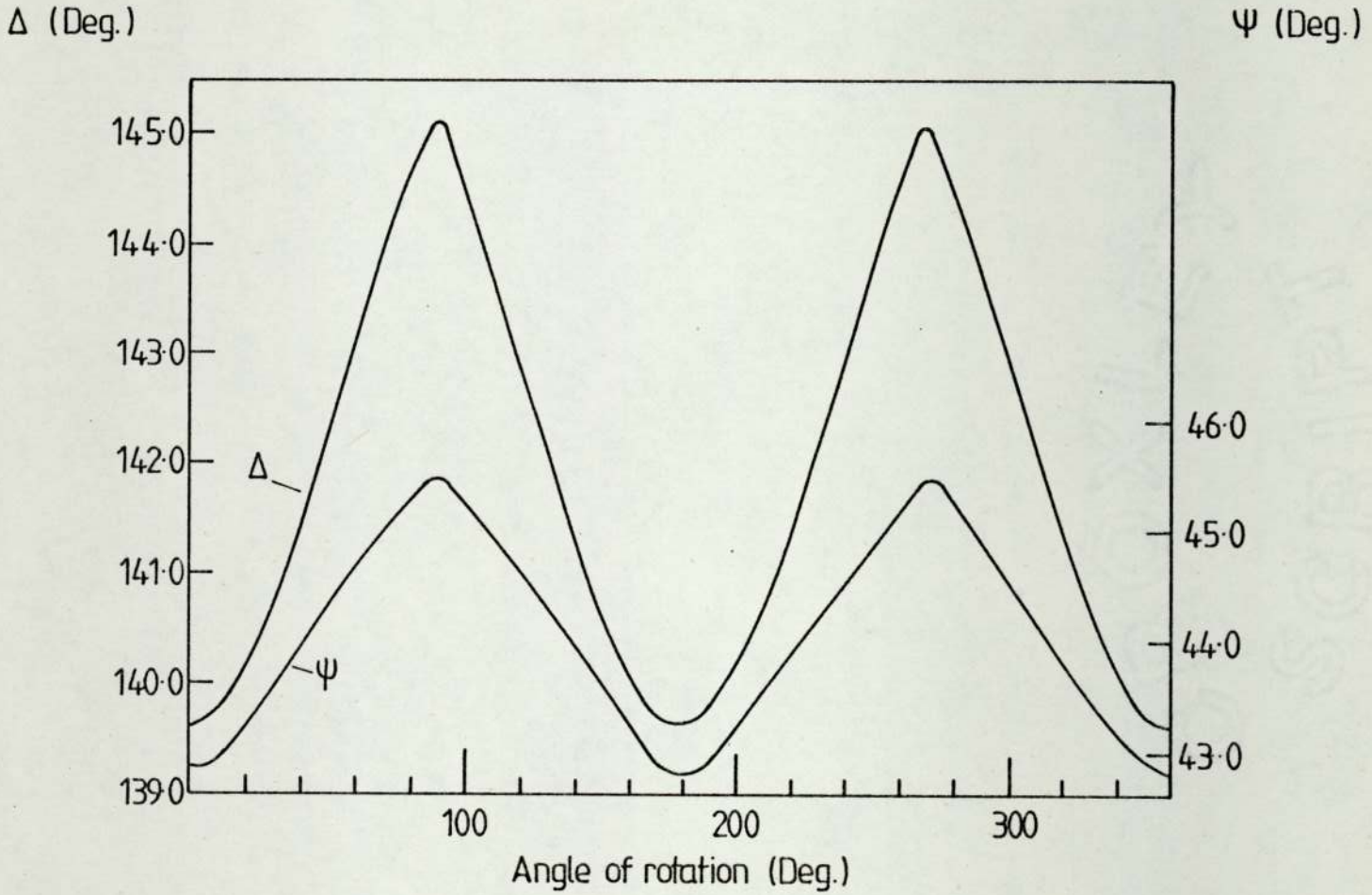

Figure 7·5 The variation in the Ψ and Δ angles as a function in the rotation angle for a polycrystalline aluminium for sample GC 1.

rotation since the angle of incidence is only 60 degrees which is well below the value of 70 degrees by Vedam[66] for reducing roughness effects. Appendix 7 gives some factors on roughness for these samples.

The refractive indices of the films on these samples were evaluated in three different positions a, b and c as shown in Fig. 7.1, because the variation in ψ and Δ during the rotation against the angle of the rotation will effect the values of n_2 and k_2 for the film of each sample as shown in Table 7.6 which also gives the degree of optical anisotropy in the samples. We found that sample GB3 had the lowest value of $\delta N_{ac} = 0.0325$ for a polycrystalline aluminium and the highest value of δN_{ac} was in sample GC1, where $\delta N_{ac} = 0.562$. All these samples in which optical anisotropy was observed were cleaned in an ultrasonic bath (see Section 4.3.6) and no diamond polishing or electropolishing technique was used. Later some samples were diamond polished and electropolished but no variation in the Ψ and Δ angles when rotated about a normal to its surface was observed after polishing, which means no optical anisotropy was detected after the diamond or electropolishing processes. In fact, the polishing technique removes the majority of the oxide layer formed in the production process (see Table 7.7). Therefore, the polishing reduces the anisotropy to a point where it was not detectable by ellipsometry.

7.1.1 Annealing to Reduce Optical Anisotropy

The optical anisotropy could be minimized by annealing the samples at 500 °C for more than one hour and if the annealing

Table 7.6

The change in the film refractive index at three different points a, b, and c (see Fig.7.1) for group A, B, and C.

Sample	n_a	n_b	n_c	N_{ac}
GA 1	1.599	1.639	1.679	0.8×10^{-1}
GA 2	1.662	1.5535	1.445	2.17×10^{-1}
GA 4	1.825	1.6300	1.435	3.9×10^{-1}
GA 5	1.756	1.627	1.498	2.58×10^{-1}
GA 6	1.189	1.435	1.6812	4.92×10^{-1}
GB 1	1.414	1.457	1.500	0.86×10^{-1}
GB 2	1.514	1.5425	1.583	0.69×10^{-1}
GB 3	1.3965	1.4128	1.429	0.33×10^{-1}
GC 1	1.871	1.5900	1.309	5.62×10^{-1}
GC 2	1.867	1.5940	1.321	5.46×10^{-1}

Table 7.7

The value of n_2 and k_2 for diamond polishing and electropolishing for polycrystalline aluminium samples.

	Sample	Δ Degree	Ψ Degree	Pseudo Constant n´	k´
diamond polishing	GA2	146.77	42.90	0.6729	4.8704
	GA5	147.60	42.76	0.7122	4.990
	GC	146.03	42.78	0.6815	4.7489
Electropolishing	GA2	149.15	42.80	0.8096	5.2559
	GB2	148.85	42.88	0.7670	5.2109
	GB3	149.89	42.91	0.8066	5.4010

lasted for four hours it was possible to reduce the optical anisotropy by 91%, as shown in Table 7.8. It is reasonable to assume that the optical anisotropy occurs in the oxide layer as a result of the stress and strain in the surface introduced during the production process[168]. Table 7.8 shows that annealing samples for different periods of time reduces the δN.

It was found that annealing reduces optical anisotropy and roughness but as mentioned earlier the roughness does not influence the variations of ψ and Δ on rotation of the sample.

7.2 Optical Anisotropy in Single Crystal Aluminium

The optical anisotropy phenomena was observed in an electropolished single crystal as prepared in 4.3.6.1 (111), (311) and (110) (as shown in Table 7.9) as the sample rotated about a normal to its surface (as shown in Fig. 7.6). The difference in the amplitude of both Ψ and Δ between the polycrystalline and the single crystal aluminium are large. In the polycrystalline samples, the amplitude was in the range of 2.5 degrees and 2 degrees where as in the electropolished single crystal it was 0.5 and 0.1 degrees for Ψ and Δ respectively, see Table 7.10. The pseudo constants of the single crystal are nearer to the values of the substrate as can be seen in Table 7.11. If the values of n_3 and k_3 in the vacuum are assumed to be 1.12 and 6.40 respectively, the oxide film which forms on the surface was calculated to be 5 nm thick which is as would be expected.

Optical anisotropy arises from the stress and the strain in the surface which we can be minimized by annealing the sample at room temperature for a few days as shown clearly in Fig. 7.7. By

Table 7.8

The annealing effect in the aluminium samples for different periods of time at 500 degrees.

Sample	Annealing time in hours	Ψ Degree	Δ Degree	δN_{ac}
GA 2	0	43.18	140.18	2.17×10^{-1}
GA 2	2	43.43	126.16	1.30×10^{-1}
GA 3	0	43.90	141.94	3.45×10^{-1}
GA 3	.5	46.25	132.59	2.91×10^{-1}
GA 4	0	43.01	136.97	3.90×10^{-1}
GA 4	3	43.32	127.15	0.73×10^{-1}
GA 5	0	42.16	141.35	2.58×10^{-1}
GA 5	1	43.63	128.99	1.70×10^{-1}
GA 6	0	43.48	132.45	4.90×10^{-1}
GA 6	3	43.12	133.41	0.83×10^{-1}
GA 6	4	43.63	133.99	0.40×10^{-1}

Table 7.9

The optical anisotropy for oxide on single crystal aluminium (311), (111) and (110) (electropolished samples), where n_3 = 1.109 to 1.3, k_3 = 6.33 to 6.689, Φ = 60 degrees and λ = 632.8 nm.

Sample	Ψ Degree	Δ Degree	n_2	δN_{ac}
GE 1(111)	42.83	150.59	1.174	8.0×10^{-1}
GE 2(311)	42.79	148.80	1.960	7.6×10^{-1}
GE 3(110)	42.85	148.90	1.220	7.6×10^{-1}
GE 4(311)	42.79	149.51	1.2581	7.2×10^{-1}
GE 5(111)	42.80	148.66	1.155	5.0×10^{-1}
GE 6(311)	42.86	144.53	1.650	4.5×10^{-1}
GE 7(110)	42.76	148.99	1.990	7.9×10^{-1}
GE 8(111)	42.99	149.42	1.200	6.0×10^{-1}
GE 9(111)	42.99	150.01	1.790	3.6×10^{-1}
GE 10(111)	42.98	148.44	1.999	5.78×10^{-1}
GE 11(110)	42.99	150.33	1.790	5.72×10^{-1}
GE 12(110)	42.98	150.19	1.901	7.12×10^{-1}
GE 13(110)	42.97	149.41	2.018	7.20×10^{-1}
GE 14(110)	42.93	150.95	1.830	6.00×10^{-1}

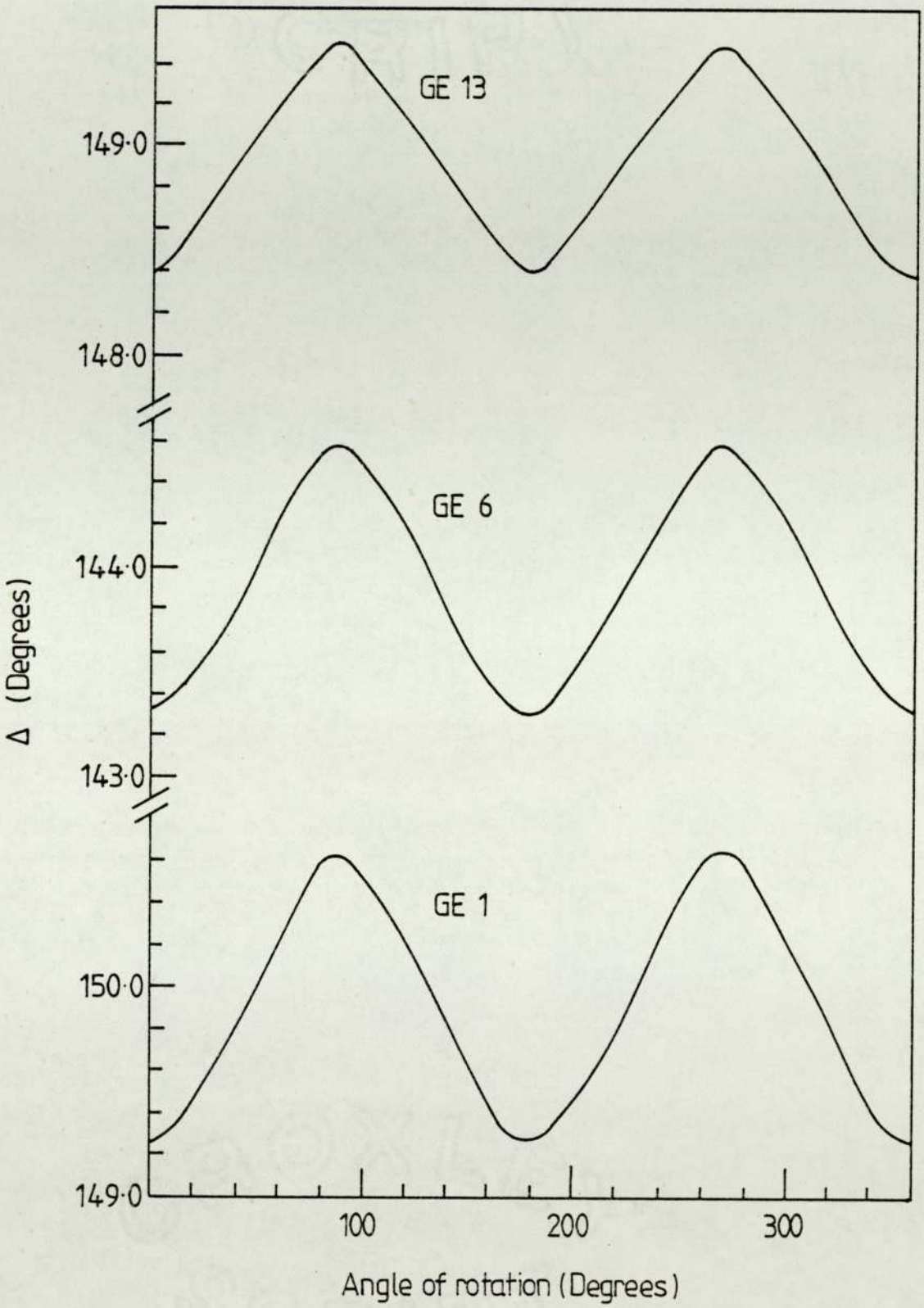

Figure 7·6 The variation in the ellipsometer parameter Δ , for three electropolished single crystal samples GE 1, 6 and 13.

Table 7.10

The difference in the amplitude of ψ and Δ angles between the polycrystalline (as supplied) samples and the single crystal (electropolished) samples of aluminium.

Sample	Amplitude ψ Degree	Amplitude Δ Degree
GA 1	1.95	2.6
GA 2	1.375	2.39
GB 1	1.9	2.06
GC 1	1.22	2.50
GC 3	1.265	1.975
GE 1	2.0×10	5.0×10^{-1}
GE 2	4.5×10	5.1×10^{-1}
GE 3	3.0×10	4.5×10^{-1}

Table 7.11

The value of the pseudo refractive index for electropolished single crystal aluminium.

Sample	Ψ Degree	Δ Degree	Pseudo Refractive Index n'	k'
GE 1	42.83	150.59	0.8744	5.5250
GE 2	42.79	148.80	0.7960	5.1937
GE 3	42.85	148.90	0.7799	5.2168
GE 4	42.79	149.51	0.8313	5.3192

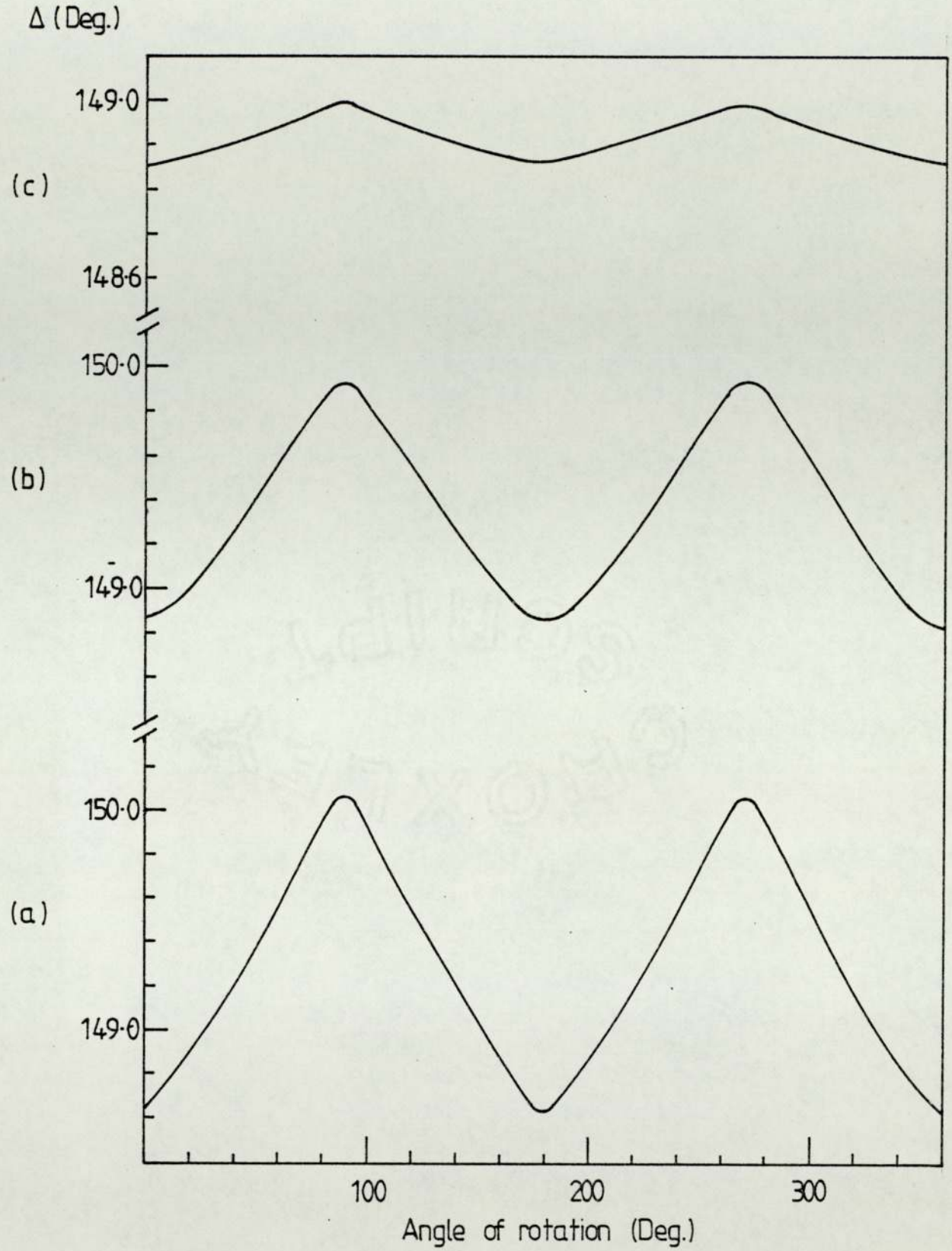

Figure 7·7 The reduction in the amplitude of Δ angles after annealing the sample (leaving the sample in air for five days) of electropolished single crystal aluminium sample GE 5. Annealing (a) one day, (b) two days, (c) five days.

leaving the sample for five days optical anisotropy is reduced by 85% i.e. After electropolishing optical anisotropy in sample one is $\delta N = 0.80$ and after leaving the sample for five days $\delta N = 0.12$ as shown in Table 7.12.

7.3 Discussion

The variation in ψ and Δ angles in the polycrystalline aluminium is relatively high. It is in the range of 2.6 degrees for Δ and 1.95 degrees for ψ in sample GA1 and 0.56 degrees and 0.39 for Δ and ψ degrees respectively for an electropolished single crystal, sample GE7. Table 7.6 shows the variation in the value of the refractive index of the composite surface as the surface is rotated. The variation is from 1.309 to 1.871 for sample GC1 (polycrystalline). The difference in electropolished single crystal samples are of the same order of magnitude. The value of δN for electropolished single crystal samples are in the range of 7.2×10^{-1} for sample GE4 and equal to 5.62×10^{-1} for sample GC1 which is a polycrystalline sample and this shows a small difference between the two kinds of samples which in some cases are almost equal (see Tables 7.6 and 7.9).

Stress and the related optical anisotropy could be minimized by annealing the polycrystalline sample at 500 degrees and the single crystal at room temperature. The polycrystalline sample was annealed for four hours in order to achieve 91% optical anisotropy reduction (Table 7.8). The same optical anisotropy reduction was achieved in the single crystal samples after an annealing period of six days at room temperature as shown in Table 7.12. Polycrystalline samples GA 2,3,4,5 and 6 were

Table 7.12

The life time of the optical anisotropy (annealed at the room temperature) for several days for electropolished (111) and (110) single crystal aluminium.

Sample	Annealing Time in Days	Ψ Degree	Δ Degree	δN_{ac}
1(111)	0	42.83	150.59	0.8
	1	42.80	150.18	0.71
	2	42.81	150.27	0.495
	5	42.79	149.26	0.12
5(111)	1	42.86	148.66	0.50
	2	42.85	148.83	0.334
	4	42.82	149.63	0.188
	5	42.82	148.86	0.114
7(110)	0	42.76	148.99	0.79
	1	42.78	148.82	0.62
	2	42.76	148.82	0.551
	3	42.79	149.66	0.40
	6	42.79	149.12	0.07
8(111)	1	42.99	149.42	0.60
	2	42.98	149.31	0.35
	3	42.97	149.67	0.20
	4	42.95	150.43	0.10
	5	42.95	150.55	0.05

annealed for 2, 0.5, 3, 1 and 4 hours respectively and the annealing effect in each sample reduced the optical anisotropy by 20%, 15%, 81%, 34% and 91% respectively. From this annealing process which reduces stress (and as a result, optical anisotropy) and surface roughness see Appendix 7, we can draw the same conclusions that we had for the silicon dioxide, that annealing the samples is a mechanism of re-crystallizing the system of Al - Al 0 . We annealed the polycrystalline at 500 degrees where oxides were formed at possibly 600 degrees or higher during the preparation process, and the single crystal annealed at room temperature where it needed to be kept under -10 degrees during the electropolishing, because it is an exothermic reaction.

Different values of the substrate refractive index are needed for calculating optical anisotropy, as shown in Table 7.15. The differences in the values of n and k could occur because of surface roughness.

We found that diamond polishing andelectropolishing removes the thicker oxide layer produced during the production of polycrystalline aluminium, and it reduce the anisotropy to a point where it is was not detectable by ellipsometer. The layer of oxide formed after electropolishing single crystal aluminium exhibited anisotropy.

Table 7.13

The refractive index of the four groups of aluminium which we used for the optical anisotropy calculations.

Group	n_3	k_3
GA	1.3-1.9	7.1-7.5
GB	1.699	3.09
GC	1.15	6.33
GE	1.109-1.299	6.33-6.689

CHAPTER VIII

SUMMARY OF CONCLUSION

In this chapter we will summarize the conclusions which have been presented in this work.

We studied the sensitivity of the ellipsometer for measuring properties of surfaces (optical properties of film free surfaces and thicknesses of surface layers). The studies have been presented in theoretical and experimental sections. We investigated the effect of the variation in the refractive index of the film, the substrate and changes in the angle of incidence on the measured thickness of surface layers:

(1) A change of ± 0.1 in n_2 (if $n_2 = 1.7$ for the surface layer) was studied. The sensitivity was very good in the range of thicknesses between 0 - 15 nm, but as the thickness increased the difference between the values of Ψ and Δ increased to ($\delta\Psi = 2.7$ and $\delta\Delta = 18.58$ as n_2 changed from 1.69 to 1.71). This will give rise to an error in thickness measurement. The same effect was observed when k_2 changed.

(2) The change of ± 0.1 in n for the substrate (if $n_3 = 0.7926$) was studied. The change in $\delta\Delta$ was small, compared to the change in $\delta\Psi$ in the range between 0 - 60 nm and from 75 - 90 nm also. This will affect the measured value in the thickness. But when k_3 the substrate absorption value changed by ± 0.1 (if $k_3 = 4.6229$) the error arising in the thickness measurement is small.

(3) The effect of changing the angle of incidence by ± 1 (if $\Phi = 61$) gives rise to an error in the thickness measurement all

around the ψ and Δ loop (see Fig.5.6). Therefore the smallest error in the thickness measurement will occur when the assumed k_3 value is in error.

The measurement sensitivity of ψ and Δ (by keeping all the parameters unchanged) was investigated. From this study we found that the most sensitive regions lie in the bottom and the top of the ψ and Δ loop when the change in ψ is small for a change in thickness. After this theoretical study, we presented experimental results and showed in each table the sensitivity of instruments at that particular thickness.

The importance of the angle of incidence encouraged us to find the optimum angle of incidence for samples on which optical properties has already been measured in this work. We found that the optimum angle of incidence for detecting Si_3N_4 on Si is 74, SiN_{34} on Al is 77 and SiO_2 on Si is 75 and we also presented a further five cases.

Examination of the silicon/silicon dioxide complex by ellipsometry, showed that optical anisotropy existed in silicon dioxide thermally grown at 1100°C. The detection of optical anisotropy in silicon oxide was observed on samples which have thicknesses greater than 400 nm. The optical anisotropy values vary from 1×10^{-3} to 8×10^{-3} in samples with a thickness of 400 nm to 995.9 nm respectively (see Table 6.5). Optical anisotropy can be attributed to the stress in the oxide film, which possibly arises from the difference between thermal expansion coefficient of the silicon and silicon dioxide during the cooling process. The stress was reduced by annealing the sampls at 950°C in a nitrogen atmosphere, which is lower than the oxidation temperature

of 1100 C. Fig. 6.15 shows the reduction in stress when sample 24 was annealed for 30 minutes, 60 minutes and 90 minutes from 1.28 x 10 N/M before annealing to 1.71 x 10 N/M after annealing. The reduction by 41%, 81% and 86% in the optical anisotropy was reached after annealing for 30 minutes, 60 minutes and 90 minutes (Sample 24). Silicon dioxide was found to exhibit optical anisotropy all around the loop of and (except at the bottom of the curve).

Optical anisotropy was observed in oxide layers on polycrystalline aluminium "as supplied" and in oxide layers on electropolished single crystals. The refractive index of polycrystalline aluminium was divided into three different groups, to be able to calculate optical anisotropy in the samples. Optical anisotropy in the oxide was found to vary from one group to another, where it lay between 0.8 x 10 - 4.9 x 10, 0.3 x 10 - 0.8 x 10 and 5.4 x 10 - 5.6 x 10 for Groups A, B and C respectively (see Table 7.6). The same order of magnitude was found for the oxide on single crystal aluminium, where it lies in the range of 3.6 x 10 - 8.0 x 10 (see Table 7.9). Optical anisotropy was reduced by annealing and the polycrystalline samples were annealed at 500 C and the single crystal samples were annealed at room temperature. The optical anisotropy was reduced by 81% - 91% when polycrystalline samples were annealed (at 500 C) for four hours (see Table 7.8). Single crystal aluminium was annealed at room temperature and a reduction of 85% optical anisotropy was obtained, when the sample was left for five days.

We were unable to detect any change in the ellipsometer parameters

and in the r.f. prepared Si N on Si, Si N on Al, Si N (glow discharge), amorphous silicon and SiO nor in the diamond polished polycrystalline and single crystal aluminium (pure 99.999%) when samples were rotated about a normal to their surfaces. The thickness of r.f. prepared silicon oxide samples were less than 400 nm, which according to our results is the minimum thickness for detecting optical anisotropy in thermally grown samples of silicon oxide.

Optical anisotropy was high in aluminium oxide compared to that of silicon dioxide where changes in refractive index were of the order of 10 and 10 for the aluminium oxide and silicon dioxide respectively. We attribute anisotropy to the result of stress in both types of surface films.

APPENDIX 1

ELLIPSOMETRY OF ANISOTROPIC FILMS

Reflection and refraction of electromagnetic wave at an interface between medium I (homogeneous isotropic) with medium II (homogeneous anisotropic) has been investigated by several authors (see Section 2.3).

This study was carried out by Den Engelsen[69]. He theoretically examined a uniaxial film with an optic axis in the direction of stratification (parallel to the Z-direction (see Fig A1 .1). The refractive index of the system will be

$$n_z = n_{\parallel} \quad (1-ik_{\parallel})$$

$$n_x = n_y = n_{\perp} \quad (1-ik_{\perp})$$

therefore Fresnel's equation is

$$\cos^2\Phi / n_{\perp}^2 + \sin^2\Phi / n_{\parallel}^2 - 1/n_e^2 = 0$$

$$1/n_o^2 = 1/n_{\perp}^2$$

where n_o and n_e the refractive index of the ordinary and extraordinary, respectively. Snell's law was applied in the direction of the wave normals in media I and II. To obtain the reflectance, the electric field E will resolve into parallel (TM) and perpendicular (TE) components. Therefore Fresnel's reflectance for an ordinary will be given as follows:

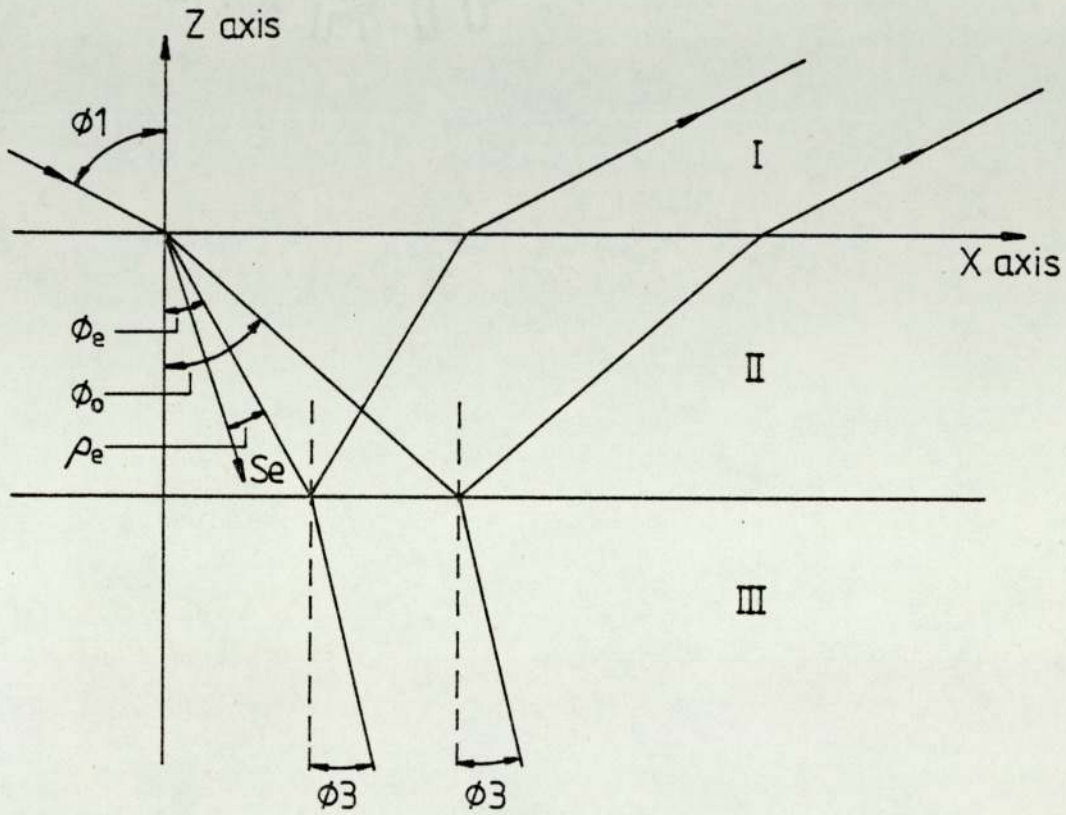

Figure A1.1 Three phase system, medium I and III are isotropic, where medium II is an uniaxial symmetry medium with optic axis parallel to the Z axis. The XZ plane is plane of incidence.
[After Den Engelsen]

$$r = \frac{n_1 \cos\Phi_1 - n_\perp \cos\Phi_0}{n_1 \cos\Phi_1 + n_\perp \cos\Phi_0}$$

$$r = \frac{n_\perp \cos\Phi_0 - n_3 \cos\Phi_3}{n_\perp \cos\Phi_0 + n_3 \cos\Phi_3}$$

where r and r are Fresnel's reflectance at the interface medium I and II, and medium II and III respectively . The phase difference for the ordinary wave will be :

$$\beta = \frac{2\pi d(n_\perp^2 - n_1^2 \sin^2\Phi_1)^{1/2}}{\lambda}$$

where λ are the wavelength of the light, and d is the thickness of the anisotropic compound layer.

The Fresnel reflectance for the extraordinary wave (TM) will be given as:

$$r_1'' = \frac{n_{//} n_\perp \cos\Phi_1 - n_1 (n_{//}^2 - n_1^2 \sin^2\Phi_1)^{1/2}}{n_{//} n_\perp \cos\Phi_1 + n_1 (n_{//} - n_1^2 \sin^2\Phi_1)^{1/2}}$$

$$r_2'' = \frac{n_3 (n_{//}^2 - n_1^2 \sin^2\Phi_1)^{1/2} - n_{//} n_\perp \cos\Phi_3}{n_3 (n_{//}^2 - n_1^2 \sin^2\Phi_1)^{1/2} + n_{//} n_\perp \cos\Phi_3}$$

The phase difference β is

$$\beta = 2\pi d\, n_\perp (n_{//}^2 - n_{//}^2 \sin^2\Phi_1)^{1/2} / \lambda n_{//}$$

The only difference between the ellipsometic formulas for isotropic and uniaxial anisotropic are the Fresnel coefficients. He presented Drude's formula for an anisotropic medium as follows:

$$\text{Tan}\,\Psi\, e^{i\Delta} = \text{Tan}\,\bar{\Psi}\, e^{i\bar{\Delta}} \left[1 - i\left(\frac{4\pi d n_1 \cos\phi_1 \sin^2\phi_1\, n_3^2 \left[(n_1^2 + n_3^2) - n_1^2 n_3^2 - n_{11}^2 n_1^2\right]}{\lambda\, n_{11}^2 (n_1^2 - n_3^2)\,(n_1^2 \sin^2\phi_1 - n_3^2 \cos^2\phi_1)}\right)\right]$$

where $\bar{\Psi}$ and $\bar{\Delta}$ are the values of Ψ and Δ for the substrate.

```
5 PRINT"OPCON 1 N&K"
10 PRINT"IN BASIC"
11 PRINT"A=PHI;B1=MIN PSI;B2=MAX PSI B3=STEP PSI;C1;C2;C3;=MIN;MAX;STEP DELTA
20 INPUTA,B1,B2,B3,C1,C2,C3
21 OPEN1,4:PRINT#1,TAB(6);"N";TAB(16);"K";TAB(24);"B";TAB(11);"C" :CLOSE1
30 FORB=B1TOB2STEPB3
31 FORC=C1TOC2STEPC3
40 D=(SIN(A*π/180))↑2
50 F=(TAN(A*π/180))↑2
60 Q=(COS(2*B*π/180))↑2
62 R=(SIN(2*B*π/180))↑2
70 M=(1+SQR(R)*COS(C*π/180))↑2
72 S=(SIN(C*π/180))↑2
80 LET2=D+(F*D*(Q-R*S))/M
82 F=SIN(C*π/180)
90 Y=((D*F)*F*SIN(4*B*π/180))/M
111 V=(-.5*Z)+(SQR(16*Z↑2+16*Y↑2))/8
112 K=SQR(V)
120 N=Y/(2*K)
122 OPEN1,4
124 PRINT#1,N;TAB(6);K,TAB(6);B;TAB(6);C: CLOSE1
125 NEXTC
126 NEXTB
127 END
```

APPENDIX 3

```
10 PRINT"OPCON PSI DEL"
20 DIMA(14),B(14),K(3),N(13),R(5),X(5),Y(5)
30 READN(2),K(2),N(3),K(3),T,L,D0,D9,S0
50 PRINT"N2="N(2),"K2="K(2),"N3="N(3)
51 PRINT"K3="K(3),T,L,D0,D9,S0
60 PRINT"PRINT WAVELENGTH=",L
70 PRINTTAB(1);"THICKNESS"TAB(15);"DELTA";TAB(30);"PSI"
90 FOR D=D0TOD9 STEPS0
100 I=0
110 X0=K(2+I)*K(2+I)
120 T4=T
130 X(4)=SIN(T4)
140 X(4)=X(4)*X(4)
150 N(4+I)=N(2+I)*N(2+I)
160 X(2+I)=N(4+I)-X0-X(4)
170 Y(2+I)=2*N(2+I)*K(2+I)
180 X(4+I)=X(2+I)*X(2+I)
190 Y(4+I)=Y(2+I)*Y(2+I)
200 R0=SQR(X(4+I)+Y(4+I))
210 A0=SQR((R0+X(2+I))/2)
220 A(4+I)=N(2+I)*A0
230 A(7+I)=SQR((R0-X(2+I))/2)
240 A(9+I)=A(7+I)*K(2+I)+A(4+I)
250 A(4+I)=X0+N(4+I)
260 A(2+I)=A(9+I)/A(4+I)
270 B0=K(2+I)*A0
280 B(4+I)=N(2+I)*A(7+I)
290 B(2+I)=(B0-B(4+I))/A(4+I)
300 IFA(2+I)>0THEN560
310 A(2+I)=-A(2+I)
320 B(2+I)=-B(2+I)
330 GOTO560
340 X(I)=K(2+I)*K(2+I)
350 T4=T
360 X(4)=SIN(T4)
370 X(4)=X(4)*X(4)
380 N(4+I)=N(2+I)*N(2+I)
390 X(2+I)=N(4+I)-X(I)-X(4)
400 Y(2+I)=2*N(2+I)*K(2+I)
410 X(4+I)=X(2+I)*X(2+I)
420 Y(4+I)=Y(2+I)*Y(2+I)
430 R(I)=SQR(X(4+I)+Y(4+I))
440 A(I)=SQR((R(I)+X(2+I))/2)
450 A(4+I)=N(2+I)*A(I)
460 A(7+I)=SQR((R(I)-X(2+I))/2)
470 A(9+I)=A(7+I)*K(2+I)+A(4+I)
480 A(4+I)=X(I)+N(4+I)
490 A(2+I)=A(9+I)/A(4+I)
500 B(I)=K(2+I)*A(I)
```

```
510 B(4+I)=N(2+I)*A(7+I)
520 B(2+I)=(B(I)-B(4+I))/A(4+I)
530 IFA(2+I)>0THEN560
540 A(2+I)=-A(2+I)
550 B(2+I)=-B(2+I)
560 I=I+1
570 IFI=1THEN340
580 C=COS(T4)
590 C1=N(2)*C
600 C2=A(2)-C1
610 E2=C1+A(2)
620 D1=K(2)*C
630 D2=D1+B(2)
640 F2=B(2)-D1
650 E=C2*E2
660 E1=D2*F2
670 G2=E+E1
680 G=E2*E2
690 G1=F2*F2
700 G=G+G1
710 G2=G2/G
720 F=C2*F2
730 F1=D2*E2
740 H2=(F1-F)/G
750 H=N(3)*A(2)
760 H1=K(3)*B(2)
770 H4=N(2)*A(3)
780 H5=K(2)*B(3)
790 C3=H4+H5-H-H1
800 H8=N(3)*B(2)
810 H9=K(3)*A(2)
820 H6=K(2)*A(3)
830 H7=N(2)*B(3)
840 D3=H9-H8+H7-H6
850 E3=H+H1+H4+H5
860 F3=H8+H7-H9-H6
870 G4=C3*E3
880 G5=D3*F3
890 G6=E3*E3
900 G7=F3*F3+G6
910 G3=(G4+G5)/G7
920 F4=C3*F3
930 H3=(D3*E3-F4)/G7
940 P=N(2)*A(2)
950 P1=K(2)*B(2)
960 P2=C-P-P1
970 P4=N(2)*B(2)
980 P5=K(2)*A(2)
990 S2=C+P+P1
1000 Q2=P4-P5
1010 T2=P5-P4
1020 U=P2*S2
1030 U1=Q2*T2
1040 U4=S2*S2
```

```
1050 U5=U4+T2*T2
1060 U2=(U+U1)/U5
1070 U7=Q2*S2
1080 U6=P2*T2-U7
1090 V2=U6/U5
1100 Q=N(3)*A(3)
1110 Q1=K(3)*B(3)
1120 P3=P+P1-Q-Q1
1130 Q4=B(3)*N(3)
1140 Q5=K(3)*A(3)
1150 Q3=P5-P4+Q4-Q5
1160 S3=P+P1+Q+Q1
1170 T3=P5-P4-Q4+Q5
1180 V=P3*S3
1190 V1=Q3*T3
1200 V4=S3*S3
1210 V5=V4+T3*T3
1220 U3=(V+V1)/V5
1230 V6=P3*T3
1240 V7=Q3*S3
1250 V3=(V6-V7)/V5
1260 M1=P+P1
1270 M=6.283185*D/L
1280 M1=M1*M
1290 L1=(P4-P5)*M
1300 M3=EXP(2*L1)
1310 M=2*M1
1320 M2=M3*COS(M)
1330 L2=M3*SIN(M)
1340 L4=G3*M2
1350 L5=H3*L2
1360 A(11)=G2+L4+L5
1370 L6=H3*M2
1380 L7=G3*L2
1390 B(11)=H2+L6-L7
1400 S4=U2*U3*M2
1410 S5=V2*V3*M2
1420 S6=L2*V3*U2
1430 S7=L2*V2*U3
1440 A(12)=1+S4-S5+S6+S7
1450 S8=V2*U3*M2
1460 S9=U2*M2*V3
1470 J=U2*U3*L2
1480 J1=V2*V3*L2
1490 B(12)=S8+S9-J+J1
1500 Q6=G2*G3*M2
1510 Q7=H2*H3*M2
1520 Q8=H2*L2*G3
1530 Q9=H3*L2*G2
1540 A(13)=1+Q6-Q7+Q8+Q9
1550 P6=H2*G3*M2
1560 P7=H3*G2*M2
1570 P8=L2*G2*G3
1580 P9=H2*H3*L2
1590 B(13)=P6+P7-P8+P9
```

```
1600 T5=U3*M2
1610 T6=V3*L2
1620 A(14)=U2+T5+T6
1630 T7=M2*V3
1640 T8=U3*L2
1650 B(14)=V2+T7-T8
1660 R(2)=A(11)*A(12)
1670 J2=R(2)-B(11)*B(12)
1680 R(3)=B(11)*A(12)
1690 J3=A(11)*B(12)+R(3)
1700 R(4)=A(13)*A(14)
1710 J4=R(4)-B(13)*B(14)
1720 R(5)=B(13)*A(14)
1730 J5=A(13)*B(14)+R(5)
1740 W1=J2*J4
1750 W2=J3*J5
1760 W3=J4*J4
1770 W4=W3+J5*J5
1780 W=(W1+W2)/W4
1790 Z1=J4*J3
1800 Z2=J2*J5
1810 Z=(Z1-Z2)/W4
1820 Z3=180*ATN(Z/W)/(4*ATN(1))
1830 IFZ3>0THEN1850
1840 Z3=180+Z3
1850 Z4=W*W
1860 Z5=180*ATN(SQR(Z4+Z*Z))/(4*ATN(1))
1870 PRINTTAB(3);D;TAB(12);Z3;TAB(25);Z5
1880 NEXTD
1900 END                                                    L=WAVE(ANGS).
1910 REM DATA N(2),K(2)=FILM.N(3),K(3)= SUBS.T=INC.ANG(RAD).L=
1911 REM DATA D0,D9,S0=MIN,MAX,STEPIN   FILM THICKNESS
1920 DATA1.655,0,0.675,4.73,1.1257,5478,0,100,10
```

APPENDIX 4

```
5 REM"N&K FOR R S"
6 REM"***THIS PROG. APPLIED FOR NS=N-IK
10 READA,B,H,Q1,Q2,Q3
12 PRINT;"NS="A,"KS="B
15 OPEN1,4:PRINT#1,"NS="A,"KS="B:CLOSE1
20 OPEN1,4:PRINT#1,TAB(6);"N";TAB(16);"K";TAB(24);"Q";TAB(11);"Q"
25 PRINTTAB(6);"N";TAB(16);"K";TAB(24);"Q";TAB(11);"Q"
30 FORQ=Q1TOQ2STEPQ3
40 A1=A*A
50 A2=B*B
70 A4=2*A*B
80 A5=A1-A2
90 A6=A5-1
100 A7=A5+2
110 B3=((A6*A7)+A4*A4)/(A7*A7+A4*A4)
120 B4=((A4*A7)-(A6*A4))/(A7*A7+A4*A4)
130 B5=1+(2*Q*B3)
140 B6=2*Q*B4
150 B7=1-Q*B3
155 E=Q*B4
160 B8=((B5*B7)-B6*E)/(B7*B7+E*E)
170 B9=((B6*B7)+(B5*E))/(B7*B7+E*E)
175 P=B9/B8
180 C1=(B8*B8+B9*B9)
190 C2=SQR(C1)
200 G=ATN(P)
210 C3=6.28*H
220 C4=(G+C3)/2
230 C5=COS(C4)
240 C6=SIN(C4)
245 C7=SQR(C2)
250 F1=C5*C7
260 F2=C6*C7
270 N=F1
280 K=F2
290 OPEN1,4:PRINT#1,N;TAB(6);K,TAB(6);H;TAB(6);Q:CLOSE1
295 PRINTN;TAB(6);K,TAB(6);H;TAB(6);Q
300 NEXTQ
310 END
320 DATA0.493,4.061,0,.1,1,.1
```

APPENDIX 5

```
10 REM"Q1 VAL FOR R S"
20 REM"THIS PROG. GIVE THE VALUE OF Q FOR A ROUGH SURFACE"
30 REM"****----------------------****"
40 REM"****(NE- IKE)= Q (NS- IKS)****"
50 REM"****----------------------****"
60 READA,B,C,D
70 PRINT;"NE="A,"KE="B
75 PRINT;"NS="C,"KS="D
80 PRINT#1,"NE="A,"KE="B
85 PRINT#1,"NS="C,"KS="D
100 PRINT#1,TAB(10);"Q1",TAB(12);"Q2"
110 PRINTTAB(6);"Q1";TAB(16);"Q2"
120 A1=A*A
130 A2=B*B
140 A4=2*A*B
150 A5=A1-A2
160 A6=A5-1
170 A7=A5+2
180 B3=((A6*A7)+A4*A4)/(A7*A7+A4*A4)
190 B4=((A4*A7)-(A6*A4))/(A7*A7+A4*A4)
200 C1=C*C
210 C2=D*D
220 C4=2*C*D
230 C5=C1-C2
240 C6=C5-1
250 C7=C5+2
260 C8=((C6*C7)+C4*C4)/(C7*C7+C4*C4)
270 C9=((C4*C7)-(C6*C4))/(C7*C7+C4*C4)
280 F1=(B3*C8+B4*C9)/(C8*C8+C9*C9)
290 F2=((B4*C8)-(B3*C9))/(C8*C8+C9*C9)
300 PRINT#1,TAB(3);F1;TAB(12);F2
305 CLOSE1
310 PRINTF1;TAB(6);F2
320 END
330 REMDATA NE,KE=EFFECTIVE N K FOR THE FILM,NS,KS FOR THE SUBS.
999 DATA3.16,1.327,.35,2.45
```

APPENDIX 6

ELECTROPOLISHING

The first optical micrographs produced by anodically dissolving a metal, rather than the traditional mechanical polishing method, were published in 1936 by Jacquet[152-157]. He also recorded the relationship between the current and anode potential.

The curve of anode potential against anode current density (Fig. A2) has been divided into five sections:

(1) The region A-B, current density increases with the potential. (Some metal dissolves, and the surface has a dull etched appearance).

(2) The region B-C, the current is unstable and fluctuates, which reflects an unstable condition.

(3) The region C-D, indicates a stable plateau, which can be obtained by increases in the potential producing little or no change in the current density.

(4) The region D-E, an increase in the potential above the point D leads to a rise in the current density, gas bubbles evolve slowly, breaking the polishing film and causing severe pitting.

(5) The region E-F, further increase in potential leads to a continued rise in the current density, this will cause a rapid gas evolution.

The optimum polishing conditions occur along C-D near D.

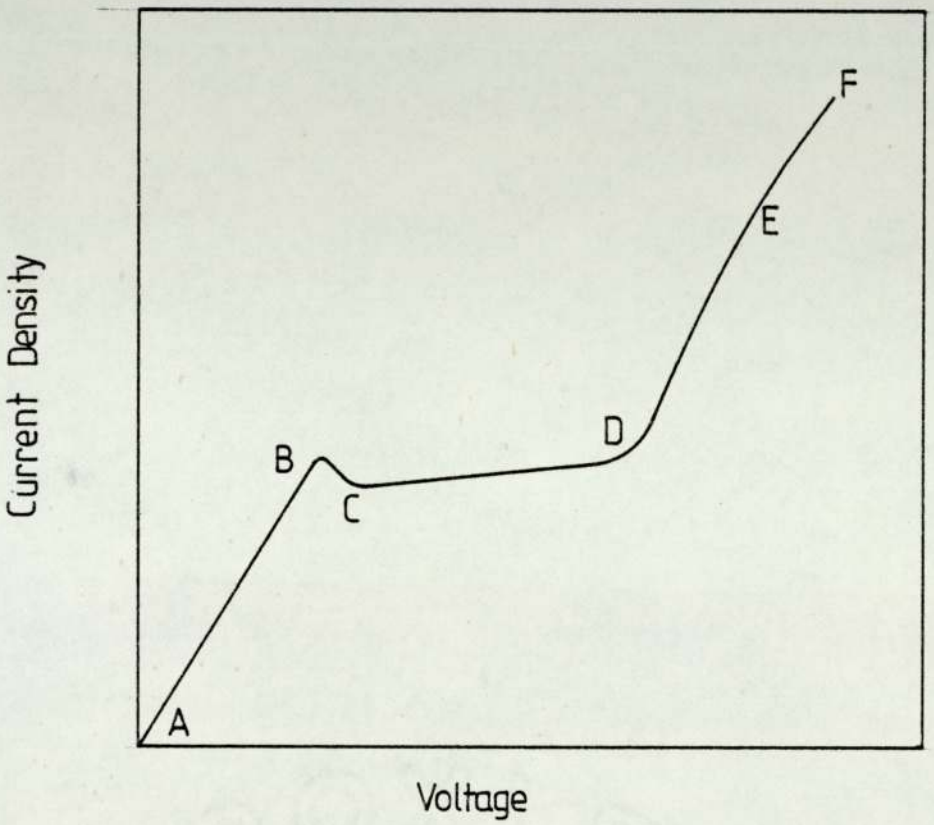

Figure A 6.1 Typical voltage - current density relationship for electropolishing.

APPENDIX 7

SURFACE ROUGHNESS

There are more than one type of surface roughness which have been used in theoretical models as explained in Section 3.3. An actual surface may be a combination of more than one of these types. If a sample has one type of surface roughness the value of " q " less than one[56] (q is the volume fraction of the substrate material which is smooth) as shown in Table A7.1. From our results and using equation 3.31 we found that $q > 1$. We assumed that there may be various reasons for this: (1) a combination of surface roughness, (2) the effect of the roughness plus the hydroxide film which forms during the production process, (3) the presence of optical anisotropy, (4) a combination of all these.

We used the talysurf technique to show the degree of roughness (as shown in Fig. A7.1) before and after annealing, and we found that the degree of roughness is decreased by annealing. Therefore annealing reduces stress, optical anisotropy and roughness which is clearly shown in Fig. A7.1. Annealing at a temperature of 500°C for three and four hours reduced the roughness by 60% and 66% in sample GA4,6.

If we take the triangle model as shown in Fig. A7.2 we can see the difference between the rough surface and the smooth surface. Fig. A7.2a shows that the undulation length of light in the film is greater than the light wavelength and this is directly related to undulation in the surface across the sample, where the value of Ψ and Δ is obtained along the rolling direction which is

Table A7.1

The change of the 'q' value from 0.1 to 1.0 to show the degree of roughness for aluminium substrate with n_3=1.45 and k_3=6.12 (in vacuum).

n_e	k_e	q
1.166	6.018 x 10	0.1
1.348	0.0134 x 10	0.2
1.555	0.0234 x 10	0.3
1.801	0.038 x 10	0.4
2.108	0.0613 x 10	0.5
2.522	0.104 x 10	0.6
3.141	0.196 x 10	0.7
4.26	0.485 x 10	0.8
7.111	2.845 x 10	0.9
6.119	1.449 x 10	1.0

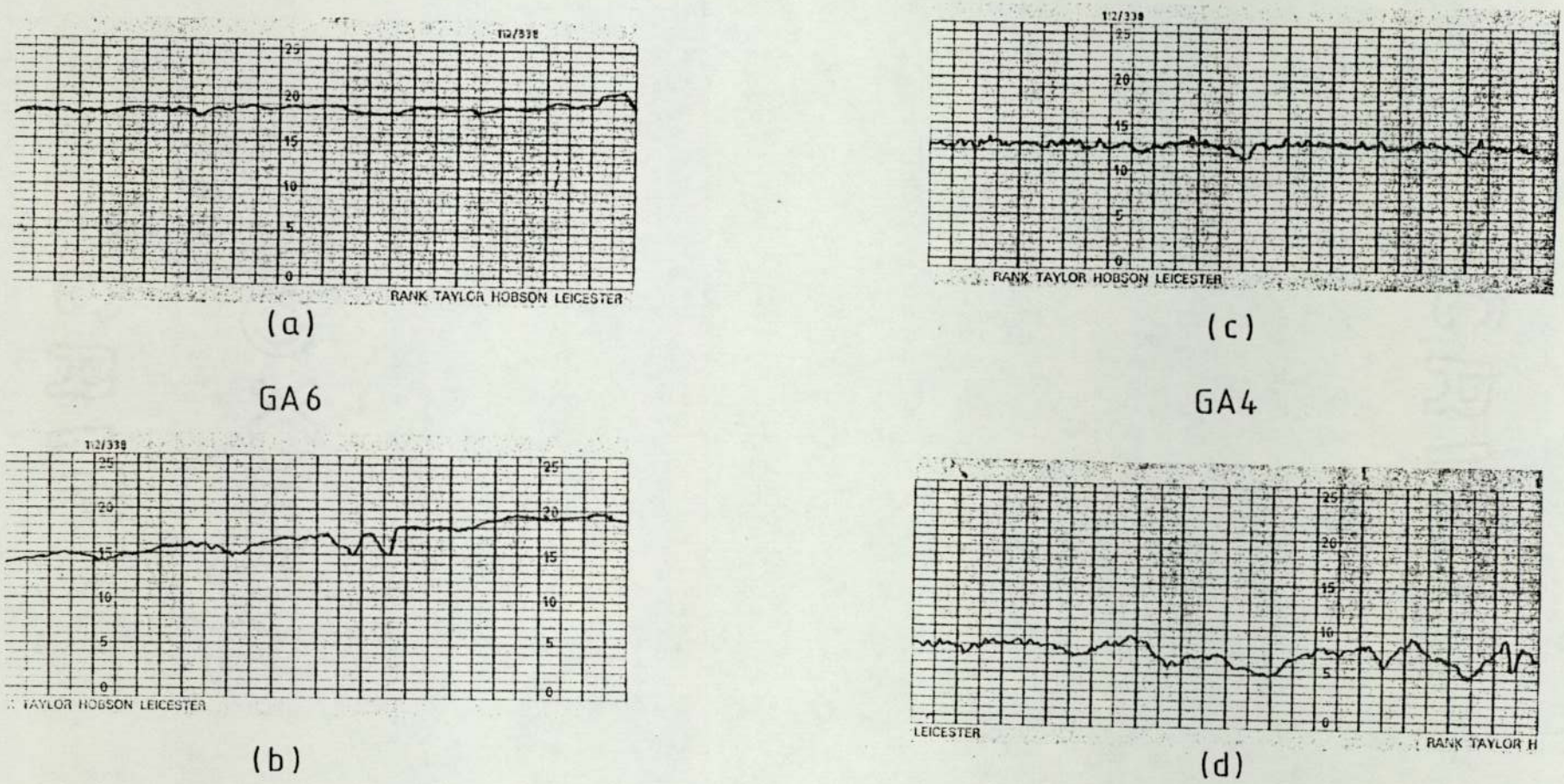

Figure A 7.1 Talysurf traces of polycrystalline aluminium (as supplied) for samples GA6 (a,b) and GA4(c,d). (a) After annealing for four hours at 500°C, (b) before annealing, (c) after annealing for three hours at 500°C, and (d) before annealing.

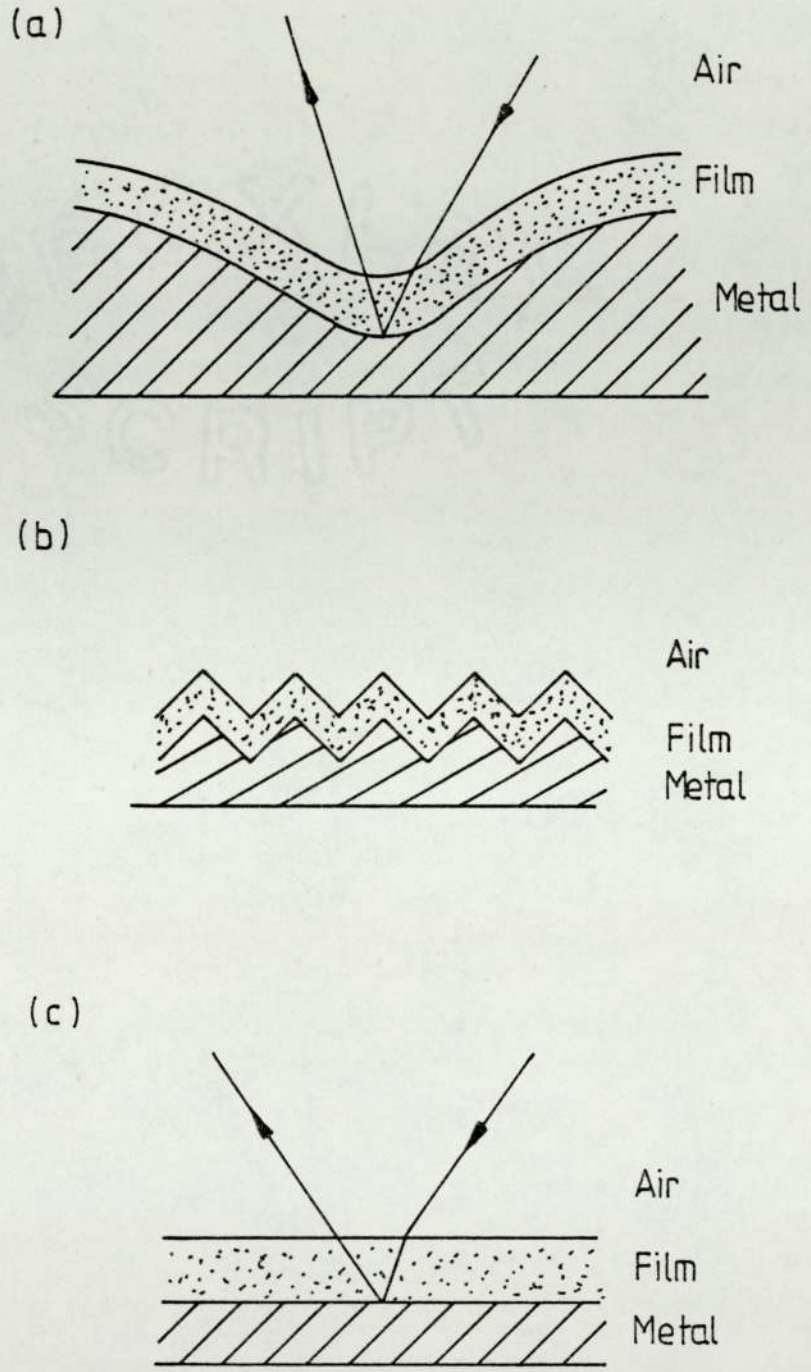

Figure A7.2 Surface roughness (triangle model)
(a) the undulation length is greater than light wavelength,
(b) the undulation length is less than light wavelength,
(c) smooth surface.

smaller than across the rolling direction. In this model we assume that the undulation wavelength is larger compared to the light wavelength, which means the rough surface does not effect the measurement at the same spot, but if the light wavelength is larger compared to the wavelength of the undulation as shown in Fig. 7.12b, the roughness must be taken into consideration. Kruger[169] suggests that this effect is small and it can be neglected but Archer[170] investigated the surface roughness by using a model of cubes where the irregularities are taken to be a periodic distribution of cubes, and he found that any surface with such roughness leads to a thinner film thickness measurement than the real film thickness. The same conclusion was approached by Kruger[171] and Fenstermaker and McCrackin[56] (see Section 3.3). The surface roughness affects the measurement of the films,i.e. for polycrystalline (as shown in Table A7.2) we can see how much difference the film thickness makes to both unpolished (polycrystalline as supplied) and electro-polished (single crystal) samples. The film thickness for unpolished samples were in the range of 15 nm or more and in the range of 5 nm for a polished sample. All this will affect the optical properties. But it is probable that the polycrystalline aluminium samples have more than one kind of roughness because when we calculated the value of 'q ' we found it to be greater than one, as shown in Table A7.3.

Table A7.2

A comparison in the thickness of the film between electropolished single crystal and polycrstalline "as supplied" aluminium samples.

Sample	Ψ Degree	Δ Degree	Thickness nm
GA 1	43.04	141.35	16.5
GB 1	39.57	108.16	48.0
GC 1	42.85	139.61	12.5
GE 2	42.79	148.80	8.5
GE 3	42.85	148.90	4.4
GE 5	42.80	148.66	4.2

Table A7.3

The 'q' value for oxide on polycrystalline aluminium (the pseudo constant was used as the effective refractive index n_e and k_e) $n_3 = 1.12$ and $k_3 = 6.40$.

Sample	n_e	k_e	q
GA 1	0.4742	4.1436	1.1102
GA 2	0.4171	4.0142	1.1250
GB 1	0.4486	1.8315	1.7744
GB 2	0.3294	1.9347	2.0276
GE 1	0.4787	3.9374	1.1305
GE 2	0.6261	4.5734	1.0728

Appendix 8

ELLIPSOMETRIC STUDIES ON SILICON DIOXIDE FILMS ON SILICON.

S. Yaghmour & W. E. J. Neal,
Department of Mathematics and Physics,
University of Aston,
Birmingham B4 7ET.

ABSTRACT

Ellipsometry is demonstrated to be an appropriate technique for measuring the thickness of silicon dioxide films grown thermally and by an r.f. glow discharge desposition technique in commercial equipment. Optical anisotropy has been observed in thermally grown oxide layers on crystalline (111) and (100) silicon by rotating samples (in an ellipsometer) about a normal to the sample surface. The degree of anisotropy films on silicon (111) was found to be dependent on oxide thickness and decreased to ∿ zero with time at an annealing temperature of 950°C. The changes in the optical constant produced by rotation increased from 1×10^{-3} to 8×10^{-3} with an increase in oxide thickness from 400 nm to 1000 nm and decreased for thicker films No anisotropy was observed in thermally grown films or for films deposited by an r.f. glow discharge for thicknesses less than 400 nm.

ELLIPSOMETRIC STUDIES ON SILICON DIOXIDE FILMS ON SILICON.

S. Yaghmour & W. E. J. Neal,
Department of Mathematics and Physics,
University of Aston,
Birmingham B4 7ET.

1. INTRODUCTION

In recent years there has been an increased interest in investigations of optical anisotropy and particularly in surface layers of oxides grown on single crystal substrates. One of the earliest reports on the use of ellipsometry for such investigations was by Cathcart et al [1] who examined oxides grown on copper (110) and (311) surfaces. Other workers have studied the phenomenon using elecro-reflectance at metal/electrolyte interfaces(see for example Furtak and Lynch [2]), Kötz and Lewerenz [3] and Huong et al [4]. Habraken and Bootsma [5] Habraken et al [6,7] and Kotz and Hayden [8] have used spectroscopic ellipsometry to investigate anisotropy in oxygen adsorption and single crystal copper and silver surfaces.

In this paper results are presented for anisotropy observed in $Si\ O_2$ using ellipsometry. The technique followed is that due to Cathcart et al [1]

The use of ellipsometry for surface examination and monitoring of surface layers has been described by many authors; see for example references [9 - 15]. If monochromatic plane polarized light is incident on a surface the reflected light is in general elliptically polarized and contains information relating to the surface and/or surface layers. If the reflected beam becomes the incident beam then plane polarizing light results. In an ellipsometer used in the former mode the elliptically polarized light is analyzed by using some form of phase compensator resulting in plane polarized light which is incident on an analyser. In the normal operation of the instrument the polarizer and analyzer components are so arranged that no light emerges. For more details see Neal [13]

The basic equation of ellipsometry is:-

$$r_p / r_s = \tan\psi \exp(i\Delta) \quad \text{------ (1)}$$

Where r_p and r_s are reflection coefficients for a surface for light with electric vectors parallel and perpendicular to the plane of incidence respectively. The two angles ψ (the direction between the incident light electric vector and the plane of incidence) and Δ (the difference in phase between the p and s components after reflection), are determined from the polarizer and analyzer settings when there is zero intensity at the detector (Fig. 1).

The optical constants n and k for a surface can be obtained from equations provided by Ditchburn [16]

$$n^2 - k^2 = \frac{\sin^2\phi_0 \tan^2\phi_0 (\cos^2 2\psi - \sin^2 2\psi \sin^2\Delta)}{(1 + \sin 2\psi \cos\Delta)^2} + \sin^2\phi_0 \quad \text{---(2}$$

$$2nk = \frac{\sin^2\phi_0 \tan^2\phi_0 \sin 4\psi \sin\Delta}{(1 + \sin 2\psi \cos\Delta)^2} \quad \text{- - - - - ---(3)}$$

Where ϕ_0 = angle of incidence.

The angles ψ and Δ can be used to characterise an ideal surface, i.e. one which is perfectly smooth, reflecting, isotropic and homogeneous. A filmed formed on an initially pure surface will modify the angles ψ and Δ for the pure surface. The magnitude of the change will be dependent on the film thickness. For an anisotropic medium, changes in ψ and Δ take place with a variation in the direction of the incident electic vector with respect to crystal directions in the surface for a given angle of incidence.

Anisotropy was observed in this work by rotating the surface under examination about the normal to the surface thus keeping the angle of incidence constant.

In order to establish that any changes in ψ and Δ , during rotation, were significant it was necessary to assess the sensitivity of the instrument for the thickness of silicon dioxide films on a silicon substrate. A range of pure silicon wafers were examined from each of three batches to determine characteristic values of ψ and Δ for the substrate. Samples from different batches of r.f. prepared silicon dioxide layers were monitored for variations in thickness across samples and differences between samples.

2. EXPERIMENTAL RESULTS

2.1 Instrument and Sensitivity

All ellipsometric measurements were performed on samples at room temperature. The arrangements of basic components in the instrument used is illustrated in Fig.1 and comprised a polarizer, sample holder, compensator (quarter wave plate) analyzer and photomultiplier detector. The angle of incidence was 60° and the radiation source was an He-Ne laser providing light of wavelength 632.8 nm. The samples used for the sensitivity tests were supplied by the Lucas Research Centre. The samples (75.0 mm x 24.5 mm) were cut after oxidation of the silicon wafers. For batches one and two the oxide was grown on (111) silicon substrates (at a temperature of 380°C) by an r.f. glow discharge technique at a pressure of 800 m T and an r.f. power of 150 w. The optical constants of the oxide layer were stated to be n = 1.5, k = 0 and the value was confirmed in this work using a computer fit to data for layers of different thicknesses. Batch three samples were prepared at a pressure of 700 m T and an r.f. power of 140 w. The optical constants for the oxide layers in this case were stated to be n = 1.45, k = 0 and this was also confirmed. For batches one and two samples were cut from the wafers perpendicular (YY$'$) and parallel (XX$'$) to the gas flow in the production chamber as shown in fig. 2 (a and b).

Table 1 shows values of ψ and Δ at three points across each of three samples from the three batches and illustrate the type of variations observed. The last column in the table gives the variation in computed thickness corresponding to the changes in ψ and Δ across the samples. According to the manufacturers of the production chamber the variation could be up to 20 nm for different preparation conditions and the results of the present investigation confirmed this in most cases.

The measured values of ψ and Δ for the centres of the samples are in reasonable agreement with computed values based on substrate optical constants of $n_1 = 3.7583, k_1 = 0.0952$ and oxide optical constants of n = 1.5, k = 0 for batches one and two and n = 1.45, k = 0 for batch three and are given in table 2. The corresponding oxide thicknesses at the centres of samples are given in the last column of table 2.

2.2 Checks for anisotropy for films prepared by the r.f. technique.

All the samples in tables 1 and 2 were rotated through 360° about the normal as mentioned in the introduction and no changes in ψ and Δ were observed. It was concluded that no anisotropy could be detected in thermally grown oxide thicknesses less than about 400 nm thick prepared by the r.f.technique.

2.3 Anisotropy in thermally grown silicon dioxide films on silicon (111).

Samples for anisotropy tests on thermally grown films of silicon dioxide were prepared in the authors' laboratory. The films were thermally grown at atmospheric pressure. Silicon (111) wafers (25 mm x 14.5 mm) of 99.999% purity were cleaned in an ultrasonic bath and heated in a nitrogen atmosphere to 1100°C. The nitrogen was then replaced by oxygen and the silicon dioxide film growth was measured by ellipsometry. The results are shown in fig.3. The films were established to be formed of $Si\ O_2$ by Electron Spectroscopy Chemical Analysis (ESCA).

The effects on the angles ψ and Δ by rotating samples of different thicknesses through 360 degrees at a constant angle of incidence are shown in figs. 4,5,6 and 7. It can be seen that the amplitudes of ψ and Δ depend on the sample thickness and for sample SS 24 (Fig. 4) were 0.22 and 0.48 degree respectively. The optical constants n_a, n_b and n_c for points a, b and c (Fig.4) are given in table 3. The difference in the optical constant between a and c was 8.0×10^{-3} for an oxide thickness of 995.9 nm. Figure 8 gives the amplitudes of

ψ and Δ for films of different thickness. Pendinoff et al (17) have shown that optical anisotropy can be reduced by annealing. In the present tests it was found that the optical anistrophy could be reduced by annealing at 950°C in a nitrogen atmosphere and the results for sample SS 24 are shown in Fig.9.

3. Discussion

From Figs. 4-9 it can be seen that silicon dioxide films grown thermally on silicon (111) at 1100°C and greater than 400 nm thick exhibit optical anisotropy and that the anisotropy is reduced by annealing. No such effect was observed in silicon dioxide layers produced by an r.f. glow discharge technique at a temperature of 380°C.

The sensitivity of the measuring equipment was such that changes in thickness of the order of less than 1 nm could be detected and variations in dioxide thicknesses of up to 20 nm were detected across samples and between samples in a batch produced by the r.f. glow discharge method.

Tests were also made on thermally grown dioxide films on silicon (100) samples. The results of rotating samples of films of thicknesses 1290 nm and 693.9 nm are given in Figs. (10a) and (10b). It can be seen that the variations in ψ and Δ are similar to those observed for (111) samples of approximately the same thickness. The corresponding changes in the optical constant n and the instrument sensitivity are given in Table 3.

Variations in the ellipsometer parameter Δ of up to $\pm$ 0.5 degree could be observed in samples exhibiting anisotropy. If interpreted in terms of thickness, such changes would represent some 2-5 nm variation. The fact that no changes in Δ were observed on rotating oxide samples less than 400 nm thick led to the conclusion that no anisotropy was present. In addition since there was an observable decrease in anisotropy with annealing this indicates that anisotropy in thermally grown silicon dioxide layers can be attributed to stress in the oxide layers.

The stress σ is given by Pedinoff et al (17) and Nye (18):-

$$\sigma = -2\Delta N / N^3 (\pi_{12} - \pi_{11}) \quad \text{---------} \quad (4)$$

where N is the refractive index of the film

Δ N is the optical anisotropy in the film

π_{ij} are stress optic constants.

Values of Δ N obtained in this work are of the same order of magnitude as those given by Pendinoff et al (17).

References

1. J.V. Cathcart, J.E. Epperson and G.F. Petersen, Acta Meta. 10(1962) 699.
2. T.E.Furtak and D.W. Lynch, Phys.Rev.Letter, 35 (1975) 960.
3. R. Kötz and H.J. Lewerenz, Surface Sci. 97(1980) 319.
4. C.N.Huong, C. Hinnen, J. Lecocur and R. Parsons, J.Electro.Chem. 92(1978) 239.
5. F.H.P.M. Habraken, G.A. Bootsma, Surface Sci., 87 (1979) 333.
6. F.H.P.M. Habraken, O.L.J. Gijzeman and G.A. Bootsma, Surface Sci., 96 (1980) 482.
7. F.H.P.M. Habraken, W. Liswski and G.A. Bootsma, Surface Sci., 118 (1982) 1.
8. R. Kötz and B.E. Hayden, Surface Sci., 135 (1983) 374.
9. W.E.J. Neal and R.W. Fane, J.Phys.E., 6 (5) (1973) 409.
10. O.S. Heavens, Thin Film Physics, 1970 Methuen.
11. K. Vedam and S. Samuel, Surface Sci., 29 (1972) 379.
12. K.H. Zaininger and A.G. Revesz, R.C.A. Revs.(1964) 85.
13. W.E.J. Neal, App.Surface Sci., 2 (1979) 445,
14. W.E.J. Neal, Surf.Technol., 6 (1977) 81.
15. E. Passaglia, R.R. Stromberg and J. Kruger, Ellipsometry in the measurem of surfaces and thin films, Symposium Proc., Washington Nat.Bur. Stand., 1963, P.201.
16. R.M. Ditchburn, J.Op.Soc.Am. 45(1955) 743.
17. M.E. Pedinoff, D.C. Mayer, O.M. Stafsudd and G.L. Dunn, App. Optics, 21 (1982) 3307.
18. J.F. Nye, Physical Properties of Crystals, Clarendon Press, Oxford, 1972

Sample and Position		ψ Degrees			Δ Degrees			δt mn
		Centre	X, Y	X', Y'	Centre	X, Y	X', Y'	
Batch 1	B(a)	23.42	23.49	23.49	155.85	155.85	155.99	± 1
	D(b)	23.61	24.17	22.27	153.75	148,35	162.85	± 3
	F(b)	22.63	22.69	23.08	173.61	177.97	175.07	± 3
Batch 2	D(a)	27.69	27.26	26.39	124.50	128.30	149.46	± 16.5
	G(a)	22.78	26.04	21.30	174.10	149.76	167.76	± 15.7
	H(a)	23.02	23.02	23.75	171.43	172.97	125.27	± 17
Batch 3	B(a)	50.50	54.75	18.03	116.37	127.27	135.57	± 13.5
	E(b)	45.88	66.56	78.18	115.40	115.56	226.54	± 22.5
	G(a)	51.46	44.96	50.22	115.22	111.91	247.42	± 20

Table (1)

The measurement of ψ and Δ for Si O_2 for batches one, two and three, in different positions of the sample. n = 1.5 for batch one and two and n = 1.45 for batch three, k = 0, λ = 632.8 nm, and the substrate value of n = 3.7583, K = 0.0952. The values of δ t show the uniformity for each sample.

Sample and Position		ψ Degrees		Δ Degrees		Thickness at Centre Position nm
		Experimental	Computed	Experimental	Computed	
Batch 1	B(a)	23.42	23.47	155.85	155.41	280
	D(b)	23.61	23.61	153.75	153.38	282
	F(b)	23.63	22.77	173.61	173.42	263
Batch 2	D(a)	27.67	27.96	235.50	235.11	199
	G(a)	22.78	22.75	185.90	185.39	252
	H(a)	23.03	22.82	188.57	188.63	249
Batch 3	B(a)	50.50	50.14	116.37	117.94	383
	E(b)	45.88	45.45	115.40	114.89	377
	G(a)	51.46	46.92	115.22	115.69	379

Table (2)

The comparison between the experimental and the computed values of ψ and Δ for the centre position only. $n = 1.5$ for batches one and two and $n = 1.45$ for batch three, and $n = 0$. $n_1 = 3.7583$ and $k_1 = 0.0952$ for the substrate.

Sample and Orientation	Thickness nm	Na	Nb	Nc	$\delta N_{(ac)}$	Instrument Sensitivity	
						$\delta t/\delta\Omega$ (nm/deg)	$\delta t/\Delta\psi$ (nm/deg)
SS 31(111)	400.2	1.4566	1.4571	1.4576	1×10^{-3}	-0.25	-2.45
SS 23(111)	692.8	1.4540	1.4559	1.4578	3.8×10^{-3}	-1.42	+1.18
SS 25(111)	995.9	1.4540	1.4575	1.4620	8.0×10^{-3}	+2.79	+3.13
SS 24(111)	1281.5	1.4566	1.4571	1.4575	0.9×10^{-3}	+1.97	+4.07
SS 36(100)	695.0	1.4549	1.4565	1.4586	3.7×10^{-3}	-1.46	+1.19
SS 40(100)	1290.0	1.4577	1.4572	1.4567	1.0×10^{-3}	+1.55	+5.25

Table (3)

The variation in the refractive index in three different positions (see fig.(4)) for different orientations of the substrate.

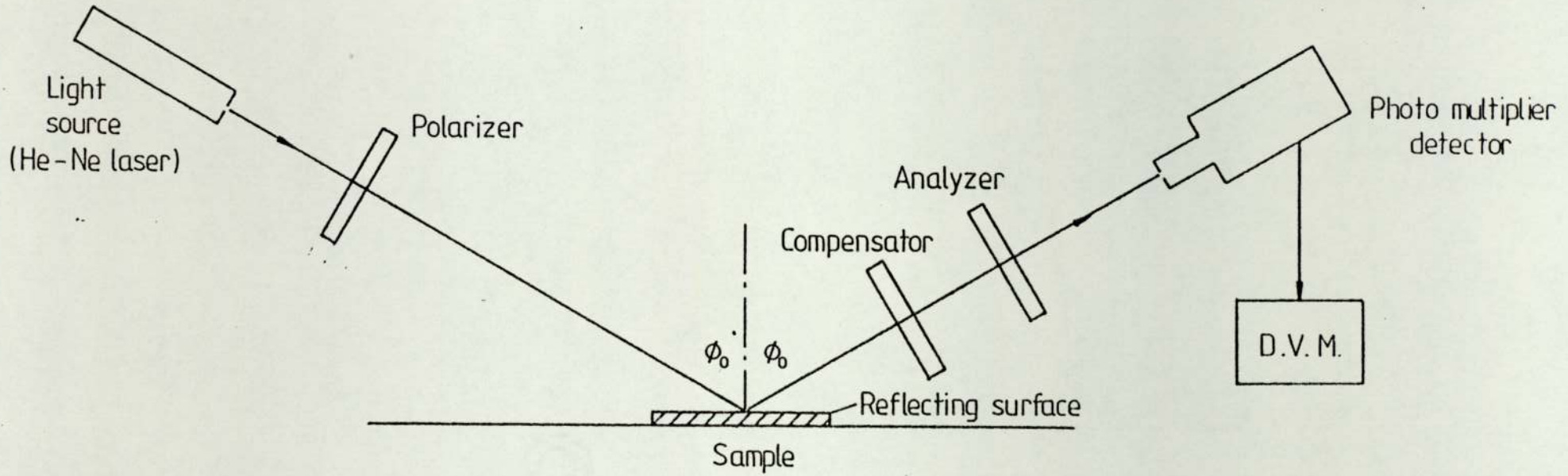

Figure 1. Components of the basic instrument.

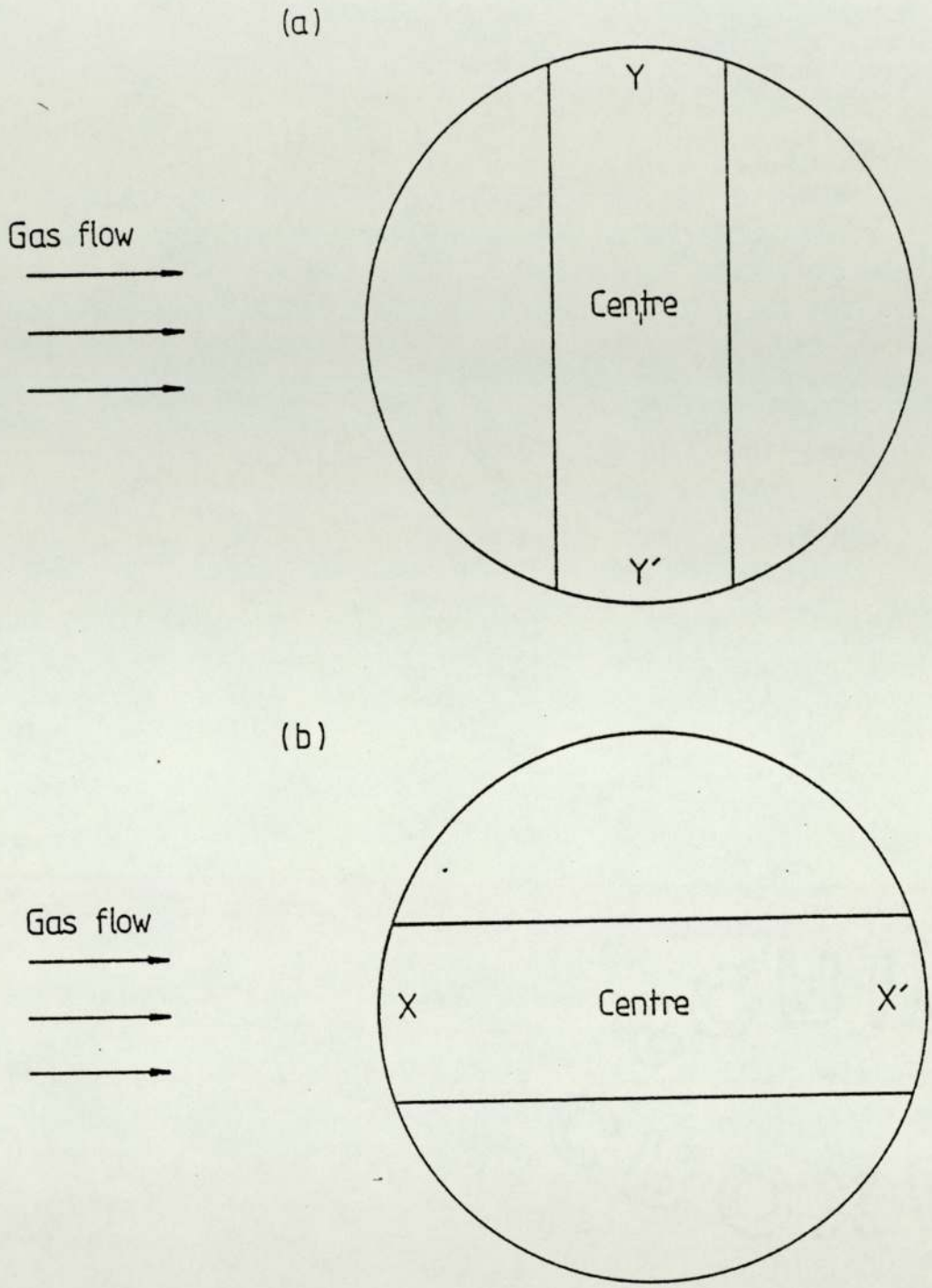

Figure 2. The position of the sample in the system during the oxidation. This shows the three positions where the measurement of Ψ and Δ were taken at the ellipsometer.

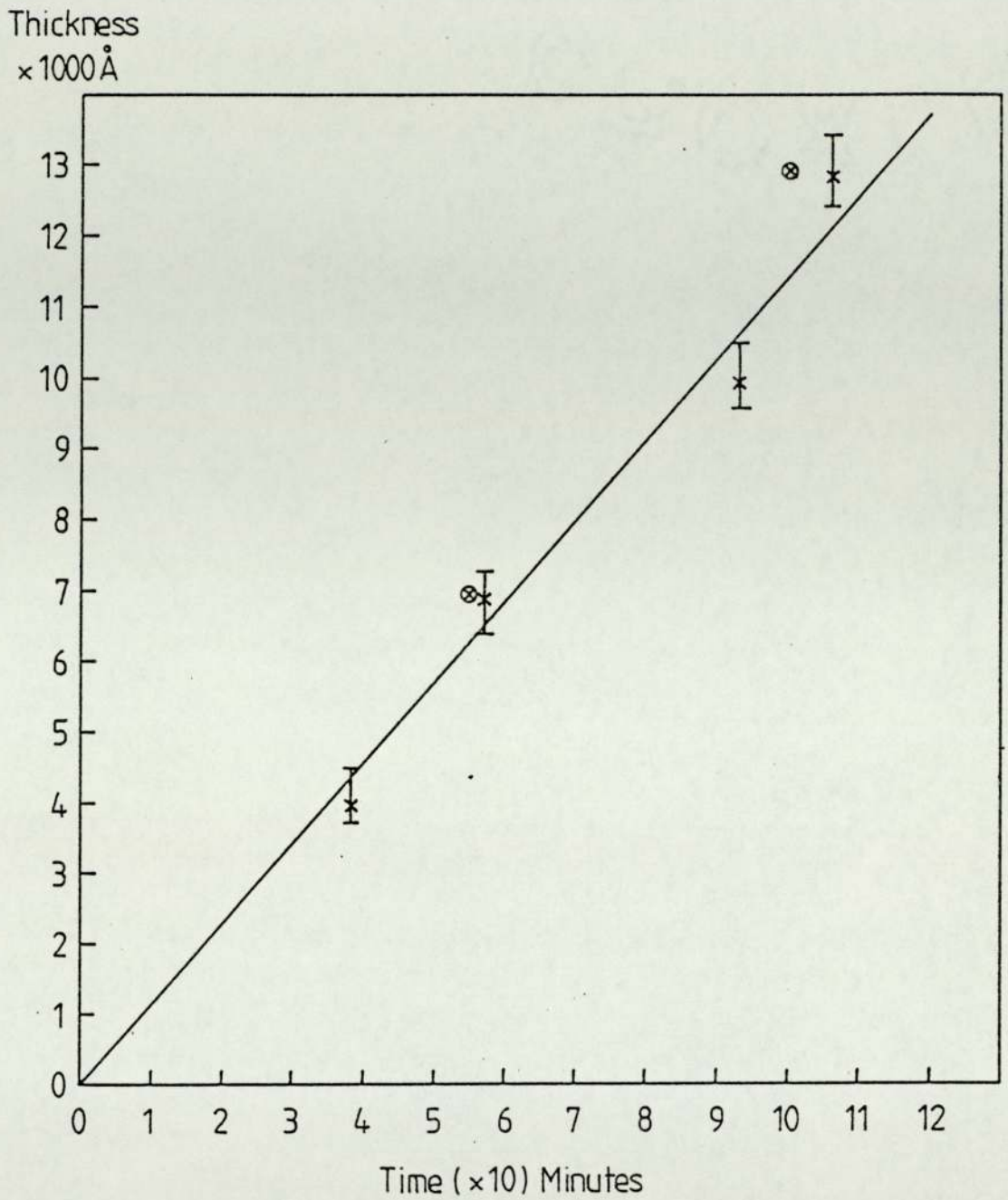

Figure 3. The growth rate for thermally grown silicon dioxide films on (111) and (100) silicon (× - 111 , ⊗ - 100)

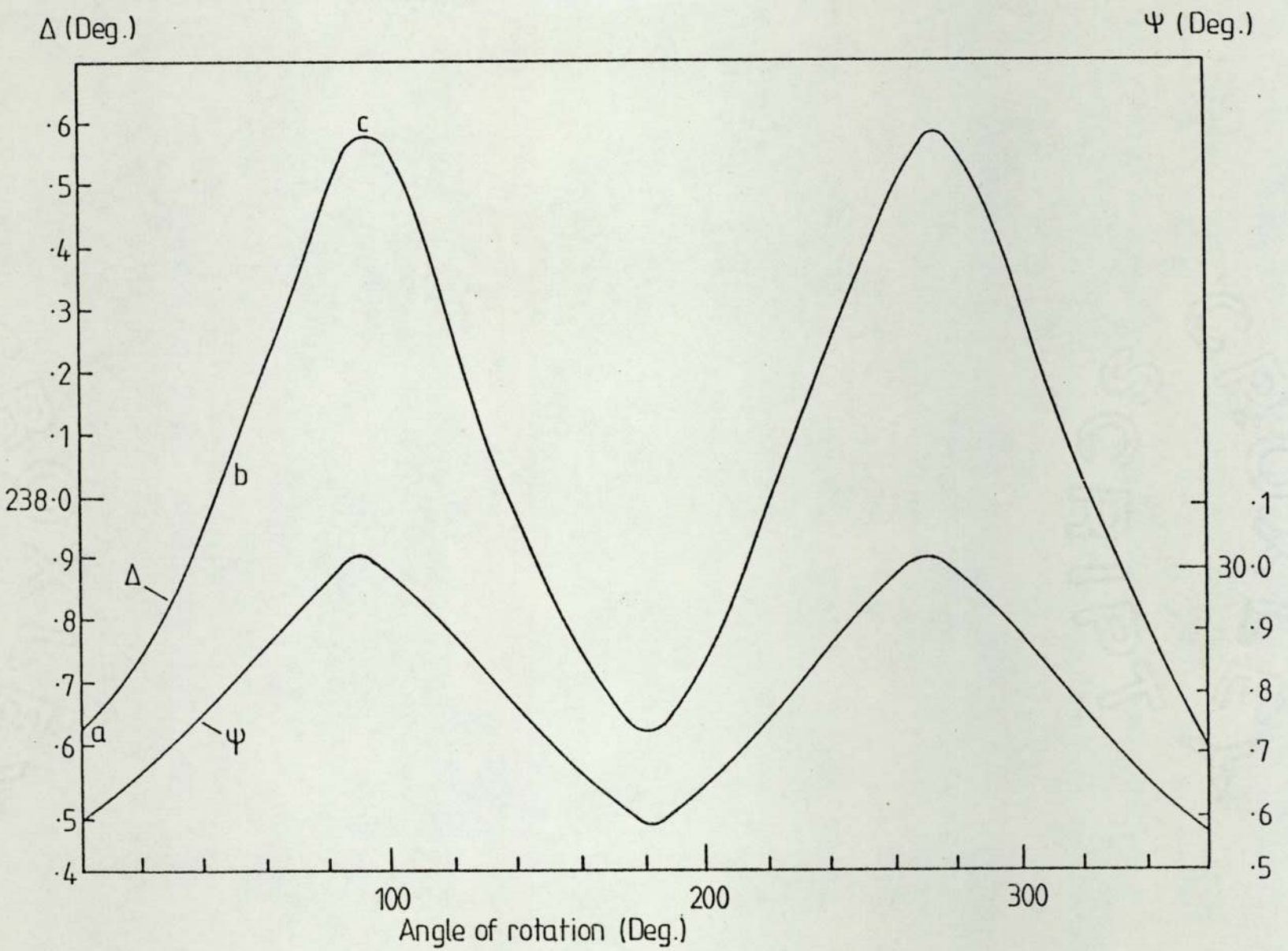

Figure 4. Plots of Ψ and Δ against angle of rotation for sample SS 24 (t = 1281·5nm). The positions a, b and c are the positions where the value of N was calculated. Instrument sensitivity at 1280nm : $\frac{\delta t}{\delta \Delta}$ and $\frac{\delta t}{\delta \Psi}$ = 1·97 and 4·07 nm / deg. respectively.

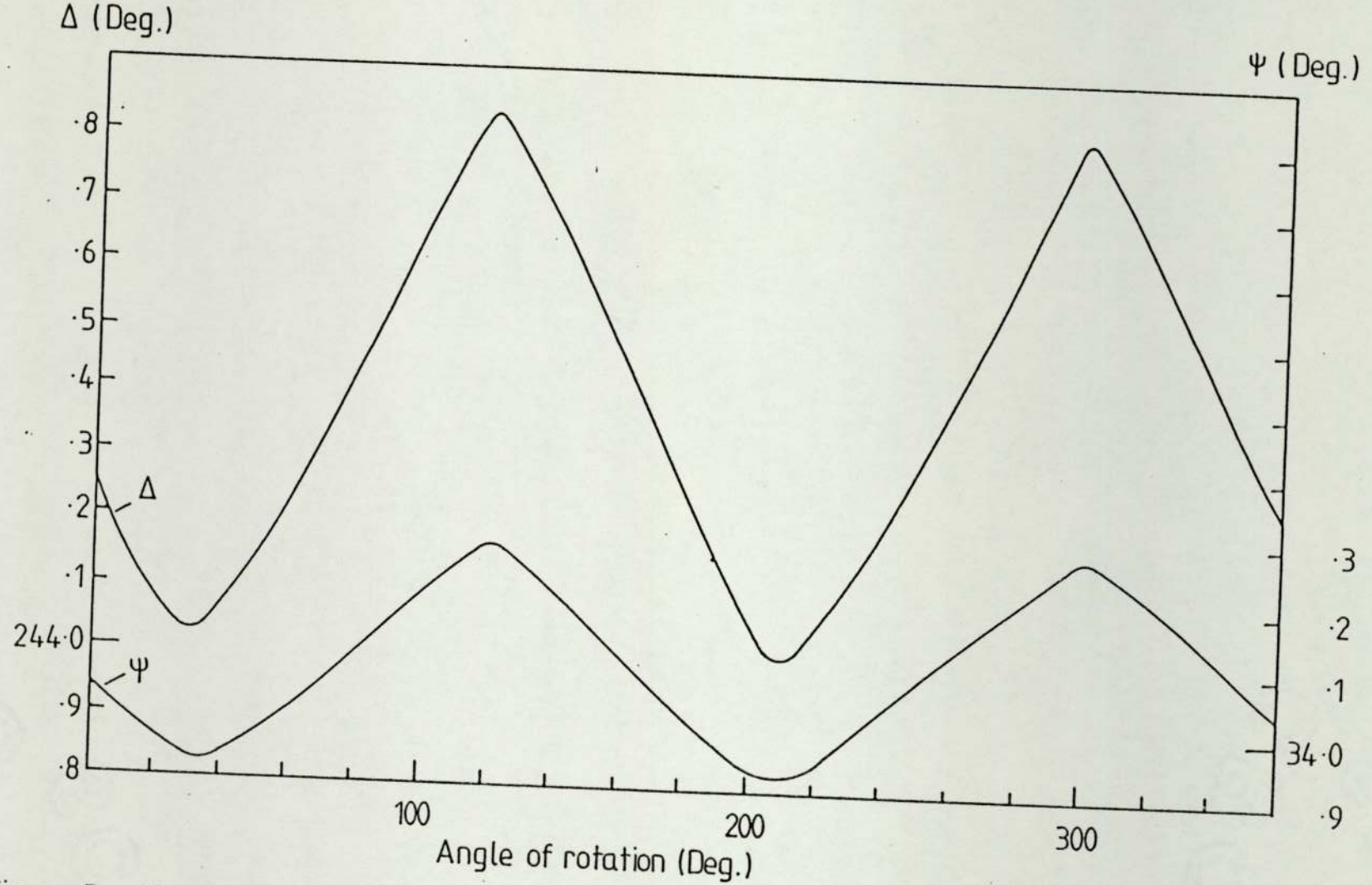

Figure 5. The variation of the values of Ψ and Δ against the angle of rotation for SS 25 (t = 995·9 nm)
Instrument sensitivity at 1000 nm : $\frac{\delta t}{\delta \Delta}$ and $\frac{\delta t}{\delta \Psi}$ = 2·79 and 3·13 nm / deg. respectively.

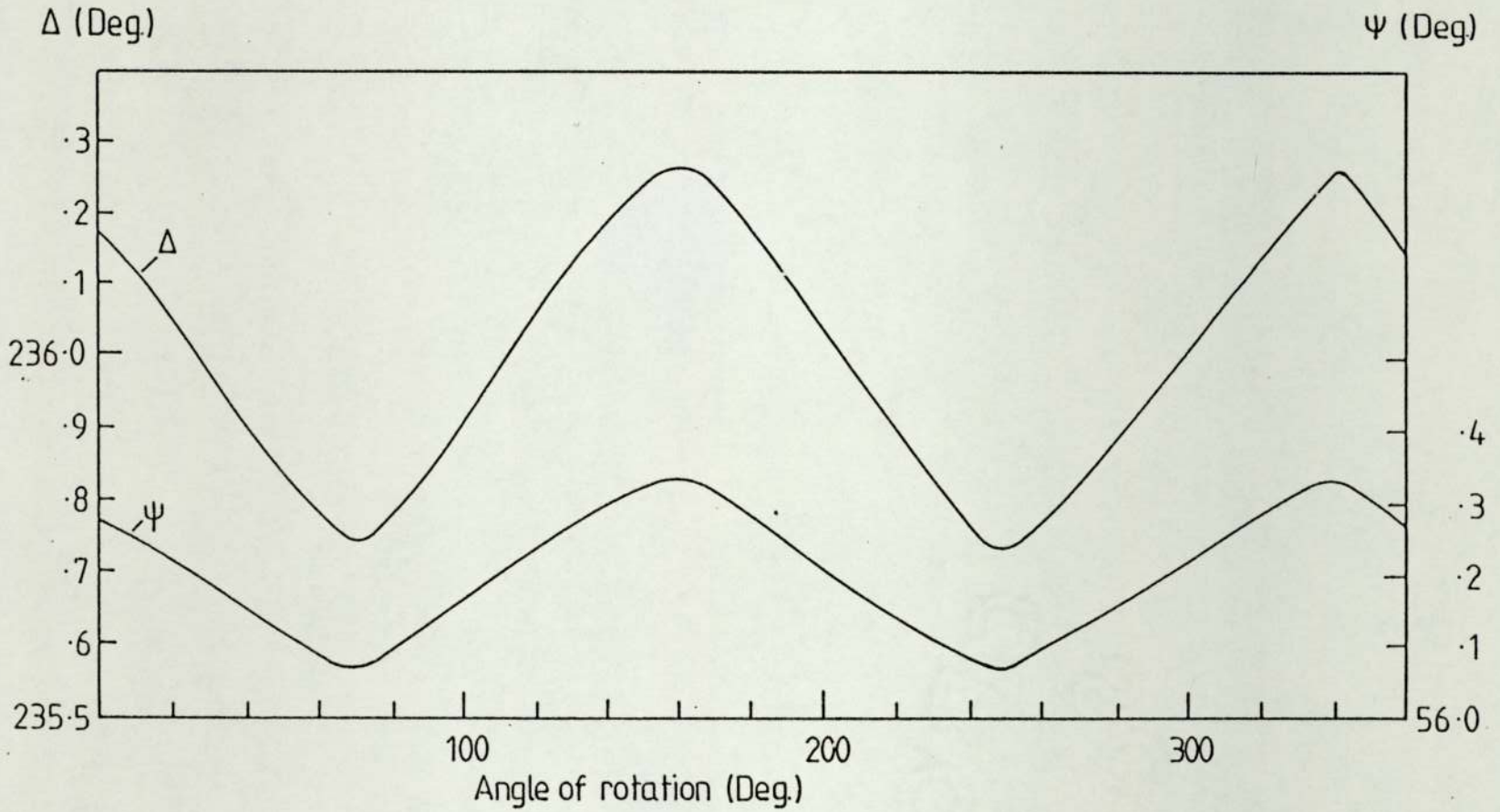

Figure 6. The variation of the Ψ and Δ as a function of the angle of the rotation for SS 23 (t = 692·8 nm)
Instrument sensitivity at 700 nm : $\frac{\delta t}{\delta \Delta}$ and $\frac{\delta t}{\delta \Psi}$ = -1·42 and 1·18 nm/deg. respectively.

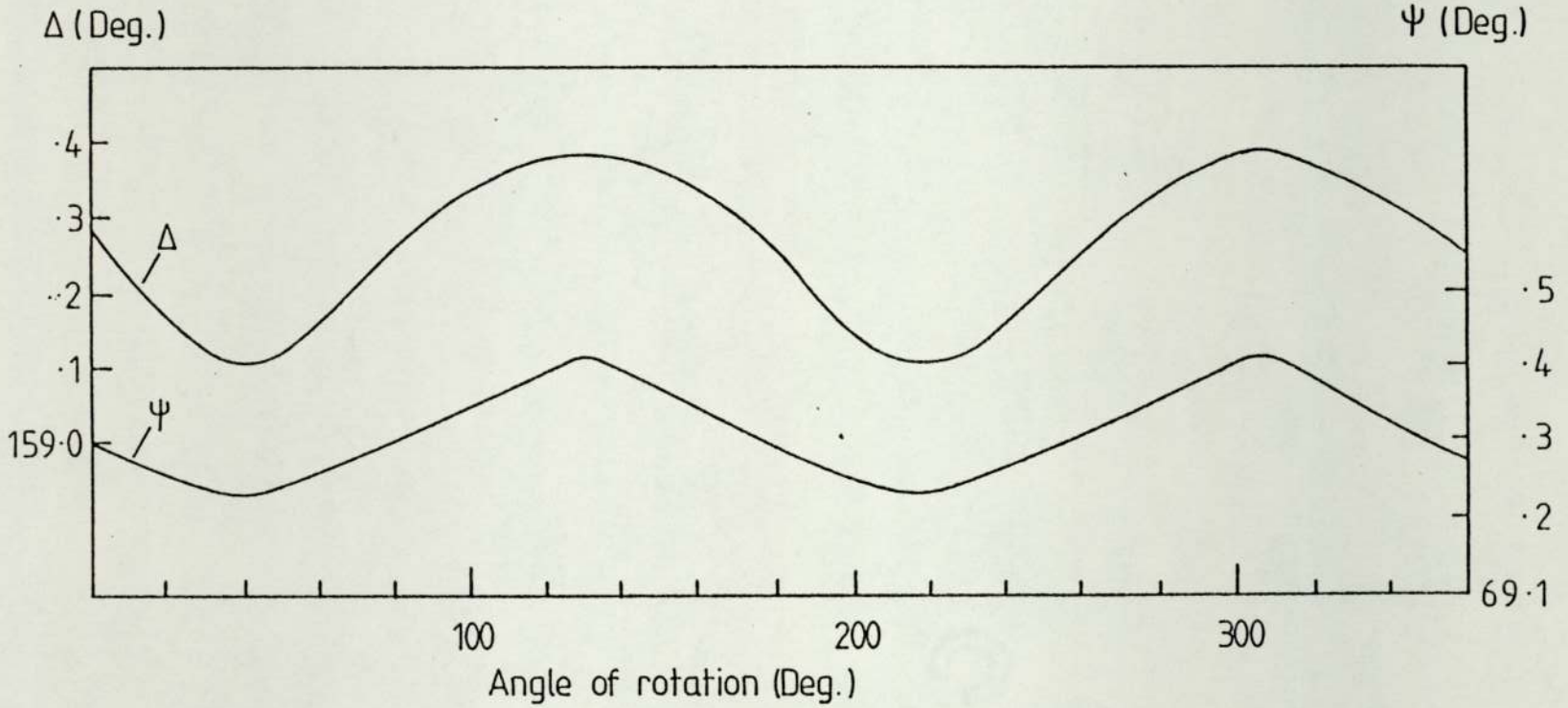

Figure 7. The change in Ψ and Δ as function of the angle of the rotation for SS31 (t = 400·2 nm)
Instrument sensitivity at 400 nm: $\frac{\delta t}{\delta \Delta}$ and $\frac{\delta t}{\delta \Psi}$ = -0·25 and -2·45 nm/deg. respectively.

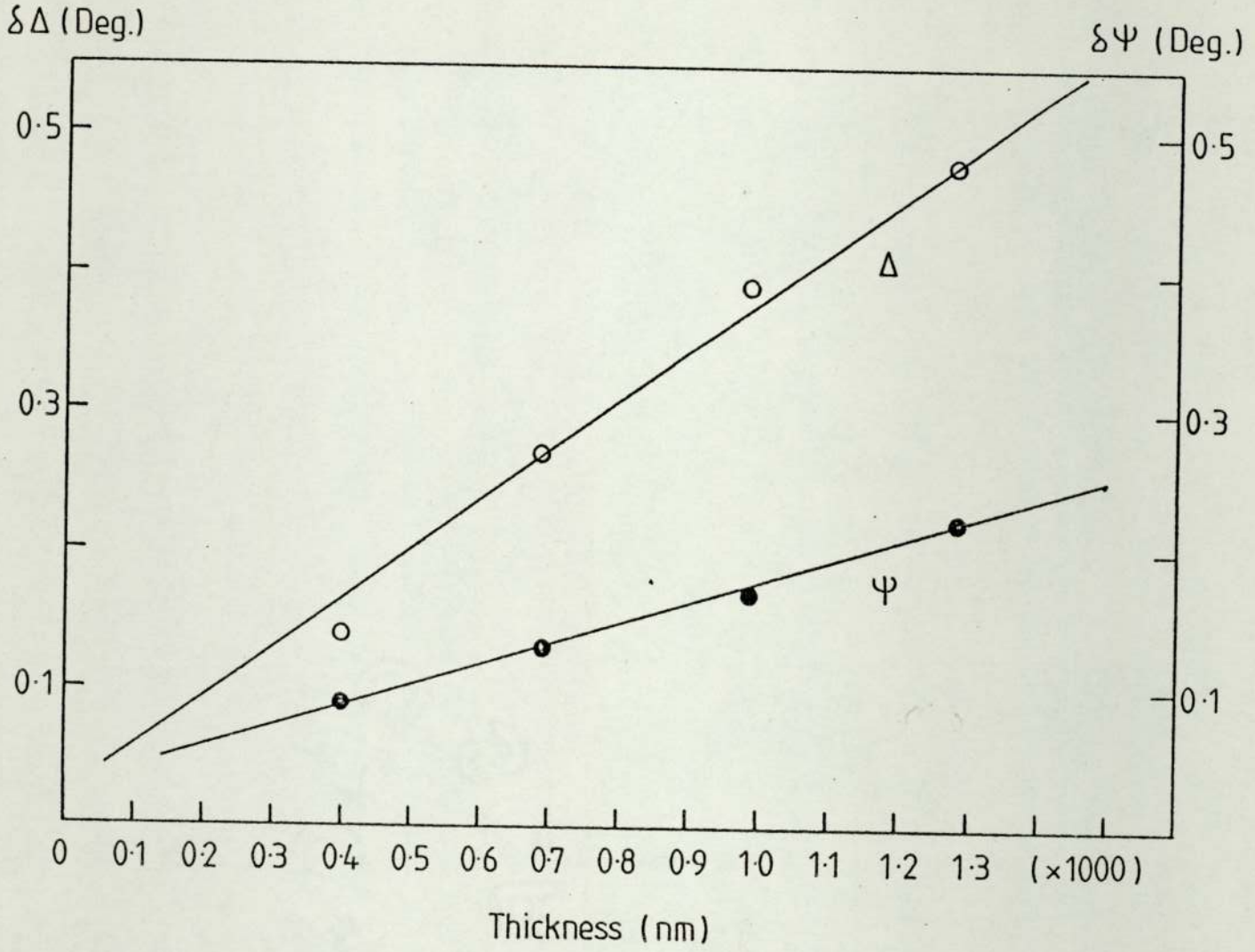

Figure 8. The changing amplitude for Ψ and Δ for oxide films of different thickness.

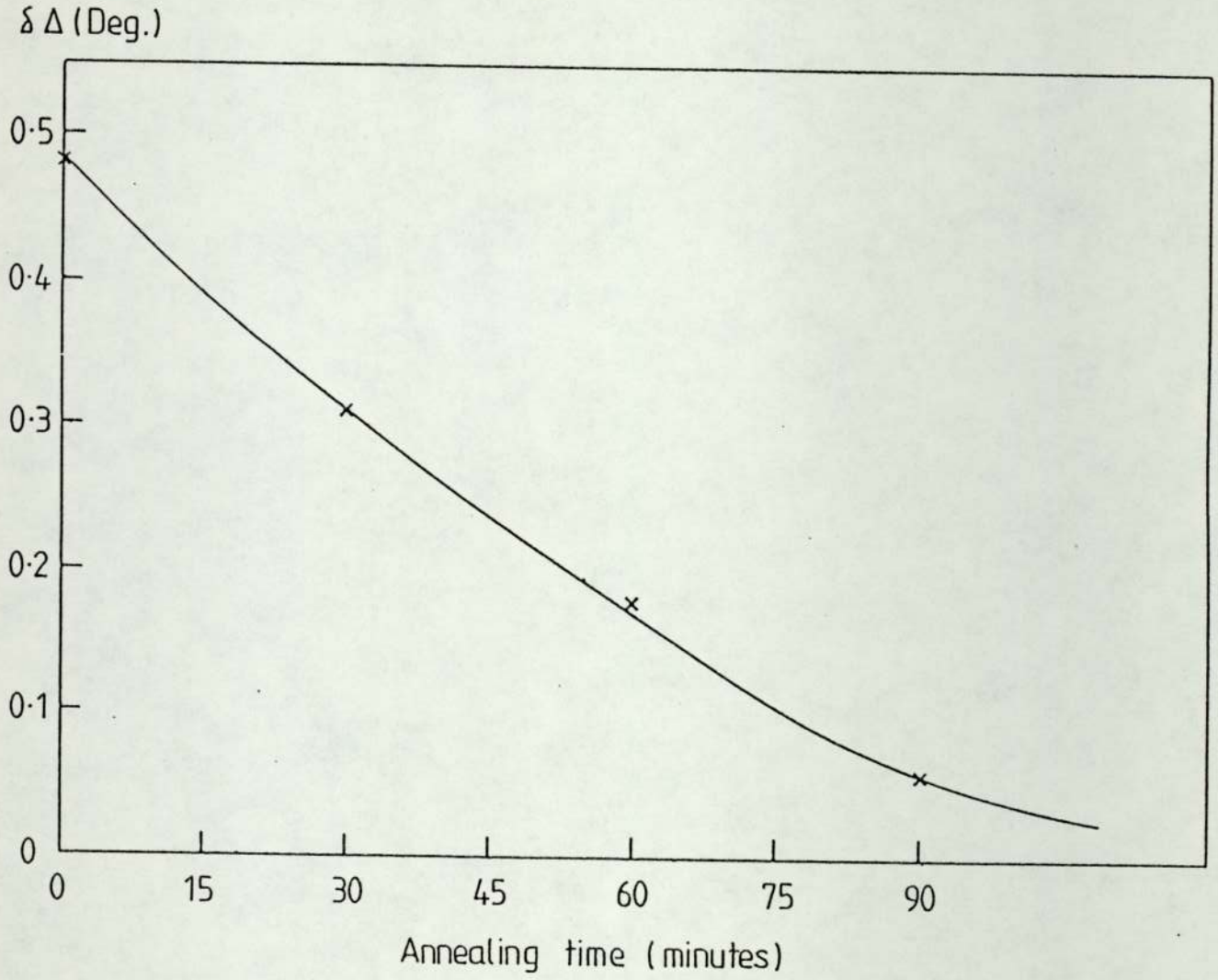

Figure 9. The reduction in the values of Δ as a result of annealing sample SS24 at 950°C in a nitrogen atmosphere.

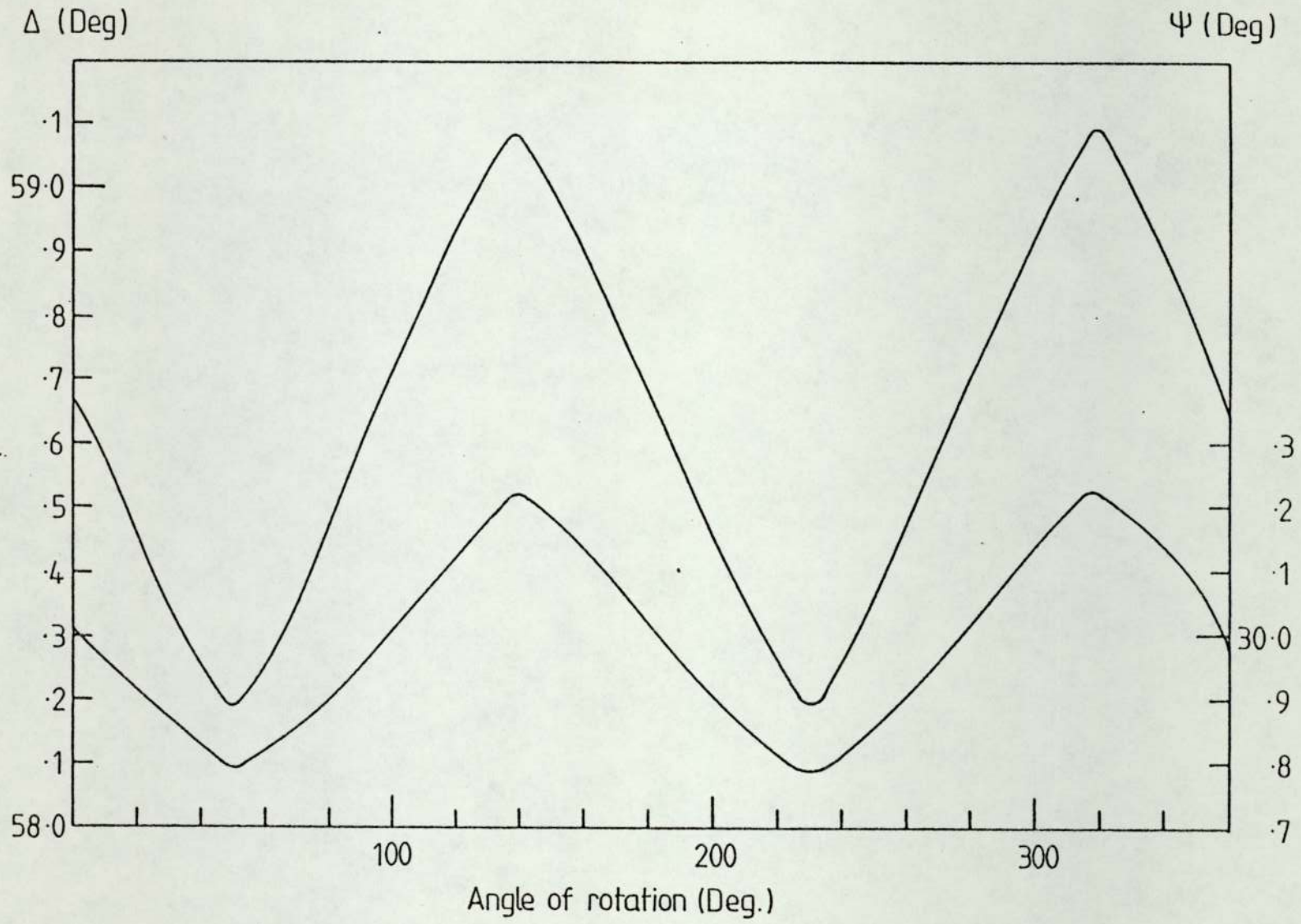

Figure 10a. The change in Ψ and Δ as a function of the angle of rotation for SS34 (t = 1280·2 nm)
The substrate orientation is (100)
Instrument sensitivity at 1290 nm : $\frac{\delta t}{\delta \Delta}$ and $\frac{\delta t}{\delta \Psi}$ = 1·55 and 5·05 nm / deg. respectively.

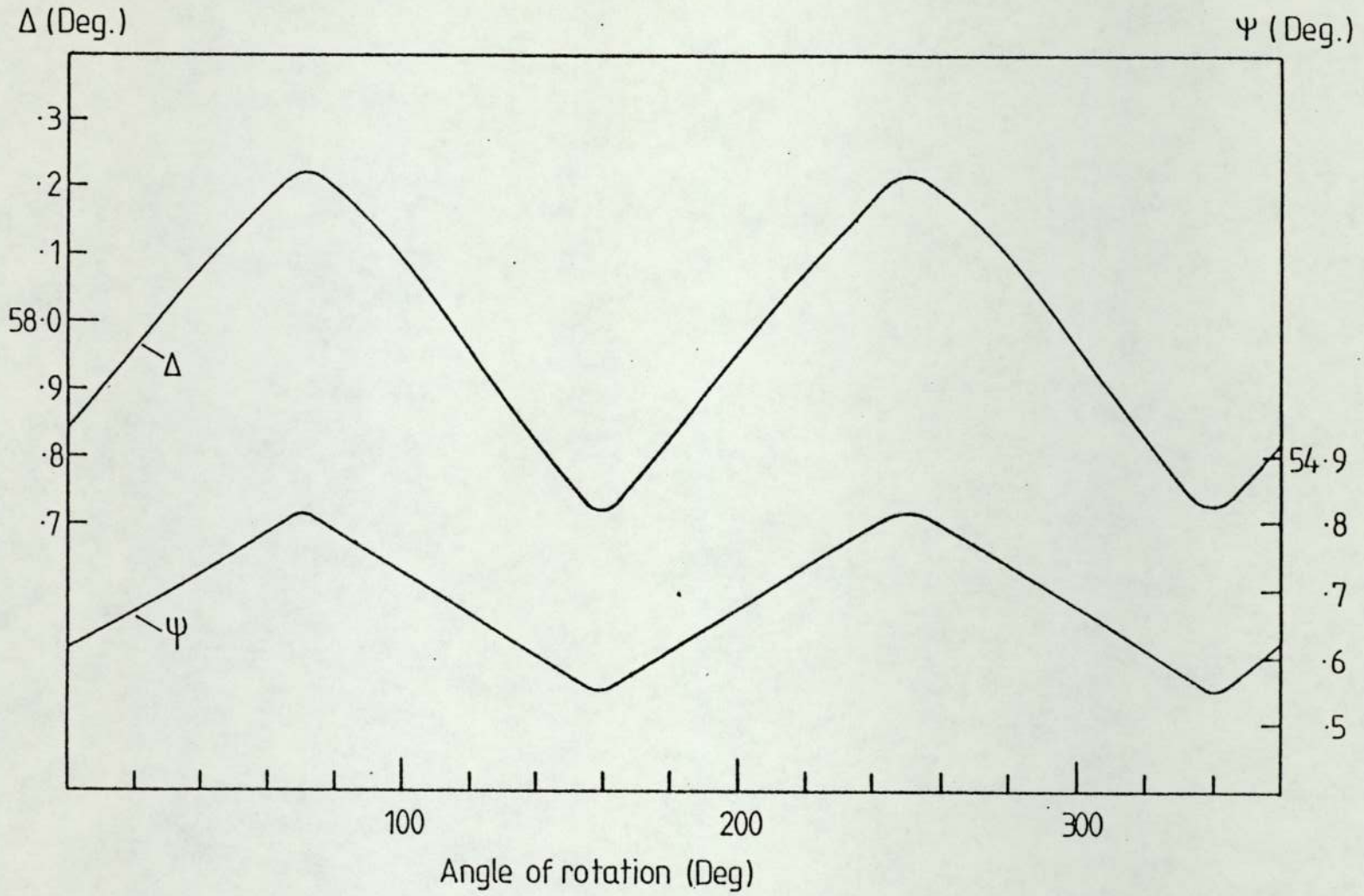

Figure 10b. The change in Ψ and Δ as a function of the angle of rotation for SS36 ($t = 695{\cdot}0$ nm) The substrate orientation is (100)
Instrument sensitivity at 700 nm: $\frac{\delta t}{\delta \Delta}$ and $\frac{\delta t}{\delta \Psi}$ = 1·46 and 1·19 nm/deg. respectively

OPTICA ACTA, 1983, VOL. 30, NO. 2, 167–170

Determination of coherence by magneto-optic diffraction

SANFORD KERN and SAUD YAGHMOUR

Department of Physics, Colorado State University, Fort Collins, Colorado 80523, U.S.A.

(*Received 26 April 1982; revision received 31 August 1982*)

Abstract. By comparing the zero-order diffraction intensity of a polarized light beam after it has passed through a magnetic thin film in the (i) normal and (ii) saturated states, we have been able to measure the degree of coherence of the light beam. The results from these magneto-optic measurements have been compared to those obtained from the classical two-slit diffraction pattern; very good agreement is obtained.

1. Introduction

The use of magneto-optic diffraction for making various measurements on magnetic thin films has been common for several years [1]. In many cases the coherence of the beam has not been a factor, much less considered. However, the transmitted intensity of the polarized Faraday-rotated light after it passes through the film and following analyser will be shown to vary with the degree of coherence [2] of the beam.

We have measured the degree of coherence by two methods. The first uses a newly devised technique that exploits the variation in diffractive intensity produced by a magnetic thin film. The results obtained from this method are then checked with a Young's double slit arrangement [2] to measure the degree of coherence of the same light beam.

2. Theory

We can describe a magnetic thin film by the fraction, p, of the domain magnetized in a given direction, the remainder of the domain width being the fraction $(1\text{-}p)$ (see figure 1 (a)). If light travelling parallel to the magnetization traverses the portion of the film denoted by p, we will say that the plane of polarization has been rotated by an angle, $+\beta$, while that light which traverses the section denoted as $(1\text{-}p)$ will be rotated by an amount, $-\beta$, as shown in figure 1 (b). If the analyser is set at an angle α, with respect to the original axis of polarization of the beam prior to its impinging on the film, then the emerging amplitudes are given by,

$$E^{+} = E(\sin\alpha\cos\beta + \cos\alpha\sin\beta)\,p,$$

$$E^{-} = E(\sin\alpha\cos\beta - \cos\alpha\sin\beta)\,(1-p),$$

where $E = E_0\exp(-\lambda l/2)$ and E_0 is the initial amplitude of the beam, λ is the attentuation coefficient and l is the thickness of the film. For a coherent light the intensity of the zero-order diffraction [2] is,

$$I^{C} = [(2p-1) + \tan\alpha\cos\beta]^2\cos^2\alpha\sin^2\beta,$$

0030-3909/83/3002 0167 $04·00

completely coherent light and $\gamma = 0$ for completely non-coherent light, we obtain

$$I_{max} = 2I(1+\gamma)$$

$$I_{min} = 2I(1-\gamma)$$

for a beam of mixed, or partial, coherence. A comparison quickly shows g and γ to be equal but we will use the different symbols to distinguish the results of the two experimental techniques.

3. Experiment

The experimental arrangement used is shown in figure 2. A polarized laser beam passes through a bubble-material thin film, whose surface is perpendicular to the beam direction, but whose domain magnetization is parallel to it. The plane of polarization of the light is Faraday-rotated, adjacent domains of opposite magnetization rotating the light in opposite directions. The magnetic field coils are used to provide a static field of sufficient strength to cause the magnetization of the film to saturate parallel or anti-parallel to the direction of the beam. The analyser is set perpendicular to the polarizer in this experimental arrangement. The emerging light will give rise to a series of diffraction spots for a parallel domain configuration (or rings for the labyrinth configuration encountered in our films). The screen is arranged to have an aperture where the zero-order diffraction spot falls; all other light is excluded from the photomultiplier detector. The aperture plate is mounted on a micrometer-driven structure. The aperture is occupied by one end of a fibre-optic light pipe. The other end inserts into a photomultiplier housing; between the end of the fibre optic and the photomultiplier face is a 'spike' filter, whose transmission maximum is centred at the laser wavelength. The photomultiplier detector's output leads to an electrometer and other recording electronics.

The 'coherence scrambler' is a milk and water mixture whose purpose is implicit in its name. Varying concentrations of milk in water were used to obtain different degrees of beam coherence.

The classical Young's two-slit diffraction experimental arrangement was employed as a check on the degree of coherence measured by this magneto-optic technique. Referring to figure 2, the magnetic field coils were replaced by a pair of precision slits. The aperture and fibre-optic light pipe were placed on the travelling slide a few metres from the slits. In this way an accurate measurement of the

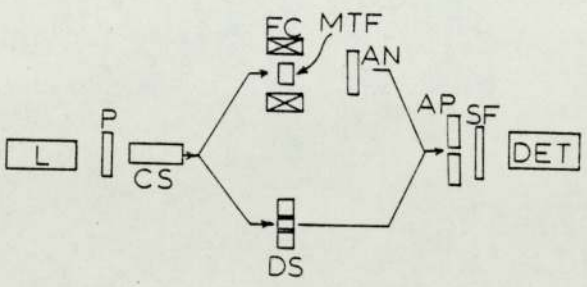

Figure 2. Experimental arrangement: L = laser, P = polarizer, CS = coherence scrambler, FC = magnetic field coils, MTF = magnetic thin film, AN = analyser, DS = double slit, AP = aperture, SF = narrow band pass filter, DET = detector and recording electronics. See the text for an explanation of the two optical paths.

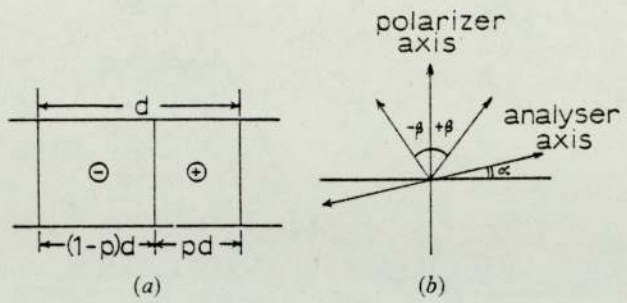

Figure 1. (*a*) The domain structure of a magnetic thin film; p represents the fraction of the domain width, d, having an 'up' magnetization. (*b*) Relative orientation of the polarizer and analyser axes; β is the Faraday rotation angle.

a result derived previously by several authors [3, 4, 5, 6]. For the non-coherent case, however,

$$I^{NC} = 2(2p-1)\sin\alpha\cos\alpha\sin\beta\cos\beta + \sin^2\alpha\cos^2\beta + \cos^2\alpha\sin^2\beta.$$

If we let g equal the coherent intensity fraction and $(1-g)$ the non-coherent fraction, then,

$$I = gI^{C} + (1-g)I^{NC}.$$

Since $0 \leqslant \alpha \leqslant \beta$ in magnetic thin film analysis and for most bubble films $\beta < 0{\cdot}1$ rad [6], we can use the small angle approximation to obtain

$$I \approx 4gp^2\beta^2 + 4p\beta[\alpha - g\beta] + [\alpha - \beta]^2.$$

In our experiments we accurately adjust the analyser to the $\alpha = 0$ position [3, 8] so,

$$I \approx 4\beta^2[gp(p-1) + 1/4].$$

Note that if we compare the intensity of the zero-order diffracted light with no applied field ($p = 1/2$) to the intensity obtained when the film is saturated ($p = 0, 1$) we obtain the simple expression

$$\frac{I(p=1/2)}{I(p=0,1)} = 1 - g;$$

again, this is for $\alpha = 0$, the crossed polarizer-analyser, or domain wall contrast position. This means that a simple measurement of these two easily obtained intensities provides a simple determination of the degree of coherence of the beam.

The degree of coherence can also be related to the intensity variation of the interference from two slits according to [2],

$$V = \frac{I_{max} - I_{min}}{I_{max} + I_{min}} = \frac{2(I_1 I_2)^{1/2}}{(I_1 + I_2)}\gamma,$$

where V, the visibility, is equal to γ when the incident intensities on the two slits are equal, i.e. $I_1 = I_2 = I$; γ is the degree of mutual coherence of the beam. I_{max} is the maximum intensity of the interference pattern formed by two slits. Using $\gamma = 1$ for

diffraction intensity as a function of distance in the diffraction plane (or, equivalently, as a function of the diffraction angle) was made.

4. Results

The table lists the results for some different degrees of beam coherence. The two techniques yield essentially the same values for the degree of coherence.

Experimental beam coherence.

γ	g
0·50	0·52
0·51	0·52
0·68	0·66
0·71	0·73
0·95	0·94

5. Conclusions

From the results listed in the table we may infer that the magnetic thin film technique represents a simple, quick and accurate means of determining the degree of coherence of a light beam. Throughout the region where the film is a good Faraday rotator (and not too absorptive), we expect accurate measurements to be easily made. The technique should prove useful for various light scattering experiments and light beam propagation where a determination of the coherence properties of the scattered or transmitted light will provide insight into various interactive processes.

Acknowledgments

We would like to thank Mr. Marvin Shipley of the Pasco Scientific Corporation for the loan of a pair of accurately formed slits, and Dr. John Fairholme of the Plessey Corporation for the magnetic film used in the experiments. We would also like to thank Dr. C. Y. She for his many helpful comments and suggestions.

En comparant l'intensité de diffraction dans l'ordre zéro d'un faisceau lumineux polarisé après son passage au travers d'une couche mince magnétique dans les états (i) normal et (ii) saturé, il est possible de mesurer le degrè de cohérence du faisceau lumineux. Les résultats de ces mesures magnéto-optiques ont été comparés à ceux obtenus à partir de la figure de diffraction classique de deux fentes; un très bon accord est obtenu.

Durch Vergleich der Beugungsintensität nullter Ordnung eines polarisierten Lichtstrahls nach Durchlaufen einer dünnen magnetischen Schicht (i) im normalen und (ii) im gesättigten Zustand konnten wir den Kohärenzgrad des Lichtstrahls messen. Die Ergebnisse dieser magnetooptischen Messungen wurden mit Ergebnissen von klassischen Doppelspaltbildern verglichen; es wurde sehr gute Übereinstimmung erzielt.

References

[1] See, for example, MALEZEMOFF, A. P., and SLONCZEWSKI, J. C., 1979, *Magnetic Domain Walls in Bubble Materials* (New York: Academic Press).
[2] BORN, M., and WOLF, E., 1970, *Principles of Optics*, fourth edition (New York: Pergamon
[3] PAPWORTH, K. R., 1974, *Phys. Stat. Sol.* (a), **22**, 373.
[4] HASKEL, H. M., 1970, *I.E.E.E. Trans. Magn.*, **6**, 542.
[5] MEZRICH, R. S., 1970, *I.E.E.E. Trans. Magn.*, **6**, 537.
[6] BOERSCH, H., and LAMBECK, M., 1964, *Z. Phys.*, **177**, 157.
[7] SCOTLAND, G. R., and LACKLISON, D. E., 1976, *I.E.E.E. Trans. Magn.*, **12**, 292.
[8] KERN, S., and CRAIK, D. J., 1976, *J. Phys.* D, **9**, L81.

REFERENCES

1. J. V. Cathcart, J. E. Epperson and G. F. Petersen, Acta Meta., 10 (1962) 699.
2. W. E. Neal, Surf. Technol., 23 (1984) 1.
3. S. Tolansky, Multiple Beam Interfrometry, Oxford Univ. Press, Oxford, 1948.
4. H. Murmann, Z. Physik., 80 (1933) 161.
5. H. Murmann, S. Physik., 101 (1936) 643.
6. O. S. Heavens, Optical Properties of Thin Solid Films, Dover, New York, 1965.
7. O. S. Heavens, Thin Film physics, Methuen and Co. Ltd., London, 1970.
8. P. Drude, Weid. Ann.(Leipzig) 39 (1890) 421.
9. P. Drude, Weid. Ann.(Leipzig) 43 (1891) 125.
10. A. B. Winterbottom, J. Sci. Instr., 14 (1937) 203.
11. P. Drude, Theory of Optics, Trans. by C. R. Mann and R. A. Millikan, London, 1902.
12. L. Rayleigh, Phil. Mag., 33 (1892) 1.
13. E. Hagen and H. Rubens, Ann. Physik., 11 (1903) 873.
14. K. Fosterling and V. Freedericksz, Ann. Physik., 40 (1913) 201.
15. L. Trowstad and C. G. Feashem, Proc. Ray. Soc., 145A (1934) 115.
16. L. Trowstad and T. Haverstad, Trans. Farad. Soc., 30 (1934) 1114.
17. C. E. Lebernight and B. Lustman, J. Opt. Soc. Am., 29 (1939) 59.

18. L. McPherson, Proc. Phys. Soc., 52 (1940) 210.

19. A. Rothen, Rev. Sci. Instrum., 16 (1945) 26.

20. A. Rothen and M. Hanson, Rev. Sci. Instrum., 28 (1957) 283.

21. A. B. Winterbottom, Optical Studies of Metal Surface, Bruns, (Trondheim) 1955.

22. A. Elliott, E. J. Ambrose and R. Temple, J. Optic. Soc. Am., 38 (1948) 212.

23. J. R. Beattie, Phil. Mag., 46 (1955) 235.

24. J. R. Beattie and G. K. Conn, Phil. Mag., 46 (1955) 22.

25. P. C. Hayfield and G. W. White, in E. Passaglia (ed.), Ellipsometry in the Measurement of Surfaces and Thin Films, National Bureau of Standards, Washington DC, 1963, p. 157.

26. W. E. Neal, R. W. Fane, N. W. Grimes, Phil. Mag., 21 (1970) 167.

27. J. C. Miller, Phil., Mag., 20 (1969) 1115.

28. F. L. McCrackin, E. Passaglia, R. Stromberg and L. Steinberg, J. Res. Nat. Bureau of Standards, 67A (1963) 363.

29. R. J. Archer, J. Opt. Soc. Am. (1962) 970.

30. E. J. Gillham, Nature (1956) 1412.

31. E. J. Gillham, J. Sci. Instrum., 34 (1957) 435.

32. E. J. Gillham and R. J. King, J. Sci. Instrum., 38 (1961) 21.

33. S. J. Williamson, J. M. Weingart and R. D. Andrews, J. Opt. Soc. Am., 54 (1964) 337.

34. R. J. King, J. Sci. Instrum., 43 (1966) 924.

35. E. Passaglia, R. R. Stromberg and J. Kruger (eds.), Proc. Symp. Ellipsometry in the Measurement of Surfaces and Thin Films, National Bureau of Standards, Washington DC, 1963.

36. N. M. Bashara, A. B. Buckman, and A. C. Hall (eds.), Proc. Symposium on Recent Developments in Ellipsometry, North-Holland Pub. Co., Amsterdam, 1969. (Surf. Sci. 16 (1969)).

37. N. M. Bashara and R. M. Azzam (eds.), Proc. Third Interna. Conf. on Ellipsometry, North-Holland Pub. Co., Amsterdam, 1976. (Surf. Sci. 56 (1976)).

38. R. H. Muller, R. M. Azzam and D. E. Aspnes (eds.), Ellipsometry, North-Holland Pub. Co., Amsterdam, 1980 (Surf. Sci., 96 (1980)).

39. R. M. Azzam and N. M. Bashara (eds.), Ellipsometry and Polarized Light, North-Holland, Amsterdam, 1977.

40. Z. Knittl, Optics of Thin Films, John Wiley and Sons, New York, 1976.

41. W. E. Neal, Surf. Technol., 6 (1977) 81.

42. W. E. Neal, Applica. Surf. Sci., 2 (1979) 445.

43. T. H. Allen, SPIE., Opt. Coatings, 40 (1978) 42.

44. W. E. Neal and R. W. Fane, J. Phys. F., 6 (1973) 409.

45. W. E. Neal, Phys. Technol., 8 (1977) 238.

46. J. B. Theeten and D. E. Aspnes, Ann. Rev. Mater Sci., 11 (1981) 97.

47. J. Sarakinos and J. Spyridelis, Thin Solid Film, 28 (1975) 167.

48. J. Shewchun and E. C. Rowe, J. Appl. Phys., 41 (1970) 4128.

49. R. H. Muller, Electrochem. Acta., 22 (1977) 951.

50. B. D. Cahan and R. F. Spanier, Surf. Sci., 16 (1969) 166.

51. S. N. Jasperson, K. K. Burge and R. C. O'Handley, Surf. Sci., 37 (1973) 548.

52. B. D. Cahan, J. Horkans and E. Yeager, Surf. Sci., 37 (1973) 559.

53. H. G. Jerrard and O. N. Henty, Opt. Laser Technol., 9 (1977) 129.

54. R. H. Muller and H. J. Mathieu, App. Opt., 13 (1974) 2222.

55. R. H. Muller, Surf. Sci., 56 (1976) 19.

56. C. A. Fenstermaker and F. L. McCrackin, Surf. Sci., 16 (1969) 85.

57. R. S. Sirohi, J. Phys. D., 3 (1970) 1407.

58. R. M. Azzam and N. M. Bashara, Phys. Rev. B., 5 (1972) 4721

59. E. C. Chan and J. P. Marton, J. Appl. Phys., 45 (1974) 5004.

60. J. P. Marton and E. C. Chan, J. Appl. Phys., 45 (1974) 5008.

61. T. Smith, Surf. Sci., 45 (1974) 117.

62. P. C. Hayfield, Surf. Sci., 56 (1976) 448.

63. M. Ohlidal, I. Ohlidal and F. Lukes, Surf. Sci., 55 (1976) 467.

64. I. Ohlidal, F. Lukes and K. Narratil, Surf. Sci., 45 (1974) 91.

65. T. Smith, Surf. Sci., 56 (1976) 252.

66. K. Vedam, Surf. Sci., 56 (1976) 221.

67. R. M. Pashley, Surf. Sci., 71 (1978) 139.

68. T. Smith and G. Lindberg, Surf. Technol., 8 (1979) 1.

69. D. Den Engelsen, J. Opti. Soci. Am., 61 (1971) 1460.

70. R. M. Azzam and N. M. Bashara, J. Opt. Soc. Am., 64 (1974) 128.

71. R. M. Azzam and N. M. Bashara, J. Opt. Soc. Am., 62 (1972) 336.

72. R. M. Azzam and N. M. Bashara, Opt. Comm., 5 (1972) 5.

73. R. M. Azzam and N. M. Bashara, J. Opt. Soc. Am., 62 (1972) 1375A.

74. R. M. Azzam and N. M. Bashara, J. Opt. Soc. Am., 62 (1972) 1521.

75. D. W. Berreman, J. Opt. Soc. Am., 63 (1973) 1374.

76. D. J. De Smet, J. Opt. Soc. Am., 63 (1973) 958.

77. D. J. De Smet, J. Opt. Soc. Am. 64 (1974) 631.

78. F. Meyer, E. E. De Kluizenaar and D. Den Engelsen, J. Opt. Soc. Am., 63 (1973) 529.

79. D. J. De Smet, J. Opt. Soc. Am. 65 (1975) 542.

80. S. Kawabata and K. Ichiji, Surf. Sci., 56 (1976) 316.

81. D. Den Engelson, Surf. Sci., 56 (1976) 272.

82. D. J. De Smet, Surf. Sci., 56 (1976) 293.

83. M. E. Pedinoff, M. Braunstein and O. M. Stafsudd, Appl. Opt., 18 (1979) 201.

84. F. H. Habraken, O. L. Gijzeman and G. A. Bootsma, Surf. Sci., 96 (1980) 482.

85. M. E. Pedinoff, D. C. Mayer, O. M. Stafsudd and G. L. Dunn, Appl. Opt., 21 (1982) 3307.

86. R. Kotz and B. E. Hayden, Surf. Sci., 135 (1983) 374.

87. J. F. Nye, Physical Properties of Crystals, Clarendon Press, Oxford, 1972, Chapter 13.

88. D. J. De Smet and J. L. Ord, J. Electrochem. Soc., 130 (1983) 280.

89. C. G. Matthews, J. L. Ord and W. P. Wang, J. Electrochem. Soc., 130 (1983) 285.

90. J. L. Ord and W. P. Wang, J. Electrochem. Soc., 130 (1983) 1809.

91. L. P. Mosteller, Jr., and F. Wooten, J. Opt. Soc. Am., 58 (1968) 511.

92. D. E. Aspnes, J. B. Theeten and R. P. Chang, J. Vac. Sci. Technol., 16 (1979) 1374.

93. P. Yeh, Surf. Sci., 96 (1980) 41.

94. L. J. Hanekamp, W. Lisowski and G. A. Bootsma, Surf. Sci., 118 (1982) 1.

95. T. M. Gardiner, H. M. Kramer and E. Bauer, Surf. Sci., 121 (1982) 231.

96. L. J. Hanekamp, S. J. Prader and G. A. Bootsma, Surf. Sci., 135 (1983) 383.

97. M. Prutton, Surface Physics, Clarendon Press, Oxford, 1983.

98. G. C. Bond, Catalysis by Metals, Academic Press, New York, 1962.

99. K. R. Lawless, Rep. Prog. Phys., 34 (1974) 231.

100. C. Wagner, Z. Physik Chem., 21 (1933) 25.

101. P. Kofstad, High Temperature Oxidation of Metal, John Wiley and Sons, Inc., New York, 1966.

102. N. Birks and G. H. Meier, Introduction to High Temperature Oxidation of Metals, Edward Arnold, London, 1983.

103. G. G. Stoney, Proc. Roy. Soc. (London) A82 (1909) 172.

104. R. W. Hoffman, Phys. Thin Films, 3 (1966) 211.

105. H. P. Murbach and H. Wilman, Proc. Phys. Soc., B66 (1953) 905.

106. H. P. Murbach and H. Wilman, Proc. Phys. Soc., B66 (1953) 911.

107. W. Buckel, J. Vac. Sci., Technol., 6 (1969) 606.

108. I. J. Hodgkinson and A. R. Walker, Thin Solid Film, 17 (1973) 185.

109. F. K. Reinhart and R. A. Logan, J. Appl. Phys., 44 (1973) 3171.

110. T. G. Beleycheva and K. K. Ziling, Avtometriya, 12 (1976) 63.

111. S. M. Rossnagel, P. Gilstrap and R. Rujkoradarn, J. Vac. Sci. Technol., 1 (1982) 1045.

112. H. K. Pulker, SPIE, Optical Thin Films, 325 (1982) 84.

113. I. T. Taylor and R. L. Edgar, Metallurg. Trans., 2 (1971) 833.

114. D. A. Vermilyea, Acta Metallurg., 5 (1957) 492.

115. J. C. Grosskreutz, Surf. Sci., 8 (1967) 173.

116. T. I. Kamins and E. S. Meieran, J. Appl. Phys., 44 (1973) 5064.

117. J. W. Menter and D. W. Pashley, in C. A. Neugebauer, J. D. Newkirk and D. A. Vermilyea (eds), Structure and Properties of Thin Films, Wiley, New York, , p. 111.

118. R. W. Hoffman, in Wilsdorf (ed.), American Society of Metals, Cleveland, Ohio, 1964, p. 99.

119. B. Yates "Thermal Expansion", Plenum Press, New York, 1972.

120. C. H. Lane, IEEE Trans. Electron Devi., ED-15, (1968) 998.

121. R. J. Jaccodine and W. A. Schlegel, J. Appl. Phys., 37 (1966) 2429.

122. M. V. Whelan, A. H. Goemans and L. M. Goossens, Appl. Phys. Lett., 10 (1967) 262.

123. E. Taft and L. Cordes, J. Electrochem. Soc., 126 (1979) 131.

124. D. E. Aspnes and J. B. Theeten, J. Electrochem. Soc., 127 (1980) 1359.

125. H. Friedrich, Solid-State Electron., 14 (1971) 639.

126. J. H. Serebrinsky, Solid-State Electron., 13 (1970) 1435.

127. S. D. Brotherton, T. G. Read, D. R. Lamb and A. F. W. Willoughby, Solid-State Electron., 16 (1973) 1367.

128. J. R. Adams and N. B. Bashara, Surf. Sci., 47 (1975) 655.

129. S. S. So and S. M. Zimmerman, Polarized Light (SPIE), 88, (1976) 119.

130. E. P. EerNisse and G. F. Derbernwick, IEEE Trans. Nucl. Sci., NS-23 (1976) 1534.

131. W. A. Martin and G. Hartung, Phys. Stal. Sol., (a) 44 (1977) K159.

132. E. A. Taft, J. Electroch. Soc., 125 (1978) 968.

133. F. J. Grunthaner, P. J. Grunthaner, R. P. Vasquez, B. F. Lewis, J. Maserjian and A. Madhukar, J. Vac. Sci. Technol., 16 (1979) 1443.

134. A. Ishizaka and S. Iwata, Appl. Phys. Lett., 36 (1980) 71.

135. G. A. Candela, K. F. Galloway, Y. M. Liu and J. Fine, Thin Solid Films, 82 (1981) 183.

136. G. E. Jellison, Jr. and F. A. Modine, J. Opt. Soc. Am., 72 (1982) 1253.

137. G. E. Jellison, Jr. and F. A. Modine, J. Appl. Phys., 53 (1982) 3745.

138. D. E. Aspnes and J. B. Theeten, Phys. Rev. Lett., 43 (1979) 1046.

139. M. Stavola, Appl. Phys. Lett., 44 (1984) 514.

140. T. J. Maloney, D. E. Aspnes, H. Arwin and T. W. Sigmon, Appl. Phys. Lett., 44 (1984) 517.

141. N. Shibata, K. Okamoto, M. Tateda, S. Seikai and Y. Sasaki, IEEE J. Quant. Electro., QE-19 (1983) 1110.

142. E. D. Palik and V. M. Bermudez, J. De Phys., 12 (1983) C10-179.

143. G. Rajeswaran, W. A. Anderson, M. Jackson and M. Thayer, Thin Solid Films, 104 (1983) 351.

144. F. Abeles, Ann. de Physique, 3 (1948) 504.

145. P. Rouard, Ann. de Physique, 7 (1937) 291.

146. A. Vasicek, J. de Phys., 11 (1950) 342.

147. R. Ditchburn, Ligh, Blackie, London, 1952.

148. J. C. M. Garnett, Phil. Trans. Roy. Soc., 203 (1904) 385.

149. J. C. M. Garnett, Phil. Trans. Roy. Soc., 237 (1905) 2237.

150. See. Ref. 87, Chapter 7.

151. W. A. Wooster, Tensors and Group Theory for the Physical Properties of Crystals, Clarendon Press, Oxford, 1973, Chapter 10.

152. P. A. Jacquet, Metal Finish, 47, No. 5 (1949) 48.

153. P. A. Jacquet, Metal Finish, 47, No. 6 (1949) 83.

154. W. J. Tegart, The Electrolytic and Chemical Polishing of Metals, Pergamon, 1959.

155. D. J. Arrowsmith, A. W. Clifford and J. C. Crowther Trans. Inst. Metal Finish, 57 (1979) 89.

156. F. L. McCrackin and J. P. Colson, in E. Passaglia (ed.), Ellipsometry in the Measurement of Surfaces and Thin Films, National Bureau of Standards Washington, DC, 1964, p. 25.

157. J. Schewchun and E. Rowe, J. App. Phys., 41 (1970) 4128.

158. J. L. Ord and D. J. De Smet, J. Electrochem. Soc., 113 (1966) 1258.

159. R. W. Fane and W. E. Neal, J. Opt. Soc. Am., 60 (1970) 790.

160. R. W. Fane, W. E. Neal and R. Latham, J. App. Phys., 44 (1973) 740.

161. R. C. Smith and M. Hacskaylo, in E. Passaglia (ed.), Ellipsometer in the Measurement of Surfaces and Thin Films, National Bureau of Standards, Washington DC, 1964, p. 83.

162. W. Primak and D. Post, J. Appl. Phys., 30 (1959) 779.

163. R. M. Waxler, D. Horowitz and A. Feldman, Appl. Opt., 16 (1977) 20.

164. J. H. Halford, F. K. Chin and J. E. Norman, J. Opt. Soc. Am., 63 (1973) 786.

165. J. Kruger, in E. Passaglia (ed.), Ellipsometry in the Measurement of Surfaces and Thin Films, National Bureau of Standards, Washington DC, 1964, p. 131.

166. R. J. Archer, in E. Passaglia (ed.), Ellipsometry in the Measurement of Surfaces and Thin Films, National Bureau of Standards, Washington DC, 1964, p. 255.

167. J. Kruger, J. Corrosion, 22 (1966) 88.

168. P. A. Jacquet, J. Electrochem. Soc., 69 (1936) 629.